Funny Hills: The Shell-Correction Approach to Nuclear Shell Effects and Its Applications to the Fission Process

M. BRACK,* JENS DAMGAARD, A. S. JENSEN, H. C. PAULI,* V. M. STRUTINSKY,† C. Y. WONG‡
The Niels Bohr Institute, University of Copenhagen, Denmark

This paper reviews various results related to the single-particle structure in spherical and deformed nuclei, discussed from the viewpoint of the so-called shell-correction method. This method stresses the importance of large-scale nonuniformities in the energy distribution of the individual particles especially near the Fermi energy. The way in which these nonuniformities affect in an essential way many nuclear properties, such as the shape stiffness, the spatial density distribution, the total mass of the nucleus, the mass and inertia of the nuclear shape variations, etc. is also discussed. Against this background, the behavior of the nuclear deformation energy is described, in particular for larger distortions relevant to the fission process. In this connection, some qualitative singularities of the phenomenological liquid-drop deformation energy at large shape distortions are pointed out, and their possible implications for fission are discussed. As the problems considered cover a wide range of nuclear properties, this paper is not a review in the narrow sense of the word. Comparison with other approaches as well as historic references are given mainly to clarify specific points, because a complete review would be a monumental undertaking.

CONTENTS

I. Introduction ... 320
II. Qualitative Considerations ... 323
1. Definition and Origin of the Shells ... 323
2. The Energy and Spatial Density Corrections and the Forces due to Shells ... 327
III. Variation in Energy and its Connection to Hartree–Fock Theory ... 330
1. The Shell Model as an Alternative for the Self-consistent Theory ... 330
2. The Renormalization of a Smooth Part of the Energy ... 332
3. The Average Field and the Shape of the Nucleus 334
4. The Smoothed Level Density ... 335
IV. The Shell Corrections ... 336
1. Quantitative Description of Level Densities ... 336
2. The Energy Shell Correction ... 337
3. The Occupation Number Representation ... 338
4. Effect of a Small Variation of the Average Field ... 338
5. The Shell Force and the Spatial Density Fluctuations ... 339
6. Contributions to Shell Corrections ... 342
7. Shell Effects in the Spatial Density Distributions ... 343
V. Equilibrium Deformations and the Pairing Correlations ... 347
1. Equilibrium Shapes ... 347
2. Shape Transition and the Influence of Pairing ... 349
3. Comparison with Some Earlier Discussions ... 352
4. Renormalization in the BCS Theory ... 356
5. Surface-Dependent Pairing ... 357
VI. Nuclear Masses in the Lead Region ... 358
1. Empirical and Theoretical Shell Corrections to Nuclear Masses ... 358
2. Shell Model Dependence of the Theoretical Mass Corrections ... 361
3. Comparison with Experiment ... 362
VII. The Liquid Drop and Shell Model for Large Distortions ... 364
1. Description of the Nuclear Shape ... 364
2. The LDM Energy Surface ... 366
3. The LDM Valley ... 367
4. The Exit Deformation ... 368
5. The Shell Model ... 371
VIII. The Deformation Energy of Heavy Nuclei ... 374
1. The Deformation Energy for Symmetric Shapes ... 374
2. The Deformation Energy for Left–Right Asymmetric Shapes ... 377
3. The Heights of the Fission Barriers of the Actinides ... 380
4. The Deformation Energy for Superheavy Nuclei ... 381
IX. On the Dynamics ... 382
1. Inertial and Friction Forces and the Dynamics of Fission ... 382
2. The Least-Action Trajectory ... 383
3. The Effective Mass Parameters ... 386
3a. The One-dimensional Case ... 388
3b. The Two-dimensional Case ... 389
4. The Trajectory for Symmetric Distortion. Lifetime Estimates ... 391
5. Moments of Inertia ... 394
Acknowledgements ... 403
Appendix ... 403
Bibliography ... 404

I. INTRODUCTION

The problems involving bulk properties of nuclei such as nucleon density distributions, nuclear masses, and nuclear deformation energies constitute some of the most pertinent problems of modern nuclear physics. They have been and are still being attacked from many different angles.

Simple models have been developed in the past to accentuate different aspects of the problem. For instance, the saturation property and low compressibility of nuclear matter have early suggested an analogy with a liquid droplet (Bohr and Kalckar, 1937). A model of this kind has formed the basis of many semiempirical mass formulae, as, e.g., the well-known Bethe–Weizsäcker approximation to nuclear masses (von Weizsäcker, 1935; Bethe and Bacher, 1936). The generalization of these phenomenological models to include the case of deformed nuclei led to the so-called liquid-drop model (LDM) for the nucleus,

* Permanent address: University of Basel, Switzerland.
† Present address: Institute for Nuclear Research, Kiev, U.S.S.R. (On leave from I. V. Kurchatov Institute for Atomic Energy, Moscow, U.S.S.R.).
‡ Permanent address: Oak Ridge National Laboratory, Tennessee, U.S.A.

which was used in the first theoretical descriptions of the fission process (Bohr and Wheeler, 1939; Frenkel, 1939).

Since then, the main field of application of the LDM has been to the description of average properties of the nuclear masses and deformation energies. Attempts have also been made to extend the analogy between the nucleus and a liquid droplet still further, e.g., by assuming a kind of irrotational and incompressible collective motion in the nucleus. These attempts have not been very successful and, at present, it is not generally believed that the LDM correctly represents the dynamic properties of nuclear matter. Against this background, it should be remembered that, whenever in the present paper we refer to the LDM, we take it only as a classical phenomenological expression for the total mass of the nucleus considered as a function of its shape and the nucleon numbers.

As an illustration of the quality of the LDM fit to nuclear masses, we show in Fig. I-1 the results obtained by using one of the recent versions, namely the liquid-drop model of Myers and Swiatecki (1966a).

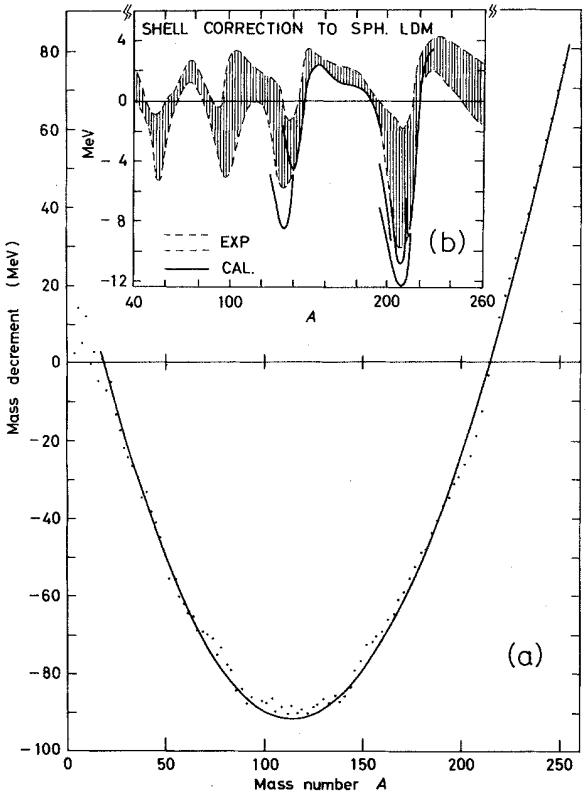

FIG. I-1. (a) Experimental nuclear masses as compared with the LDM fit used by Myers and Swiatecki (1966a). The figure is taken from that reference. (b) The total shell-correction energies to the nuclear ground-state masses, as calculated in Strutinsky (1967), are compared to the deviations of experimental masses from an LDM mass law referring to spherical nuclei (Seeger and Perisho, 1967).

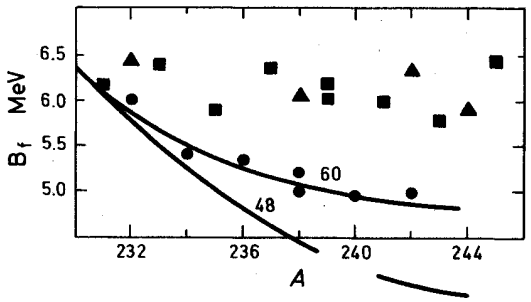

FIG. I-2. Fission threshold energies versus the mass number A obtained by an analysis of the observed fission cross sections (Androsenko *et al.*, 1969). Circles mark doubly even, squares odd A, and triangles doubly odd nuclei. The lines represent the LDM predictions for $(Z^2/A)_{crit}$ equal to 48 and 60.

When, in 1939, the fission process was discovered (Hahn and Strassmann, 1939), it was immediately related to the disintegration of a uniformly charged droplet (Meitner and Frisch, 1939). In the classic papers by Bohr and Wheeler (1939) and by Frenkel (1939), the deformation energy provided a guide to the understanding of the mechanism of the process. This original picture, however, is insufficient in many respects. As an example, we show in Fig. I-2 the fission threshold energies obtained by an analysis of the observed fission cross sections (Androsenko *et al.*, 1969). The experimental values are almost constant for the actinide nuclei. The liquid-drop model, however, predicts a rather sharp decrease of the fission barrier with increasing value of the fissility parameter $x=(Z^2/A)/(Z^2/A)_{crit}$. It would require a value of $(Z^2/A)_{crit}\approx 60$ to fit the observed weak variation, while the general trend of the barriers in a broader region of nuclei, and especially the fit to nuclear ground-state masses, lead to a value $(Z^2/A)_{crit}\approx 45$–48 (Goeppert-Mayer and Jensen, 1955). Since the fission barriers are determined as the energy difference of two stationary shapes, namely, the ground and theshold state, this discrepancy does not depend on the still poorly understood dynamic features of the fission process. Thus, the conclusion is rather straightforward, and may be taken as a serious warning that the LDM does not correctly represent these quantities, indicating that something essential is missing in that model.

Actually, already by considering the LDM mass fit in Fig. I-1, one observes the occurrence of some systematic deviations, especially pronounced in the so-called magic nuclei. While, on the average, the deviation does not exceed a few MeV, the magic nuclei can be nearly 13 MeV more bound than predicted by the LDM average fit. These deviations of the nuclear binding energy from the smooth average defined by the liquid drop were early taken as evidence for the existence of

shell structure in nuclei, similar to that found in atoms (see, e.g., Feenberg, 1955). This special aspect of nuclear structure is stressed in the shell or independent-particle model based on the idea that the nucleonic interactions create a field, which in the lowest order approximation is common to all nucleons; the latter are considered as moving independently of each other in this average field, and their energies and wave functions are found by a solution of the corresponding one-particle problem, with the potential determined on an empirical basis.

It was indeed a great success when the shell model, after introduction of the spin–orbit force (Haxel *et al.*, 1949; Mayer, 1949), predicted the gaps in the single-particle level structure corresponding to the magic numbers . . . 50, 82, 126, reflected in the increased binding energy of the magic nuclei. The model has also provided a basis for discussions of the properties of excited nuclear states and for the development of microscopic theories, which describe the collective excitations found in nuclei as coherent motion of the shell-model particles. Furthermore, the shell model in its extension to nonspherically symmetric average fields (Nilsson, 1955) correctly predicted the ground-state spins and the low excitation spectrum for most of the even–odd nuclei. It was also successfully applied to the evaluation of the nuclear ground-state deformations (Mottelson and Nilsson, 1959), where the nuclear energy as a function of deformation was estimated from the sum of single-particle energies, as given by the Nilsson model, with the constraint of constant volume for the potential. This approach and the closely related treatment based on a quadrupole interaction between the nucleons (Kumar and Baranger, 1968) were further developed with the inclusion of pair correlations by various authors. Attempts were also made to extend such a treatment to large distortions occurring in the fission process, particularly in connection with the problem of asymmetry of the fragment distribution; see, e.g., Johansson (1962). Such studies became especially intensive after the discovery in 1962 of the spontaneous fission isomers (Polikanov *et al.*, 1962); see, e.g., Gustafson *et al.*, 1966; Malov, Polikanov, and Soloviev, 1966.

Analyses of this type, based entirely upon the single-particle model, cannot be expected to adequately describe the nuclear deformation energy. Although they work reasonably well for moderate quadrupole deformations of the order of those occurring in the ground-state deformations, it is essential for larger quadrupole, or for other more complex deformations, to properly incorporate the bulk properties of the nucleus, in addition to the single-particle structure.

In general, one may also say that large distortions of the average field, which are bound to occur in fission, remains a very difficult but challenging testing ground for any nuclear theory. Thus it seems that both approaches—the phenomenological classical approach represented by the liquid-drop model as well as the summation of levels based on the single-particle model—are unable to provide a reliable picture of all essential properties; they existed peacefully side by side without links between them, each with its own virtues. Recently, a method has been developed, in which the liquid-drop and the single-particle aspects were given their balanced role (Strutinsky, 1966–68). In this method, the smooth part of the total energy of the nucleus is extracted and replaced by the phenomenological liquid-drop model expression. One tries only to evaluate the remaining oscillations (the so-called shell corrections) due to nonuniformity of the phase-space distribution of the nucleons. As it has proved successful in many applications, we shall in the following limit ourselves to consideration of this method. However, it should be stressed that many other methods have been suggested for treating the problems connected with large nuclear distortions and the fission process.

Significant insight has for example been obtained in the so-called statistical theory of fission (see Fong, 1969, and references herein). More recently there have been attempts to develop a theory, in which properties of complex nuclei are deduced from nucleon–nucleon interactions. Important progress in this approach has lately made it possible to calculate with a relatively high precision the nucleon binding energies in a number of heavy nuclei, and has also made possible a quantitative description of some other properties (see, e.g., Negele, 1970). However, it seems that still higher accuracy is required for the description of the nuclear fission process (see Bassichis *et al.*, 1971). Here, one is dealing with a significant reconstitution of the whole nucleus, and the theory should be able to predict the *total* binding energy of the nucleus with an accuracy of at least a few MeV. The development of a purely microscopic theory capable of meeting this requirement is undoubtedly a tremendous undertaking, in which one meets very serious theoretical and practical difficulties. One may even doubt that such an approach will ever result in a manageable theory of nuclear fission, where the evaluation of the energy variations in itself is only part of the problem involving also dynamical features of a distorted piece of nuclear matter.

Similar studies, as the ones presented in later sections of this paper, have recently been done by several other groups (see e.g. Nilsson *et al.*, 1969; Andersen *et al.*, 1970; Mosel *et al.*, 1971; Bolsterli *et al.* 1971; for a complete list of references see the latter reference). Though they all apply the same methods, i.e., the shell-correction approach presented below, they differ among themselves and from this presentation mainly by the use of different types of average potentials in the single-particle models. They all arrive at qualitatively similar results, which can be understood from the arguments presented below.

In this paper we have not tried to give a complete review of all the different approaches, mainly for reasons of space. We rather report on the extensive investigations of different aspects of shell structure in nuclei, undertaken at the Niels Bohr Institute in the years 1968–1970. So without being a proper review, it is the aim of the present paper to show that the presence of shells interpreted as large-scale nonuniformities in the distribution of single-particle states is a common feature of independent-particle models, and that this grouping of levels manifests itself in many important ways in deformed as well as in spherical nuclei. In Sec. II, we shall collect some qualitative arguments indicating that the bunching of levels is not so much a feature of spherical nuclei, but rather a kind of residual effect of the quantization of the single-particle motion. Therefore it may occur at any deformation of the average field. This implies necessarily a generalized concept of the shell structure as well as of nuclear magicity. The way in which the existence of such shells is connected with a contribution to the total energy, and how this shell-correction energy can be calculated from existing single-particle models, is presented in detail in Sec. IV, together with a discussion of the forces arising due to a nonuniform density distribution of the nucleons. We discuss, in Sec. III, how far it is justified, from a microscopic point of view, to divide bulk properties like the total energy into a shell contribution and a slowly varying background energy, which may be treated in a simple phenomenological way, and whether the suggested approach is self-contained.

In fact, the shell structure is almost exclusively decisive for the nuclear ground-state deformations, while residual interactions like the pairing correlations are of comparatively minor importance (Sec. V). However, they manifest themselves, for instance, in fluctuations of the ground-state masses. Although no new fit to these masses has been attempted in this paper, some conclusions (Sec. VI) are drawn, in particular concerning the nuclear masses around lead-208.

In the second part (Secs. VII–IX), we confine ourselves to a discussion of the nuclear deformation energy at larger distortions, and in particular its implications for the fission process and for the stability of the hypothetical superheavy nuclei. In this context, the shell-correction method has especially interesting applications. Large and unusual deformations of the nucleus are characteristic of fission, and the way in which we treat both the single-particle and the liquid-drop models in these cases may be found in Sec. VII. An important part of our investigation deals with the influence of asymmetry in the nuclear shape at large distortions (Sec. VIII). In the same section, we consider the possible existence of isomeric states in strongly deformed nuclei, a possibility which is confirmed by the growing body of experimental data.

The dynamic aspect of the special modes of collective motion met in fission is a nearly untouched field. In Sec. IX, we present our calculations of two important quantities of a future dynamic theory, namely, the mass and inertia tensors. In these quantities, we again find a strong correlation with the grouping of levels and sometimes pronounced "shell structure" as in the total energy. Though a dynamic theory remains a challenging problem, some success may be achieved in the calculation of spontaneous fission lifetimes by simple estimates of penetration probabilities. These are described in Sec. IX.

We consider also the moments of inertia of the rotating nucleus for a varying degree of the excitation characterized by the nuclear temperature (Sec. IX). Here, one can see that the shell effects in the single-particle level distributions become less important in excited nuclei.

II. QUALITATIVE CONSIDERATIONS

This section is devoted to a qualitative description of the simple physical picture arising from our calculations concerning the correlations between different shell-correction quantities. The precise definition of these quantities will be found in the next sections along with a detailed description of the results.

In this section, we also try to explain why the shell structure may be expected to be a common feature of nearly any independent-particle model.

1. Definition and Origin of the Shells

In the framework of the single-particle model, the distribution of energy levels found in nuclei is traditionally described in terms of shells, subshells, etc. Adapted from atomic structure, the notion of a shell is often used as just another denotation of a degenerate single-particle state in a spherical nuclear field.

As will be explained in the following, a somewhat broader and more specific definition seems, however, necessary.

We shall define a shell as a large-scale nonuniformity in the energy distribution of the individual particle states. This crude definition will become more explicit in the course of this section. So, in the specific case of a spherical field, instead of a degenerate single-particle state, we would rather interpret large distinct groups of such states as shells.

For the nuclear binding energies the level distribution near the Fermi energy is of special importance. Considering this region, we have tried to illustrate the connection between the variation of the local density of single-particle states near the Fermi energy and the nuclear binding energy in Fig. II-1. From this figure, it is seen that, compared to the case of uniform density of states, the nucleus is expected to be more bound if the

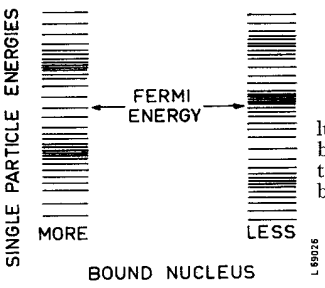

FIG. II-1. Qualitative illustration of the connection between the level density at the Fermi energy and the binding energy of the nucleus.

level density is smaller, because then the nucleons occupy deeper and more bound states. Conversely, the nucleus is less bound if the level density is increased near the Fermi energy.

This effect of the variation of the single-particle level density in the vicinity of the Fermi energy on the nuclear binding energy is, in fact, a particular example of the general rule that, in quantal systems, degeneracy leads to reduced stability. This is so because even an infinitely small perturbation of a degenerate system produces a finite response in the system due to rearrangement of many close states. In nuclei, the bunching of levels expresses, of course, only an approximate degeneracy and, therefore, it requires a finite though small perturbation to reveal this feature of the degeneracy. In all other respects, the situation is analogous to the one met in some problems of molecular and solid state physics; see, e.g., the Jahn–Teller rule in the theory of molecules (Landau and Lifshitz, 1959):

The nuclear ground state, as well as any other relatively stable state, should thus correspond to the lowest possible degeneracy or, in other words, the lowest density of states near the Fermi energy. From this, a new definition of a "magic" nucleus (or, more generally, of a shell closure) follows: it is the one, which is the least degenerate, i.e., which has the lowest density of intrinsic states at the Fermi level, among its neighbors. It should be noted that neither this definition nor the concept of shells introduced above involves any assumption concerning the nuclear shape. As the shell distribution is also a function of the nuclear shape, and pronounced shells appear in deformed nuclei, one also has to generalize somewhat the concept of "magicity". Instead of being connected only to definite nucleon numbers, "magicity" should be characterized by *both* the nucleon number *and* some characteristic deformation of the nuclear shape at which the shell closures occur. A magic nucleus need not be spherical and, in addition to the familiar magic numbers of nucleons for spherical nuclei, one can also speak of magic deformed nuclei connected to other nucleon numbers. In the same way as, e.g., the presence of the familiar shell closures for $Z=82$, $N=126$ in a spherical shape nucleus is responsible for the increased stability of spherical shapes in nuclei around lead-208, the deformed shape shell closures appearing for some other nucleon numbers (e.g., $N=100$, 152) are responsible for the increased stability of distorted shapes (corresponding to quadrupole distortions with β_2 equal to 0.2 or 0.3) for the rare-earth and actinide nuclei. Confirmation hereof can be found in some empirical data. Here one should mention an observation by W. D. Myers and W. Swiatecki who in their analysis of nuclear masses found systematic deviations in the middle of the rare-earth region and, independently of the theoretical results, found it compelling to introduce some kind of magicity also for deformed nuclei. This observation led them to improve their phenomenological shell corrections in a direction consistent with the calculations (Myers and Swiatecki, 1966a).

In order to illustrate our point of view, we present in Fig. II-2 a schematic fingerprint of single-particle level distributions in a deformed nucleus, where the magic shell closures as the regions of a locally low level density are indicated by circles. In real nuclei, these regions expose an anomalous stability depending on specific shapes and nucleon numbers.

As we shall explain later, the shell distribution is expected to change appreciably with even a relatively small variation of the nuclear shape of the order of $A^{-1/3}\approx 20\%$ and, consequently, a nucleus can have more than one shape where the condition of the lowest degeneracy is locally fulfilled. Thus, one can also speak of magic nuclei in connection with a second shell closure in a strongly deformed nucleus. An important example is found at $N=146$, where the nucleus becomes magic for a strongly distorted shape. A pronounced potential well develops in the nuclei around this nucleon number at a deformation characterized by the ratio of the two nuclear axes equal to 1.8–2.0.

In fission, the nucleus may be caught into this other well and stay there for a relatively long time. In this

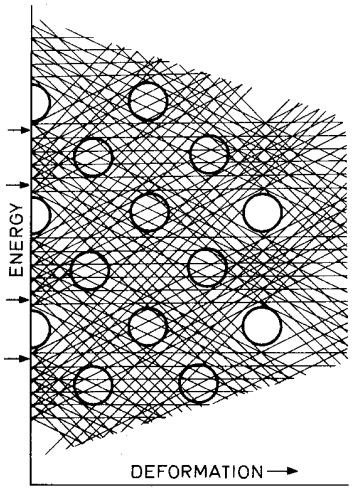

FIG. II-2. Qualitative picture of the distribution of single-particle states in the deformed nucleus. The low-density regions (shell closures) are indicated by circles.

way, the spontaneous fission isomers discovered recently (Polikanov *et al.*, 1962) are explained (Strutinsky, 1966). It also influences the fission process in nuclei around ^{240}Pu, and there one finds many experimental results in support of the quasistationary state in the strongly distorted nucleus, in addition to the spontaneous fission isomers: the grouping of the neutron fission resonances, broad collective resonances, and some anomalies in the angular distribution of the fission fragments, etc. (see, e.g., Bjørnholm and Strutinsky, 1969; Vienna Symposium, 1969).

In this paper, we describe a method which allows a quantitative evaluation of the shell-structure effects in the nuclear binding energy; the correlation between the increased binding and the shell closures mentioned above will appear as a systematic qualitative result. This connection has earlier been used in a phenomenological way; see, e.g., Swiatecki, 1963; Myers and Swiatecki, 1966a. However, considerable arbitrariness arises in connection with the phenomenologically defined shell corrections of these authors, and, furthermore, their assumption that the shells disappear for large deformations was not justified.

The latter assumption was, in fact, very common at the time. Only in a few earlier attempts to explain the asymmetry of the mass distribution of fission fragments, has it been suggested that shells in strongly distorted fragments might be partly responsible for this asymmetry, as e.g. in Geilikman, 1960. The arguments were based on a consideration of the axially symmetric deformed harmonic oscillator field in which degeneracy appears for the ratios of the frequencies equal to 1/1, 1/2, 1/3, etc. However, the pure harmonic oscillator was too much of a special case, and no such degeneracy was expected for realistic potentials. It was, therefore, usually assumed that the pronounced shell structure is a characteristic of spherical nuclei and disappears at relatively small deformations when levels of adjacent shells cross (Swiatecki, 1963; Myers and Swiatecki, 1966a, b; Geilikman, 1965; Geilikman and Khlebnikov, 1968; Strutinsky, 1966). This assumption seemed to find support in the rather chaotic level distribution resulting from the Nilsson scheme at medium deformations, where it is indeed not easy to detect any special structure on brief inspection. However, closer examination, having in mind the quantitative definition of the shell structure, still clearly reveals shell structure there, as well as in other single-particle potentials, cf. Fig. II-3.

In fact, the presence of shells appears to be a rather general phenomenon. Conversely, the absence of shells, i.e. a uniform random distribution of the single-particle states, must be considered an exception. Actually, in all investigated single-particle potentials, a similar pattern of the shell distribution is found with the shells only relatively more pronounced in the spherical case. This point has been checked in a number of calculations, e.g., with the deformed square well and the harmonic oscillator potentials, the Nilsson model with arbitrary values for the μ and κ parameters (Strutinsky, 1968), and with the Woods–Saxon potentials of various nuclear shapes, including those with a distinct waist, or with the spin–orbit force artificially increased so much that even the spherical magic numbers were significantly moved from their usual positions. Nor does the shell structure seem to have much to do with special features of the harmonic oscillator, whose shell structure appears to be only a specific case of a more general phenomenon.

This may be clear, for instance, from the finding that even stronger shells appear in the Nilsson model than in the original deformed haromic oscillator, in spite of the fact that the spin–orbit force and the l^2 term spoil the degeneracy related to special rational ratios of the frequencies. It seems that only one feature is common to all the investigated cases, namely that an average potential of a certain size and depth is considered. Thus, a plausible explanation seems to be that the large-scale fluctuations in the level distribution emerge as a residual effect due to quantization of the single-particle motion in a finite size field. The quantization imposes some restrictions on the available nucleon phase space and results in a certain statistical correlation of the spacings between the individual levels in a few-dimensional case. In order to explain this argument in more detail, let us start by considering first an arbitrary one-dimensional potential which has a certain definite size R. From Bohr's quantization rule, we find

$$p(\mathcal{E}_n)R \approx n\hbar, \tag{II.1}$$

where $p(\mathcal{E}) = (2\mathcal{E}m)^{1/2}$ is the momentum of the particle, and m is the nucleon mass. The estimate in Eq. (II.1) gives a spacing between the levels approximately equal to

$$\hbar\Omega = \mathcal{E}_{n+1} - \mathcal{E}_n \approx (\hbar/R)[(2\mathcal{E}_n/m)]^{1/2}, \tag{II.2}$$

with much smaller and larger distances not allowed.

If we equate the kinetic energy $\mathcal{E}$ with the Fermi energy λ and use the familiar relation $R = r_0 A^{1/3}$, the elementary energy quantum in Eq. (II.2) is given by

$$\hbar\Omega \approx 1.3(\lambda/A^{1/3}) \approx 5\text{–}10 \text{ MeV}. \tag{II.3}$$

In Eq. (II.3), we have further made use of the Fermi momentum

$$p(\lambda) = (\tfrac{9}{8}\pi)^{1/3}(\hbar/r_0) = 1.52(\hbar/r_0) \tag{II.4}$$

taken from the Fermi gas assumption.

Of course, in actual cases, the distance between the energy levels deviates from the estimate above. However, these model-dependent deviations are small compared to the mean distance between the states given by $\hbar\Omega$ (II.3). Thus, in a quantal problem the distribution in no instance looks like a random distribution with the mean distance $\hbar\Omega$. Instead, the positions of the individual levels are always strongly correlated.

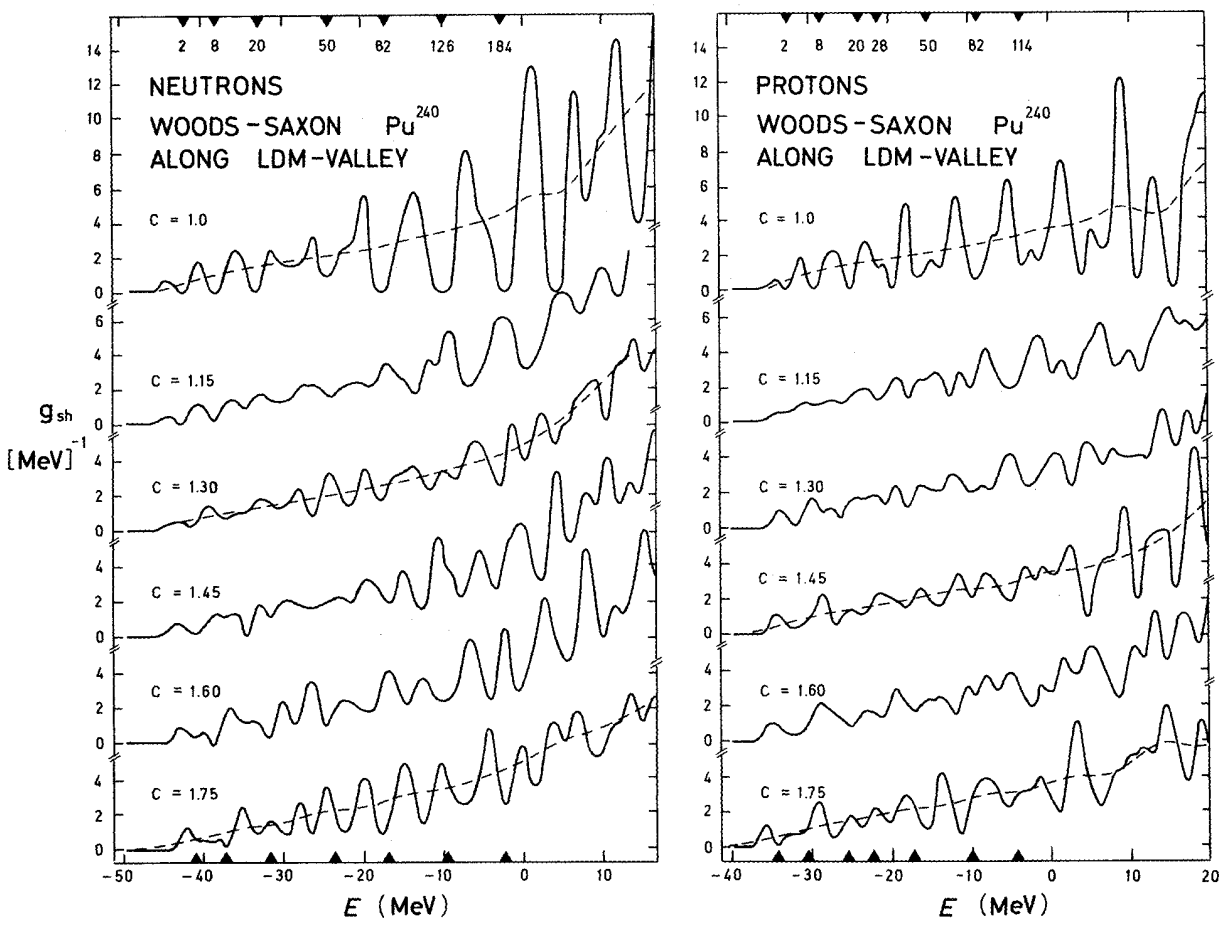

FIG. II-3. Level densities $g_{sh}(E)$ of the Woods–Saxon model for different deformations along the LDM valley (described in Sec. VII). Two times the parameter **c** denotes the elongation of the nucleus in units of the spherical radius. In the calculations $\gamma_{sh}=0.2\hbar\omega_0$ was used. The dashed lines represent the uniform density $\tilde{g}(E)$ calculated with $\tilde{\gamma}=1.0\hbar\omega_0$ (see Sec. IV). At the top and the bottom the corresponding nucleon numbers are indicated.

Turning now to two- or more-dimensional cases, we first notice that, in these cases, the level distribution may be considered approximately as a result of combining a number of one-dimensional distributions.

This leads to the familiar estimate of the mean level density in a three-dimensional potential well:

$$\tilde{g}(\lambda)\approx\tfrac{3}{2}(A/\lambda). \qquad \text{(II.5)}$$

In a heavy nucleus this estimate corresponds to 5–6 levels per MeV. Thus, had the individual levels been randomly distributed, any large-scale fluctuation of the number of particles in energy intervals of the order of a few MeV would have only a very small chance to occur. The essential point, however, is that the three-dimensional case will reflect the correlations found above in the one-dimensional distributions, with the order of magnitude of the correlation length given by Eq. (II.3).

Consequently, each shell contains as many as

$$\tilde{g}(\lambda)\hbar\Omega\approx A^{2/3} \qquad \text{(II.6)}$$

individual states.

Because the actual energies always deviate somewhat from the regular spacing in each dimension, the more dimensions the system has, the less distinct the correlations become. However, the three dimensions met in reality are hardly sufficient to wash the correlations out. So, the shell structure in the level distribution may be expected to be a general phenomenon, which is present in any shell-model field, provided that it has a finite size and a significant depth.

The above remarks concerning the origin of shell structure in finite-size potentials are only intended to give an indication of the lines along which this problem may be discussed in a way consistent with our experience. Probably, one should look for more quantitative arguments by studying the correlations in a statistical

distribution which has the described properties. As a step in this direction, it may be helpful to consider average fields which possess some special symmetries, because in these fields the arguments often have a more transparent meaning; see, e.g., the analysis of level distribution by Bloch and Balian (1969). It should be kept in mind that the presence of such symmetries in itself does not appear to be a necessary condition for the establishment of shells and also that the shells are large groups, containing as many as $\hbar\Omega\tilde{g}\approx A^{2/3}$ individual levels. The symmetry results often in a degeneracy on a smaller scale.

An interesting approach to the appearance of shell oscillations and their relation to the Hartree–Fock and Thomas–Fermi approximations has been initiated by Balian and Bloch (1970). They consider Hartree–Fock quantities smoothed over energy, γ being the smoothing width; and find that the smeared Hartree–Fock quantities resemble those appearing in the Thomas–Fermi approximation, provided γ is large. When, on the other hand, γ is small, oscillations which resemble the shell structure, and which in the classical limit are related to classical periodic orbits, arise. A similar connection between shell structure and classical periodic orbits has also been considered recently by Swiatecki and Myers (1970).

The intrinsic properties of the individual states which belong to the same shell are rather accidental. Thus, when the nuclear shape changes, some of them increase their energy while others decrease it. Therefore, redistribution of shells takes place. The characteristic distortion, at which new shells are formed, can be estimated from the fact that the slopes of the single-particle levels are on the average characterized by the particle-to-surface coupling constant κ of the order of the Fermi energy λ (see, e.g., Bohr and Mottelson, to be published). With the energy distance between the shells given by Eq. (II.3), this amounts to a characteristic increment of the shape variation equal to

$$\Delta\beta\approx\hbar\Omega/\lambda\approx A^{-1/3}, \tag{II.7}$$

i.e., to a deformation of 20%–30%.

So we find that the distribution of the shells is an approximately periodic function of both the number of nucleons and the shape variations with characteristic increments equal to $A^{2/3}$ and $A^{-1/3}$, respectively. This is qualitatively illustrated in Fig. II-2.

Examples of single-particle level densities are shown in Fig. II-3; the energy levels were evaluated using a Woods–Saxon potential for a number of nuclear shapes along the so-called liquid-drop valley, which for larger values of the shape-distortion parameter **c** also includes shapes with a significant neck-in. Both the local level density, $g_{\rm sh}(\mathcal{E})$, obtained by averaging the single-particle spectrum over an energy interval of about 1–2 MeV, and the average level density $\tilde{g}(\mathcal{E})$, obtained by averaging over an interval of about 8 MeV, are shown. Strong fluctuations of the local level density around the average, though most pronounced in the spherical case ($\mathbf{c}=1$), are observed for all deformations. In some special combinations of the energy value and deformation, the shell closures are especially clearly marked.

2. The Energy and Spatial Density Corrections and the Forces Due to Shells

In Fig. II.3, the level densities are shown as functions of the special deformation parameter **c**. In the following, we shall use the shorthand sign β to denote one or more unspecified deformation parameters.

The difference between the two level densities shown in Fig. II-3,

$$\delta g(\mathcal{E},\beta)=g_{\rm sh}(\mathcal{E},\beta)-\tilde{g}(\mathcal{E},\beta), \tag{II.8}$$

gives a convenient measure of the fluctuations in the level density (the shell structure). Thus, a negative value of $\delta g(\mathcal{E},\beta)$ indicates a local density lower than the average. The fluctuations in the level density lead, as we have seen, to variations $\delta U(N,\beta)$ in the total energy. In $\delta U(N,\beta)$, we have replaced the energy variable $\mathcal{E}$ by the nucleon number N, which in fact is taken to be twice the number of levels found below the energy $\mathcal{E}$. Then, $\mathcal{E}$ and N are equivalent variables. We also consider N as the nucleon number in real nuclei; this is possible only insofar as the level distribution does not change considerably in a number of neighbor nuclei. We assume this throughout the paper.

The varying part of the total binding energy of the nucleus δU, due to shell structure, is called the shell-correction energy or simply the energy correction.

As, later on, we shall consider other quantities which are affected by the shell structure, we introduce the following notation. The shell deviations (shell corrections) are denoted by writing δ in front of their symbols: δU, δg, δQ, etc. Here $\sim$ is used to denote the averaged quantities $\tilde{U}$, $\tilde{g}$, $\tilde{Q}$ defined for the renormalization. These quantities, discussed here only qualitatively, are derived and explained in more detail in Sec. IV.

There is a simple qualitative relation between $\delta U(N,\beta)$ and $\delta g(N,\beta)$. Both are approximately periodic functions of the nucleon numbers and the shape variations, and both should have their local minima and maxima at the same places. This feature is observed in the actual calculations; see Fig. II-6 and the more detailed discussion in Sec. IV.

We will show how one calculates the shell-correction energy $\delta U(N,\beta)$. It appears, however, that $\delta U(N,\beta)$ depends on the shell structure only in a relatively narrow energy interval of the order of $\pm$(5–10) MeV around the Fermi energy, while the contributions from more distant single-particle states average out. This is an important feature of the shell-correction approach,

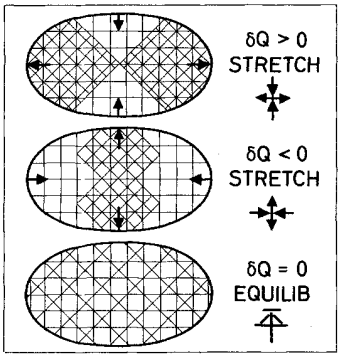

FIG. II-4. Qualitative figure illustrating the relationship between the shell forces (indicated by arrows) and the spatial density fluctuations.

because, at the present time, one can hardly have any confidence in the independent-particle model outside this region. This feature also ensures that the energy correction $\delta U(N,\beta)$ as well as other corrections are reasonably insensitive to changes in the single-particle model used, and can be found in a unique way. This is in marked contrast to the results obtained by summation of the energies of all individual levels; cf. Sec. I.

As will be shown, the ground-state equilibrium shapes are very accurately determined by the position of the minima of $\delta U(N,\beta)$. Furthermore, the value of $\delta U(N,\beta)$, evaluated for the ground-state shape, can be compared to the empirical shell corrections to the nuclear masses.[1] The results (Strutinsky, 1967; Seeger, 1967; Nilsson, Thompson and Tsang, 1969) agree rather well with the empirical data, especially in the deformed nuclei. The mean deviation of the calculated masses is not worse than in the best (and very complicated) phenomenological fits, as can be seen by comparing the theoretical curves in Fig. I-1(b). A more detailed discussion is to be found in Sec. VI, where additional data are presented.

The shell effects in the deformation energy may also be described in terms of restoring or distorting forces due to the shell structure. As the energy correction depends, in particular, on the parameters $\beta_1, \beta_2, \cdots, \beta_n$, specifying the shape of the average nuclear potential, the shell forces restoring—or stretching—the nuclear shape are given simply by the partial derivatives of the shell correction energy

$$\delta\mathcal{F}_{\beta_i} = \partial\delta U(N,\beta_1,\beta_2,\cdots,\beta_n)/\partial\beta_i. \qquad \text{(II.9)}$$

Moreover, the shell forces are closely related to undulations, $\delta\rho(\mathbf{r},\beta)$, in the spatial density as a function of deformation, and such density variations entail naturally fluctuations in the density moments, as, e.g., in the quadrupole moment

$$\delta Q(\beta) = \int d\tau \hat{q}\delta\rho(\mathbf{r},\beta), \qquad \text{(II.10)}$$

due to the shell structure. The quadrupole restoring force $\delta\mathcal{F}_q$ is proportional to δQ, and, in general, analogous relationships are found; see Sec. IV.[2] For the sake of simplicity, we shall in this section only consider the shell correction to the quadrupole moment δQ.

Thus, the four shell corrections, δg, δU, $\delta\mathcal{F}$, and δQ, are intimately connected. In a smoothed density distribution $\delta\rho = 0$ and, in this case, the shell force $\delta\mathcal{F}$ turns to zero. According to Eq. (II.9), this situation corresponds to an extremal value of the energy correction δU, i.e., as far as the nuclear interior is concerned, it should be a stationary state of the nucleus.

The relationship between the force arising from the shell structure and the spatial density fluctuations is illustrated in Fig. II-4, which recalls the original ideas of Rainwater, 1950, and of Bohr and Mottleson (Bohr, 1952; Bohr and Mottelson, 1953) concerning the origin of nuclear equilibrium deformations: the restoring ("alignment") force tends to distort the nucleus in the direction of maximal nucleon density. Note, however, that, in the present context, δQ describes the undulations of the nuclear density related to the nonuniformity of the energy distribution of single-particle states and is generally different from the "quadrupole moment of the extra nucleons" in the unified model (Bohr and Mottelson, 1953).

When the nucleus is deformed, variations of the nucleon spatial density are paralleled with the redistribution of the energy shells. As a result, δQ is an oscillating function of the deformation, in the same way that the other shell corrections are. This is indicated schematically in Fig. II-5.

At deformations where the shell-correction energy

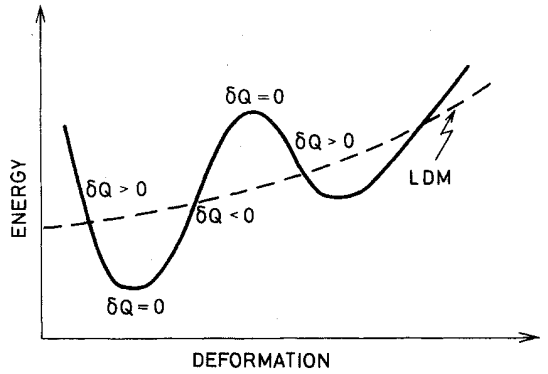

FIG. II-5. Schematic picture illustrating the connection between the total deformation energy and the quadrupole moment δQ. The curve represents the deformation energy (LDM+δU) as a function of deformation, oscillating around the slowly varying LDM part (dashed curve). The qualitative value of δQ is indicated in different regions.

[1] For simplicity, in this section we ignore some less important contributions to energy variations, such as the pairing correlation energy (see Secs. IV–VI).

[2] This is only true in the case of small distortions of a harmonic oscillator potential. Similar results are obtained in all investigated cases.

$\delta U(N,\beta)$ and the level density $\delta g(\mathcal{E},\beta)$ have their local extrema, δQ and, as a result of the nucleon redistribution, the restoring force change their signs there. An example of the results obtained with a realistic shell-model potential is shown in Fig. II-6. The oscillating behavior is a typical feature of all other cases, too. In the instance shown, $Z=82$, the stability of the spherical shape is increased due to a "negative" response ($\delta Q<0$) of the shell distribution to a quadrupole perturbation of the shape. This is also true for other magic nuclei with spherical shapes and some nuclei around them.

The shell forces, represented in our calculations by $\delta\mathfrak{F}$, constitute only one—and a relatively small—part of the generalized forces acting on the nuclear shape. The other component is represented by classical forces present in the liquid-drop model. Then, the total force can be written

$$\mathfrak{F}_{\text{tot}}=\mathfrak{F}_{\text{cl}}+\delta\mathfrak{F}. \qquad \text{(II.11)}$$

This division is enforced in our calculation by the normalization of the uniform energy-distribution terms to the phenomenological LDM energy.

The two main components of $\mathfrak{F}_{\text{cl}}$ are the Coulomb and the surface tension forces, and each of them is, in general, much stronger than the shell force $\delta\mathfrak{F}$. However, $\mathfrak{F}_{\text{cl}}$ is relatively small for shapes not very different from the spherical shape, which is an extremal shape for the LDM energy alone. There, the shell force $\delta\mathfrak{F}$, or equivalently the shell correction energy δU, is the most essential factor in determining the equilibrium shape of the nucleus. Consequently, the condition $\delta\mathfrak{F}=0$ must be fulfilled at the equilibrium. So we see that, for not too large distortions, the ground-state equilibrium shapes are determined by the position of the minima of $\delta U(N,\beta)$.

At larger distortions, the liquid-drop model forces increase and the presence of shells is generally insufficient to form an equilibrium state, even in the regions of very pronounced shell closures. This is not the case, however, in the very heavy nuclei; there one finds a relatively large region of space spanned by the nuclear shape coordinates, where the increase in the surface energy is largely compensated for by the decreasing Coulomb energy—it is the region of the so-called LDM valley. The resulting classical force is weaker and the shell force again plays a significant role. This makes possible the existence of pronounced potential wells in the deformation energies of some very distorted heavy nuclei.

At first sight, a formal estimate of the amplitude of the energy variations related to the shell structure may be obtained as a characteristic energy of the shell, equal, by the order of magnitude, to the intershell spacing $\hbar\Omega$ times the number of states in the shell

$$U_{\text{shell}}\approx\hbar\Omega A^{2/3}\approx 200\text{–}300\ \text{MeV}. \qquad \text{(II.12)}$$

This quantity should also be related to the spatial

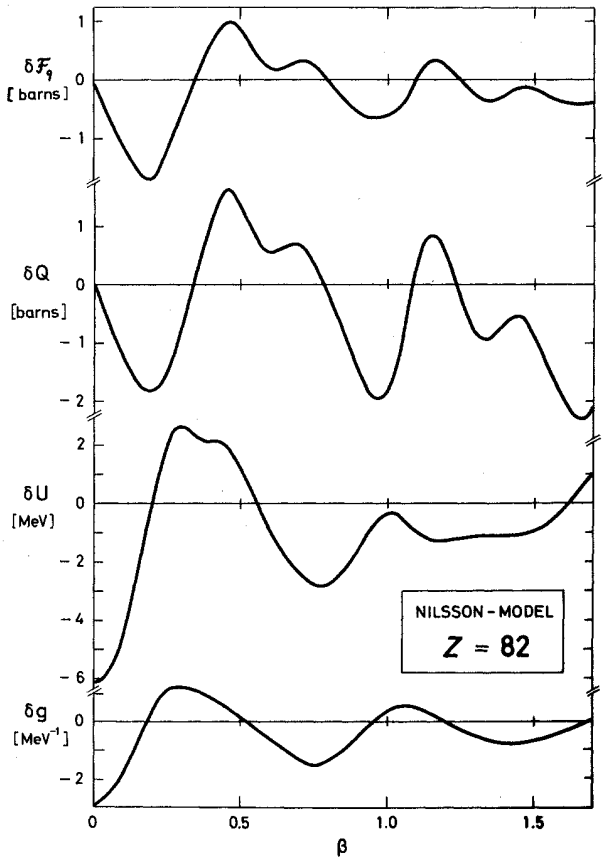

FIG. II-6. The quadrupole shell force $\delta\mathfrak{F}_q$, the quadrupole moment δQ of the spatial density nonuniformity, the energy correction δU, and the level density variation δg as functions of the quadrupole deformation β of the Nilsson potential, calculated for $Z=82$ protons. The deformation parameter β used here is defined by $\beta=d-1$, where d is the ratio of the oscillator frequencies, $d=\omega_\perp/\omega_z$. For small deformations, $\beta\approx\delta+\frac{2}{3}\delta^2+\cdots$ with δ as used in Mottelson and Nilsson, 1959.

density fluctuations by the relationship

$$U_{\text{shell}}\approx\int V(\mathbf{r})\delta\rho(\mathbf{r})\,d\tau, \qquad \text{(II.13)}$$

where V is the average nuclear potential of the order of λ. The two quantities are the same if the average magnitude of $\delta\rho$ in Eq. (II.13) is of the order of $A^{-2/3}$ relative to the total density $\rho(\mathbf{r})$

$$\delta\rho/\rho\approx A^{-2/3}. \qquad \text{(II.14)}$$

The estimate (II.14) agrees with the expected fluctuation of the nucleon density in a shell, as this fluctuation is proportional to the square root of the number of individual uncorrelated states in the shell adjacent to the Fermi energy,

$$\delta\rho/\rho\approx(A^{2/3})^{1/2}/A=A^{-2/3}.$$

Stronger fluctuations are expected if some of the states have identical density distributions, as e.g., in the case

of spherical degeneracy [though, even in this case, the amplitude of the variations of the shell-model density does not seem to differ much from the estimate (II.14)].

However, the energy corrections δU found in actual calculations are an order of magnitude smaller than the quantity (II.12). Apparently, this is so because the considerations leading to both (II.12) and (II.13) ignore essential factors: Eq. (II.12) disregards completely the spread of the energy shell, while using (II.14), the oscillating character of δp has not been considered.

A much better estimate can be given by making use of Eq. (IV.38). There it is shown that the shell correction $\Delta(\delta U)$, produced by a small change ΔV of the average nuclear potential, equals

$$\Delta(\delta U)=\int(\Delta V)\delta\rho d\tau. \tag{II.15}$$

In this equation we substitute, instead of ΔV, the change of the potential produced by increasing the number of particles in the nucleus by an amount equal to one-half of the number of states in the shell, $\Delta N=\frac{1}{2}A^{2/3}$. The most important effect in V due to the increase in particle number is the corresponding increase in the nuclear radius

$$\Delta R\approx\Delta(r_0A^{1/3})=\tfrac{1}{6}r_0. \tag{II.16}$$

The depth of the potential remains approximately constant equal to λ. Using $\delta\rho\approx A^{-2/3}\rho$, we then find the following estimate for the variation of δU from magic to mid-shell nucleus

$$\Delta(\delta U)\approx\lambda\delta\rho\Delta v\approx\tfrac{1}{2}\lambda\approx 20\text{ MeV}. \tag{II.17}$$

Here Δv is the variation in the volume of the potential

$$\Delta v=\tfrac{1}{2}v_0A^{-1/3},$$

where v_0 is the nuclear volume. The quantity (II.17) agrees better with the numerical results concerning the variation of the energy correction in spherical nuclei. In deformed nuclei, the amplitude of δU is two or three times less.

The relative magnitude of the shell-correction quantities is very small, indeed. While the total binding energy in nuclei is of the order of a few GeV, the shell-correction energy amounts only to 5–10 MeV.

With respect to the magnitude of the shell part of the quadrupole moment δQ, it is only 1–2 b or less, whereas the typical quadrupole moment Q of a deformed nucleus is of the order of 10 b. The relative smallness of the shell corrections was probably one of the reasons why the rather regular shell structure in deformed nuclei remained unnoticed until recently; it was difficult to observe these small variations on the background of a much larger and poorly determined quantity. These variations were undoubtedly present in all single-particle calculations of the total single-particle energy and of the quadrupole moment (cf., e.g., Fig. 5 in Bès and Szymánski, 1961; Gustafson *et al.*, 1966).

III. VARIATION IN ENERGY AND ITS CONNECTION TO HARTREE–FOCK THEORY

The equations of the shell-correction method may be obtained by starting from the Hartree–Fock (HF) expression for the total energy. The subsequent steps to be taken can be summarized as follows:

One assumes that there exists some smooth, generally nonlocal, but not necessarily self-consistent average field, which is close to the HF field. Such a field may be identified with the shell-model potential. In other words, the shell model is defined as a model in which the potential is constructed without regard to the shells.

The self-consistent quantities in the HF equation are substituted for by the solutions of the shell model. In the expression for the total energy, this gives only an error of second order in the difference between the HF and the shell-model field.

In the expression obtained in this way for the total binding energy, the shell-structure effects are contained only in the sum of the shell-model single-particle energies. A smooth part of this sum is extracted and taken together with the already smooth potential energy term. The sum of these two terms is considered as representing a "smooth" part of the total energy, which may be considered an analog to the liquid-drop energy. The result is further simplified and improved by replacing the smooth part by the phenomenological expression of the liquid-drop model (LDM) for the energy of the nucleus. The remaining part of the sum of single-particle energies (after extraction) constitutes what we call the shell-correction energy of the nucleus. This quantity can be evaluated for any given shell-model field. Added to the LDM energy, it gives an approximate expression for the total nuclear energy.

The pair correlation energy is added to the final expression.

1. The Shell Model as an Alternative to the Self-Consistent Theory

In a first step, we show that one makes only a relatively small error in the total energy by replacing the self-consistent single-particle energies and wave functions by the analogous quantities of the not self-consistent shell model.

The single-particle density matrix

$$\rho(\mathbf{r},\mathbf{r}')=2\sum_\nu n_\nu\varphi_\nu^+(\mathbf{r})\varphi_\nu(\mathbf{r}') \tag{III.1}$$

plays a fundamental role in HF theory. In this equation n_ν is the occupation number (either 0 or 1), and $\varphi_\nu(\mathbf{r})$

is the solution of a Schrödinger equation

$$[-(\hbar^2/2m)\Delta+V]\varphi_\nu=\varepsilon_\nu\varphi_\nu. \quad \text{(III.2)}$$

The self-consistent single-particle potential V is built up by the density matrix ρ and the effective nucleon interaction G

$$V(\mathbf{r})=\int d\tau'\rho(\mathbf{r}',\mathbf{r}')G(\mathbf{r},\mathbf{r}')+\text{ exchange terms.} \quad \text{(III.3)}$$

In addition to the density matrix ρ, one can define a quantity $\tilde{\rho}(\mathbf{r},\mathbf{r}')$ which is ρ properly averaged over a number of nuclei or an equivalent average over a sufficient number of states in the same nucleus. A characteristic feature of the nuclear shell structure is an approximately periodic variation with the nucleon numbers with a period $\Delta A\approx A^{2/3}$. Thus, the interval over which the average should be taken must at least contain that many nuclei. This corresponds to an interval $\hbar\Omega$ in the single-particle energy spectrum. Quantities averaged in this way represent the smooth behavior of the original quantities and this can also be assumed for $\tilde{\rho}(\mathbf{r},\mathbf{r}')$.

In analogy to Eq. (III.3) we can use $\tilde{\rho}$ to define a smooth single-particle potential $\tilde{V}(\mathbf{r})$,

$$\tilde{V}(\mathbf{r})=\int d\tau'\tilde{\rho}(\mathbf{r}',\mathbf{r}')G(\mathbf{r},\mathbf{r}')+\text{ exchange terms.} \quad \text{(III.4)}$$

Apparently, $\tilde{\rho}$ is not related to $\tilde{V}$ in the same way as ρ is to V, since the latter two are connected by the self-consistent HF equation. The average or smooth quantities $\tilde{\rho}$ and $\tilde{V}$ are not self-consistent and do not correspond to any real physical system. We may assume, however, that apart from some relatively small deviations due to the shell structure in specific nuclei, these quantities are close to those in real nuclei. As $\tilde{V}$ by the definition varies smoothly from one nucleus to another, it may be close to a "good" shell-model field. From the solutions of the shell-model Schrödinger equation

$$[-(\hbar^2/2m)\Delta+\tilde{V}]\varphi_\nu{}^S=\varepsilon_\nu{}^S\varphi_\nu{}^S, \quad \text{(III.5)}$$

we can form the shell-model density matrix ρ^S

$$\rho^S(\mathbf{r},\mathbf{r}')=2\sum_\nu n_\nu\varphi_\nu{}^S(\mathbf{r})^+\varphi_\nu{}^S(\mathbf{r}'). \quad \text{(III.6)}$$

The three densities ρ, $\tilde{\rho}$, and ρ^S differ from each other, but differences between them are of the same order of magnitude, and are all linear in

$$\delta V=V-\tilde{V}\propto\delta\rho, \quad \text{(III.7)}$$

with

$$\delta\rho=\rho-\tilde{\rho}. \quad \text{(III.8)}$$

Considering δV as small, one finds in first-order perturbation for the density

$$\rho=\rho^S+\rho'+O[(\delta\rho)^2] \quad \text{(III.9)}$$

with

$$\rho'(\mathbf{r},\mathbf{r}')=2\sum_{\nu\neq\mu}[(n_\nu-n_\mu)/(\varepsilon_\nu-\varepsilon_\mu)]\langle\nu\mid\delta V\mid\mu\rangle\times\varphi_\nu{}^+(\mathbf{r})\varphi_\nu(\mathbf{r}'), \quad \text{(III.10)}$$

where the neglected terms are of second order in $\delta\rho$. Correspondingly, one finds for the self-consistent single-particle energies

$$\varepsilon_\nu=\varepsilon_\nu{}^S+\langle\nu\mid\delta V\mid\nu\rangle+\sum_{\mu\neq\nu}|\langle\nu\mid\delta V\mid\mu\rangle|^2/(\varepsilon_\nu-\varepsilon_\mu). \quad \text{(III.11)}$$

In the matrix elements of Eq. (III.11) and Eq. (III.10), the index ^{S} has been dropped for the shell-model wave functions $\varphi_\nu{}^S$. The fluctuation $\delta\rho$ of the self-consistent density ρ can be related in a simple way to the analogous quantity of the shell model, i.e. to

$$\delta\rho^S=\rho^S-\tilde{\rho}^S. \quad \text{(III.12)}$$

Noting that the average value of δV is zero, one obtains up to second order in $\delta\rho$

$$\tilde{\rho}=\tilde{\rho}^S+O[(\delta\rho)^2]. \quad \text{(III.13)}$$

From Eq. (III.9) it follows that

$$\delta\rho=\delta\rho^S+\rho'+O[(\delta\rho)^2]. \quad \text{(III.14)}$$

If we express δV in Eq. (III.10) in terms of $\delta\rho$ by means of Eqs. (III.3) and (III.4), we obtain

$$\delta\rho=\delta\rho^S+2\sum_{\mu\neq\nu}(n_\nu-n_\mu)/(\varepsilon_\nu-\varepsilon_\mu)\varphi_\nu{}^+(\mathbf{r})\varphi_\mu(\mathbf{r}')\times\sum_{\alpha,\beta}\langle\nu\alpha\mid G(1-\mathcal{P})\mid\beta\mu\rangle\langle\alpha\mid\delta\rho\mid\beta\rangle. \quad \text{(III.15)}$$

Here we have used the exchange operator $\mathcal{P}$ and the notation

$$\langle\nu_1\nu_2\mid G\mid\nu_3\nu_4\rangle=\int d\tau\int d\tau' G(\mathbf{r},\mathbf{r}')\varphi_{\nu_2}{}^+(\mathbf{r}')\times\varphi_{\nu_1}{}^+(\mathbf{r})\varphi_{\nu_3}(\mathbf{r})\varphi_{\nu_4}(\mathbf{r}'). \quad \text{(III.16)}$$

In a symbolic form, Eq. (III.15) can be written as

$$\delta\rho=\delta\rho^S+\mathfrak{A}G\delta\rho. \quad \text{(III.17)}$$

The matrix elements of $\mathfrak{A}$ are

$$\langle\nu\mid\mathfrak{A}\mid\mu\rangle=2(n_\nu-n_\mu)/(\varepsilon_\nu-\varepsilon_\mu);\qquad\langle\nu\mid\mathfrak{A}\mid\nu\rangle=0. \quad \text{(III.18)}$$

By means of Eq. (III.17), $\delta\rho$ can be expressed directly in terms of $\delta\rho^S$ and the so-called scattering amplitude Γ. The latter satisfies the equation

$$\langle\nu'\mu'\mid\Gamma\mid\nu\mu\rangle=\langle\nu'\mu'\mid G(1-\mathcal{P})\mid\nu\mu\rangle+2\sum_{\alpha\neq\alpha'}\langle\nu'\alpha'\mid G(1-\mathcal{P})\mid\nu\alpha\rangle\times(n_\alpha-n_{\alpha'})/(\varepsilon_\alpha-\varepsilon_{\alpha'})\langle\mu'\alpha'\mid\Gamma\mid\mu\alpha\rangle \quad \text{(III.19)}$$

or

$$\Gamma=G+G\mathfrak{A}\Gamma. \quad \text{(III.20)}$$

Thus one obtains

$$\delta\rho=(1+\mathfrak{A}\Gamma)\delta\rho^S. \quad \text{(III.21)}$$

The virtue of this equation lies in the fact that the

fluctuation $\delta\rho$ of the self-consistent density ρ is expressed in terms of the nonself-consistent quantity $\delta\rho^S$, which can be easily found.

Otherwise any attempt to evaluate $\delta\rho$ would require that one solve the full self-consistent problem.

Using the above formalism, the HF energy of the system

$$E_{\mathrm{HF}}=2\sum_{\nu}\varepsilon_\nu n_\nu-\tfrac{1}{2}\,\mathrm{tr}\,[\rho G(1-\mathcal{P})\rho] \quad \text{(III.22)}$$

can be transformed in such a way that only shell-model quantities appear. The new approximate expression for the energy is

$$E_{\mathrm{HF}}=2\sum_{\nu}\varepsilon_\nu^S n_\nu-\tfrac{1}{2}\,\mathrm{tr}\,[\tilde{\rho}G(1-\mathcal{P})\tilde{\rho}]+\delta_2E[(\delta\rho)^2]+O[(\delta\rho)^3], \quad \text{(III.23)}$$

where the second-order term is given by

$$\delta_2E[(\delta\rho)^2]=\tfrac{1}{2}\int d\tau\int d\tau'\delta\rho^S(\mathbf{r},\mathbf{r})G(\mathbf{r},\mathbf{r}')\delta\rho(\mathbf{r}',\mathbf{r}'), \quad \text{(III.24)}$$

which can be expressed in terms of $\delta\rho^S$ alone.

From Eqs. (III.20) and (III.21) we find

$$\delta_2E[(\delta\rho)^2]=\tfrac{1}{2}\int d\tau\int d\tau'\delta\rho^S(\mathbf{r},\mathbf{r})\Gamma(\mathbf{r},\mathbf{r}')\delta\rho^S(\mathbf{r}',\mathbf{r}'). \quad \text{(III.25)}$$

It is important to note that in Eq. (III.23) all terms linear in $\delta\rho$ cancel identically. The neglected terms are of third order in an expansion in which $\delta\rho/\rho$ plays the role of a small parameter.

The arguments presented in this section only reflect the familiar feature of the HF energy, that it is stationary with respect to small variations of the single-particle density matrix. The aim of presenting them here is to show how this feature can be used in the discussion of the accuracy and meaning of the shell model and its connection to the self-consistent calculations.

The smooth potentials used in shell-model calculations may be interpreted as the result of a two-step averaging procedure. The self-consistent field for a definite state in a definite nucleus is a quantum-mechanical average quantity which, when averaged over many nuclear states, in a number of nuclei leads to the shell-model average field which in this sense is rather a statistical average quantity.

If, therefore, the self-consistent quantities were known for many nuclear states in a large number of nuclei, the best shell-model field could be found simply by means of a least-deviation fit of a proper phenomenological expression containing a number of free parameters. However, one hardly needs to do so because the shell model is fitted directly to experimentally known features of nuclei and, at present, one may have more confidence in the shell-model average field and the LDM than in the available HF solutions.

2. The Renormalization of a Smooth Part of the Energy

Technically, Eq. (III.23) is simpler than the original HF equation (III.22), which contains self-consistent quantities, but even this simpler form can hardly be used in practice and, of course, it has all the ambiguity of the original HF expression as an independent-particle model approximation for a strongly bound system.

However, Eq. (III.23) forms a good basis for a renormalization procedure, in which a phenomenological liquid-drop model expression is used to replace the smoothly behaving part of the energy (III.23).

It has been proved by many authors that the quasiclassical Thomas–Fermi type approximation ("statistical model") is equivalent to a phenomenological droplet model (see, e.g., Myers, 1968; Myers and Swiatecki, 1969). In particular, the condition of equilibrium density distribution of the statistical model in a deformed nucleus is equivalent to the familiar equation of equilibrium of the nuclear surface considered in the liquid-drop model (Strutinsky and Tyapin, 1963).

The liquid-drop model is in fact even more general, because its phenomenological terms may contain any contributions of the same functional type, not necessarily only those which appear in the Thomas–Fermi approximation (Bethe, 1968; Siemens, 1970). Therefore, one probably does not make things worse by replacing the smooth part of Eq. (III.23) by a phenomenological LDM. The essential assumption is that the LDM, being a classical model, is characterized by smoothly behaving terms, such as e.g. the volume and the surface energies. It may also contain any other correction terms which have this feature.

These quasiclassical approximations naturally ignore completely any kind of shell-structure effects, which appear as relatively small variations (of the order of a few percent) around the average in both the sum of the single-particle energies and the potential energy term[3] in Eq. (III.22).

The shell effects are also present in the approximate shell-model expression (III.23) for the total energy, but the latter equation is different in one important respect: The shell structure appears there mainly in the first relatively simple term, while the second term, representing the average shell-model potential energy, is already a smooth quantity.

These considerations may clarify some arguments concerning calculations of the nuclear deformation energy in which the latter was identified with the variation of the sum of shell-model single-particle energies only (Mottelson and Nilsson, 1959; Bès and

[3] The shell fluctuations of the total quadrupole moment of the nucleus, discussed in Sec. IV, constitute an example of shell effects in a quantity of the same type as the potential energy integrals in Eq. (III.22).

Szymánski, 1961). Equally strong shell-structure effects in the self-consistent potential energy term were, presumably, ignored.[3]

Equation (III.23) shows, however, that within an accuracy of $(\delta\rho)^2$, only a smooth component, containing no shell structure, was missing in such calculations. This means that at least some of the shell-structure effects could indeed be reproduced in this way provided that the variation of the omitted smooth term was small. This requirement is not easily dealt with and has not always been fulfilled for larger quadrupole or more complicated distortions of the nuclear shape.

The criticism would be completely justified, however, based on the original Eq. (III.22), where the self-consistent quantities appear.

Although the difference between the shell model and the self-consistent solutions is expected to be small, it appears as a significant factor, when sums over many nuclear states are considered.

The microscopic theory is now left with the much simpler task of evaluating that part of the total binding energy which fluctuates due to shell structure. The main contribution to the latter comes from linear terms in $\delta\rho$, which in Eq. (III.23)—but not in Eq. (III.22)—is contained in the relatively simple sum of U of the single-particle energies. This shell structure part of the energy can be obtained by subtracting from U the smooth quantity

$$\tilde{U}=2\int_{-\infty}^{\tilde{\lambda}}\varepsilon\tilde{g}(\varepsilon)\,d\varepsilon, \tag{III.26}$$

where $\tilde{g}(\varepsilon)$ is the mean density of single-particle levels at the energy ε, which is obtained by averaging the shell-model level density

$$g_0(\varepsilon)=\sum_\nu \delta(\varepsilon-\varepsilon_\nu{}^S) \tag{III.27}$$

over a finite energy interval $\tilde{\gamma}$ around the Fermi energy λ, where

$$\tilde{\gamma}\approx\hbar\Omega\approx\lambda A^{-1/3}. \tag{III.28}$$

Thus we define

$$\begin{aligned}\tilde{g}(\varepsilon)&=\tilde{\gamma}^{-1}\int_{-\infty}^{\infty}\xi\left(\frac{\varepsilon-\varepsilon'}{\tilde{\gamma}}\right)g_0(\varepsilon')\,d\varepsilon'\\&=\tilde{\gamma}^{-1}\sum_\nu\xi[(\varepsilon-\varepsilon_\nu{}^S)/\tilde{\gamma}].\end{aligned} \tag{III.29}$$

The smoothing function $\xi(x)$ can (but must not necessarily) be defined by (see Sec. IV.1)

$$\xi(x)=(\pi)^{-1/2}\exp(-x^2)\sum_{k=0,2}^{2m}a_kH_k(x), \tag{III.30}$$

with $H_k(x)$ being the Hermite polynomials. The coefficients are then given by the recurrence relation

$$a_k=-(1/2k)\,a_{k-2}$$

for $k>2$ and $a_0=1$.

The first-order energy correction is then[4]

$$\delta U\equiv\delta_1E=U-\tilde{U}=2\sum_\nu\varepsilon_\nu{}^Sn_\nu-2\int_{-\infty}^{\tilde{\lambda}}\tilde{g}(\varepsilon)\varepsilon\,d\varepsilon. \tag{III.31}$$

In this equation $\tilde{\lambda}$ is the Fermi energy corresponding to $\tilde{g}$, and is determined from the condition of number conservation

$$N=2\int_{-\infty}^{\tilde{\lambda}}\tilde{g}(\varepsilon)\,d\varepsilon. \tag{III.32}$$

The next step is to replace Eq. (III.23) by

$$E_{\rm HF}=\tilde{E}+\delta E, \tag{III.33}$$

where the fluctuating part of the energy, δE, is the sum of the first-order shell correction δ_1E—given by Eq. (III.31)—and the second-order shell correction δ_2E—given by Eq. (III.25)—i.e.,

$$\delta E=\delta_1E+\delta_2E. \tag{III.34}$$

The quantity $\tilde{E}$ is the smooth part of the energy in Eq. (III.23),

$$\tilde{E}=\tilde{U}-\tfrac{1}{2}\,\mathrm{tr}\,\tilde{\rho}G\tilde{\rho}, \tag{III.35}$$

and it is now replaced by the liquid-drop energy $E_{\rm LDM}$. Then the final expression for the energy becomes

$$E_{\rm HF}=E_{\rm LDM}+\delta E. \tag{III.36}$$

The smooth energy $\tilde{E}$ does not literally correspond to a phenomenological mass equation fitted to the ground-state masses. One should rather make a new fit of the LDM and shell-model parameters, in which the evaluated shell corrections δE to the ground-state masses are taken into account. A calculation of this kind has recently been performed by Seeger (1967). Without doing such a fit, the use of Eq. (III.36) may result in smoothly varying and relatively small deviations, which at the present stage are insignificant.

It will be shown in Sec. IV that the contribution to the energy shell correction [Eq. (III.31)] comes only from a relatively narrow region of the order of 10–15 MeV around the Fermi energy. All more distant states can be ignored in the evaluation of the difference of the two energies Eq. (III.31).

This is important for the applicability of the renormalization expressed by Eq. (III.36), because the use of approximately independent quasiparticles with relatively small residual correlations, as in the Fermi liquid model, can be justified only for this narrow region. Also in this respect, the shell-correction approach differs in principle from the traditional approach to the problem of nuclear deformations, in

[4] In Sec. IV we will discuss another important form of δ_1E, making use of an occupation number representation.

which the total sum of single-particle energies is considered to represent the nuclear deformation energy.

As to the LDM part, there is little doubt that at present it is an accurate and reliable model for describing the average properties of the nuclear masses and deformation energies. Thus, we find Eq. (III.36) as an approximation for the total energy of the nucleus. The accuracy expected of this expression should be significantly better than that of the LDM alone, i.e., it should on the average be of the order of at least a few hundred keV. Comparison of the results with a number of empirical data seems to demonstrate that such an accuracy is indeed achieved.

The shell-correction approach should be compared with attempts to evaluate the total mass of the nucleus starting from "first principles" and a "good" nucleon–nucleon interaction (e.g., Negele, 1970). There, far less accuracy has been reached at present, and attempts to raise the level of accuracy involve many model-dependent assumptions and some phenomenological relations concerning, e.g., the density dependence of the nuclear forces.

An approach from the other end, namely, from a many-body theory, in which one tries to describe only small changes in the system without evaluating the total quantities, seems more justified for heavy nuclei. The shell-correction approach is an approximation of the latter type.

A foundation of the shell-correction method can also be given on the basis of the Fermi-liquid theory (Bunatyan, Kolomietz, and Strutinsky, 1972). The result is formally the same as obtained above by means of the Hartree–Fock theory. The difference is that the single-particle energies are to be interpreted as quasiparticle excitations in the vicinity of the Fermi energy. The amplitude Γ in Eq. (III.25) is replaced by Migdal's quasiparticle amplitude found from an equation analogous to Eq. (III.19), in which the nucleon interaction G is replaced by the universal amplitude Γ^{ω} (Migdal, 1968).

The energy shell correction, determined as the energy difference between the self-consistent energy of the nucleus and the energy related to a smooth statistical-model approximation, is a quantity of the first order in the difference between the real density matrix and an average density distribution. A formal estimate of the energy correction was presented in the previous section. This should be compared to inaccuracies originating from the $(\delta\rho)^2$ terms in Eq. (III.25).

An estimate of the $(\delta\rho)^2$ terms may be obtained from Eq. (III.4) using the fact that the average potential is by order of magnitude equal to the Fermi energy λ. From this we find that the neglected terms are of the order of

$$\lambda A(\delta\rho/\rho)^2. \tag{III.37}$$

With $(\delta\rho/\rho)\sim A^{-2/3}$, this gives an inaccuracy of the order of $\lambda A^{-1/3}$, i.e., a quantity formally $A^{1/3}$ smaller than the leading-order term. There are reasons to believe, however, that Eq. (III.37) gives much too large an estimate.

A somewhat better quantitative estimate of the second-order term can be obtained if we neglect the difference between $\delta\rho^S$ and $\delta\rho$ in Eq. (III.24). With $\delta\rho^S$ defined as in Sec. IV of this paper and the use of a δ force approximation for the nucleon interaction, one gets

$$\delta_2 E\approx(\delta_2 E)_0\approx V_0(4\pi/3)r_0\int d\tau[\delta\rho^S(\mathbf{r})]^2. \tag{III.38}$$

With $V_0\approx$40–50 MeV, this quantity may amount to a few MeV and is thus essentially smaller than the leading shell correction term of the order of 10 MeV (Kolomietz *et al.*, 1971). Again, we have however only an upper-limit estimate, since Eqs. (III.24) and (III.25) have integrands which are oscillating functions. Calculations of $\delta_2 E$ using the amplitude Γ of Migdal's theory (Bunatyan *et al.*, 1972) result in fractions of MeV for $\delta_2 E$. The variation with the nucleon numbers exposes even less fluctuation. The appreciable difference of these results from the estimate (III.38) suggests not only that the amplitude of the effective interaction V_0 has been overestimated, but also that the difference between $\delta\rho$ and $\delta\rho^S$ is significant. One may slso say, that the range of the effective nucleon correlation Γ in Eq. (III.25) is of the same order of magnitude as the period of the spatial oscillations of $\delta\rho^S$ due to the shell structure.

These results lead to the conclusion that the particle–hole interaction, represented by $\delta_2 E$, is only of secondary importance. We shall therefore neglect this term throughout the paper. More essential are the nucleon pairing interaction and some uncertainties related to the evaluation of the first-order term. These will be discussed in detail later in this paper.

3. The Average Field and the Shape of the Nucleus

No detailed assumptions have thus far been made for the average field $\tilde{V}$. It may be local or nonlocal, spherical or deformed. It should only be consistent with the LDM term in (III.36). We shall, as argued above, identify ε_ν^S, φ_ν^S, and $\tilde{V}$, with the corresponding quantities of a phenomenological shell model. Fortunately, the evaluated shell corrections are rather insensitive to details of the average field.

The consistency of the shell model with the LDM is not a very severe condition. It essentially requires an approximate equality between the shape and the volume of the shell-model potential, and the shape and the volume used in the LDM expression. In our calculations, the shape of the nucleus is defined in a transparent classical-like manner as that of the effective surface of the nucleon distribution by the largest density gradient condition. The shell-model potential may now be

defined in terms of this nuclear surface (Damgaard *et al.*, 1969). The above requirement is then easily fulfilled by using the same nuclear surface in both the LDM and the shell-model term (see also Sec. VII).

The definition of the nuclear shape in terms of the nuclear surface ensures also the consistency with the shell-model density distribution in an average field defined in this way. In another description of the nuclear form, e.g., by prescribing the value of the quadrupole moment, the same is achieved by making use of the Lagrange multiplier method in which the very notion of the nuclear surface and its shape is lost. Moreover, such a description is more complicated.

The definition in terms of the shape of the nuclear surface makes it possible to distinguish the concept of nuclear surface distortions from static or dynamic variations of the nucleon distribution within the nuclear volume. Examples of the latter are the static undulations of the mean nucleon density due to the shell structure, and some nucleon quadrupole vibrations analogous to the density vibrations in a macroscopic body. These quantities are not so easily obtained, if e.g., the total quadrupole moment is used to determine the shape of the nucleus. The relatively small but undoubtedly important contribution from the shell structure will be completely lost in the total quantity where the main contribution comes from the common distortion of all the nucleon wave functions.

On the basis of this discussion, another important conclusion can be drawn, namely that, with the nuclear surface so defined, one may consider the parameters that appear in its definition as adiabatic collective variables of the shape distortion without subsidiary conditions. This possibility is exploited in Sec. IX, which deals with the effective inertia of nuclear shape variations.

4. The Smoothed Level Density

The definition of the smooth level density $\tilde{g}$ does not follow uniquely from the arguments presented above. One could, in fact, define an infinite number of smoothly behaving level density functions representing the same discrete distribution of single-particle energies. For further specification of this important quantity, we use the following qualitative arguments. The renormalization to the phenomenological LDM energy in Eq. (III.36) has a meaning only if the energy correction δE, defined by Eq. (III.34), does not contain any smooth terms analogous to those already present in the LDM part; the phenomenological LDM terms in the total energy should account for all contributions of a given type. However, the sum of single-particle energies is known to contain a certain contribution proportional to the area of the surface region where the nucleon density gradient is the largest. This feature is most easily seen in the Thomas–Fermi approximation where it appears in higher-order terms in the quasiclassical expansion (Kirzhnits, 1967). It has also been proved in a very general way by Bloch and Balian (1969) in their recent calculations on the level density of the independent-particle model.

Therefore, the shape dependence of the uniform energy integral $\tilde{U}$ (III.26) should be the same as that of the total single-particle energy in order not to have the surface energy component in the shell correction. To achieve this, the level density $\tilde{g}(\varepsilon)$ which formally corresponds to a quasiclassical level density where the quantum numbers are treated as continuous variables, must contain the higher-order corrections in the expansion in the Planck constant h. Unfortunately, such a level density can be found practically only in a few simple cases, far from any physically reasonable shell-model potentials.

One might then attempt to use a simple definition of $\tilde{g}$ and to take the "surface energy" into account by a separate calculation. However, it is not easy to evaluate this term with any reasonable accuracy even in the relatively simple case of Thomas–Fermi theory (Siemens, 1970).

A simple practical solution of this problem is to average the discrete single-particle spectrum, obtained for the chosen field $\tilde{V}$, over an energy interval $\lambda \pm \tilde{\gamma}$ around the Fermi energy λ, with $\tilde{\gamma}$ of the order of $\lambda/A^{1/3} \approx (5\text{–}15)$ MeV as described above (Sec. III.2) and in more detail in Sec. IV.

Such a procedure requires, of course, the knowledge of the single-particle spectral distribution around the Fermi energy. This can be found in the usual way by solving the independent-particle model problem for a given shell-model field $\tilde{V}$, spherical or deformed. Moreover, the use of the same spectrum in both terms of Eq. (III.31) automatically ensures numerical consistency between the two large terms, which is important as the difference is relatively small. Otherwise, even a very small error in these terms would lead to completely erroneous results for the energy correction δU.

An indication that the uniform energy $\tilde{U}$ indeed contains a "surface energy" part has been found in actual calculations. In cases of a "good" volume conservation, it varies approximately proportional to the area of the nuclear surface; see also Strutinsky (1968).

It is interesting that the single-particle "surface tension" constant found in this way often exceeds the empirical LDM value which should include all contributions. But it may also become negative, as is found, for example, for protons in the Woods–Saxon potential to which the Coulomb potential is added, probably because the sum of the single-particle energies contains a doubled magnitude of the average Coulomb potential energy decreasing in the deformed nucleus.

All this is, however, insignificant for our calculations, in which all kinds of the surface energy contributions, realistic or not, are replaced by the phenomenological

LDM term. Neither is it necessary that U and $\tilde{U}$ behave in a physically reasonable manner as a function of the nuclear shape or volume. In fact, these features are not so easily achieved for a reasonable shell-model potential, for which no volume conservation condition can even be formulated with the required accuracy. This does not affect the shell corrections which are proved to be much less sensitive to the volume conservation condition. For them, the approximate volume conservation, formulated above, is completely sufficient.

IV. THE SHELL CORRECTIONS

In this section, we first define some of the main quantities used in the shell-correction method and derive an approximate formula for the energy correction δU. An occupation number representation is introduced and the quantities of the shell-correction method are given in this representation. Then we discuss the influence of small variations in the average field and the connection between spatial density fluctuations and the shell forces. Finally, the origin of the contributions to the shell-corrections is discussed.

1. Quantitative Description of Level Densities

To account for the average properties of a single-particle spectrum, we introduce, as outlined in the preceding section, a smooth function $\tilde{g}(\mathcal{E},\beta)$. By β we denote, as a shorthand notation, a set of one or more parameters β_1, β_2, $\cdots$, β_i, $\cdots$, used to characterize nuclear deformations. In order to define the function $\tilde{g}$, we introduce the auxiliary function

$$\tilde{G}(\mathcal{E},\beta)=(\pi^{1/2}\tilde{\gamma})^{-1}\sum_{\nu}\exp\left(-\{[\mathcal{E}-\mathcal{E}_\nu(\beta)]/\tilde{\gamma}\}^2\right). \tag{IV.1}$$

In this section, we shall for convenience leave out the superscript "S" used in Sec. III to distinguish shell-model quantities such as $\mathcal{E}_\nu^S$ and φ_ν^S from the corresponding self-consistent quantities.

The averaging interval $\tilde{\gamma}$ in Eq. (IV.1) is chosen to be of the order

$$\tilde{\gamma}\approx\hbar\omega_0\approx 7\text{–}10\ \text{MeV}, \tag{IV.2}$$

i.e., we represent the intershell distance (denoted $\hbar\Omega$ in Secs. II and III) by $\hbar\omega_0\approx 41/A^{1/3}$, the shell spacing of a harmonic oscillator spectrum.

Thus, the function $\tilde{G}(\mathcal{E},\beta)$ [Eq. (IV.1)], is obtained by smearing out the single-particle energies $\mathcal{E}_\nu$ over an energy range of the order $\hbar\omega_0$. It is therefore a smooth function of the energy and does not reflect the existence of shells in the spectrum $\mathcal{E}_\nu$.

Care should be taken that the local value of the level density is reproduced when the procedure (IV.1) is applied to a uniform level distribution. This is achieved by introducing a curvature correction (Strutinsky, 1968), which contains higher derivatives of the sum defined by Eq. (IV.1). Thus, we define the uniform level density as

$$\tilde{g}(\mathcal{E},\beta)=\tilde{G}-\tfrac{1}{4}\tilde{\gamma}^2(\partial^2\tilde{G}/\partial\mathcal{E}^2)+\tfrac{1}{32}\tilde{\gamma}^4(\partial^4\tilde{G}/\partial\mathcal{E}^4)\\ -\cdots+a_{2m}\tilde{\gamma}^{2m}(\partial^{2m}\tilde{G}/\partial\mathcal{E}^{2m}), \tag{IV.3}$$

which is identical to Eq. (III.29). From this form, however, it is possible to estimate the order of magnitude of the curvature corrections. Qualitatively, Eq. (IV.3) corresponds to an expansion of $\tilde{g}(\lambda,\beta)$ in powers of the small quantity $\tilde{\gamma}/\lambda\approx A^{-1/3}$:

$$\tilde{g}(\lambda,\beta)\approx\tilde{G}(\lambda,\beta)[1+c_2(\tilde{\gamma}/\lambda)^2+c_4(\tilde{\gamma}/\lambda)^4+\cdots]. \tag{IV.4}$$

In analogy to Eq. (IV.3), other smooth quantities like the uniform energy $\tilde{U}$ Eq. (III.26) can be expanded in powers of $\tilde{\gamma}/\lambda$.

As we already have mentioned in Sec. III, the shell-correction method is not limited to the use of the Gaussian function as the averaging function $\xi(x)$ in Eq. (III.29). In fact, any other averaging function with a correct asymptotic behavior may be used (see e.g., Brack and Pauli, 1971). In any case, the role of the curvature corrections is very important for the technical realization of the shell-correction method. As argued in Sec. III, the shell-correction energy δU should not contain smooth terms already present in the phenomenological liquid-drop model part of the total energy, Eq. (III.35), (see also Strutinsky, 1968); otherwise such terms would be accounted for twice. This is avoided by the requirement that the integral (III.29), or correspondingly the sum (IV.3), reproduce identically any component of the level density, which can be written as a polynomial in energy of order less than or equal to $2m$. This requirement leads, in fact, directly to a series of the form (IV.3), the numerical coefficients in front of the derivatives being dependent on the averaging function $\xi(x)$. In the case of Gaussian averaging, this can be recognized by the fact that Eq. (III.30) is equal to the sum of the first m terms in the expansion of a delta function in Hermite polynomials, as pointed out by Tsang (1968). For the general case, we refer to Brack and Pauli (1971).

For the uniform energy $\tilde{U}$, the lowest order ($m=1$) of the curvature correction contributes up to a few tens of MeV, and is thus an important part of it. However, for the level density $\tilde{g}(\mathcal{E},\beta)$ itself, the curvature corrections are less important and have only a negligible effect on the relationships derived below. In the qualitative discussions of this section, we shall therefore omit these corrections.

As the parameter $\tilde{\gamma}$ in itself has no physical meaning, the results obtained for $\tilde{g}(\lambda,\beta)$ (and for δU, of course) should not depend on the exact value of $\tilde{\gamma}$ used. It has, in fact, been shown (Strutinsky 1968, Nilsson *et al.*, 1969) that the results are independent of $\tilde{\gamma}$ within an interval of $\hbar\omega_0\lesssim\tilde{\gamma}\lesssim 2\hbar\omega_0$, when a harmonic oscillator or

a Nilsson model potential is used for the calculation of the single-particle levels ε_ν. With the use of finite depth potentials, this problem becomes more delicate; it has been argued, however, that the correct value of $\tilde{\gamma}$ can be found in these cases by the condition

$$\partial(\delta U)/\partial\tilde{\gamma}=0 \qquad \text{(IV.5)}$$

(Brack and Pauli, 1971; compare also Bunatyan, Kolomietz, and Strutinsky, 1972).

As we shall discuss in more detail below, the essential contributions to the level density (IV.3) come from the energies ε_ν within a region $\pm\tilde{\gamma}$ around the Fermi energy λ, i.e., with the value (IV.2) for $\tilde{\gamma}$, within $\lambda\pm(7$–$10)$ MeV. It is thus important to know *all* single-particle energies ε_ν in this region. Frequently, the use of an improper basis for the diagonalization results in the omission of some appreciable fraction of the levels; consequently, erroneous results for the shell correction are obtained.

In calculations with finite depth potentials, as, e.g., the Woods–Saxon potential, the nucleon binding energy is often less than $\tilde{\gamma}$, and the number of bound states is insufficient for the averaging in Eq. (IV.1), especially with larger values of $\tilde{\gamma}$. This difficulty is avoided by adding to the bound-state spectrum also the lower quasistationary unbound states. These unbound states should represent a reasonable extrapolation corresponding to the transition to nuclei with larger A values. Such an extrapolation of the bound spectrum is obtained by the diagonalization, provided that the size of the basis functions is close to the size of the potential well. The energies of these states depend on the number of basis states used, when the energies are found by a diagonalization method. However, this dependence is rather weak and influences most strongly the low spin states, which contribute less to the smearing procedure. Therefore, in the present paper, we have not given any special treatment of these states. For a more detailed discussion of this problem, we refer to the works of Bolsterli *et al.* (1971), and of Brack and Pauli (1971).

For qualitative discussions, it is convenient to introduce another density function $g_{\rm sh}(\varepsilon,\beta)$ in order to describe the local level density of the single-particle spectrum, defined analogous to (IV.1) and (IV.3). As $g_{\rm sh}(\varepsilon,\beta)$ shall reflect shell nonuniformities, the smearing interval $\gamma_{\rm sh}$ has to be chosen considerably smaller than $\hbar\omega_0$. On the other hand, $g_{\rm sh}$ should be a continuous function of energy and therefore the interval $\gamma_{\rm sh}$ should still contain many levels (in the limiting case when $\gamma_{\rm sh}\to 0$, $g_{\rm sh}$ turns into a sum of delta functions). In our calculations, we have normally used

$$\gamma_{\rm sh}\approx\lambda A^{-2/3}\approx 1\text{–}2\ \text{MeV}. \qquad \text{(IV.6)}$$

With this choice, $g_{\rm sh}(\varepsilon,\beta)$ represents a locally averaged level density, which is a wiggly function of energy and deformation parameters, oscillating around the "uniform" level density $\tilde{g}(\varepsilon,\beta)$, see Fig. II–3.

2. The Energy Shell Correction

With the definitions above, the variations in the single-particle level density caused by the shells can be described by the function

$$\delta g(\varepsilon,\beta)=g_{\rm sh}(\varepsilon,\beta)-\tilde{g}(\varepsilon,\beta). \qquad \text{(IV.7)}$$

Furthermore, the sum of single-particle energies

$$U=2\sum_\nu \varepsilon_\nu(\beta), \qquad \text{(IV.8)}$$

can be replaced by

$$U=2\int_{-\infty}^{\lambda_{\rm sh}(\beta)}\varepsilon g_{\rm sh}(\varepsilon,\beta)\,d\varepsilon. \qquad \text{(IV.9)}$$

In the limiting case $\gamma_{\rm sh}\to 0$, the integral (IV.9) is the sum of the single-particle energies $\varepsilon_\nu(\beta)$ in Eq. (IV.8). The Fermi energies $\lambda_{\rm sh}(\beta)$ and $\tilde{\lambda}(\beta)$ appearing in Eqs. (IV.9) and (III.32) are determined from the condition that the number of particles (protons or neutrons) is fixed and is the same for both distributions

$$N=2\int_{-\infty}^{\lambda_{\rm sh}(\beta)} g_{\rm sh}(\varepsilon,\beta)\,d\varepsilon=2\int_{-\infty}^{\tilde{\lambda}(\beta)}\tilde{g}(\varepsilon,\beta)\,d\varepsilon. \qquad \text{(IV.10)}$$

The energy shell correction can be written as

$$\delta U=2\left[\int_{-\infty}^{\lambda_{\rm sh}}\varepsilon g_{\rm sh}d\varepsilon-\int_{-\infty}^{\tilde{\lambda}}\varepsilon\tilde{g}d\varepsilon\right]. \qquad \text{(IV.11)}$$

Normally, the difference between the two Fermi energies $\lambda_{\rm sh}(\beta)$ and $\tilde{\lambda}(\beta)$ is small compared to their absolute values

$$\lambda_{\rm sh}(\beta)-\tilde{\lambda}(\beta)=\delta\lambda(\beta)\lesssim 1/\tilde{g}(\tilde{\lambda},\beta)\ll\tilde{\lambda}. \qquad \text{(IV.12)}$$

For the pure single-particle model, a value of $\lambda_{\rm sh}$ must be taken between the last occupied and the first empty level. Inserting $\lambda_{\rm sh}(\beta)=\tilde{\lambda}(\beta)+\delta\lambda(\beta)$ into Eq. (IV.10), we find

$$\delta\lambda(\beta)=-\left[\int_{-\infty}^{\lambda_{\rm sh}(\beta)}\delta g(\varepsilon,\beta)\,d\varepsilon\right]\Big/\tilde{g}[\lambda_{\rm sh}(\beta),\beta]. \qquad \text{(IV.13)}$$

Expanding Eq. (IV.11) around $\lambda_{\rm sh}(\beta)$, one obtains, using Eq. (IV.13),

$$\delta U(\beta)=2\int_{-\infty}^{\lambda_{\rm sh}(\beta)}[\varepsilon-\lambda_{\rm sh}(\beta)]\delta g(\varepsilon,\beta)\,d\varepsilon-(\delta\lambda)^2\tilde{g}(\lambda_{\rm sh})+O[(\delta\lambda)^3]. \qquad \text{(IV.14)}$$

To a good accuracy, one can use only the first term in (IV.14). This expression is stationary with respect to small changes in λ. Thus, without specifying any more the Fermi energy, we obtain the approximate formula

$$\delta U=2\int_{-\infty}^{\lambda}(\varepsilon-\lambda)\delta g(\varepsilon)\,d\varepsilon+O[(\delta\lambda)^2]. \qquad \text{(IV.15)}$$

In practice there is no advantage in using Eq. (IV.15); on the contrary, the definition of δU given in Sec. III with summation for U (i.e., using $\gamma_{sh}=0$) is simpler. In the qualitative discussion here, however, Eq. (IV.15) is of interest, especially because it shows the connection between δU and δg. It will also be used later in this section.

Keeping in mind that the shell-model potential, and therefore all quantities introduced here, depend on the deformation β, we shall in the following, for simplicity, omit the argument β of the functions $\tilde{g}$, g_{sh}, $\tilde{\lambda}$, λ_{sh}, etc.

3. The Occupation Number Representation

The physical content of the relations obtained above will become more transparent, when these relations are expressed in an occupation number representation. The assumption of independent-particle motion in a shell-model potential allows the introduction of occupation numbers n_ν describing the filling of the νth shell-model state (being 1 or 0, if ε_ν is occupied or empty, respectively). The particle number and the sum of single-particle energies [Eq. (IV.8)] can then be written as

$$N=2\sum_\nu n_\nu; \qquad U=2\sum_\nu \varepsilon_\nu n_\nu. \tag{IV.16}$$

The smearing procedure considered above [Eq. (IV.1)] can now be interpreted as a kind of reoccupation of the levels, whereby the steplike distribution corresponding to (IV.16) is smoothed out over a region $\pm\tilde{\gamma}$ around the Fermi level. Such an interpretation can be described by introducing occupation numbers $\tilde{n}_\nu$ which are not restricted to having the values 0 and 1. These "average" occupation numbers can be defined by the equation

$$N=2\sum_\nu \tilde{n}_\nu=2\int_{-\infty}^{\tilde{\lambda}} \tilde{g}(\varepsilon)\,d\varepsilon. \tag{IV.17}$$

Inserting in this equation the expression (III.29) for the smooth level density and interchanging the integration and the summation, leads to the following explicit form for $\tilde{n}_\nu$

$$\tilde{n}_\nu=\tilde{\gamma}^{-1}\int_{-\infty}^{\tilde{\lambda}} \xi\left(\frac{\varepsilon-\varepsilon_\nu}{\tilde{\gamma}}\right)d\varepsilon. \tag{IV.18}$$

By means of the occupation numbers $\tilde{n}_\nu$, the uniform energy Eq. (III.26) can after some calculations (see Brack and Pauli, 1971) be written as

$$\tilde{U}=2\sum_\nu \varepsilon_\nu\tilde{n}_\nu+\tilde{\gamma}(\partial\tilde{U}/\partial\tilde{\gamma}). \tag{IV.19}$$

This relation holds independent of the averaging function $\xi(x)$. In the special case of Gaussian averaging, the second term in Eq. (IV.19) can also be written as

$$\tilde{\gamma}(\partial\tilde{U}/\partial\tilde{\gamma})=(\tilde{\gamma}/\pi^{1/2})a_{2m}\sum_\nu H_{2m}[(\tilde{\lambda}-\varepsilon_\nu)/\tilde{\gamma}] \times\exp\left(-[(\tilde{\lambda}-\varepsilon_\nu)/\tilde{\gamma}]^2\right), \tag{IV.20}$$

and is thus proportional to the $2m$th derivative of the function $\tilde{G}(\tilde{\lambda},\beta)$ [Eq. (IV.1)]; compare also Bunatyan *et al.* (1972).

As $\tilde{\gamma}$ in all cases considered has been chosen to fulfill Eq. (IV.5), the term involving $\partial\tilde{U}/\partial\tilde{\gamma}$ vanishes. Therefore the first-order shell-correction energy δU can be expressed in the simple form

$$\delta U=2\sum_\nu \varepsilon_\nu\delta n_\nu, \tag{IV.21}$$

where

$$\delta n_\nu\equiv n_\nu-\tilde{n}_\nu. \tag{IV.22}$$

The occupation number representation introduced here can be used to express the expectation values of all one-body operators. We have for instance for the quadrupole moment

$$Q=2\sum_\nu q_{\nu\nu}n_\nu, \tag{IV.23}$$

where $q_{\nu\nu}$ is the diagonal matrix element of the quadrupole operator in the state φ_ν. Correspondingly, the uniform part of the quadrupole moment can be defined by

$$\tilde{Q}=2\sum_\nu q_{\nu\nu}\tilde{n}_\nu \tag{IV.24}$$

(see Sec. IV.5 below).

Finally, the total shell-correction energy δE [Eq. (III.34)], including $\delta_2 E$ [Eq. (III.25)], can in this representation be brought into the simple form

$$\delta E=\delta_1 E+\delta_2 E=2\sum_\nu \varepsilon_\nu\delta n_\nu+2\sum_{\nu\nu'}\langle\nu\nu'\mid\Gamma\mid\nu\nu'\rangle\delta n_\nu\delta n_{\nu'}. \tag{IV.25}$$

This demonstrates that $\delta_2 E$ is of second order in δn_ν, and thus only a correction to the leading term $\delta_1 E=\delta U$.

4. Effect of a Small Variation of the Average Field

We now consider the effect of a small change V' of the average shell-model field on the shell corrections. The change of the νth energy level is, in first-order perturbation theory, equal to

$$\varepsilon_\nu'=\int d\tau V'\mid\varphi_\nu(\mathbf{r})\mid^2. \tag{IV.26}$$

Then, we have

$$\varepsilon_\nu=\varepsilon_\nu^{(0)}+\varepsilon_\nu'. \tag{IV.27}$$

The corrections to the level densities introduced in Sec. IV.1 are obtained directly from their definition. In the following, we denote both functions $\tilde{g}$ and g_{sh} by g_γ, and the corresponding occupation numbers by n_ν^γ, not specifying the values of γ for the moment. Inserting ε_ν into Eq. (III.29), and assuming that the perturbation V' does not explicitly depend on ε, we obtain

$$g_\gamma(\varepsilon)=g_\gamma^{(0)}(\varepsilon)-\gamma^{-1}\sum_\nu \varepsilon_\nu'(d/d\varepsilon)\xi[(\varepsilon-\varepsilon_\nu^{(0)})/\gamma]. \tag{IV.28}$$

Here, the derivative of $\xi(x)$ with respect to ε_ν has been substituted for by the derivative with respect to ε.

In Eq. (IV.28) the essential contributions come from states with $|\varepsilon-\varepsilon_\nu^{(0)}| \lesssim\gamma$, and therefore we have used in the derivation of Eq. (IV.28)

$$|2(\varepsilon-\varepsilon_\nu^{(0)})\varepsilon_\nu'| \ll\gamma^2, \tag{IV.29}$$

which implies that the perturbation of the individual energies must be small as compared to the smearing effect of γ, instead of the usual quantum-mechanical condition

$$|\varepsilon_\nu'| \ll |\varepsilon_\nu^{(0)}-\varepsilon_{\nu'}^{(0)}|. \tag{IV.30}$$

The perturbation of the level density $g_\gamma(\varepsilon)$ can now be written as

$$g_\gamma'(\varepsilon) = -\gamma^{-1}\int d\tau V'(\mathbf{r}) \times \frac{d}{d\varepsilon}\{\sum_\nu |\varphi_\nu(\mathbf{r})|^2\xi[(\varepsilon_\nu^{(0)}-\varepsilon)/\gamma]\}$$
$$= -\int d\tau V'(\mathbf{r})\frac{d}{d\varepsilon}\rho_\gamma(\varepsilon,\mathbf{r}). \tag{IV.31}$$

Here, we have introduced a new quantity

$$\rho_\gamma(\varepsilon,\mathbf{r}) = \gamma^{-1}\sum_\nu |\varphi_\nu(\mathbf{r})|^2\xi[(\varepsilon_\nu^{(0)}-\varepsilon)/\gamma], \tag{IV.32}$$

which may be interpreted as an averaged phase-space density of the nucleons. Its volume integral is equal to the level density $g_\gamma(\varepsilon)$:

$$\int d\tau\rho_\gamma(\varepsilon,\mathbf{r}) = g_\gamma(\varepsilon). \tag{IV.33}$$

The averaged spatial density distribution of the nucleons is obtained as an energy integral over $\rho_\gamma(\varepsilon,\mathbf{r})$

$$\rho_\gamma(\mathbf{r}) = 2\int_{-\infty}^{\lambda_\gamma} d\varepsilon\rho_\gamma(\varepsilon,\mathbf{r}) = 2\sum_\nu |\varphi_\nu(\mathbf{r})|^2 n_\nu^\gamma. \tag{IV.34}$$

Inserting the two different averaging parameters $\gamma_{\rm sh}$ and $\tilde\gamma$ in Eqs. (IV.28)–(IV.34), we define the local densities $\rho_{\rm sh}(\varepsilon,\mathbf{r})$, $\rho_{\rm sh}(\mathbf{r})$ which contain shell effects, and the uniform densities $\tilde\rho(\varepsilon,\mathbf{r})$, $\tilde\rho(\mathbf{r})$ reflecting an averaged nucleon distribution. The shell corrections to the phase density and the spatial density are thus

$$\delta\rho(\varepsilon,\mathbf{r}) = \rho_{\rm sh}(\varepsilon,\mathbf{r})-\tilde\rho(\varepsilon,\mathbf{r}) \tag{IV.35}$$

and

$$\delta\rho(\mathbf{r}) = \rho_{\rm sh}(\mathbf{r})-\tilde\rho(\mathbf{r}) = 2\int_{-\infty}^{\lambda_{\rm sh}} d\varepsilon\rho_{\rm sh}(\varepsilon,\mathbf{r}) - 2\int_{-\infty}^{\tilde\lambda} d\varepsilon\tilde\rho(\varepsilon,\mathbf{r}). \tag{IV.36}$$

The quantity $\delta\rho(\mathbf{r})$ is the density fluctuation, which was called $\delta\rho^S$ in Sec. III. In spite of the fact that there is no simple relation to the self-consistent density fluctuation $\delta\rho$ [see Eq. (III.21)], it is an important quantity in itself. It describes fluctuations of the spatial single-particle density, which are related to the non-uniform distribution of the single-particle states near the Fermi energy. It will be discussed in some detail below.

Finally, we can express the change of the shell correction $(\delta U)'$ caused by the perturbation V' in terms of $\delta\rho(\mathbf{r})$. Using Eq. (IV.15) and the above definitions, we find

$$(\delta U)' \approx 2\int_{-\infty}^{\lambda} d\varepsilon(\varepsilon-\lambda)(g_{\rm sh}'(\varepsilon)-\tilde g'(\varepsilon))$$
$$= -2\int_{-\infty}^{\lambda} d\varepsilon(\varepsilon-\lambda)\int d\tau V'(\mathbf{r})\frac{d}{d\varepsilon}\delta\rho(\varepsilon,\mathbf{r}), \tag{IV.37}$$

and, after partial integration,

$$(\delta U)' \approx \int V'(\mathbf{r})\delta\rho(\mathbf{r})d\tau = 2\sum_\nu (V')_{\nu\nu}\delta n_\nu. \tag{IV.38}$$

The Eqs. (IV.31), (IV.37), (IV.38) are analogous to Eqs. (32)–(36) in the paper by Strutinsky (1968) where a smooth WKBlike density distribution, determined by a continuous spectral function $\nu=\nu(\varepsilon)$ was considered, and the deviation from a spherical shape was taken as a perturbation V'. The smooth density function $\tilde g(\varepsilon)$ is here determined as it appears in the shell-correction calculations, and therefore, the above equations hold also for small variations of a deformed field.

5. The Shell Force and the Spatial Density Fluctuations

Equation (IV.38) shows the direct relation between the change in the energy-shell correction, which is caused by a small perturbation of the average field, and the spatial density fluctuations. This relation is of relevance especially in connection with the discussion of the stretching—or restoring—forces related to the shell structure, which we shall just call the shell forces.

Defining the force, as usual, as the derivative of the potential energy taken with respect to a certain coordinate, we can define the shell forces $\delta\mathcal{F}_i$ as the derivatives of the energy correction with respect to the deformation variables β_i. These quantities can be found by means of Eq. (IV.38).

Assuming

$$V' = (\partial V/\partial\beta_i)\delta\beta_i,$$

we find the related force

$$\delta\mathcal{F}_i = -\partial(\delta U)/\partial\beta_i = -\int d\tau[\partial V(\mathbf{r})/\partial\beta_i]\delta\rho(\mathbf{r}) = -2\sum_\nu (\partial V(\mathbf{r})/\partial\beta_i)_{\nu\nu}\delta n_\nu. \tag{IV.39}$$

In addition to the forces (IV.39) related to the intrinsic shell structure in the nucleus, we must consider also the classical forces $\mathcal{F}_{\rm cl}$ of the surface tension and the Coulomb field. These are described in our calculations by the LDM energy terms in Eq. (III.36) for the

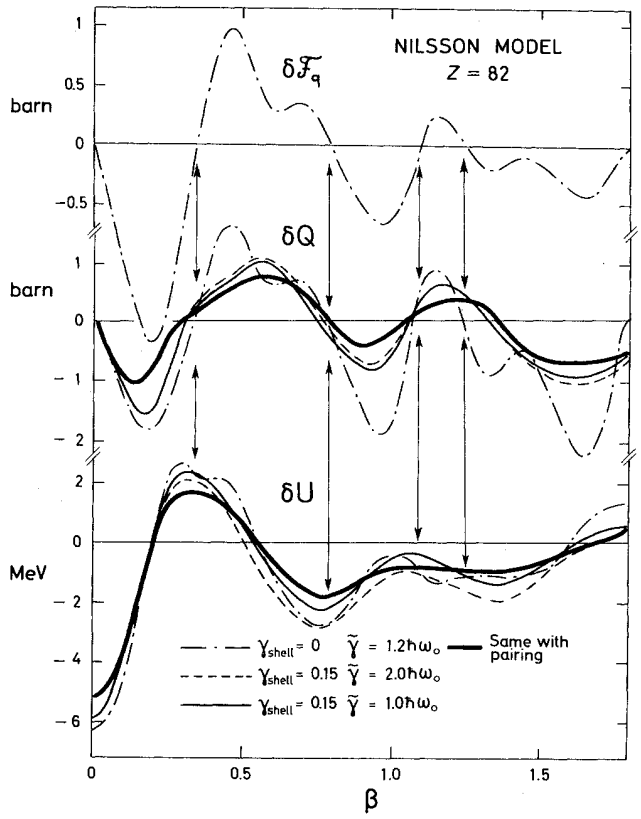

FIG. IV-1. Curves $\delta Q(\beta)$ and $\delta U(\beta)$ obtained with the Nilsson model. (The definition of the deformation parameter β in this and the following figures is given in the caption to Fig. II-6). Thin lines are without and thick lines are with the pairing correlations included (cf. Sec. V; $\tilde{\Delta}=0.8$ MeV). The coincidence of the nodes of δQ with the extrema of δU is shown by arrows. In addition, $\delta\mathcal{F}_q$ is shown for the case $\gamma_{sh}=0$ and $\tilde{\gamma}=1.2\ \hbar\omega_0$.

total energy of the nucleus. So we have

$$\mathcal{F}_{\rm tot}=\mathcal{F}_{\rm cl}+\delta\mathcal{F}.$$

With the exception of very large distortions, the classical forces are, however, weaker than the local value of the structural force $\delta\mathcal{F}$. Consequently, they are less significant for establishing the equilibrium shape β_i^* which is determined by

$$\delta\mathcal{F}_i(\beta_i^*)=0. \qquad \text{(IV.40)}$$

Hence, the shell forces are a measure of the trend of the system to change its deformation until it reaches a shape where the energy is stationary and the condition (IV.40) is fulfilled.

As the average potential varies most around the nuclear surface, $\partial V/\partial\beta_i$ is largest there and, consequently, the surface region is relatively more essential for determining the shell force $\delta\mathcal{F}$, see Eq. (IV.39). This is not the case for the energy correction δU, to which the whole region of variation of $\delta\rho$ contributes.

As an example, we consider the special case of quadrupole distortions β of a spherical average field. The derivative $-\partial V(\mathbf{r})/\partial\beta$ is then approximately proportional to the single-particle quadrupole operator $\hat{q}(\mathbf{r})$ in harmonic oscillatorlike potentials (e.g., in the Nilsson model). To the same accuracy, the quadrupole shell force $\delta\mathcal{F}_q$ is then proportional to the quadrupole moment of the shell undulations of the spatial density distribution

$$\delta\mathcal{F}_q\propto\delta Q=\int d\tau\hat{q}(\mathbf{r})\delta\rho(\mathbf{r})=Q_{\rm sh}-\tilde{Q}, \qquad \text{(IV.41)}$$

where $Q_{\rm sh}$ and $\tilde{Q}$ are the quadrupole moments of the two density distributions, $\rho_{\rm sh}(\mathbf{r})$ and $\tilde{\rho}(\mathbf{r})$. For example,

$$\tilde{Q}=\int d\tau\hat{q}(\mathbf{r})\tilde{\rho}(\mathbf{r}) \qquad \text{(IV.42)}$$

[see also Eqs. (IV.23, 24)].

The relationship between δQ and $\delta\mathcal{F}_q$, expressed in Eq. (IV.41), has already been discussed qualitatively in Sec. II; see also Fig. II-4.

As a special case of Eq. (IV.40), it follows that, at the equilibrium deformation β^*,

$$Q_{\rm sh}(\beta^*)=\tilde{Q}(\beta^*). \qquad \text{(IV.43)}$$

The more general condition is that

$$(\partial V/\partial\beta)_{\rm sh}=(\partial V/\partial\beta)_{\tilde{\gamma}}, \qquad \text{(IV.44)}$$

where the average values of $\partial V(\mathbf{r})/\partial\beta$ are evaluated with $\rho_{\rm sh}(\mathbf{r})$ and $\tilde{\rho}(\mathbf{r})$.

Equations (IV.43) and (IV.44) imply that, at equilibrium, the shell inhomogeneity of the density distribution is uniformly spread over the nucleus (especially near the surface) so that no specific shell force arises.

Although the proportionality of $\delta\mathcal{F}_q$ [Eq. (IV.39)] and δQ [Eq. (IV.41)] does not hold for larger deformations, their zeros along the β axis always coincide, even for very large distortions. In the calculations with the Nilsson model, the two quantities are easily compared; see, e.g., Fig. IV–1. The Woods–Saxon model does not seem to make an exception, however, as can be seen from Fig. IV–2.

Concerning the quadrupole moment $\tilde{Q}$ of the uniform density distribution, all results of our calculations prove that for this quantity, only the deformation of the average field is significant. Thus, it may be regarded as representing the quadrupole distortion of the average field, and is practically identical to the quadrupole moment of a uniform density distribution which has the same shape as the shell-model potential.

Therefore, Eqs. (IV. 43) and (IV.44) may be considered to be just another expression for the consistency condition that, at equilibrium, the quadrupole moment of the average field and that of the nucleon density distribution must be the same (Bohr and Mottelson, to be published). Equations (IV.39) and (IV.40) express the same condition for the general case.

These relationships have been checked in calculations

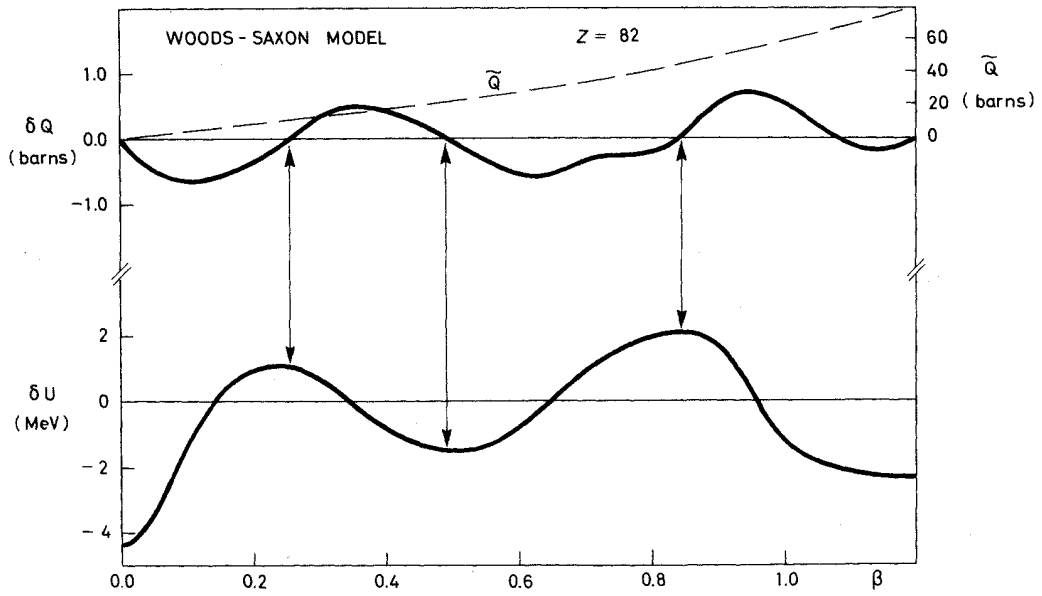

FIG. IV-2. The same as Fig. IV-1 for the Woods–Saxon model, calculated with pairing correlations only. $\gamma_{sh}=0$, $\tilde{\gamma}=1.2\hbar\omega_0$. The uniform quadrupole moment is shown by a dashed line. The deformation of the potential well is not purely ellipsoidal; at higher deformations, the shape has a small neck at the center (cf. Sec. VII).

with different potentials, which shall be briefly presented here.

In the case of a pure deformed harmonic oscillator, the relationship between the positions of the extrema of the energy correction δU and the zeros of δQ holds exactly, even for nonanalytic maxima where δQ and the derivative of δU are discontinuous; see Fig. IV–3. It holds undistorted by the addition of the pairing correlation (thick lines).

An example of the data showing the correlation between the energy correction, the quadrupole shell force $\delta\mathfrak{F}_q$, and the fluctuation of the quadrupole moment of the spatial density distribution is shown in Fig. IV–1 above which is calculated with the Nilsson model.

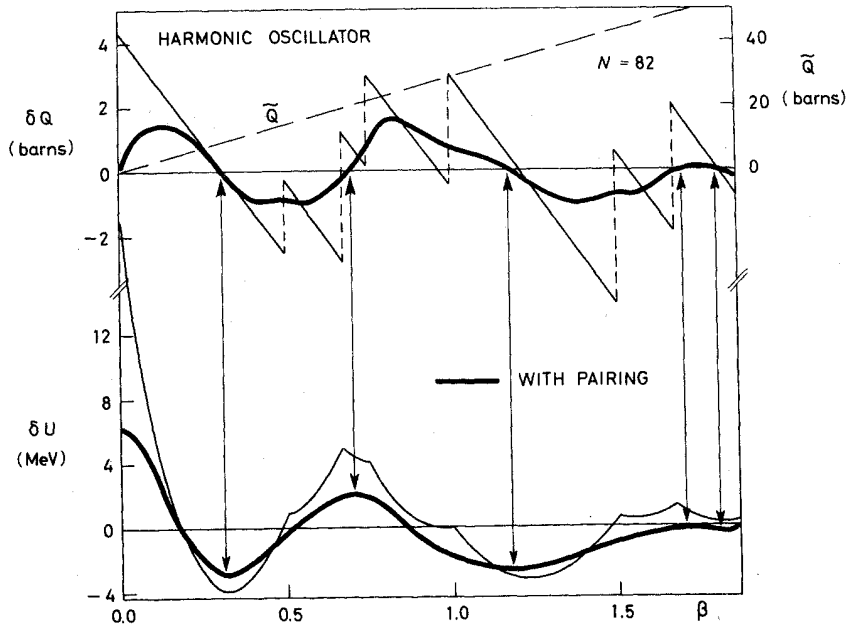

FIG. IV-3. The same as Fig. IV-2 for an axially symmetric deformed harmonic oscillator. Note the finite value of δQ and the finite slope of the δU curve for the case $\delta P=0$ at $\beta=0$ due to the Rainwater effect in an unfilled degenerate spherical state. This as well as similar anomalies of a smaller scale in the deformed case disappear when the pairing is included, thereby revealing more distinctly the shell structure. Strict proportionality of $\tilde{Q}$ to β shows that $\tilde{Q}$ is determined by the deformation of the average field, only.

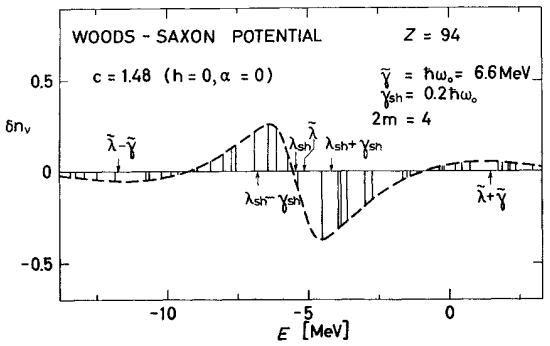

FIG. IV-4. Proton level spectrum of a deformed Woods–Saxon potential around the Fermi energy (for details of the potential, see Sec. VII). The positions of the vertical lines along the energy axis are those of the levels ε_ν, their lengths are equal to the values of δn_ν. The curvature-correction order is $2m=4$.

Different values of γ_{sh} and $\tilde{\gamma}$ are used, and pairing is added. The insensitivity of the results to these variations is clearly demonstrated. The minor deviations from the general rule for the $\gamma_{sh}=0$ and nonpairing case are probably due to the fact that for the calculated values of $\delta\mathcal{F}_q$, in the derivative $\partial V/\partial\beta$ [Eq. (IV.39)] only the main (coordinate) part of the average field is taken into account. The agreement is improved when some additional smearing is present, as in the case where the pairing correlation is included and $\gamma_{sh}=0$.

Very similar results were obtained in the calculations with the Woods–Saxon model, see, e.g., Fig. IV–2.

The agreement of all these results illustrates the insensitivity of the shell correction to the detailed features of the shell model.

6. Contributions to Shell Corrections

It is important to know, which part of the single-particle spectrum contributes to the quantities δU, $\delta\mathcal{F}$, and δQ. This can most easily be seen, if we use the occupation number representation introduced in Sec. IV.3. We have from Eqs. (IV.21), (IV.39), and (IV.41)

$$\delta U=2\sum_\nu \varepsilon_\nu\delta n_\nu$$
$$\delta\mathcal{F}_i=-2\sum_\nu (\partial V/\partial\beta_i)_{\nu\nu}\delta n_\nu$$
$$\delta Q=2\sum_\nu q_{\nu\nu}\delta n_\nu. \qquad \text{(IV.45)}$$

The fluctuations δn_ν are shown in Fig. IV-4. It is seen that they differ significantly from zero only in a relatively narrow region of width $\tilde{\gamma}$ around the Fermi energy. Consequently, the quantities in Eq. (IV.45) get their main contribution from the same energy region, and the states far away from the Fermi energy do not contribute at all. Actually, the Fermi energy λ, which is found from the condition that the total number of particles is conserved, is the only quantity for which the lower states, or at least their number, are important.

Taking into account the behavior of the function δn_ν (Fig. IV-4), one can also represent δQ in Eq. (IV.45) as the difference between two terms $Q_<$ and $Q_>$, which are the averaged quadrupole moments in an energy region below and above the Fermi energy, respectively:

$$\delta Q=Q_<-Q_>. \qquad \text{(IV.46)}$$

The same holds for the general case of shell forces $\delta\mathcal{F}_i$, determined as in Eq. (IV.39), as well as for δU. As the quantity $(\partial V/\partial\beta)_{\nu\nu}$ in Eq. (IV.45) determines the slope of the νth level in the Nilsson-type diagrams, the strength of the shell force $\delta\mathcal{F}_q$ can thus also be expressed as the difference between the averaged slopes of the states above and below the Fermi energy,

$$[(\partial V/\partial\beta)_>]_{Av}-[(\partial V/\partial\beta)_<]_{Av},$$

the average being taken over a sufficiently large energy interval of the order of $\lambda/A^{1/3}$.

A detailed picture of the contributions to the shell force is given in Fig. IV-5. In this figure, the matrix elements $(\partial V/\partial\beta)_{\nu\nu}$ of the single-proton states in the Nilsson model are plotted against the energy. The lengths of the vertical lines, in upward or downward directions depending on the sign of $(\partial V/\partial\beta)_{\nu\nu}$, represent the absolute values of the matrix elements. Two characteristic deformations have been chosen, $\beta=0.16$ (lower part) and $\beta=0.46$ (upper part), and the weighting functions $\delta n(\varepsilon-\lambda)$ for different Fermi energies, corresponding to the proton numbers $Z=82$, 88, and 92, are represented by dotted lines.

At both deformations, the distribution A (belonging to $Z=82$) leads to extremal values of the shell force $\delta\mathcal{F}_q$ which means that the slope of δU is maximal (cf. Fig. IV-1). By shifting the Fermi energies (i.e., moving the dotted curves along the energy axis), the weighting factors δn_ν in Eq. (IV.45) are changed, until for a certain nucleon number ($Z=82$ for $\beta=0.16$, and $Z=92$ for $\beta=0.46$) the value of $\delta\mathcal{F}_q$ becomes zero. At these points the contributions from both sides of the Fermi energy cancel, although it hardly can be seen in the figure.

A similar picture of the distribution of the individual quadrupole moments $q_{\nu\nu}$ contributing to δQ is shown in Fig. IV-6, calculated also for the Nilsson model with $\beta=0.46$ for $Z=82$. Due to the prolate distortion of the average field, the positive value of $q_{\nu\nu}$ predominate. Nevertheless, this does not affect δQ.

Although many states near the Fermi energy contribute to the sum (IV.45), most of the contributions cancel, so that the remaining coherent shell effect in δQ does not exceed 1–2 b, a small quantity as compared, e.g., to the typical value of $Q\approx 10$ b for the quadrupole moment of a deformed nucleus. The value of δQ oscillates around zero when the deformation changes, which shows that it is related to a volume nonuniformity of the nucleon distribution.

In Fig. IV-7, some results are shown which demon-

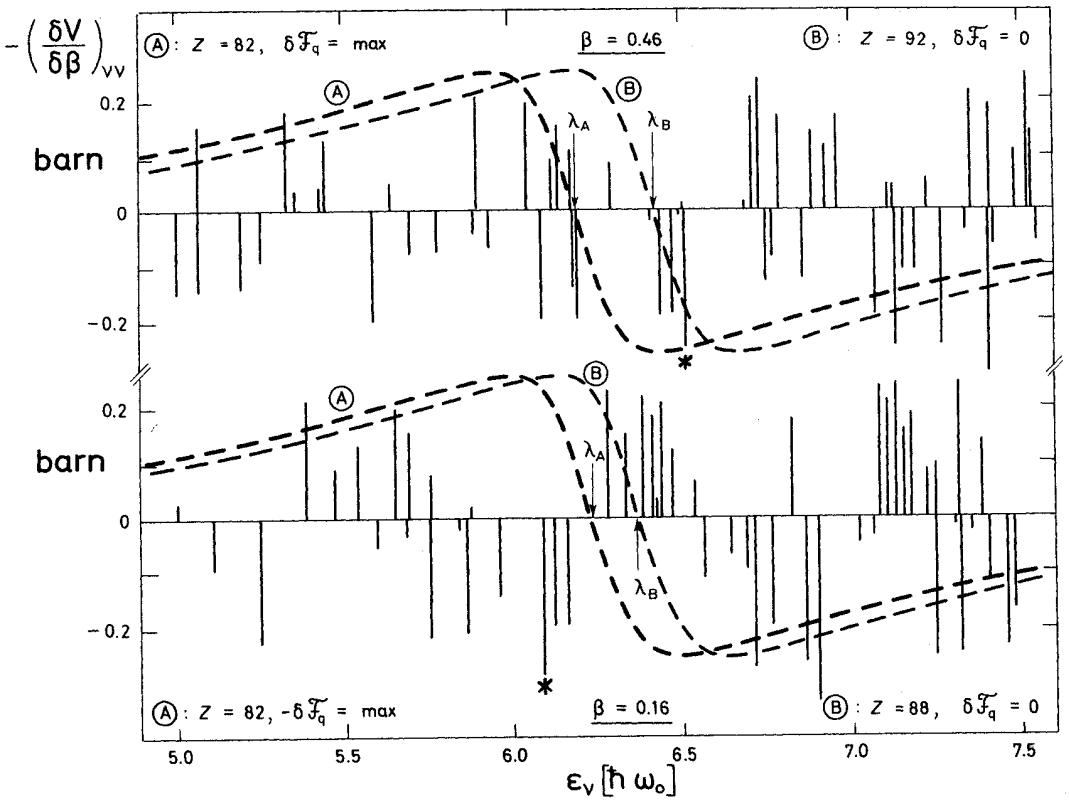

FIG. IV-5. Plot of the matrix elements $-(\partial V/\partial\beta)_{\nu\nu}$, which contribute to the stretching force $\delta\mathcal{F}_q$ according to Eq. (IV.45). The spectrum is taken for the Nilsson model at two different deformations, $\beta=0.16$ in the lower part, and $\beta=0.46$ in the upper part of the figure. The lengths of the vertical lines are proportional to the absolute values of $(\partial V/\partial\beta)_{\nu\nu}$. Their positions along the energy axis correspond to the single-particle energies ε_ν. The dashed curves represent, in an arbitrary normalization, the function δn_ν (cf. Fig. IV-4) with $\gamma_{sh}=0.2\ \hbar\omega_0$ and $\tilde{\gamma}=2.0\ \hbar\omega_0$. At each deformation, two positions of the Fermi energy are chosen to correspond to extremal values of $\delta\mathcal{F}_q$ in cases A, and to $\delta\mathcal{F}_q=0$ in cases B. (The respective nucleon numbers are given in the figure.) The asterisk (*) denotes the state [505 11/2] mentioned in the text.

strate the effect of varying $\tilde{\gamma}$ on the shell corrections δQ. The features of δQ discussed above are insensitive for $\tilde{\gamma}\gtrsim 1\hbar\omega_0$, in analogy to the behavior of the quantities δU and $\delta g(\lambda)$ (see also Fig. IV.1).

By increasing γ_{sh}, the centers of the contributing regions are moved away from the Fermi energy, which can easily be seen from Fig. IV-4. This affects considerably only the amplitudes of δQ and δU, but not their general behavior. This result demonstrates that no single state at the Fermi energy is particularly important. Thus, it is not correct to say, e.g., that the large deformations of some nuclei are due to especially strong coupling to the surface of certain high-spin states, as, e.g., the [505 11/2] state (Bès and Szymánski, 1961; Mottelson and Nilsson, 1955). In Fig. IV-5, the latter state is one of a few states with large negative slopes (it is marked by an asterisk). It is clear that its contribution is of no special significance, and positive and negative contributions of many other states from above and below the Fermi energy must also be considered.

The data in Figs. IV-1–IV-7 demonstrate clearly that the shell force is the result of a delicate balance of contributions of many states around the Fermi energy.

7. Shell Effects in the Spatial Density Distributions

The spatial variation of the nucleon density in nuclei constitutes an important problem in nuclear physics. It is usually assumed that this density distribution is smooth, as exemplified by, e.g., the Fermi distribution. Recently, however, from electron scattering experiments (Heisenberg *et al.*, 1969), evidence has been obtained that the nucleon density does deviate, in an oscillating manner, from such a smooth distribution. Hopefully, with further refinements of these experiments, more detailed quantitative information will soon become available.

The discussion above shows that the energy effects of the shell structure—which are the main goal of this paper—are also closely related to variations of the spatial density. Thus, it may be instructive to have a closer look at the origin of the oscillations of the nucleon density as they appear in the shell model.

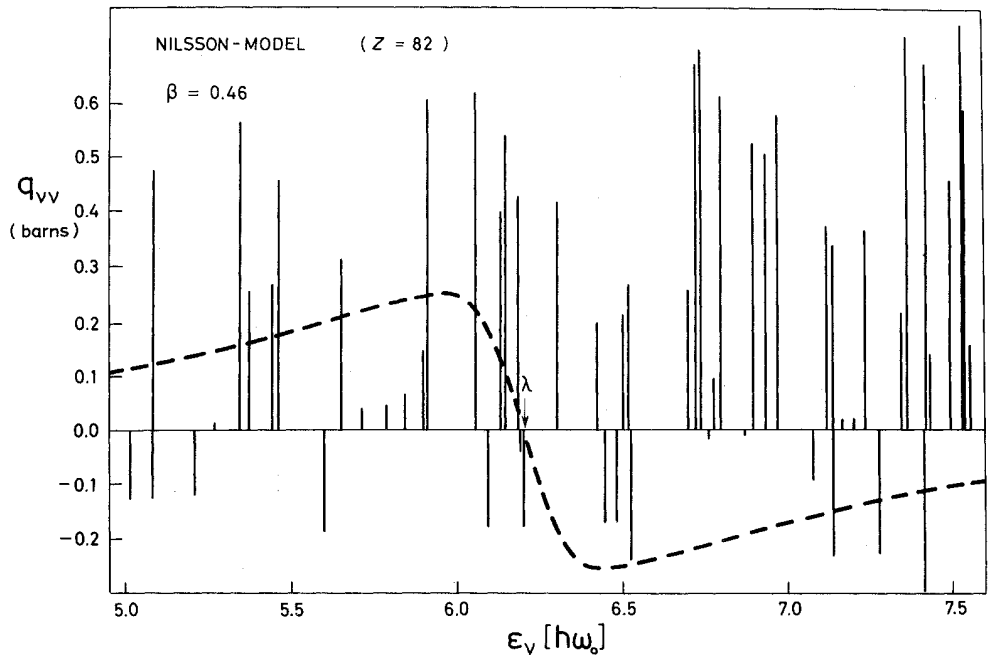

FIG. IV-6. The same as Fig. IV-5, but for the single-particle quadrupole moments $q_{\nu\nu}$. Only the case of $Z=82, \beta=0.46$ is shown, which is the same as case A, upper part in Fig. IV-5. Note the predominance of large positive values of $q_{\nu\nu}$, which is due to the prolate deformation of the average field.

It should be noted that, contrary to the total energy of the nucleus, the spatial density distribution does not have the property of being stationary against small variations of the density matrix. Therefore, the results presented below do not pretend to accurately reproduce the real density distribution in the nucleus. This is even more true as we shall consider the fluctuations of the shell-model density, denoted $\delta\rho^S$ in Sec. III, and not the fluctuations of the self-consistent density, which is connected to $\delta\rho^S$ by Eq. (III.21). Nevertheless, it is of a certain interest to investigate more thoroughly the density distribution of the shell model. It was represented in Eq. (IV.36) as the sum of the energy-smoothed distribution $\tilde{\rho}$ and of $\delta\rho$ describing the variations due to the nonuniform energy distribution of the individual states. The comparison of the energy-smoothed distribution $\tilde{\rho}$ with the familiar Thomas–Fermi distribution is also of some interest.

Examples of density distributions and the shell corrections $\delta\rho$ are presented in Fig. IV-8. The proton densities of ^{208}Pb, calculated with the commonly used Nilsson model and a Woods–Saxon shell model are compared in this figure.

The thick solid lines represent the single-particle distribution functions $\rho_{\rm sh}(\mathbf{r})$ calculated as the "shell" sum over the single-particle densities of the occupied states. The dashed lines are the energy-smeared density distributions $\tilde{\rho}(\mathbf{r})$ obtained by means of Eq. (IV.32) with $\tilde{\gamma}=2\hbar\omega_0\approx 14$ MeV. In the lower part of Fig. IV-8, the spatial density corrections $\delta\rho$ are shown. The calculated $\delta\rho$ are found to be insensitive to the specific value of $\tilde{\gamma}$ and are rather similar for the two variants of the shell model, although there are some noticeable differences in their magnitudes. This resemblance appears in spite of the fact that the total densities $\rho_{\rm sh}$ and $\tilde{\rho}$ are quite different for the two models. Note

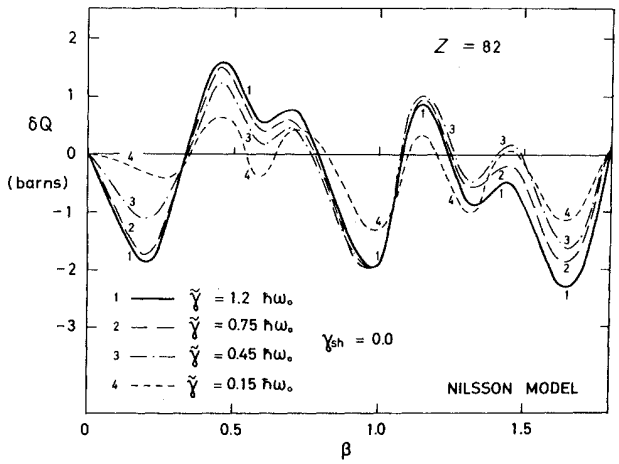

FIG. IV-7. The quadrupole moment δQ of the spatial density fluctuations, calculated with the Nilsson model ($Z=82$) for different values of the smearing parameter $\tilde{\gamma}$ ($\gamma_{sh}=0$). Starting from the smallest values of $\tilde{\gamma}$ (lines *4* and *3*), the full value of δQ is essentially reached for $\tilde{\gamma}=0.75\hbar\omega_0$.

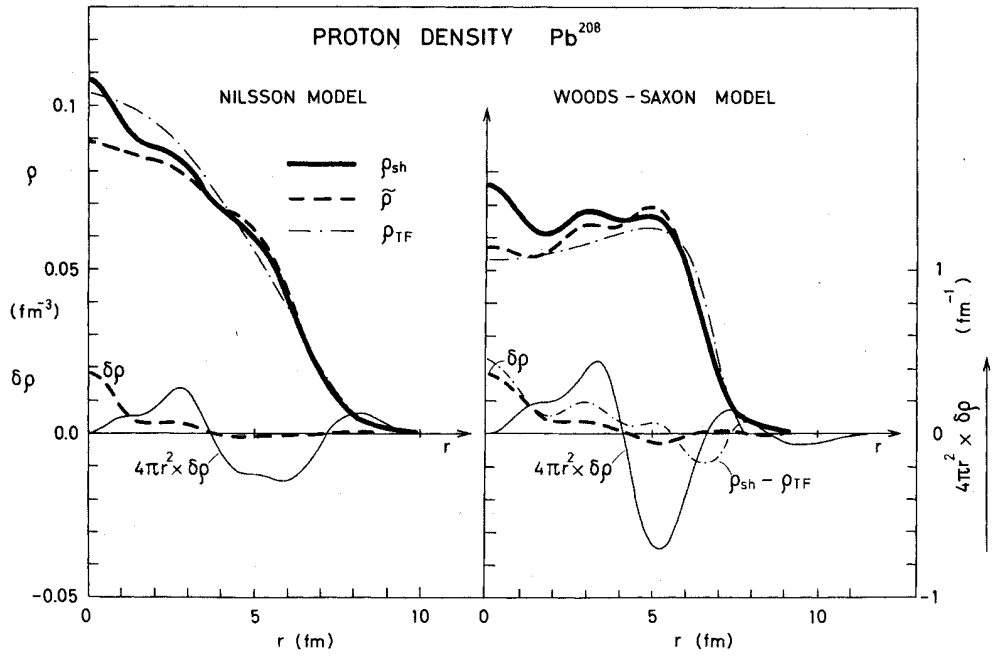

FIG. IV-8. Proton density distributions and their shell corrections $\delta\rho$ for ^{208}Pb, calculated for the Nilsson model and the Woods–Saxon model. The thick and the dashed curves represent ρ_{sh} ($\gamma_{sh}=0$) and $\tilde{\rho}$ ($\tilde{\gamma}=2.0\hbar\omega_0$), respectively. The Thomas–Fermi distributions ρ_{TF} (thin dash-and-dot lines) are calculated without the $\mathbf{l}\cdot\mathbf{s}$ term (and in the Nielsson case, without the $\mathbf{l}^2$ term) in the potential. (The Coulomb energy is included in ρ_{TF} for the Woods–Saxon curve). Note the very similar behavior of the curves $\delta\rho$ in both cases.

also that no Coulomb energy is contained in the Nilsson model; in the Woods–Saxon model it causes a clear rise of $\tilde{\rho}$ in the surface region.

The smoothed density $\tilde{\rho}$ describes the spatial nucleon distribution of the independent-particle model, smeared over the shell structure in the energy spectrum. Neither this definition of $\tilde{\rho}$ nor its role in the calculations of the energy shell corrections excludes that this quantity also may contain some oscillating component. The uniform distributions $\tilde{\rho}(\mathbf{r})$ in Fig. IV-8 were found, indeed, to have some oscillations, though, in the Nilsson model, these were much less pronounced than those of the total single-particle density $\rho_{sh}(\mathbf{r})$.

In the Woods–Saxon model, the oscillations of $\tilde{\rho}$ are more pronounced, while $\delta\rho$ oscillates less than the total density does. The same result was found in other spherical and deformed nuclei including shapes with very large distortions. This suggests that, in the Woods–Saxon model, distant shells contribute more appreciably to the single-particle density than they do in the Nilsson model or in the harmonic oscillator potential.

In order to compare the energy-smoothed density distribution $\tilde{\rho}(\mathbf{r})$ with the analogous Thomas–Fermi quantity, some special calculations were performed with simple shell-model potentials for which the Thomas–Fermi distribution could easily be found.

The Thomas–Fermi density is defined as

$$\rho_{TF}(\mathbf{r})=\rho_0[\lambda-V(\mathbf{r})]^{3/2}, \qquad \text{(IV.47)}$$

where ρ_0 is a normalization constant.

In general, the calculated energy-smeared $\tilde{\rho}(\mathbf{r})$ turns out to be close to the corresponding Thomas–Fermi distribution $\rho_{TF}(\mathbf{r})$. In the case of a pure harmonic oscillator potential, the two distributions are practically identical. The only difference is that $\rho_{TF}(\mathbf{r})$ has a finite maximal radius, whereas $\tilde{\rho}(\mathbf{r})$ has a "tail". This feature is seen in Fig. IV-9a where the calculated distributions for a magic number of nucleons are shown. In these cases, $\rho(\mathbf{r})$ has no oscillations at all and can hardly be distinguished from $\rho_{TF}(\mathbf{r})$ except for the tail. In the tail region, $\tilde{\rho}$ is so close to ρ_{sh} that the figure cannot show the difference. Addition of a spin–orbit term to the harmonic oscillator potential does not change $\tilde{\rho}(\mathbf{r})$ (cf. Fig. IV-9b). The insensitivity of $\tilde{\rho}(\mathbf{r})$ to the spin–orbit term was found also in the case of a Woods–Saxon potential.

The only difference between the two potentials used in Fig. IV-9b and Fig. IV-8a is the presence of the $\mathbf{l}^2$ term in the Nilsson potential. It is clearly seen that this term brings the averaged distribution $\tilde{\rho}$ closer to a Woods–Saxon density distribution: the density at the

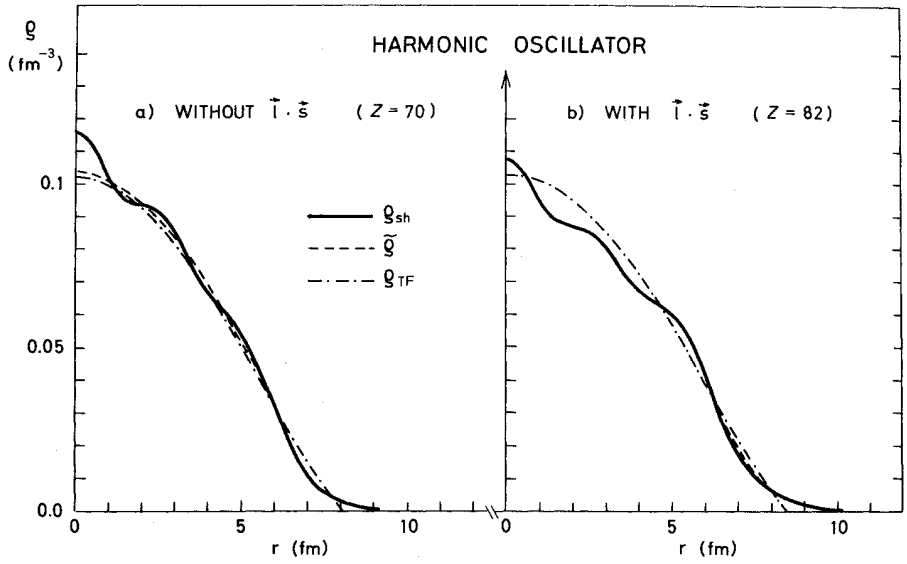

FIG. IV-9. Proton density distributions for (a) a purely harmonic oscillator potential and (b) a harmonic oscillator with spin–orbit interaction calculated for a magic number of nucleons. (Notation and parameters as in Fig. IV-8.) The curves for $\tilde{\rho}$ and ρ_{TF} are very close in case (a) and they completely coincide in case (b), except for the region $r \geq 6$F. Note that the density ρ_{sh} obtained for a harmonic oscillator with only $\mathbf{l}\cdot\mathbf{s}$ interaction (case b) is the same as in the case with an additional $\mathbf{l}^2$ in the potential (Fig. IV-8).

center is lowered as compared to that at the surface region.

Contrary to that, the single-particle density ρ_{sh} is, in the case of $Z=82$, not affected by the $\mathbf{l}^2$ term. This is because with $\mathbf{l}$ being a good quantum number in the spherical case, it changes neither the wave function of the individual states nor the occupied states and, therefore, the total density remains the same. The energies of the single-particle states, however, are affected and therefore the weights which appear in the evaluation of $\tilde{\rho}$ are different, resulting in a change in $\tilde{\rho}$.

The remaining oscillations in $\tilde{\rho}$ mentioned above are found to be most pronounced in the Woods–Saxon model. They seem to become stronger, the steeper the potential well is at the surface. The oscillations of $\tilde{\rho}$ are not related to the degeneracy of the subshells in the spherical case, because they are equally pronounced in the deformed Woods–Saxon potential. As all occupied states contribute to $\tilde{\rho}$ (in contrast to $\delta\rho$), it seems important that different shells have the same radius in a potential with steeper walls. In fact, it is reasonable to assume that this effect is a characteristic feature of the independent-particle distribution near the walls of a steep reflecting potential, where all individual wavefunctions are in phase. A more detailed discussion of this point is given by Kolomietz *et al.* (1971).

The residual oscillations in $\tilde{\rho}$ have no influence on the smooth behavior of quantities such as $\tilde{Q}$ or the uniform single-particle energy $\tilde{U}$. Considered as functions of the nuclear shape, these latter quantities do not exhibit any significant oscillations.[5] Thus it seems reasonable to assume that this residual effect in $\tilde{\rho}$ disappears when some additional averaging is present, as, e.g., the integration in Q or a variation of the radii in different shells distant from the Fermi level.

Anyway, we assume that these fluctuations in $\tilde{\rho}$ are not significant for δU, which is the quantity of interest.

One should recognize that the shell effects in the spatial density distribution will be counteracted by residual interactions which tend to restore a constant density. This is of course only true for the fluctuation of the real self-consistent density, which is related to the shell-model density fluctuation by Eq. (III.21).

However, even a relatively strong interaction is not expected to change the qualitative character of the density oscillations represented by the density correction $\delta\rho$. This is because the characteristic energy interval of the shell distribution is of the order of 7–10 MeV, and it would require a very strong mixing to wash out the shell-structure effect near the Fermi energy. This would account also for the role of the virtual and real excitations in the electron scattering process.

In particular, the amplitude of the oscillations of $\delta\rho$ in the presence of a strong pairing force is reduced by a factor of up to 2, but the qualitative behavior as well as the positions of the nodes of $\delta\rho$ remain unchanged.

Some calculations of the electron scattering cross section were performed for the case of lead-208, in which the spatial density distribution used was obtained by adding $\delta\rho$ to the smooth phenomenological distribution. Preliminary results indicate that the oscillations represented by $\delta\rho$, although weaker than in the single-particle density ρ_{sh}, are still too strong. This result is consistent with the investigations on the size of the so-called $(\delta\rho)^2$ term. Also there we came to the conclusion that the amplitude of $\delta\rho^S$ is considerably larger than the one of the self-consistent density.

[5] This may not be true, however, in the case of a "poor" volume conservation.

It is likely that the use of the phenomenological density-dependent interaction, which hinders large-scale variations of the density, will improve the results. Such an interaction is known to improve greatly the results obtained by the Bruckner–Hartree–Fock theory; see, e.g., Negele, 1970.

V. EQUILIBRIUM DEFORMATIONS AND THE PAIRING CORRELATIONS

This section is devoted mainly to a discussion, kept in rather general terms, concerning the connection between level densities, pairing correlations, and the ground-state equilibrium deformations.

1. Equilibrium Shapes

As the lowest possible density of single-particle states at the Fermi energy—or lowest degeneracy in the sense described in Sec. II—is a characteristic feature of ground state shapes, the equilibrium deformations should coincide with the minima of the function $\delta g(N, \beta)$ calculated at the Fermi energy. Some contour maps of this function are shown in Fig. V-1. The experimental equilibrium deformations are not plotted in the figure because they depend significantly on more than one deformation parameter. This will be discussed below, and it will also be shown that the minima of $\delta g(N, \beta)$ in fact give a good representation of the experimental equilibrium deformations. The figure shows the results obtained in an actual calculation and will be used as a basis for a more general discussion. In Fig. V-2 the landscape of neutron and proton energy shell corrections are illustrated. This figure exhibits essentially the same features as those seen in the level density diagrams in Fig. V-1. The contour maps shown in Figs. V-1 and V-2 were evaluated using four variants of the Woods–Saxon shell model, namely, with parameters corresponding to neutrons and protons in ^{170}Yb and ^{240}Pu (see Table VIII.1). Actually, the level schemes obtained for these two nuclei may be used in broad regions of nuclei around them, in the same way as if we worked with, e.g., the Nilsson model. Although the parameters of the Woods–Saxon potential depend explicitly on Z and N, this dependence is weak and does not appreciably change the shell distribution near the Fermi energy. This feature can be seen by comparing the right- and left-hand side maps in Fig. V-1. The figures referred to above show the behavior of the different quantities for a one-parameter sequence of the nuclear shapes along the so-called liquid-drop valley, see Sec. VII. For small distortions, this corresponds approximately to quadrupole deformations. It may, however, not be sufficient to consider distortions of this type. Recently, it was found, both experimentally (Hendrie *et al.*, 1968) and theoretically (Nilsson *et al.*, 1969; Gareev *et al.*, 1969), that many ground-state shapes seem to involve an appreciable P_4-type component. The most direct experimental evidence came from detailed measurements of elastic α particle scattering cross sections, but also the presence of $l=4$ transitions between the levels in the lowest rotational band seems to be established.

These data are summarized in Fig. V-3 along with the calculated values based on the Nilsson model (Nilsson *et al.*, 1969). In this reference the theoretical values were obtained in two different ways, namely, by means of the traditional Mottelson–Nilsson prescription, i.e., by minimizing the total sum of the single-particle energies, and by the shell correction method. Good agreement with experiment was found in the latter case, while the values obtained by minimization of the single-particle energy sums are in clear disagreement with the empirical values. Thus, this result may also be considered as an additional evidence in favor of the shell correction approach. (For the quadrupole distortion of the ground-state shapes, the two methods give close results.) Although relatively small, corrections of the P_4 type in many cases lower the ground-state minimum of the deformation energy by up to 2 MeV, as compared to purely ellipsoidal deformations. This is the case in particular in the actinide region, see also Sec. VIII. Besides the Nilsson model calculations mentioned above, calculations of ground-state hexadecapole deformations have been performed successfully, using the Woods–Saxon model (Gareev *et al.*, 1970).

Using the deformed Woods–Saxon model adopted in this paper, we have also briefly investigated the equilibrium deformations in the rare-earth region.

In Fig. V-4, contour diagrams for a few nucleon numbers are shown, which give more detailed data concerning the energy corrections as functions of the two variables, $\mathbf{c}$ and h, representing respectively the elongation of the nucleus and the degree of necking-in (the meaning of these parameters is explained in detail in Sec. VII).

This parametrization of the nuclear surface was chosen because of its advantages in connection with fission problems. However, in earlier experimental as well as theoretical works concerning ground-state deformations, the nuclear surface was described by an expansion of the form

$$R=R_0[1+\beta_2 Y_{20}+\beta_4 Y_{40}+\beta_6 Y_{60}+\cdots].$$

Therefore, in order to be able to compare our results with those expressed in terms of the expansion coefficients β_2, β_4, etc., Fig. V-5 was drawn. It shows the connection between our parameters $\{\mathbf{c}, h\}$ and $\{\beta_2, \beta_4\}$.

As it seemed difficult to establish an analytic connection between the two sets of parameters, the figure was obtained by making a least-square fit of the parameters β_2 and β_4 in the equation above to our shapes described by $\{\mathbf{c}, h\}$. (Terms involving β_6 and so on are neglected). Using this connection, one easily obtains the β_2 and β_4 values corresponding to the minima of contour maps as those shown in Fig. V-4. The points

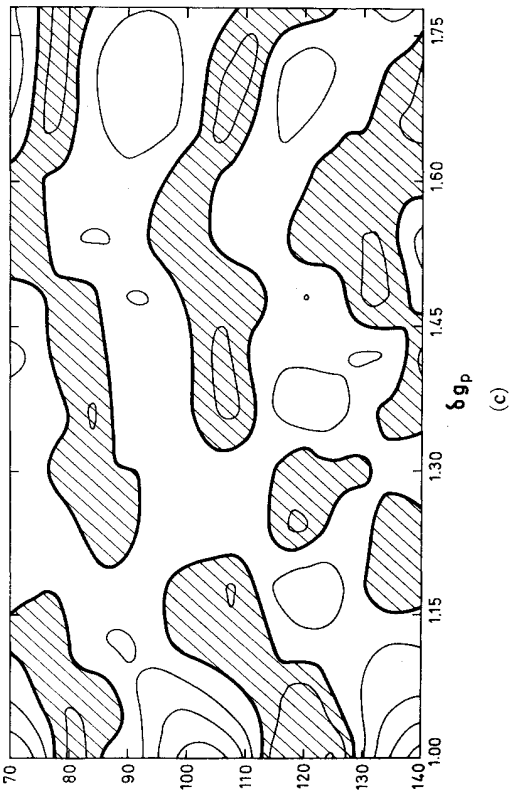
70
80
90
100
110
120
130
140
1.00
1.15
1.30
1.45
1.60
1.75
δg_p

(c)

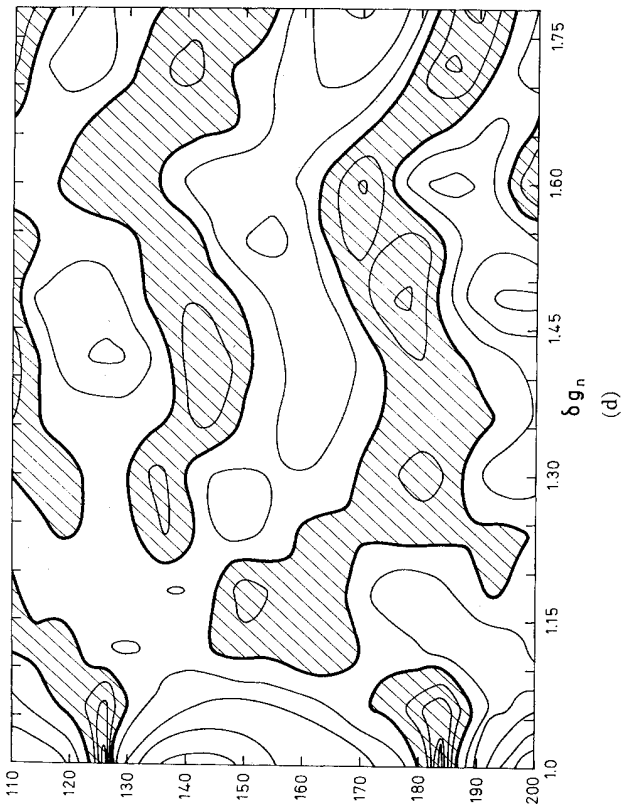
110
120
130
140
150
160
170
180
190
200
1.0
1.15
1.30
1.45
1.60
1.75
δg_n

(d)

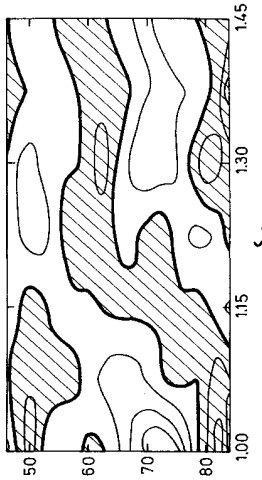
50
60
70
80
1.00
1.15
1.30
1.45
δg_p

(a)

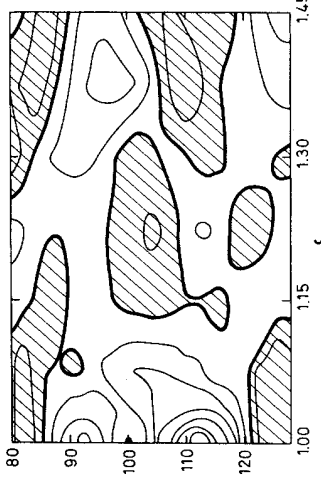
80
90
100
110
120
1.00
1.15
1.30
1.45
δg_n

(b)

FIG. V-1. Some contour maps of the function $\delta g(N, \beta)$. The nucleon numbers are along the ordinate, while a deformation parameter **c** is along the abscissa. As discussed in text, the figure has been made on the basis of only 4 Woods-Saxon spectra, namely ^{170}Yb protons (upper left), ^{170}Yb neutrons (lower left), ^{240}Pu protons (upper right), and ^{240}Pu neutrons (lower right). In all cases $\gamma_{sh}=0.2\,\tilde{\gamma}$ was used. The {**c**, h} parametrization (see Sec. VII) has been used to describe the nuclear shape. The contour maps are drawn for $h=0$, which for small deformations (**c** small) is approximately equivalent to quadrupole deformations (comp. Fig. V-5). The thick curves are zero lines and the increment per line is 0.2/MeV. The shaded areas have negative values of δg.

designated by crosses in Fig. V-3 have been obtained in this way. Normally the equilibrium deformations inferred from contour maps are rather well defined, but in some cases the minimum in the deformation energy is not clearly defined (see the ^{168}Er map in Fig. V-4) and no simple equilibrium configuration may be found.

As seen from Fig. V-3, the theoretical determined β_4 values agree quite well with the experimental data and with the results obtained in Nilsson *et al.*, 1969 once more indicating the relative insensitivity of the shell corrections to the specific nuclear model used.

In Fig. V-6, we show analogous results for β_6 values corresponding to equilibrium deformations in the rare-earth nuclei.

2. Shape Transitions and the Influence of Pairing

An interesting feature seen in both Figs. V-1 and V-2 is the presence of rather well-defined nucleon numbers, which separate regions of minima of spherical shapes and regions of deformed shapes. That is, in all nuclei with nucleon numbers near to spherical magic numbers, $\delta g(N, \beta)$ taken at the Fermi energy considered as a function of deformation, has its minimum for a spherical shape. But for nucleon numbers beyond the critical values, the minimum of this function occurs at a deformed shape. This is due to a redistribution of the shell closures, brought about by the formation of new shells in deformed nuclei, magic at $N=100$, 152, etc.

It is characteristic of nuclei with nucleon numbers equal to transitional values that in them essential shell structure near the Fermi energy develops neither at spherical nor deformed shape: The level density at the Fermi energy remains nearly constant for all not too large deformations. Consequently, the shell corrections remain small and the deformation energy stays close to the mean LDM value with the effect that the nuclear shape is relatively soft in these nuclei.

As the variation of the nuclear deformation energy for small deformations is mainly determined by the energy correction (see Sec. IV), the total deformation energy, in which the energy corrections are added to the LDM energy, also reflects the behavior of the energy correction described above. The critical nucleon numbers set the limits of the region of nuclei deformed in their ground states. In Figs. V-1 and V-2 we find the transitional numbers equal $N\approx 88$, 136, 196 for neutrons, and $Z\approx 56$, 88, 130 for protons. They agree rather well with values known from experiments.

Because the presence of the transition point is due to a change in the gross structure of the level distribution, it is independent of the residual interactions, and about the same transitional nucleon numbers are found in the contour maps of the energy corrections δU shown in Fig. V-7 evaluated with or without taking pairing correlations into account. However, in the latter case δU has some additional shallow minima, which occur for slightly distorted shapes and which are not found in the δg distributions; compare Figs. V-1 and V-2.

These secondary minima are due to grouping of the spherical levels in degenerate j states, i.e., the subshell structure. They disappear if this degeneracy is lifted by the presence of pairing correlations or any other residual interactions, which spoil the spherical symmetry of the average field and mix the independent-particle states over energy intervals comparable to intersubshell spacings of the order of 1 or 2 MeV. Consequently, the same result as obtained by taking pairing into account may be achieved in a formal way by artificially mixing the single-particle states, for example, using $g_{\rm sh}(\varepsilon, \beta)$ with a $\gamma_{\rm sh}=2$–3 MeV, which is slightly larger than in Eq. (IV.6).

Whenever either the strength of the pairing correlations or $\gamma_{\rm sh}$ is increased, the subshell structure disappears first, while the gross-shell effects remain until $\gamma_{\rm sh}\approx\tilde{\gamma}$, in which case the shells are completely smeared out. This difference in behavior of the shell and subshell structures, when the pairing strength is varied, is illustrated in Fig. V-8. The figure shows the changes in energy shell corrections $\delta U+\delta P$ brought about by varying the pairing strength, characterized by the parameter $\tilde{\Delta}$, whose physical meaning is that of the energy gap parameter for the smoothed energy distribution of the single-particle states. (Explicit definitions of δP and $\tilde{\Delta}$ are given in Sec. V.4.) The calculations have been done for several nucleon numbers, namely, for nearly magic numbers $N=86$, 120, a spherical mid-shell number $N=94$, and also for transitional nucleon numbers $N=88$, 90, 112–116.

The first thing we notice in the figure is the disappearance of the above-mentioned shallow minima in nearly spherical nuclei for rather weak pairing, somewhat smaller or equal to its empirical value $\tilde{\Delta}\approx 0.8$ MeV. In contrast hereto, the shell-structure minima and maxima remain, although their amplitude progressively decreases with the increase of pairing strength. For the largest value of $\tilde{\Delta}$ shown in the figure, the amplitude of the pairing correlations becomes comparable to the shell structure, and the shell correction then behaves rather erratically.

The influence of the subshell structure in nearly spherical nuclei on the equilibrium deformations is also

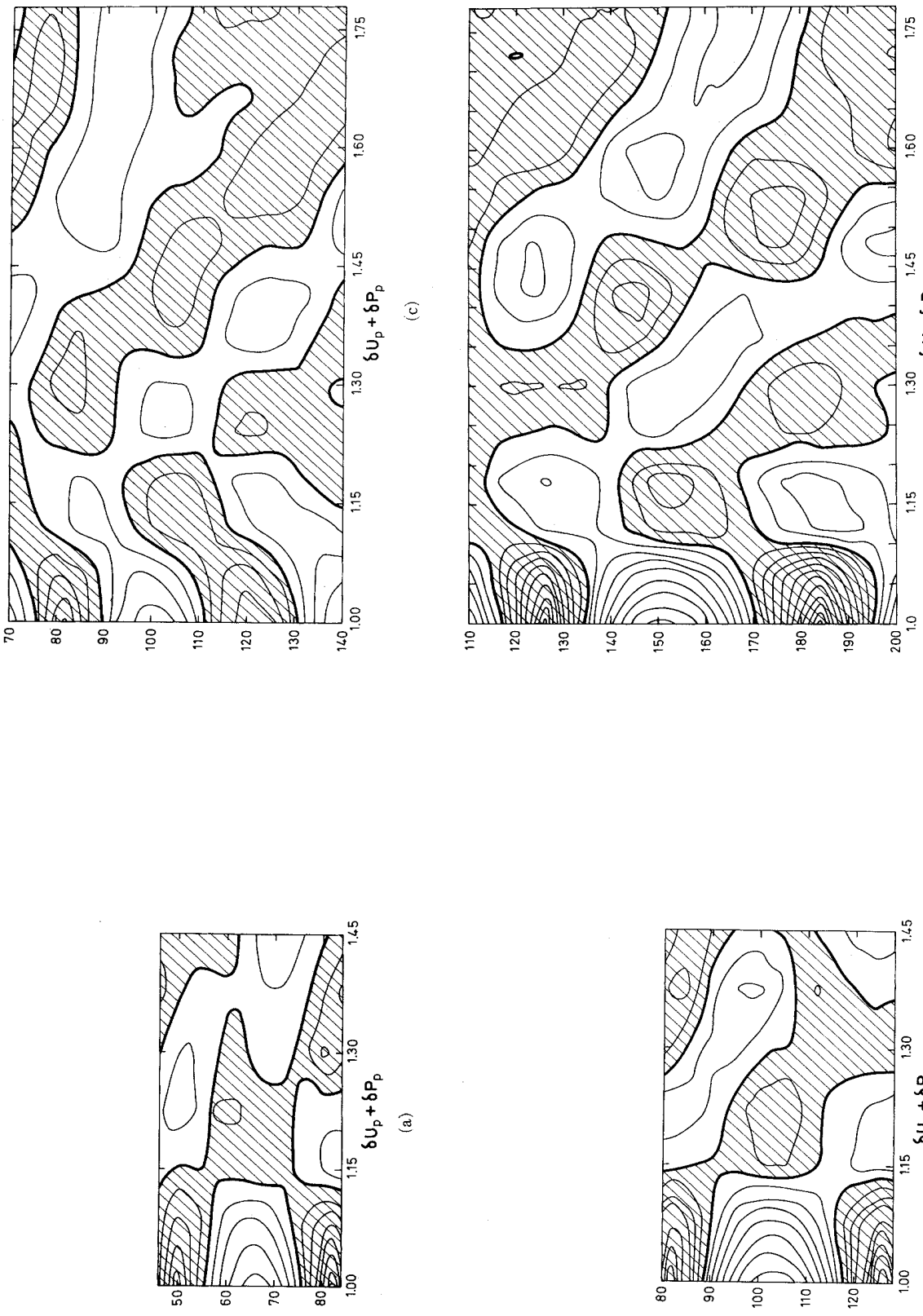

FIG. V-2. Contour maps of the energy shell correction corresponding to the maps in Fig. V-1. The thick curves are zero lines and the increment per line is 1 MeV. The shaded areas have negative values.

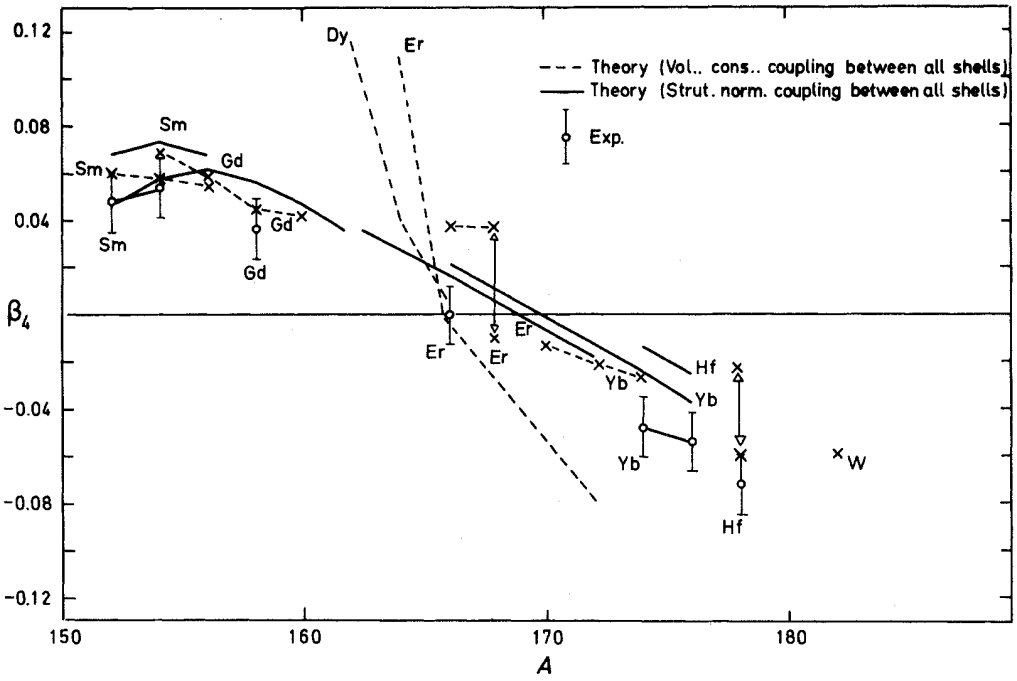

FIG. V-3. Experimental and theoretical β_4 values for ground-state shapes in the rare-earth region. The full lines and the dashed lines for Dy and Er are the results obtained by Nilsson *et al.* (1969) by the shell-correction method and the summation method, respectively. The crosses are the results obtained in this paper using a deformed Woods–Saxon potential. Note the uncertainty found, e.g., for ^{168}Er (compare Fig. V-4).

illustrated in Fig. V-9. There, for each neutron number between $N=82$ and 126 are shown the values of the quadrupole deformation parameter β_2* of the first minimum of the neutron shell correction $\delta U_n+\delta P_n$. The "transition" points from spherical to nonspherical equilibrium shapes, and vice versa, are clearly seen, and they remain practically unchanged even for unrealistically high values of the pairing strength. They change by only a couple of units of the nucleon number for the whole range of pairing strength from zero to $\tilde{\Delta}\approx 3$ MeV.

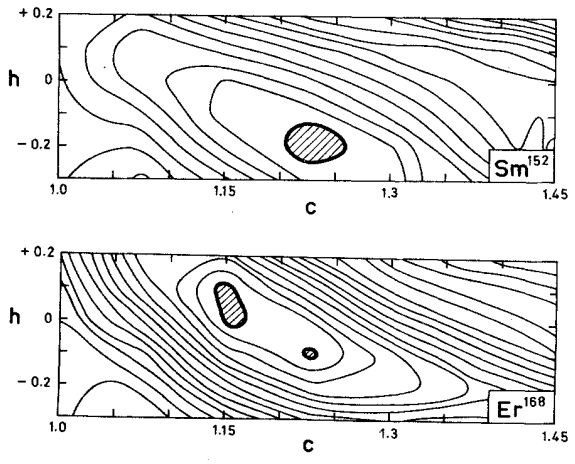

FIG. V-4. Contour diagrams of the total deformation energy for ^{152}Sm and ^{168}Er. The **c** and *h* are deformation parameters (compare Sec. VII). The LDM energy is normalized to be zero at spherical shape. Each contour line corresponds to an increment equal to 1 MeV. The deformation energy is negative in the shaded regions. In cases such as ^{168}Er no clear-cut ground-state deformations are found (see also Figs. V-3 and V-6).

In the figure it may also be noted that the presence of the transition points can be traced even in the data evaluated without pairing correlations ($\tilde{\Delta}=0$). It appears in a step-like change of the slope of the curve $\tilde{\Delta}=0$ at $N\approx 88$–90 and 114–116. This feature is not clearly seen if the single-particle proton and neutron energies are summed up (Mottelson and Nilsson, 1959). Some experimentally known equilibrium deformations are also shown in Fig. V-9.[6] They practically coincide with the values β_2* of the first minima of the neutron energy corrections $\delta U_n+\delta P_n$. This demonstrates that the shell closures occurring at these deformations in the neutron shell distribution are apparently most important in determining the equilibrium deformations. However, in many deformed nuclei in the rare-earth region, the proton shell closures occur at approximately the same deformation as those of the neutron shells. The depth of the ground-state minimum of the deformation energy is then increased, but its position remains unchanged.

[6] Taken from Coulomb excitation measurements and ignoring values of β_4, β_6 etc. different from zero.

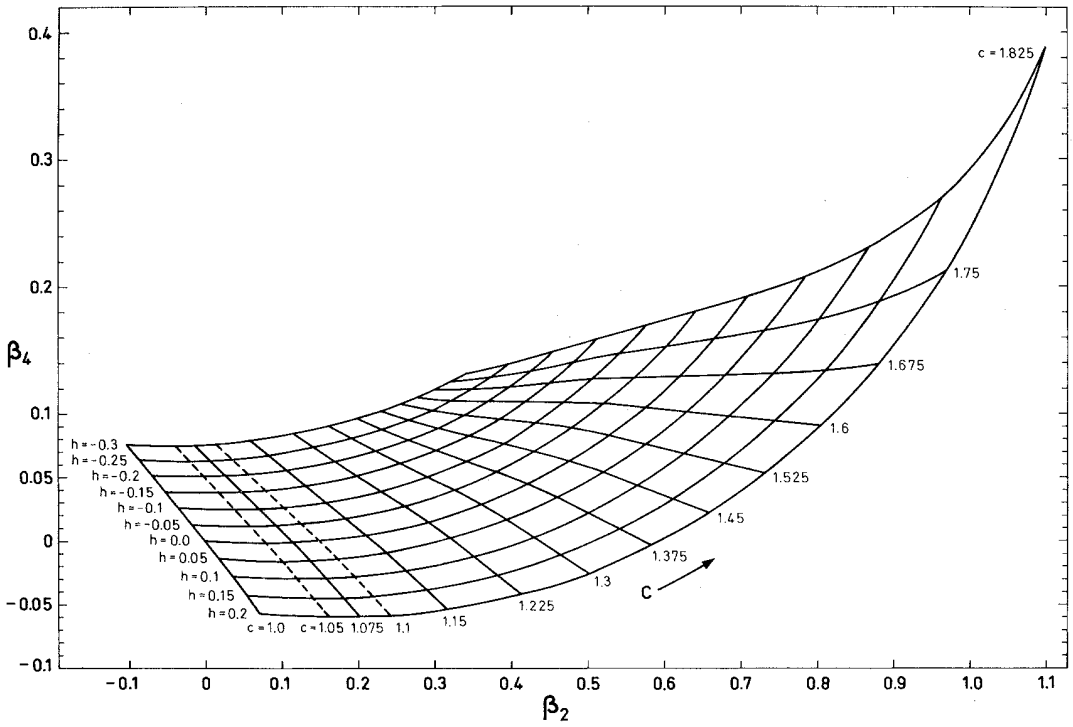

FIG. V-5. Relation between the parameters $\{\mathbf{c}, h\}$ and $\{\beta_2, \beta_4\}$

3. Comparison with Some Earlier Discussions

The results mentioned above seem to be in disagreement with a number of earlier conclusions (Belyaev, 1959; Bès and Szymánski, 1961). Therefore, in this section, we dwell on these discrepancies. With respect to the points relevant to this discussion, the conclusion reached in these earlier calculations may be summarized briefly as follows. The pairing correlations would have a great influence on the variation of the deformation energy and in particular would play a central role for the transition between spherical and deformed shapes, as the transition was predicted to take place when a certain occupation of a shell, proportional to the pairing

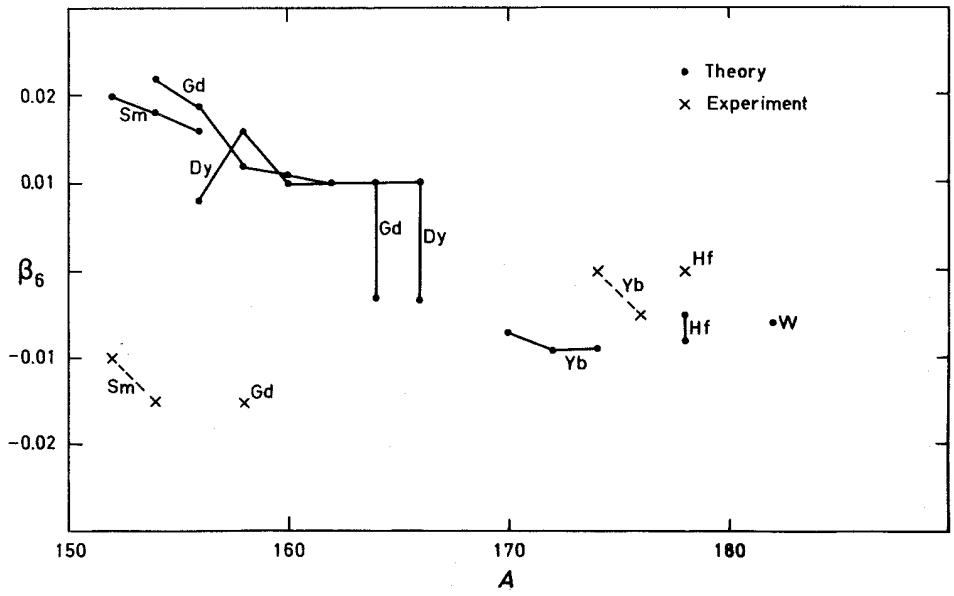

FIG. V-6. Similar to Fig. V-3 for our equilibrium β_6 values in the rare-earth region.

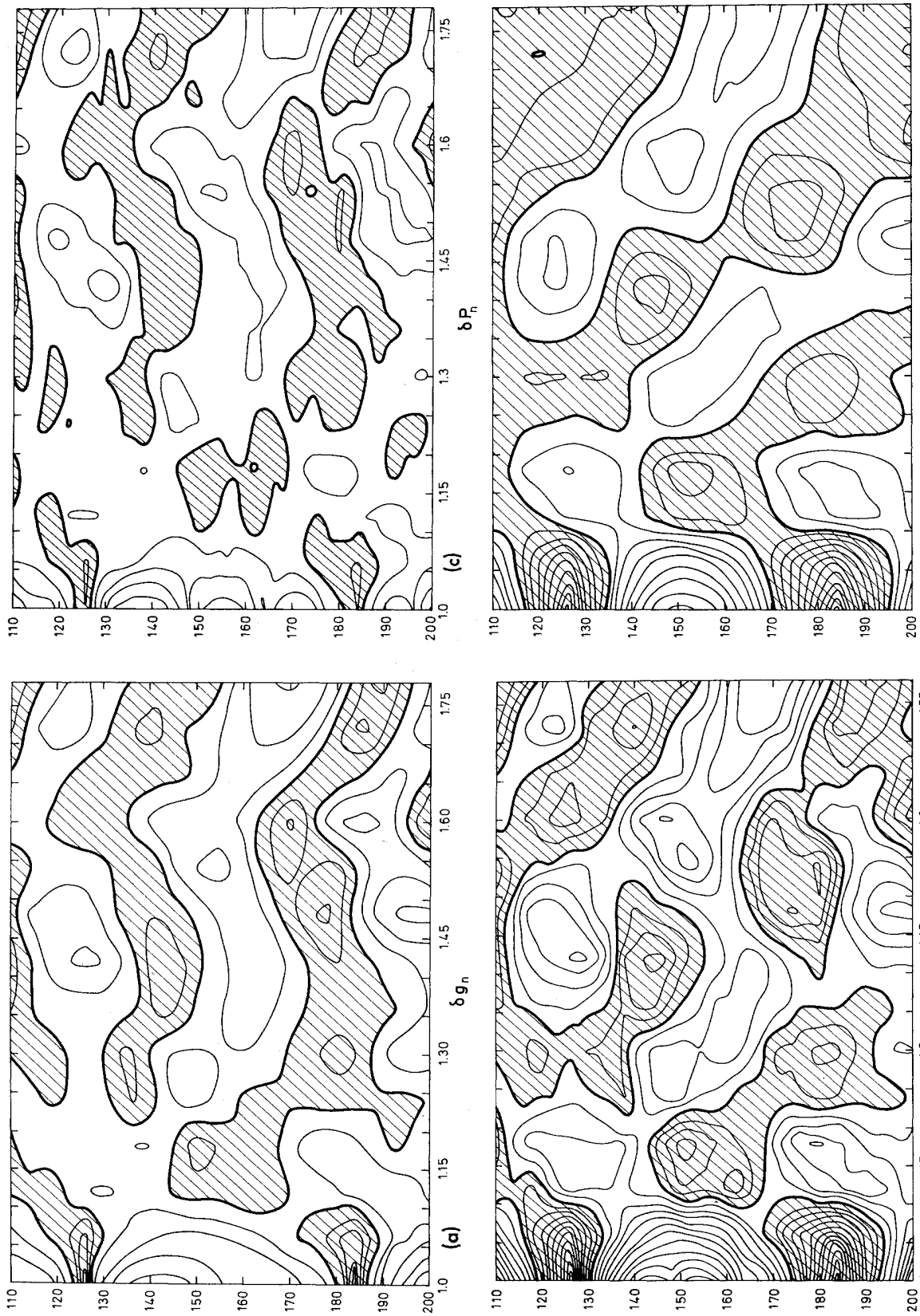

FIG. V-7. Figure showing the connection between contour maps of the quantities δg (upper left), δU (lower left), δP (upper right), and $\delta U+\delta P$ (lower right). The figure has been made on the basis of the neutron levels of ^{240}Pu as used in Figs. V-1 and V-2.

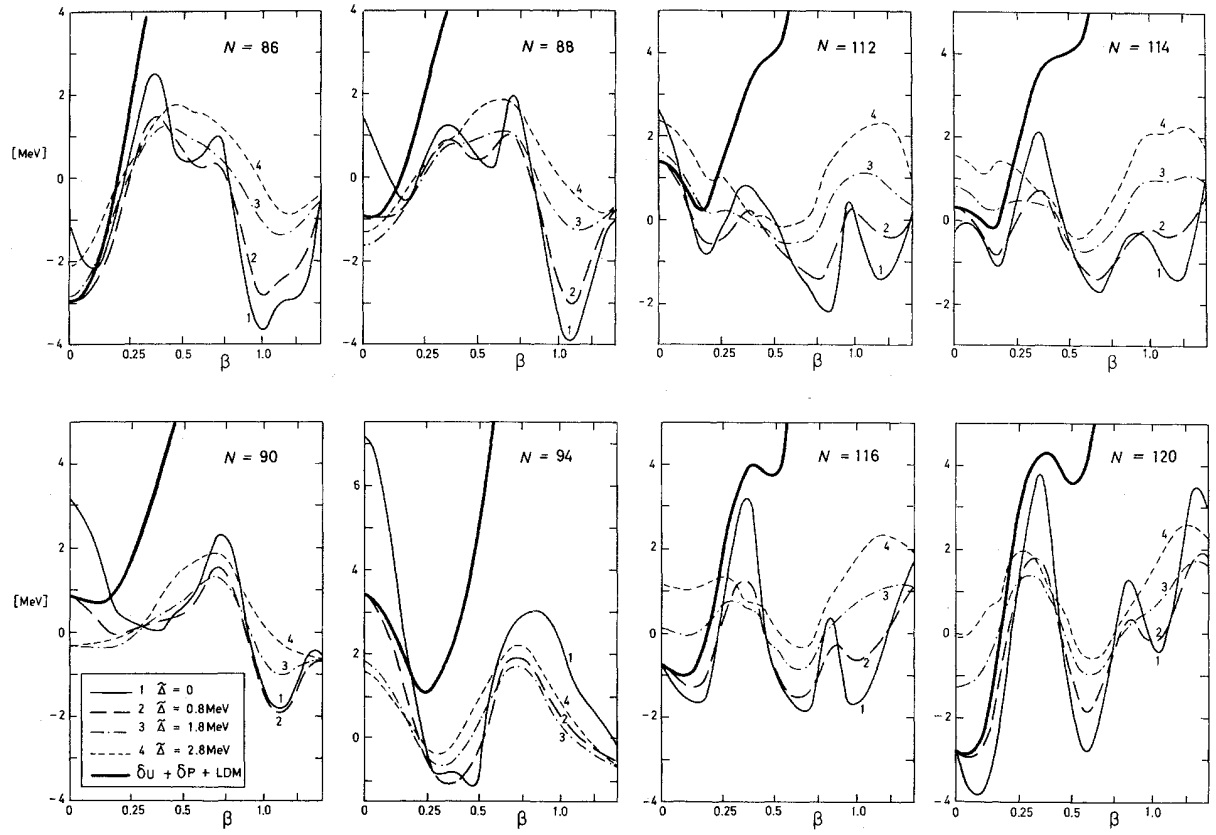

FIG. V-8. The influence of the pairing strength $\tilde{\Delta}$ on the energy shell correction $\delta U+\delta P$ for some nucleon numbers. The results are based on the Nilsson model. The deformation parameter β is defined in the caption to Fig. II-6. The thick full line shows the total deformation energy $LDM+\delta U+\delta P$ (with $\tilde{\Delta}=0.8$ MeV).

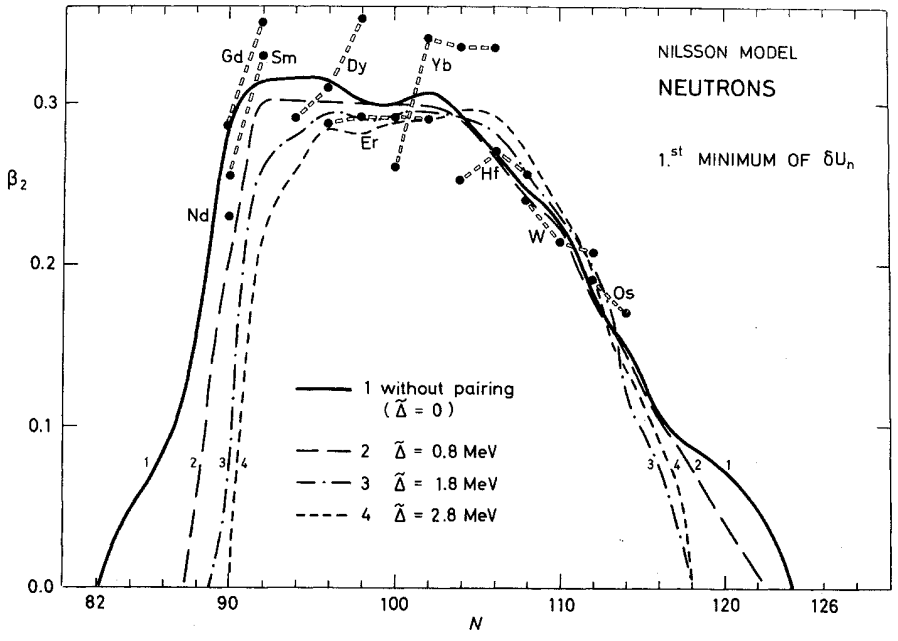

FIG. V-9. The variation in the position of the first minimum of the neutron shell correction $\delta U_n+\delta P_n$ brought about by varying the pairing strength $\tilde{\Delta}$. The Nilsson model was used as in Fig. V-8. Some experimental equilibrium deformations obtained by Coulomb excitation measurements are also shown.

strength, is reached. This conclusion was originally based on qualitative considerations using a simplified model of the competition between quadrupole forces and the pairing correlations within an unfilled shell. The "shell" was pictured as a highly degenerate spherical state, which splitted in a fanlike manner when the magic core was distorted (Belyaev, 1959). Such a model, in our point of view, not only exaggerated the role of the pairing correlations at smaller deformations; it also ignored decisive effects due to crossing of single-particle levels as well as formation of new shell closures in the deformed nucleus.

The importance of the pairing correlations in reducing the distorting effect of the unfilled shell is emphasized in the simplified model. However, real shells in nuclei consist of many degenerate states, each splitting in a fanlike way. Thus, even a very small distortion of the average field normally creates a rather random mixture of states, which by itself reduces appreciably the distorting effect of the unfilled shell already for small deformations. In fact, the crossings of individual states near the Fermi energy influence in a decisive way the distorting force arising in the unfilled shell, characterized by the quadrupole moment Q_λ of the unfilled shell in Belyaev (1959). This is so, because the two crossing levels have opposite slopes and, therefore, opposite signs of their quadrupole moments; at each crossing at the Fermi energy, the contribution of the occupied state to Q_λ changes its sign. This circumstance alone makes Q_λ a function of deformation determined by some average distribution of the level's slopes and the crossings, and by the variation of this distribution with deformation. However, in the simplified model, Q_λ was assumed constant in the absence of pairing.

The function $Q_\lambda(\beta)$ changes even its sign at certain deformations, when the levels of higher or lower shells systematically come into the vicinity of the Fermi energy and replace those of the original unfilled spherical shell. Consequently, the interaction energy of the core and the extra nucleons considered in the model (Belyaev, 1959)

$$H_{\text{int}} = \kappa Q_\lambda Q_{\text{closed}}, \qquad \text{(V.1)}$$

even in the absence of pairing correlations, becomes an oscillating function of the deformation. The presence of an inversion point of $Q_\lambda(\beta)$, where the restoring force determined by the interaction (V.1) changes its sign, will then determine the equilibrium deformation. The pairing interaction plays only a secondary role here, producing some additional smearing of the strengths of the individual states.

Normally, the degeneracy of spherical levels plays no significant role except at meaningless deformations formally as small as $A^{-2/3} \approx 0.03$–0.05%. However, this degeneracy becomes significant at the edges of the gross shells, where the distorting effect of the few last spherical single-particle levels is not weakened by crossings with the other levels until at a relatively large deformation, where levels of the next shell approach the Fermi energy. Therefore, the distorting power of only a few particles or holes outside the closed shell is sufficient to produce a relatively large deformation in the transition region; compare e.g., the contour maps of δU in Figs. V-1 and V-2.

In contrast to the qualitative considerations referred to above, the level crossing effect was implicitly included in actual calculations of equilibrium deformations by minimizing the sum of single-particle energies, when one assumed at each deformation all states below the Fermi energy to be filled. Consequently, good agreement with the empirical values was obtained already in the very first simple calculations of this kind, with a rather poor version of the Nilsson model and not taking into account such, presumably, essential factors as the pairing correlations and the Coulomb forces (Mottelson and Nilsson, 1959). Actually, when in some later calculations the pairing correlations and the Coulomb energy were taken into account, the equilibrium deformations were found almost unchanged.

As the above-mentioned qualitative considerations had pointed to a large influence of the pairing correlations, this was an unexpected result. Some authors have drawn the conclusion that the result was due to a mutual compensation of the two factors (Nilsson *et al.*, 1969). Such a conclusion seems not convincing to us. We feel that all results of concrete calculations point to the conclusion that neither the pairing correlations nor the Coulomb forces are as important for determining the equilibrium shape as the formation of "magic" shell closures in the mid-shell nuclei at a deformation $\beta \approx 0.2$–0.3.

One of the essential difficulties of the summation method is that all occupied single-particle energies contribute to the deformation energy, and therefore, all model-dependent errors in the single-particle level distribution add, so that their total may be considerably larger than the expected effect due to single-particle structure. The latter amounts only to a few MeV modulation of the nuclear deformation energy compared to a background energy in the GeV region. Furthermore, it remains unclear to what extent the model is able to reproduce such quantities as the volume and the surface energy.

Actual calculations employing the summation of single-particle energies clearly show these difficulties. The instability of the method to small changes either in the volume conservation condition (Strutinsky, 1968) or in the potential (Quentin and Barbinet, 1970) has been pointed out. Furthermore, an attempt to improve the volume conservation failed to predict even the ground-state deformations (Albrecht *et al.*, 1970), and calculations using an approximately self-consistent potential, with respect to quadrupole deformations, failed badly at large deformations (Belyakov, 1964).

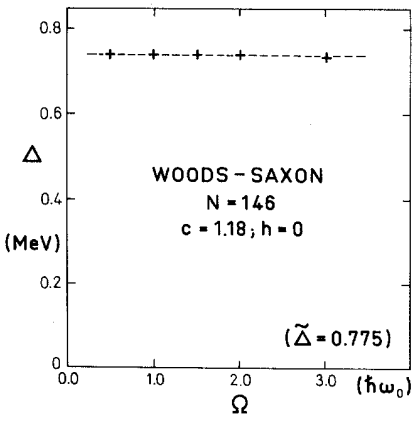

FIG. V-10. Figure showing that Δ is nearly independent of the cutoff parameter Ω.

Other attemps to describe the total energy at large deformations, using the summation method, have also failed, since they were not able to reproduce even qualitatively the fission barriers (Szymánski, 1961; Gustafson *et al.*, 1966).

The arguments above exhibit clearly a correspondence between our approach and the original ideas of the unified model. In fact, the renormalization of the shell-correction method may be considered a version of the unified model approach, in which the distinction between the core and independent nucleon features is based on a different principle. Thus, the quantity δQ introduced in the shell-correction calculations plays a role which in many respects is analogous to the one played by the quadrupole moment Q_λ of the unfilled shell in the unified model, and the same is true for the LDM part whose role is analogous to that of the magic core. The resemblance is especially clear at smaller deformations (Strutinsky, 1968). In particular, the relationship between the shell undulations quadrupole moment δQ and the shell force is qualitatively the same as was assumed in the unified model, (Secs. II and IV), although the specific definitions of the shell-correction quantities are different in many respects, too.

4. Renormalization in the BCS Theory

In our calculations, the pairing correlation energy was evaluated according to the commonly used prescriptions of the BCS approach. We have found it very useful, however, to apply the idea of a renormalization based on the extraction of a smooth part also to the calculations of the pairing energies (Strutinsky, 1968). In this way, one evaluates only the essential variations of the energy gap Δ and the pairing energy due to the shell structure, while the same quantities for a uniform model distribution of the single-particle states are described phenomenologically by means of the smoothed distribution gap parameter $\tilde{\Delta}$. The use of $\tilde{\Delta}$ as an input parameter determining the intensity of the pairing correlations was found very convenient because the value of $\tilde{\Delta}$ varies relatively little throughout the Periodic Table, and it is easy to find a good approximation for it. In fact, using the relation

$$\tilde{\Delta}=(12.0/A^{1/2})\ \text{MeV} \tag{V.2}$$

gives good agreement, throughout the Periodic Table, between the calculated values of the energy gap Δ in specific nuclei and the values deduced from experiment (see also Nilsson *et al.*, 1969).

The main advantages, however, in using $\tilde{\Delta}$ as a parameter are that it absorbs the divergency characteristic of the BCS theory and that it appears to be the only essential parameter in the treatment of the pairing correlations. Such a treatment usually requires two parameters, namely, the effective strength of the interaction G and the number of states n_c affected by the interaction. The latter parameters have no unique physical meaining and it is difficult to connect them in such a way that for several nuclei one gets reasonable values of Δ.

We start with the following BCS equation

$$2/G=\sum_\alpha{}'[(\mathcal{E}_\alpha-\lambda)^2+\Delta^2]^{-1/2},\qquad \sum_\alpha{}'=\sum_{\alpha=n-n_c}^{n+n_c} \tag{V.3}$$

and

$$\frac{2}{G}=\int_{\tilde{\lambda}-\Omega}^{\tilde{\lambda}+\Omega}\frac{\tilde{g}(E)\,dE}{[(E-\tilde{\lambda})^2+\tilde{\Delta}^2]^{1/2}}\approx 2\tilde{g}(\tilde{\lambda})\ln\left(\frac{2\Omega}{\tilde{\Delta}}\right), \tag{V.4}$$

where the integral is a uniform-distribution analog of the sum (V.3). In the integral (V.4), the cutoff energy Ω is related to the number of states $2n_c$ taken into account in the sum (V.3) by the relationship

$$2\Omega=2n_c/\tilde{g}(\tilde{\lambda}), \tag{V.5}$$

where $\tilde{g}(\tilde{\lambda})$ is the average level density at the Fermi energy. The BCS equation must be solved with the constraint that the particle number

$$N=2\sum_\nu v_\nu{}^2 \tag{V.6}$$

is conserved. Here, we have

$$v_\nu=\left(\tfrac{1}{2}\{1-(\mathcal{E}_\nu-\lambda)/[(\mathcal{E}_\nu-\lambda)^2+\Delta^2]^{1/2}\}\right)^{1/2}. \tag{V.7}$$

Equation (V.6) together with (V.3) determines the two parameters Δ and λ in terms of the pairing strength and the cutoff parameter n_c.

Both Eqs. (V.3) and (V.4) diverge logarithmically, which leads to familiar inconveniences of the BCS theory. Therefore, instead of using these equations directly, we now consider the difference

$$\sum_\alpha{}'[(\mathcal{E}_\alpha-\lambda)^2+\Delta^2]^{-1/2}-2\tilde{g}(\tilde{\lambda})\ln(2\Omega/\tilde{\Delta})=0, \tag{V.8}$$

where the two cutoff parameters n_c and Ω are connected by (V.5). In the difference, the parameter G is not present and, furthermore, it is seen that the divergency

in each of the terms in (V.8) cancel in the difference. Consequently, the quantity of interest, Δ, is now found to be a function of the only parameter Δ. The specific values of the cutoff parameters n_c and Ω have no significance provided that $\Omega \gg \tilde{\Delta}$.

As an illustration we present Fig. V-10, where it is seen that the change in Δ, brought about by varying the cutoff by more than a factor of four, is negligible. Furthermore, the energy gap Δ is practically a linear function of $\tilde{\Delta}$ (see Fig. V-11) as long as one chooses $\Omega \gg \Delta$. In our calculations, we have fixed Ω to have the order of intershell spacing, i.e., $\Omega = 10$ MeV, and the quantities Δ, λ, and $\tilde{\lambda}$ are found by an iteration method[7] described in Baranger and Kumar, 1968. As the inclusion of the pairing correlations has practically no effect on the uniform Fermi energy $\tilde{\lambda}$, this quantity was found as in the pure independent-particle model, see Eq. (IV.10). The pairing quantities evaluated in this way were found to be in good agreement with the known experimental values (see also, Strutinsky, 1968). The pairing strength Δ varies significantly when comparing different nuclei in their ground state. It varies, for instance, by a factor of 2 over the rare-earth region. Furthermore, Δ varies with deformation when the nucleon numbers are kept fixed. These variations reflect the periodic behavior of the local level density at the Fermi energy. Small values for the pairing gap are obtained in the middle of the rare-earth and the actinide regions and also in spherical nuclei. This is always near the centers of the shell closures characteristic of deformed and spherical nuclei, where the level density is low.

Now, we define the energy P of the pairing correlations as the difference of the sums of single-particle energies evaluated with and without the pairing correlations. This quantity is found equal to

$$P = \sum_\nu \{(\varepsilon_\nu - \lambda) \operatorname{sign} [\varepsilon_\nu - \lambda_0] - [(\varepsilon_\nu - \lambda)^2 + \tfrac{1}{2}\Delta^2]/[(\varepsilon_\nu - \lambda)^2 + \Delta^2]^{1/2}\}, \quad \text{(V.9)}$$

analogous to Eq. (9) in Strutinsky (1967) where, however, the change of the Fermi energy due to pairing correlations was ignored. In Eq. (V.9), λ_0 is the Fermi energy for $\Delta = 0$, i.e., $\lambda_0 = (\varepsilon_n + \varepsilon_{n+1})/2$. The sum in (V.9) converges and no cutoff problem arises.

The shell correction in the pairing energy is now determined as

$$\delta P = P - \tilde{P}, \quad \text{(V.10)}$$

where $\tilde{P}$ is the pairing correlation energy for the uniform distribution

$$\tilde{P} = -\tfrac{1}{2}\tilde{g}(\tilde{\lambda})\tilde{\Delta}^2. \quad \text{(V.11)}$$

The variation of δP with the shape of the nucleus and with the nucleon number is similar to that of the other shell correction quantities. But the pairing is stronger, i.e., the energy P takes larger negative values, where the Fermi level density is increased ($\delta g > 0$) and is weaker or even becomes zero in regions of the shell closures ($\delta g < 0$). Its oscillations follow rather closely those of the energy correction δU and, when added to this quantity, the pairing correction smooths the shell oscillations of the deformation energy. It always remains smaller, however, than the shell effects in the deformation energy, and plays only a secondary role.

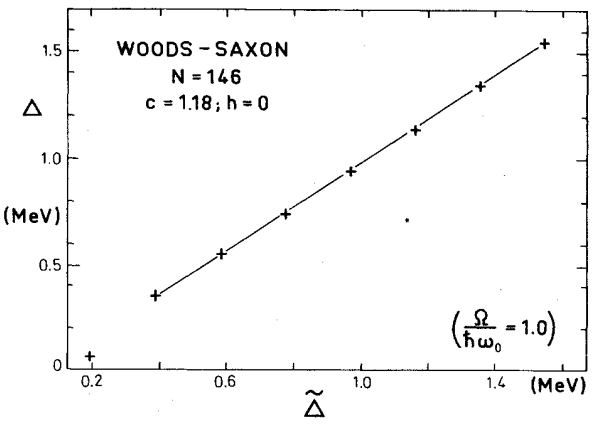

FIG. V-11. The gap parameter Δ as a function of the strength $\tilde{\Delta}$ keeping the cutoff parameter constant.

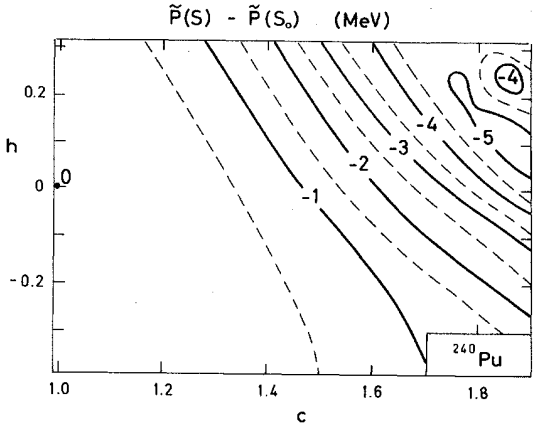

FIG. V-12. Contour map of the function $\tilde{P}(S) - \tilde{P}(S_0)$ appearing in Eq. (V.16). The map may be applied in a region around ^{240}Pu as $\tilde{P}(S) - \tilde{P}(S_0)$ changes only slowly with the nucleon numbers.

5. Surface-Dependent Pairing

It has been suggested recently that, for the pairing correlations, the region of the nuclear surface may be especially significant because the residual nucleon interaction is predominantly attractive there. The assumption of a surface-dependent pairing was extensively used

[7] The authors are indebted to Dr. K. Kumar for letting them use his computer code for solving the BCS problem.

by Nilsson *et al.* (1969). These authors have demonstrated that such an assumption makes no difference for smaller distortions as, e.g., for the ground-state deformation, but that it has an appreciable effect on the nuclear deformation energy at large distortions by lowering the energy, which may be an important factor in the theory of nuclear fission. So far one has no direct evidence for such an assumption, and the theoretical arguments are not too solid either. The well-established feature of empirical Δ values, that they decrease as the size of the nucleus increases, seems to contradict it, or at least to suggest that the situation is not so very simple.

However, in some of our calculations, we have included a surface dependence in the pairing. At the time this was done in the hope of reducing the heights of the so-called second barrier in the deformation energy of heavy nuclei, as described below. It was found later, however, that this effect may be achieved in a more natural way by other means; in particular, by introducing asymmetry in the nuclear shape at the second barrier.

In the surface-dependent pairing calculations, one assumes that the pairing coupling constant G is proportional to the surface area S (Nilsson *et al.*, 1969)

$$G \propto S/S_0 \tag{V.12}$$

where S_0 is the surface area of the nucleus with a spherical shape. Within our approximation, this is equivalent to the assumption that the average gap parameter increases from its spherical value $\tilde{\Delta}=\tilde{\Delta}_0$—given by (V.2)—rather appreciably with the increased surface at large distortions, i.e.,

$$\tilde{\Delta}=2\Omega(\tilde{\Delta}_0/2\Omega)^{S_0/S}. \tag{V.13}$$

Being a linear function of $\tilde{\Delta}$ (cf. Fig. V-11), the actual gap Δ will, on the average, behave in the same way. Now the question arises whether the surface-dependent pairing should be thought of as already taken into account in the phenomenological liquid-drop model. If this is assumed not to be the case, the nuclear deformation energy may be written

$$E_{\rm def}=P(S)+\delta U+\text{LDM}, \tag{V.14}$$

while the opposite assumption leads to

$$E_{\rm def}=P(S)-\tilde{P}(S)+\delta U+\text{LDM}. \tag{V.15}$$

In the latter case, the surface dependence would practically be confined to the LDM part, because the pairing energy $P(S)$ and its uniform part $\tilde{P}(S)$ vary in very much the same way, making the difference nearly independent of the nuclear shape.

We have found that the surface-dependence correction to the pairing energy contributes only to the smooth component of the deformation energy and, in the interesting region of large distortions of the actinide nuclei, affects it in exactly the same way as some change of the surface tension parameter in the LDM would do. Thus, it seems more reasonable to us, if the surface pairing should be considered at all, to assume that it is already included in a phenomenological way in the LDM. Since, however, so many unanswered questions are involved in the application of a surface-dependent pairing, in the sections below dealing with the behavior of the deformation energy at large distortions, we present only the results obtained with a constant pairing parameter $\tilde{\Delta}$. If required, the results can always be corrected for the surface pairing. For this purpose, we present in Fig. V-12 a contour map of the difference

$$\tilde{P}(S)-\tilde{P}(S_0)=-\tfrac{1}{2}[\tilde{g}_n(\tilde{\lambda}_n)+\tilde{g}_p(\tilde{\lambda}_p)][\tilde{\Delta}^2(S)-\tilde{\Delta}^2(S_0)] \tag{V.16}$$

considered as a function of the elongation parameter c and the neck parameter h of the nuclear shape.

VI. NUCLEAR MASSES IN THE LEAD REGION

As the shell-correction method may become an important tool for the calculation of nuclear masses, we shall try in this section to elucidate some points pertinent to such an application of the method.

1. Empirical and Theoretical Shell Corrections to Nuclear Masses

In Sec. II we have referred to the mass fluctuations in order to introduce the shell-correction method. Now, we return to this point and investigate whether this method is in fact able to improve the LDM fit to nuclear masses. The necessary procedure may be put as follows: Evaluate for some nucleus the ground-state deformation as described in Sec. V. Then, at this deformation, find the shell correction and add it to the liquid-drop mass. The question is then whether this total mass agrees better with the empirical one than does the liquid-drop mass alone.

Such an approach to nuclear masses has the advantage of relating the evaluated mass corrections directly to the distribution of single-particle states, i.e., to the spectroscopic experience and thus does not introduce additional parameters.

The separation of the empirical mass into a smooth average—given by the liquid-drop mass formula—and a remaining shell correction is somewhat ambiguous. However, the empirical shell corrections available in the literature (Myers and Swiatecki, 1966b; Zeldes *et al.*, 1967) are found relatively independent of the specific ansatz for the liquid-drop mass formula, and therefore may be regarded as more or less uniquely determined empirical data. An example, obtained by Myers and Swiatecki (1966b), is shown in Fig. VI-1. There, the difference between the experimental binding energies

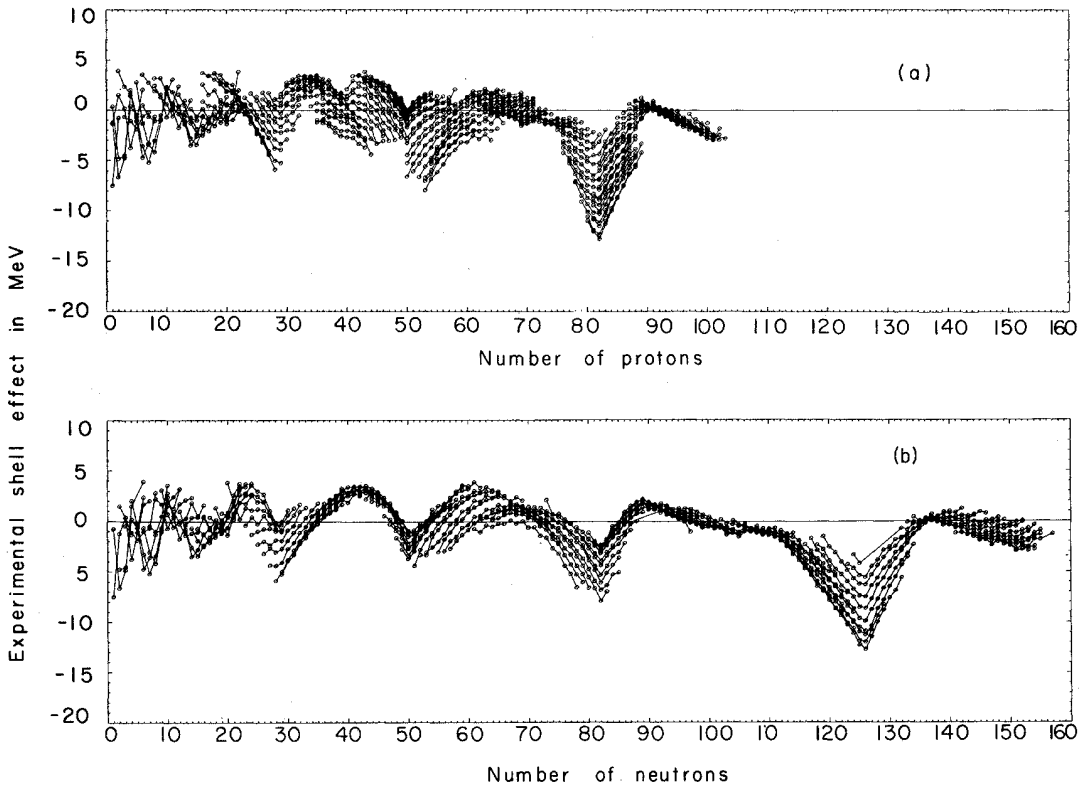

FIG. VI-1. Deviations of nuclear masses from the spherical *LDM* values, plotted as a function of neutron number N (lower part) and proton number Z (upper part) as found by Myers and Swiatecki, 1966a. We are indebted to W. D. Myers and W. J. Swiatecki for permitting us to use this figure.

and the calculated liquid-drop value, i.e.,

$$\Delta M_{\rm exp} = M_{\rm exp} - M_{\rm LDM}, \qquad \text{(VI.1)}$$

are plotted both as functions of neutron number N, and proton number Z; systematic odd–even effects due to the pairing interaction have been removed already. In this figure the same characteristic fluctuations of $\Delta M_{\rm exp}$ can be observed as in Fig. II-1.

The experimental mass correction $\Delta M_{\rm exp}$ is calculated by using a liquid-drop formula adapted to spherical nuclei. In deformed nuclei, the total energy also gets a contribution from the liquid drop, $\Delta M_{\rm LDM}(\beta)$ [see Eq. (VII.13)], and therefore the theoretical quantity to be compared with the shell correction $\Delta M_{\rm exp}$ is given by

$$\Delta M_{\rm th} = [\Delta M_{\rm LDM}(\beta) + (\delta U(\beta) + \delta P(\beta))_p + (\delta U(\beta) + \delta P(\beta))_n]_{\beta=\beta^*}, \qquad \text{(VI.2a)}$$

where the liquid drop deformation energy is defined by

$$\Delta M_{\rm LDM}(\beta) = M_{\rm LDM}(\beta) - M_{\rm LDM}(0). \qquad \text{(VI.2b)}$$

In Eq. (VI.2a), $\delta U(\beta)_{p,n}$ are the shell corrections as defined in Eq. (IV.11), and $\delta P(\beta)_{p,n}$ the pairing corrections as defined in Eq. (V.10) for protons and neutrons, respectively; all quantities should be evaluated at the ground-state deformation $\beta = \beta^*$.

It should be noted that by its very definition the quantity defined in Eqs. (VI.2) does not contain contributions from the leading spherical liquid-drop model terms. This allows a broad comparison with empirical mass corrections of many individual nuclei such as shown in Fig. VI-1. In the more usual microscopic theories such as the Fermi liquid approach of Migdal (1968), one is forced to consider more complicated combinations of individual masses in order to get rid of contributions of the liquid-drop model type.

To which assumptions are the computed mass corrections sensitive?—Let us start our considerations with the liquid-drop model part in Eqs. (VI.2). At the moderately small deformations of the nuclear ground states, the liquid-drop deformation energy $\Delta M_{\rm LDM}(\beta)$ is small compared to the leading shell-correction terms $\delta U + \delta P$. Therefore, we may confine ourselves to a rather simple expression of the liquid-drop formula, having only a Coulomb and surface energy component without the refinements of e.g. the droplet model (Myers and Swiatecki, 1969) or a curvature dependence. For the

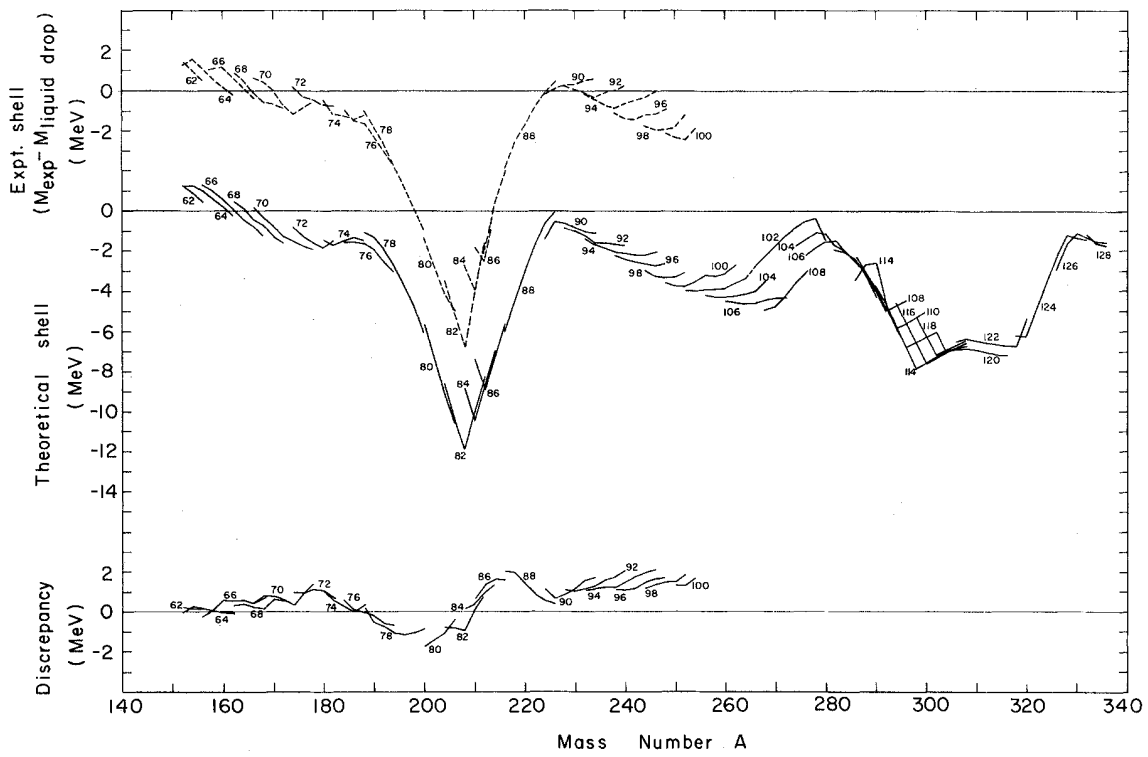

FIG. VI-2. The theoretical mass corrections obtained with one of the most recent versions of the Nilsson model are compared to the experimental values (Nilsson, Thompson, and Tsang, 1969). We thank these authors for giving us this figure.

discussion of the nearly spherical nuclei in this section, $\Delta M_{\mathrm{LDM}}(\beta)$ may be neglected.

As all of the available shell models (using different types of average potentials) are tailored to fit the sequence and the distribution of the levels around the Fermi energy, i.e. to fit the quantities on which the shell corrections depend, we would expect that the size and sign of the shell corrections to the ground-state masses are almost model independent. Though this argument will be discussed to some extent later in this section, it was strongly supported by the first calculations of this kind (Strutinsky 1967, 1968) in which a relatively poor version of the Nilsson model (Nilsson, 1955) was used. They demonstrated a clear correlation with the empirical data both in position and amplitude, as shown in Fig. II-1.

A calculation connected to the one proposed here, but with a somewhat different scope, has been done by Seeger and Perisho (1967). With a suitably chosen initial set of Nilsson model parameters, these authors first computed the shell corrections, then substracted them from the empirical masses, and fitted these supposedly smooth quantities with the parmeters of the liquid-drop model. They then iterated the Nilsson model parameters in order to fit the experimental masses. The values for which the rms deviation was minimized were close to the ones obtained from spectroscopic information (fit of single-particle states). A rather good fit was obtained for more than 1000 nuclei with an rms deviation of 0.6–0.7 MeV, an accuracy which competes with the more phenomenologically oriented approaches (Zeldes *et al.*, 1967; Myers and Swiatecki, 1966b). In the more recent calculations by Nilsson, Thompson, and Tsang (1969)—using the Lysekil version of the parameters for the Nilsson model (Gustafson *et al.*, 1966), the gross features of the experimental shell corrections are quite well reproduced, as can be seen in Fig. VI-2. There remain, however, some discrepancies. The smooth over-all trend with too small theoretical masses (LDM) is not so much a problem for the present discussion, and could certainly be improved by a new fit of the liquid-drop parameters. Its regular and oscillating structure, however, expecially around the doubly magic lead, is more intriguing since it must be correlated directly with the shell structure and the shell corrections.

Obviously, the spherically or near spherically magic nuclei play a special role in understanding the ground-

state mass corrections. In order to discuss the problem in greater detail, we shall restrict ourselves in the following to lead-208.

2. Shell Model Dependence of the Theoretical Mass Corrections

The experimental ground-state mass correction for lead-208, using the revised LDM formula of Myers and Swiatecki (1966b), is $\Delta M = -12.8$ MeV. The Nilsson model gives a result of -11.9 MeV (Nilsson, Thompson, and Tsang, 1969), while a Woods–Saxon potential, adjusted to fit the experimental positions of the single-particle subshells in lead, gives a significantly higher value (-17.6 MeV). Thus, the experimental value is rather well reproduced by the Nilsson model in spite of the fact that this model gives a very poor reproduction of the experimental single-particle levels in lead.

In order to understand this result, it may be of interest to know what the values of the shell corrections would be if the shell-model level distribution had reproduced exactly the empirical single-particle spectrum of lead. This can easily be checked by performing calculations with an artificial single-particle spectrum in which some of the single-particle energies are substituted for by their empirical values.

One may also perform calculations using directly the experimental single-particle energies. The possibility of making reasonable calculations with only a limited number of single-particle states follows directly from the conclusions reached in Sec. IV. There, it was shown that only an energy region ± 5 MeV around the Fermi surface contributes appreciably to the shell corrections. As the positions of a sufficient number of single-particle states in such an energy interval have recently been determined experimentally (see, e.g. Stein, 1969) calculations of this kind are quite feasible. For lead-208 such calculations result in a mass correction of $\Delta M_{\text{th}} = -20.6$ MeV. This value exceeds the experimental one by more than 7 MeV, a discrepancy which cannot possibly be due to the approximation made by using a limited set.

However, it may not be so surprising as it seems that the value of ΔM obtained on the basis of the experimental spectrum differs significantly from the experimental value. An explanation as to why apparently still "imperfect" shell models might do well in shell-correction calculations may be found in the arguments given in Sec. III. There it has been shown that not the realistic self-consistent energy spectrum of the single-particle states, but rather the shell-model spectrum, is to be used in the shell-correction approach. Indeed, even for the best possible shell-model potential, i.e., the one deviating the least from the actual nuclear field, there must always be some difference between the shell-model energies and the actual single-particle energies due to nonsmooth terms in the real nuclear average potential. Considering the effect of this difference, one comes to the conclusion that if the actual single-particle energies were used in the calculations, then the fluctuating part of the average potential energy should be taken into account as well, see Sec. III.

Thus, the quality of the shell-model potential used in shell-correction calculations should not be judged by the accuracy reached in reproducing the positions of the individual single-particle states in real nuclei. And one should not be discouraged by the fact that none of the existing variants of the shell model reproduces the positions of the empirical single-particle states with the desired degree of accuracy. It seems more justified to require that the shell-model distribution should reproduce some important quantities related to the single-particle state distribution averaged over the essential shell intervals.

As such properties it seems sensible to consider quantities like the average distance between the mean energies of the major shells and their dispersion relative to these energies. Calculating these quantities in a number of existing single-particle potentials it has been found, that there are, in nearly all cases, an appreciable discrepancy in the difference between the mean energies of the theoretical gross shells adjacent to the lead-208 gap. This difference is systematically larger than the experimental value. At the same time, the theoretical shells are significantly broader. These features are especially pronounced in the neutron case, where the mean distance between the shells equals ~ 7.5 MeV, compared to the value 6.5 MeV evaluated for the experimental single-particle level distribution in the lead region. A better agreement was found for models using a radius for the neutron well, considerably larger than that used in determinations of spectroscopic factors (see Rost, 1968; Batty and Greenless, 1969; and Batty, 1970). Another way to achieve the same result is to take the effective nucleon mass larger than the free mass. This may be justified by the residual particle–hole interaction (see, e.g., in Brown, 1969) or by the recent self-consistent field calculations with a modified effective δ interaction (Vautherin and Brink, 1970; Moskowski, 1970). Actually, with the normal value for the radii, the use of a neutron or a proton mass higher than the free nucleon mass by 20% and 5%, respectively, is sufficient to improve the agreement with the experimental level distribution.

In order to illustrate this point, we show in Fig. VI-3 a comparison between the results obtained with and without the use of an effective nucleon mass. In that figure, case (A) shows the single-particle spectra obtained with the Woods–Saxon potential ordinarily used in our calculations. This potential is described in detail in Sec. VII below. In case (B), the spectra resulting from the use of an effective mass are presented; in case (C), the spectra of the Nilsson model; and finally in case (D) the experimentally observed level distributions of protons and neutrons are shown. In

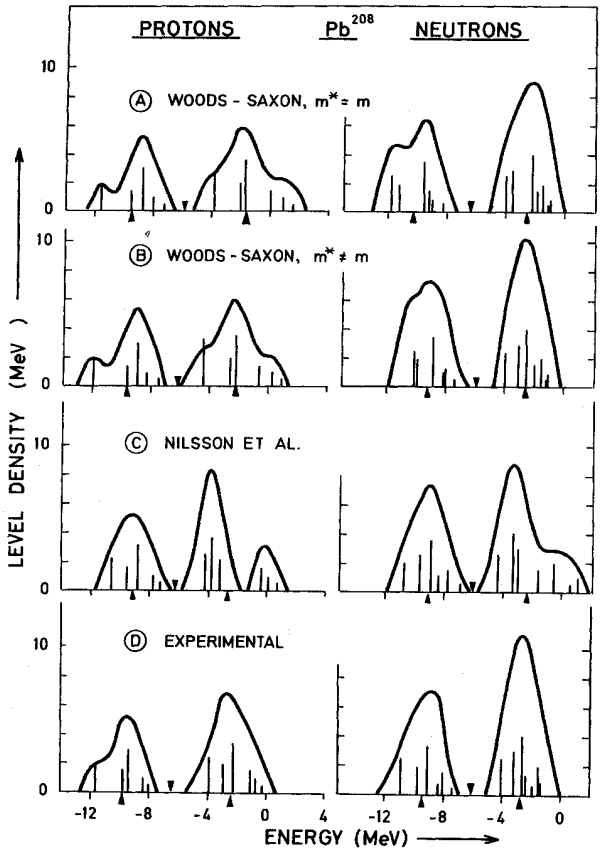

FIG. VI-3. Single-particle energies and shell level densities of ^{208}Pb. The shell level density is calculated with $\gamma_{sh}=1.5$ MeV. The arrows show the positions of the Fermi energies, and the triangles mark the mean energies of the gross shells. The lengths of the vertical lines, marking the energies ε_i, are proportional to their degeneracies n_i. The following cases are considered: A: Woods-Saxon potential with free nucleon masses; B: Woods-Saxon potential with effective nucleon masses; C: Nilsson model (Nilsson *et al.*, 1969), D: Experimental single-particle energies, taken from the spectra of ^{207}Tl, ^{209}Bi, ^{207}Pb, and ^{209}Pb (see e.g., Bohr and Mottelson, 1969).

each case is shown the local level densities obtained by averaging with $\gamma_{sh}=1.5$ MeV. The curves $g_{sh}(\varepsilon)$ resemble each other in the sense that they behave like gaussians, centered around the middle of each shell. The mean value and widths of these guassians, however, differ from one single-particle spectrum to another. It is reasonable to believe that these features of the spectra are more important for the shell corrections than for the specific positions of the individual states.

The triangles in the figure mark the positions of the mean energies of the gross shells adjacent to the lead-208 gap. The distances between these positions are just the mean shell energies mentioned above. For the four distributions shown in Fig. VI-3, these quantities equal 7.70 MeV [case (A)], 6.58 MeV [case (B)], 6.71 MeV [case (C)], and 6.64 MeV [case (D)] for the neutron distributions, and respectively, 7.75 MeV, 7.42 MeV, 6.45 MeV, and 7.46 MeV for the proton distributions.

3. Comparison with Experiment

Contrary to the level distances within the shells, the lead-208 gap (in the following called D_p for protons and D_n for neutrons) cannot be taken from experiments without making assumptions on the effect of pairing interactions in the even target and odd compound nuclei. It is therefore not surprising that Bromley and Weneser (1968, Fig. 1) arrive at somewhat different values for D_n and D_p than ours shown in Fig. VI-3 (D), which were taken from Bohr and Mottelson (1969, p. 325). The latter have been found by separation energy differences, i.e., by

$$D_n=S_n(^{208}\text{Pb})-S_n(^{209}\text{Pb})=3.44\text{ MeV},$$

$$D_p=S_p(^{208}\text{Pb})-S_p(^{209}\text{Bi})=4.23\text{ MeV}. \quad \text{(VI.3)}$$

The difference between these values and the experimentally observed ones reflects mainly the pairing energy.

Now we note that in the shell-correction approach the total mass correction is the sum of two terms, one for protons and one for neutrons, which for a fixed average potential are independent of each other

$$\Delta M(N,Z)=\Delta M_p(Z)+\Delta M_n(N). \quad \text{(VI.4)}$$

Calculating the corrections ΔM_p for a set of l proton numbers, and ΔM_n for m neutron numbers, one can by combinations get the total mass corrections for lm nuclei. Looking now at the experimental data of Fig. VI-1, one sees that this assumption is valid only in a limited region of nuclei: Should it hold strictly, then all curves in Fig. VI-1 connecting isotopes and isotones should be parallel to each other. As can be seen, this holds only for five or six isotopes or isotones around ^{208}Pb. Moving away from ^{208}Pb, the slopes decrease systematically, which may be due to changes in the shape of the nucleus and therefore cannot be accounted for in this calculation, where we use a fixed set of experimental levels of a spherical nucleus.

However, for nearly 20–30 even nuclei around the magic lead-208, the experimental values of ΔM can indeed be reproduced as a sum of the two independent neutron and proton partial mass corrections ΔM_n and ΔM_p. The inaccuracy brought about by this approximation is less than 0.5 MeV, as can be seen from the empirical ΔM curves in Fig. VI-1.

It should be noted that the separability of the proton and neutron contributions to the masses in this region may be taken as an indication of the smallness of the $(\delta\rho)^2$-term in Eq. (III.24), as we know that the n–p interaction is as important for this term as the n–n or p–p interactions are.

The results obtained for the lead-208 region using Woods–Saxon potentials with and without the use of an effective nucleon mass are compared with the experimental mass corrections in Fig. VI-4.

The theoretical curves are normalized to the experi-

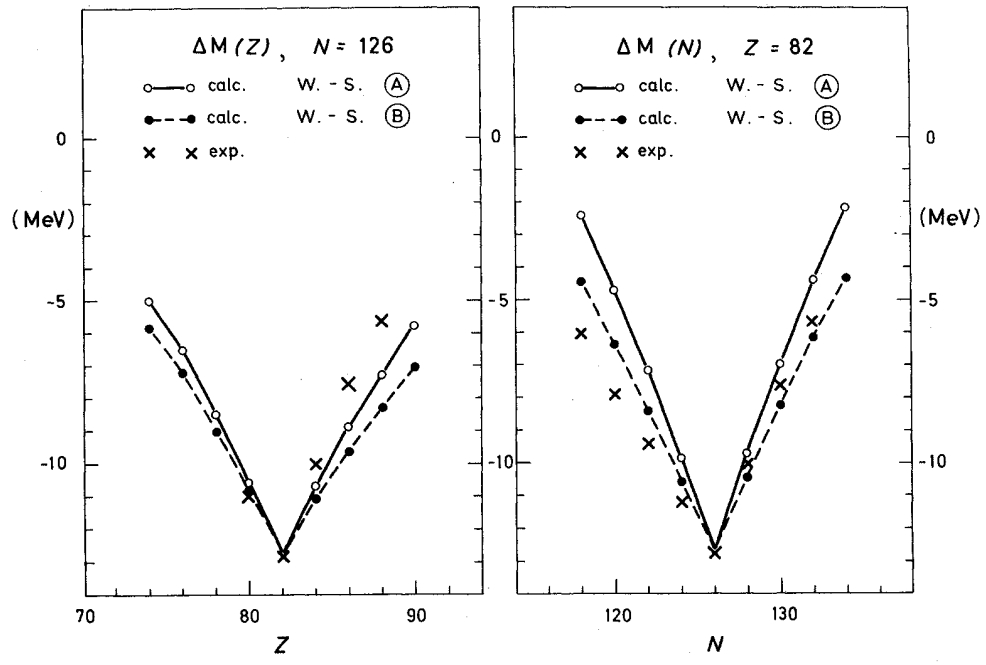

FIG. VI-4. Total mass corrections ΔM in the lead region, plotted as function of proton number Z (left) and neutron number N (right). The crosses are the experimental values as taken from Myers and Swiatecki (1966b). Case A (open circles): Theoretical values calculated according to Eqs. (VI.2) and (VI.4), using the Woods-Saxon potential described in Sec. VII. Case B (filled circles): The same as A, but using the effective masses $m_p^* = 1.05\ m$ and $m_n^* = 1.20\ m$ in the Woods-Saxon shell-model calculations. All curves are adjusted to the value of ^{208}Pb.

mental mass correction in ^{208}Pb. As the figure shows, none of the slopes on either side of ^{208}Pb agree with the experimental results.

In Fig. VI-5, the results of similar calculations using directly the experimental single-particle levels are shown. As mentioned above, the absolute values differ even more from the experimental ones in this case and no improvement in the slopes is seen.

Because of the uncertainties in the relative positions of the two shells on one hand, and in the importance of the pairing interaction for magic nuclei on the other, some special calculations have been done using again

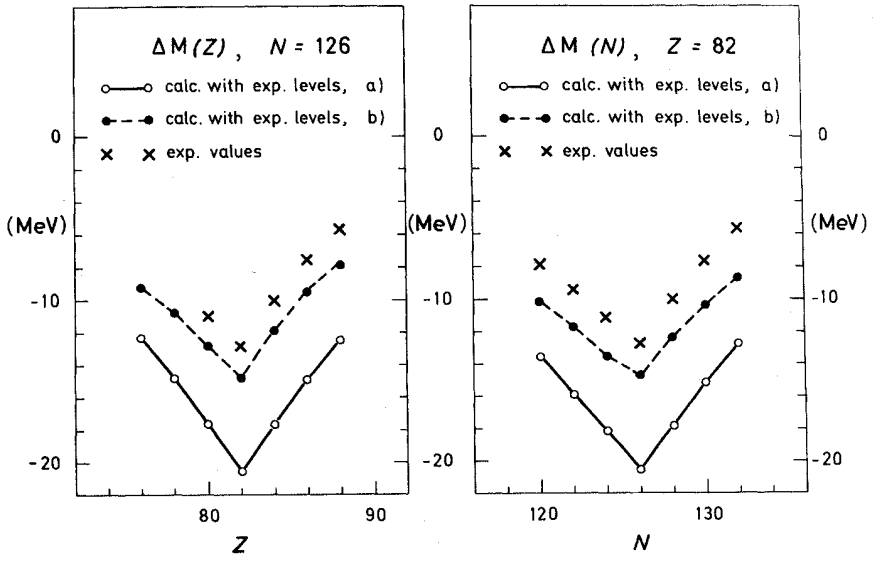

FIG. VI-5. Mass corrections in the lead region, as Fig. VI-4. (a) Calculated with the unshifted experimental levels; pairing included. (b) As (a), but the energy difference between particle and hole states is reduced by 1.5 MeV; pairing correction omitted. The crosses show the experimental mass corrections (as in Fig. VI-4).

the experimental single-particle spectrum in which, however, the distances between all states belonging to the upper and lower shells were artifically reduced and, instead, no pairing was taken into account. A rather good agreement with experimental values was obtained in these calculations when both the proton and neutron shell distances were reduced by 1.5 MeV compared to the values shown in Fig. VI-3(D). The results for this case are also shown in Fig. VI-5. The mass increments in "particle" and "hole" nuclei fit now the experiments much better and over a larger region of nuclei than in the "normal" calculations with the shell-model single-particle spectrum and the BCS pairing. The discrepancy does not, on the average, exceed 0.2–0.3 MeV. In the absolute values of ΔM, however, a common deviation of $\sim$2 MeV remains.

The significance of these calculations with the reduced distance between the shells is not very clear to us, but the agreement obtained seems suggestive and the reasons for it must be understood better.

This and the other results described above in this section probably indicate a still inadequate treatment of the nucleon interactions in spherical nuclei.

We feel that the problem of shell effects in masses of spherical nuclei still requires a deeper understanding of these phenomena and a more rigorous treatment of the residual interactions. It could be one of the important lines in the future improvement of the theory. It is, however, not of great importance for this paper in which problems of deformed nuclei are considered.

VII. THE LIQUID DROP AND SHELL MODEL FOR LARGE DISTORTIONS

In this section, we consider the specific definitions of the two nuclear models involved in our calculations. These are the liquid-drop model and the shell model. Special attention is paid to some qualitative features, which are important for the use of these models at large distortions, so significant for the fission process.

1. Description of the Nuclear Shape

Even in simple classical models, fission is a many-dimensional process, in the sense that many deformational degrees of freedom are involved. Therefore, any reasonable theory requires at least a few parameters to describe even the most important variation of the nuclear shape.

In a complete dynamic theory of the process, these parameters would appear as generalized coordinates. At the present time we have, however, no reliable dynamic theory, which can guide us in choosing these parameters. As the variety of possible shapes, and with it the computational time, increases extremely fast with the number of independent variables, we are forced to limit ourselves to a few parameters (more than three is practically impossible), chosen by physical intuition. Since any restraints in the degrees of freedom are equivalent to introducing some infinitely strong "restriction forces", the choice of parameters may result in a rather artificial model of the process. In order to avoid as much as possible *a priori* restraints of this kind, we have tried to express the important physical quantities in a way which at least makes a change in the number and meaning of the shape parameters very easy. In our calculations, it is practically required only that the shape of the effective nuclear surface be defined in some way. As was mentioned in Sec. III, this may be done consistently, both for the LDM and the shell model; how this is done is described in more detail in this section. In these calculations, the only significant limitation we impose on the shapes is that they shall be axially symmetric. In cylindrical coordinates, which we use throughout, the *shape* of the nuclear surface is given by an equation

$$\pi(\beta, u, v) = 0, \tag{VII.1}$$

where β is a set of deformation parameters, and u and v are dimensionless coordinates proportional to the ordinary cylindrical coordinates

$$z = Cu,$$
$$\rho = Cv. \tag{VII.2}$$

Here and in the following the origin of the coordinate system coincides with the center of mass of the assumed shape. This is achieved as in Damgaard *et al.* (1969a).

The real nuclear surface may be obtained from Eq. (VII.1) by imposing the volume conservation condition, thereby determining the proper value of the scale factor C in Eq. (VII.2)

$$C = R_0 \left[\frac{3}{4} \int_{u_1}^{u_2} v_s^2(u)\, du \right]^{-1/3}, \tag{VII.3a}$$

where the function $v_s(u)$ is determined implicitly by Eq. (VII.1), u_1 and u_2 are the two end points at which $v_s(u)$ becomes zero, and R_0 is the radius of the sphere. For the following, it is convenient to introduce a dimensionless elongation paratmer $\mathbf{c}$, which is defined by

$$\mathbf{c} = C/R_0. \tag{VII.3b}$$

In the volume conservation condition [Eq. (VII.3a)], we replace the real distribution of nucleons by a uniform density distribution which is constant within the effective nuclear surface determined by Eqs. (VII.1)–(VII.3a). This volume is kept constant for all variations of the nuclear shape.

This formulation of the volume conservation condition is, of course, only a crude approximation. It is, however, sufficient for the definition of the phenomenological equation of the LDM as well as the shell-model potential with the accuracy required for the shell correction calculations (see Strutinsky, 1968, Sec. 9).

After trying a number of different parameterizations

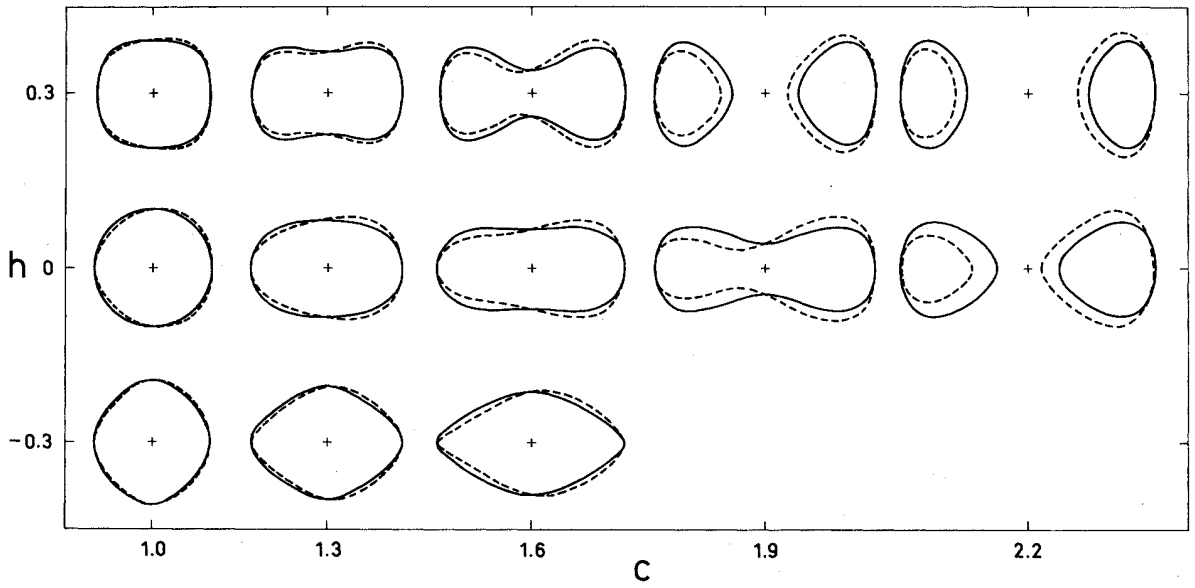

FIG. VII-1. Some shapes in the $\{\mathbf{c}, h\}$ parametrization [Eqs. (VII-4) and (VII-5)]. The solid lines show symmetric shapes ($\alpha=0$); the dotted lines are shapes with an asymmetry parameter $\alpha=0.2$.

of the shape, we have found that the following simple polynomial expression is in rather good agreement with the known results of exact LDM calculations, where practically no restrictions were imposed on nuclear shapes (Strutinsky *et al.*, 1963; Cohen and Swiatecki, 1963)

$$\pi(u, v)=v^2-(1-u^2)(A+Bu^2+\alpha u). \quad \text{(VII.4)}$$

The parameter α describes the asymmetry of the shape in the z direction. When $\alpha=0$, one obtains a family of symmetric shapes ranging from the spherical shape ($A=1$, $B=0$) to two-fragment shapes ($A<0$). These were first studied by Lawrence (1965) and later considered by Hasse (1969). When both α and B are equal to zero, one has a set of oblate ($A>1$), and prolate ($A<1$) ellipsoids. In general, the shape described by Eqs. (VII.1), (VII.4) is more necked-in, if β is positive, than the ellipsoidal shape with the same longer axis.

For the description of the ground-state shapes of many deformed nuclei, which seem to require more diamond-like shapes, the shapes obtainable from Eq. (VII.4) were found to be insufficient. Therefore, Eq. (VII.4) is replaced by

$$\pi(u, v)=v^2-(1-u^2)[(A+\alpha u)\exp(B\mathbf{c}^3u^2)] \quad (B<0) \quad \text{(VII.5)}$$

as soon as B becomes negative. The two definitions join smoothly for small absolute values of B.

We assume that the two most important modes of deformation appearing in the fission process are elongation and formation of a neck. It is convenient to connect the formal parameters introduced above with some other parameters, which can be related more directly to these two modes.

With respect to the nuclear elongation, this is easily done with the parametrization we use here. Indeed, if the shape is defined by Eqs. (VII.4) or (VII.5), it will always have its end points at $u=\pm1$ in dimensionless coordinates u, v.

The volume normalization scale factor $\mathbf{c}$ in Eq. (VII.3) is equal to

$$\mathbf{c}=(A+\tfrac{1}{5}B)^{-1/3} \quad \text{(VII.6)}$$

for the parametrization (VII.4), and approximately equal to this number when (VII.5) is used. Thus, the total length of the longer axis of the density distribution, in units of R_0, equals simply $2\mathbf{c}$, independently of the asymmetry parameter α.

A second parameter h describes the variation of the thickness of the neck without changing the length $2\mathbf{c}$ of the nucleus, and is chosen in such a way that the $h=0$ line fits approximately the bottom of the liquid drop valley described below. The connection between the parameter sets $\{A, B\}$ and $\{\mathbf{c}, h\}$ is given by

$$B=2h+\tfrac{1}{2}(\mathbf{c}-1)$$
$$A=(1/\mathbf{c}^3)-\tfrac{1}{5}B. \quad \text{(VII.7)}$$

Figure VII-1 shows some selected shapes, connected with our $\{\mathbf{c}, h\}$ parametrization. It should be noted that Eq. (VII.4) describes also separated shapes, as soon as A is less than zero, or as we see easily from Eq. (VII.7), $h\geq(5/2\mathbf{c}^3)-\frac{1}{4}(\mathbf{c}-1)$.

2. The LDM Energy Surface

When investingating the deformation energy of the nucleus, two terms emerging from the liquid-drop model are especially important. These terms are the surface energy E_s and the Coulomb energy E_c, which we express in units of the corresponding energies of a sphere (see Hill and Wheeler, 1953):

$$B_s=\frac{E_s}{E_s^{(0)}}=\frac{1}{2}\left(\frac{C}{R_0}\right)^2\int_{u_1}^{u_2}du\left\{v_s^2\left[1+\left(\frac{dv_s}{du}\right)^2\right]\right\}^{1/2}, \tag{VII.8}$$

$$B_c=\frac{E_c}{E_c^{(0)}}=\frac{1}{2}\frac{R_0}{Ze^2}\left(\frac{C}{R_0}\right)^3\int_{u_1}^{u_2}du\left[v_s^2-\tfrac{1}{2}u\frac{dv_s^2}{du}\Phi(v_s,u)\right], \tag{VII.9}$$

where the energies of a sphere are

$$E_s^{(0)}=4\pi\sigma R_0^2,$$
$$E_c^{(0)}=\tfrac{3}{5}(Z^2e^2/R_0), \tag{VII.10}$$

and Φ is the Coulomb potential. The surface tension coefficient was fixed to the value

$$\beta=4\pi\sigma r_0^2=E_s^{(0)}/A^{2/3}=17\text{MeV},$$

where

$$R_0=r_0A^{1/3}.$$

The function $v_s(u)$ in Eqs. (VII.8) and (VII.9) is the same as that introduced in Eq. (VII.3). As a rule, it can be found by solving Eq. (VII.1) numerically. In our case, it is given explicitly as

$$v_s^2=(1-u^2)(A+Bu^2+\alpha u), \qquad (B\geq 0)$$
$$v_s^2=(1-u^2)(A+\alpha u)\exp(Bc^3u^2). \qquad (B<0). \tag{VII.11}$$

The derivatives occurring in the integrands are found by

$$\frac{dv_s^2}{du}=2v_s\frac{dv_s}{du}=-\left(\frac{\partial\pi/\partial u}{\partial\pi/\partial v^2}\right)=-\frac{\pi_u}{\pi_{v^2}}.$$

They are evaluated at the integration points. The Coulomb potential is evaluated as

$$\Phi(v_s,u)=\frac{3}{4\pi}\frac{Ze^2}{R_0^3}C^2\int_{u_1}^{u_2}du'\left\{E(a,b)+F(a,b)\times\left[v_s^2(u')-v^2(u)-(u-u')^2\frac{dv^2(u')}{du'}\right]\right\}, \tag{VII.12}$$

where the complete elliptic integrals of the first and second kind (Abramowitz and Segun, 1964) are described by $E(a,b)$ and $F(a,b)$, and their arguments are

$$a=\{[v(u)+v(u')]^2+[u-u']^2\}^{1/2},$$
$$b=\{[v(u)-v(u')]^2+[u-u']^2\}^{1/2}.$$

The function $\Phi(v,u)$, which in Eq. (VII.9) is taken only in surface points (v_s,u), applies also to all other points in the space, and is used in the Coulomb part of the Woods–Saxon potential for the protons.

In terms of these quantities, the deformation energy of the nucleus—normalized to the spherical case—is then

$$E_{\text{LDM}}=E_s^{(0)}[B_s-1+2x(B_c-1)], \tag{VII.13}$$

where x is the fissility parameter

$$x=E_c^{(0)}/2E_s^{(0)}. \tag{VII.14}$$

Using Eq. (VII.10), we get

$$x=(Z^2/A)/(Z^2/A)_{\text{crit}}, \tag{VII.15}$$

where the critical value of Z^2/A is simply related to r_0 and the surface tension σ:

$$(Z^2/A)_{\text{crit}}=4\pi\sigma\tfrac{1}{3}(r_0^3/e^2). \tag{VII.16}$$

In the earlier versions of the liquid-drop model this value was taken to be independent of Z and A. In more general versions—such as in the droplet model of Myers (see, e.g., Myers and Swiatecki, 1969)—the introduction of a critical value of Z^2/A is no longer a unique concept, as this quantity may vary with the nuclear isospin. However, the liquid-drop coefficients are determined by a fit of the liquid-drop formula and, as pointed out by several authors, this can be done in an unambiguous way only by taking the fission thresholds into account, where the shell corrections become extremely important and no simple LDM equation is applicable. Therefore, we keep the ratio of the liquid-drop surface and Coulomb energy as a free parameter, and in most cases we use

$$(Z^2/A)_{\text{crit}}=45$$

keeping in mind that a better and consistent value may be obtained by a final fit with a better quantitative knowledge of the shell corrections at large distortions (see Pauli and Ledergerber, 1971).

The LDM energy surface has some important qualitative features, which become clear when the physical parameters of elongation and neck formation are used for the description of the shape. These features are related to the presence of a certain LDM valley with its characteristic of relative smallness of effective classical forces arising from shape variations, and also to the existence of a critical deformation at which, according to the LDM, the elongatated nucleus becomes unstable against scission. The latter feature determines the physical scission point and is directly connected with the kinetic energy release to the fission fragments.

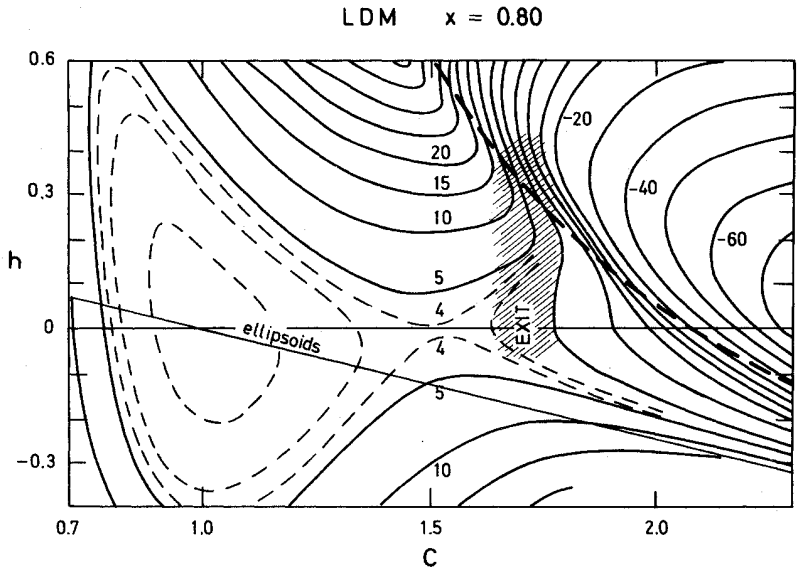

FIG. VII-2. LDM-energy surface for a nucleus with $x=0.8$ ($E_s^{(0)}=635$ MeV). The curves are lines of constant deformation energy (in MeV) which is normalized to zero for the spherical shape ($c=1$, $h=0$). The straight line denoted "ellipsoids" connects the points of ellipsoidal shapes [$B=0$ in Eq. (VII.4) or (VII.5)]. The thick dashed line is the scission line ($A=0$). In the region above this line, the shapes are separated. The shadowed region is the "exit" described in the text.

3. The LDM Valley

What we call the LDM valley may be viewed as a region in the space spanned by the deformation coordinates, in which the LDM energy varies less than elsewhere. That is a region where the Coulomb repulsion and the surface tension nearly compensate each other as, e.g., is reflected in the relatively low fission barriers (of the order of 5–7 MeV) found in the valley region for heavy nuclei. These barrier heights should be compared with typical values of the Coulomb and surface energies separately, which near the fission barrier increase to a few hundred MeV. The reason for introducing this concept may be understood by recognizing the orders of magnitude of the three main forces involved in fission. These are the classical Coulomb and surface tension forces and the shell force arising from the intrinsic structure. An estimate of the latter may be obtained from a typical variation of the shell-energy corrections of the order of a few MeV over the characteristic deformation $R_0A^{-1/3}$:

$$\delta\mathfrak{F}\approx 5\ \text{MeV}/R_0A^{-1/3}\approx 30\ \text{MeV}/R_0.$$

This force is significantly smaller than the two others. The average value of the Coulomb force can be estimated as the Coulomb repulsion energy of a couple of hundred MeV gained by a distortion of the order of R_0. The surface tension force is comparable in magnitude to the Coulomb force, but with opposite sign. Thus, in regions where the two strong forces are not in balance, they result in a strong effective force which either restores the equilibrium by bringing the nucleus back to the region of the valley or tends to split the elongated nucleus into pieces.

From this consideration, an important conclusion may be drawn. To a certain extent, any reasonable "trajectory" of the fissioning nucleus is determined by the static relationship between the two classical forces and must therefore be close to the LDM valley. This statement may be considered as part of a rough model of the fission process.

Outside the valley region where the resulting classical force is much larger than the force related to shell structure, the deformation energy is not expected to be influenced considerably by any specific structure in the nucleus. However, within the valley region, the otherwise smooth relief of the LDM deformation energy surface is strongly affected by the shell structure. This shell-structure effect, together with the inertia and possible damping properties of the nuclear matter, may influence the fission process in many important ways, and is presumably responsible for a variety of observed features of nuclear fission. Therefore, in considering this process, one may, as a first step, restrict oneself to investigating the shell structure only within the valley region, which is convenient at least in reducing the amount of work involved.

The LDM valley may be found as the locus of conditional minima of the LDM deformation energy, with the condition that some elongation parameter has a given value D. The sequence of the minimal energy values $W(D)$, corresponding to the bottom of the valley, is usually regarded as a static model for the energy variation in fission, while the corresponding sequence of shapes is treated as a kind of LDM fission trajectory. The definition of the LDM valley is not unique, but fortunately the sequence of shapes determined in this way is not too sensitive to the specific choice of the elongation parameter, as long as it is a physically reasonable one.

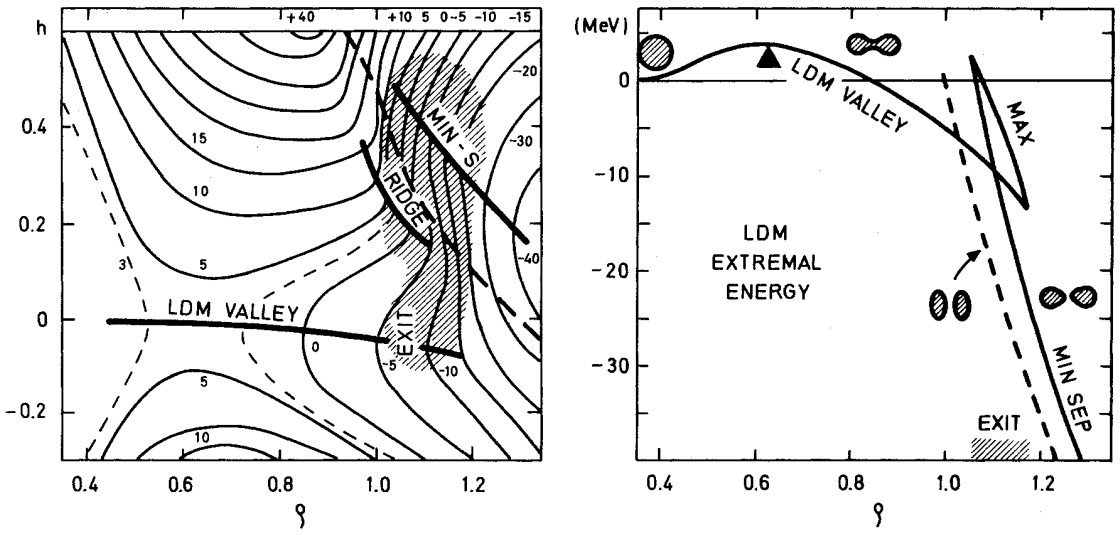

FIG. VII-3. Left side: The same as in Fig. VII-2, but in the $\{\rho, h\}$ representation, i.e., using the mass-center distance ρ_{cm} as elongation parameter instead of **c**. The three branches of conditional extrema are clearly indicated. Right side: Plot of the deformation energy of the three branches of conditional extrema as a function of ρ_{cm}. A triangle indicates the saddlepoint. For $\rho_{cm} \geq \rho^* \approx 1.16$ there exist only separated stable shapes. The dotted curve is calculated for the case of two equal oblate ellipsoids whose energy was minimized for a given distance ρ_{cm} of their centers.

In our $\{\mathbf{c}, h\}$ parametrization, the region of the LDM valley can be confined to a rectangular region determined by $1.0 \lesssim \mathbf{c} \lesssim 1.8$, and $-0.3 \lesssim h \lesssim 0.3$. This can be seen, e.g., in Fig. VII-2, which shows a contour map of the LDM energy surface, calculated for a nucleus with $x=0.80$ in the $\{\mathbf{c}, h\}$ parametrization. The line of ellipsoids is indicated as well as the line $h=0$, which approximately follows the bottom of the LDM valley. The thick dashed line shows the scission line ($A=0$), beyond which the shapes are separated into two fragments.

4. The Exit Deformation

An important feature of the LDM valley is the existence of a well-defined exit at the deformation $\mathbf{c} \approx 1.7$–1.8. Here, the energy surface drops steeply down in a waterfall manner and a force arises in the direction of reducing the neck radius of the stretched nucleus, thus leading to an abrupt scission.

The original of this critical point can be understood if one considers that, already at somewhat smaller distortions, the separated fragment shapes become much lower in energy than the continuous shapes of the same elongation. For this region of deformations, one finds three shapes of the same elongation, which give three different conditional extrema of the LDM deformation energy (Strutinsky *et al.*, 1963, Sec. 2.1). Two of them correspond to minima of the deformation energy, one for usual continuous shapes of the LDM valley, and another for separated two-fragment shapes. The valley of these minima for two-fragment shapes can be recognized in Fig. VII-2, lying above the scission line. The third extremum corresponds to the maximum of the potential barrier which separates the two minima at the same elongation. Considered as a function of the elongation parameter, the energies of these extrema form three branches of the extremal energy curve. Conversely, one finds at smaller distortions only one extremum, namely the conditional minimum of the deformation energy for continuous shapes of the LDM valley.[8]

The barrier between the two minima disappears at the exit. For distortions larger than the exit deformation, again, only one minimum corresponding to separated fragment shapes exists. From this point, the minimum energy curve reflects actually the energy of the Coulomb repulsion between the two distorted fragments. The elongation parameter used by Strutinsky *et al.* (1963) was half the distance between the centers of mass of the two halves of the nucleus, ρ_{cm}, which can be defined by

$$\rho_{cm} = 2\mathbf{c}\left(\int_{u_1}^{u_2} |u|\, v^2(u)\,du \Big/ \int_{u_1}^{u_2} v^2(u)\,du\right). \quad \text{(VII.17a)}$$

It was found in this reference, that the exit deformation shapes are characterized by a relatively thick neck,

[8] There is also an infinite number of other continuous-shape solutions with two and more "necks" as well as asymmetric solutions. These are of no interest here; see, however, Strutinsky *et al.*, 1963.

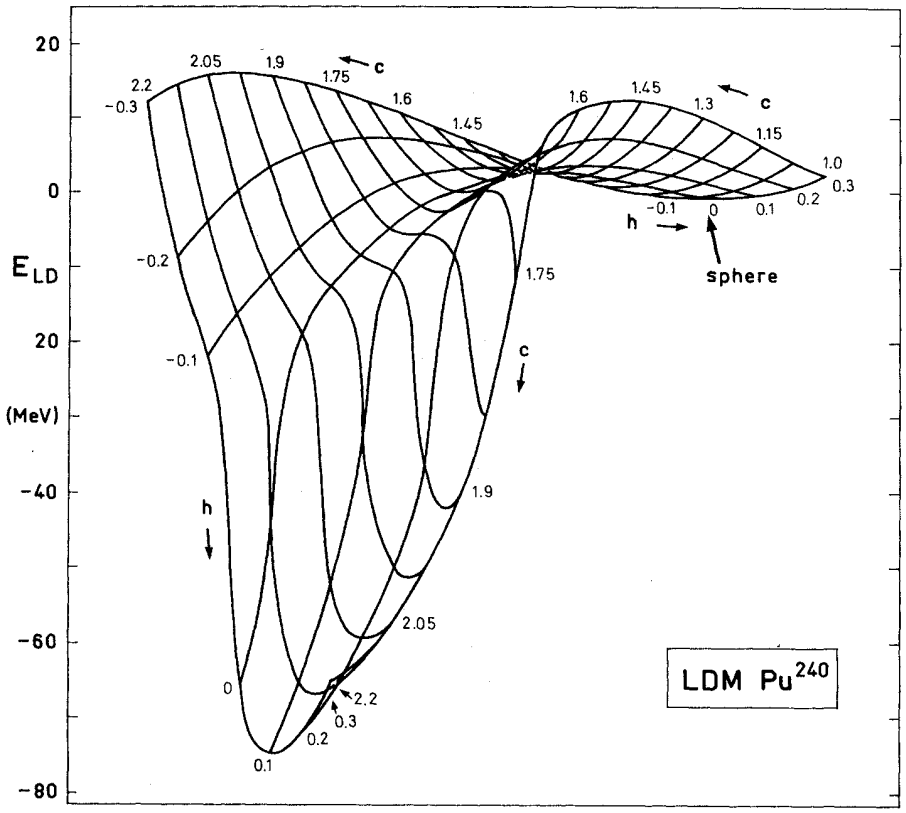

FIG. VII-4. Perspective plot of the LDM deformation energy surface of ^{240}Pu (x= 0.818, $E_s^{(0)}$=631.5 MeV), as described in the text.

occurring at a mass-center distance of

$$\rho_{cm}=\rho^*\approx 1.16R_0 \qquad \text{(VII.17b)}$$

which is almost independent of the fissility parameter x.

This general result is confirmed in our calculations with a limited set of shapes determined by the shape functions (VII.4) and (VII.5). This is obvious from Fig. VII-3, which shows—on the left side—the same energy surface as in Fig. VII-2, but plotted in the $\{\rho_{cm}, h\}$ representation. The curves of conditional minima for the continuous shapes of the LDM valley and the separated shapes ("MIN SEP") are clearly marked in the map. The ridge separating the two valleys is also well discernible. On the right-hand side of Fig. VII-3, the energy extremal along these three branches is plotted against ρ_{cm}. One clearly observes a characteristic singularity occurring in the exit region where the continuous shape minimum disappears. Note also the strongly increased slope after the exit. There, the deformation energy is determined merely by the Coulomb repulsion of the two forming fragments. This feature can also be seen in Fig. VII-4, where a perspective plot of the LDM energy surface of ^{240}Pu is shown. The viewpoint is chosen at a large distance; its direction is parallel to the **c**, h plane in an angle of 45° to the **c** axis, i.e., looking from the region of separated fragments towards the saddle. The cataract-like falling off of the deformation energy after the exit from the LDM valley can easily be recognized.[9] The maximal value of ρ_{cm}, at which a stable continuous shape still exists, is seen in Fig. VII-3 to agree very well with the value ρ^* (VII.17). In fact, the data on the right-hand side of Fig. VII-3 are similar in all respects to Fig. 2 of the paper by Strutinsky *et al.* (1963) where the exit singularity was obtained in a more general treatment of the LDM energy. For the separated shapes, our parametrization should be improved. The humps on the inner side of the fragments make the surface energy too high. This can be seen from the results of calculations in which the fragments are described by two oblate ellipsoids with a mass center distance ρ_{cm}. Minimizing the total LDM energy for constant ρ_{cm}, one obtains values which are lower by 5–10 MeV than those of the $\{\rho_{cm}, h\}$ parametrized fragments; see the dotted curve on the right-hand side of Fig. VII-3. For the discussion of the exit region, this is of no consequence.

When we use asymmetric shapes, we still find a well-defined exit, as can be seen from Fig. VII-5. The presence of the exit deformation is an important feature of the liquid-drop model and may be used for the

[9] We would like to thank Dr. F. Dickmann for his help in preparing Fig. VII-4.

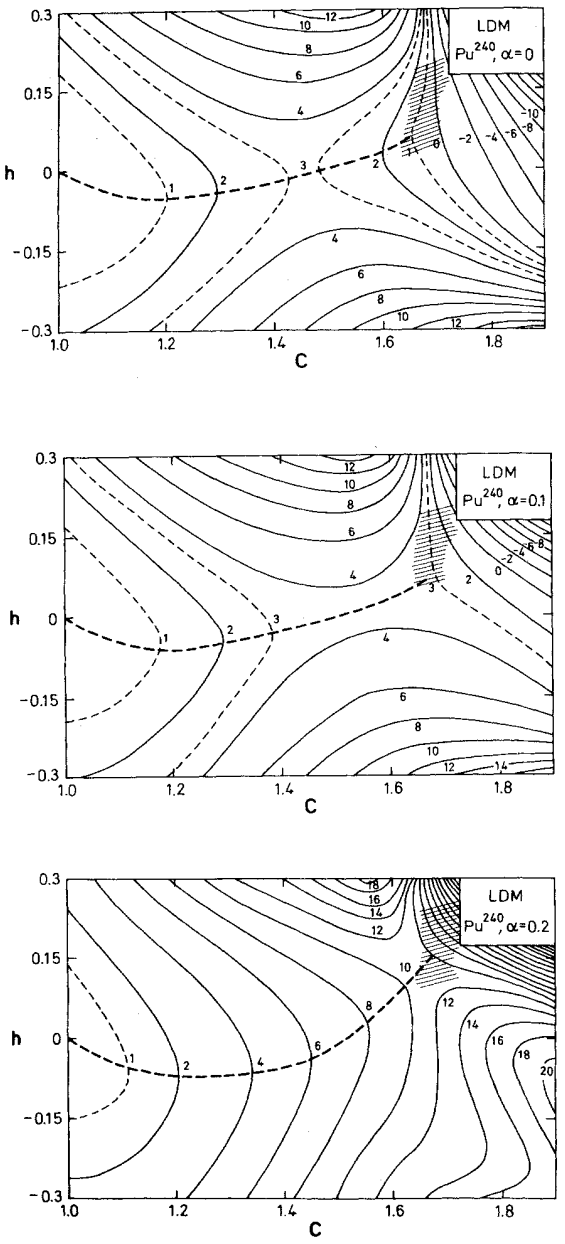

FIG. VII-5. LDM–energy surface for ^{240}Pu ($x=0.818$, $E_s^{(0)}=631.5$ MeV) for symmetric shapes ($\alpha=0$, uppermost figure), and asymmetric shapes ($\alpha=0.1$ and 0.2). The shadowed regions are the exits as in Figs. VII-2 and VII-3, and the dotted lines are the "static ways to fission" along the LDM valley, for given values of the asymmetry parameter α.

determination of the physical scission point. Such a determination seems more natural than the usual condition that the neck radius becomes zero. The latter condition is very ambiguous as it depends completely on the specific choice of the shapes: The more general parametrization of shapes used, the less meaning such a scission shape has. In addition, one can hardly treat the nucleus by means of the liquid-drop model when the neck radius becomes comparable to the internucleon distance.

The interpretation of the exit as the scission point receives some support from experimental evidence concerning the mean kinetic energy of the fission fragments $\bar{T}_f$. This quantity taken as the Coulomb repulsion energy at scission, is almost uniquely determined by the mass center distance at the exit, ρ^*, and is found to be insensitive to the details of the shape. Moreover, as the exit shape does not depend on the fissility parameter, $\bar{T}_f$ should be proportional to $Z^2/A^{1/3}$ and, indeed, this feature is well known from systematics of the empirical values, see, e.g., Terrell (1959). (More recent data can be found in Nix, 1969.) Measured in units of the surface energy $E_s^{(0)} \propto A^{2/3}$, T_f should thus be proportional to Z^2/A:

$$T_f \approx Dx. \qquad \text{(VII.18)}$$

In Fig. VII-6, known experimental fission fragment kinetic energies are plotted against x. A straight line in the figure is drawn through the experimental points and the origin of the coordinate system. Its slope agrees rather well with the estimate based on the above interpretation of the scission point. In fact, the theoretical value of the proportionality coefficient D in (VII.18) can be obtained directly from the calculated Coulomb interaction energy of the two "halves" of the

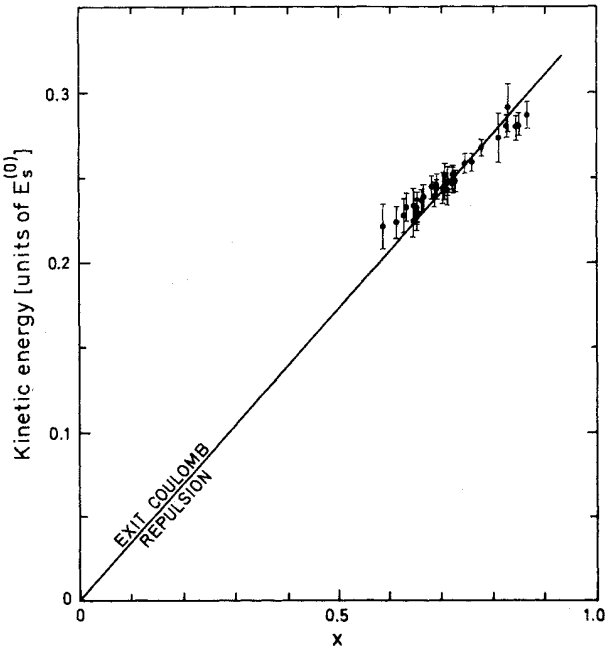

FIG. VII-6. Experimental average kinetic energies $\bar{T}_f$ of fission fragments, plotted against fissionability parameter χ. The straight line drawn through the points shows the approximate proportionality of $\bar{T}_f$ to the parameter x. [The experimental points are taken from R. Nix's paper (1970).]

nucleus at the exit. In this way, one gets

$$D=0.35\pm0.02.$$

The experimental slope of the straight line in Fig. VII-6 corresponds to $D=0.33$. This value should also be compared with Terrell's estimate (1959), based on a smaller number of experimental points in a region of smaller values. Nevertheless, this result corresponds to the same value of D. The agreement strongly suggests that at least the major part of the kinetic energy of the fragments does come from the Coulomb repulsion at scission, which takes place as an abrupt splitting of the elongated nucleus, when the exit deformation is reached. If so, one can probably not deduce from the quoted experimental evidence that an appreciable part of the kinetic energy of the fragments comes from sliding downhill after the saddlepoint, an alternative considered recently by Nix (1969).

On the other hand, some evidence concerning the kinetic energy distribution of α particles formed in fission seem to demonstrate that the fragments already have considerable kinetic energy at the moment of emission of the α particles (private communication by Halpern, 1970). An explanation of this controversy may probably be found in the fact that normally the α particles are not emitted in fission events which contribute appreciably to the mean kinetic energy of the fragments in low-energy fission. Other data shown in Fig. VII-6 refer to fission of highly excited compound nuclei formed in heavy-particle bombardment. No detailed data on the kinetic energies of α particles are available for these reactions.

For the exit shapes, the neck radius is still sufficiently thick and amounts to about one-third of the nuclear radius R_0. One may hope, therefore, that the situation just before the exit still can be treated by means of the usual quasistationary theory, considering the whole nucleus as an entity. As any significant opposing forces are absent, scission should be a very fast process. Consequently, one may assume that not only the mean kinetic energy, but also other distributions in the fission fragments are identical to those formed just before the exit deformation. We shall come back to this point later (see Sec. VIII.2).

5. The Shell Model

The single-particle energies and wavefunctions used in our calculations are evaluated in a generalized shell model. It is evident from the previous sections that the shell model should be easily applicable to very general shapes which the nucleus may take during the process of fission. We shall therefore define a deformed Woods–Saxon potential in such a way that the shape determined by the function [Eq. (VII.1)] easily can be varied. For the evaluation of the single-particle energies and wavefunctions, we use a fast numerical method recently suggested (Pashkevich and Strutinsky, 1969; Damgaard *et al.*, 1969a). In this method, all parts of the single-particle Hamiltonian are defined in terms of the nuclear surface. The accuracy of the numerical method and the required computer time are approximately independent of the shape of the surface, in contrast to some other formulations of the deformed Woods–Saxon potential. (See, e.g., Nemirovsky and Chepurnov, 1966; Ford *et al.*, 1970).

In order to solve the Schrödinger equation, we diagonalize the Hamiltonian

$$H=T+V(l)+V_{so}+V_{Coul} \qquad \text{(VII.19)}$$

where T is the kinetic energy in a deformed, axially symmetric oscillator basis. This basis has the following desirable features. The shape and size $\hbar\omega_0$ of the basis may easily be adjusted to the form and volume of the nucleus considered. The matrix elements of the Hamiltonian can be expressed as two-dimensional integrals in a way appropriate to the application of Gaussian quadrature formulae. In evaluating the integrals, simple recurrency relations are used for the Hermite and Laguerre polynomials in terms of which the basis functions are expressed.

Furthermore, the truncation of the basis also varies depending upon the deformation of the average field, and is different along the main deformation (i.e., the z axis) and in the perpendicular direction. This contrasts with the usually used truncation of the basis with a definite number of spherical shells, where, in order not to miss the states of very high quantum numbers in strongly deformed nuclei, one is forced to use very many states in the spherical basis. The use of the basis and truncation adjustable to the deformation of the average field helps to avoid this problem completely.

Furthermore, in the applications, it is also often convenient to have the wave functions expressed in terms of Hermite and Laguerre polynomials because of the simple recurrency relations which connect these functions. Finally, it is possible to write the computer program in such a way that the computer time required is determined mainly by the time used for the diagonalization, which means that the computer time involved is comparable to the time used when one is working, e.g., with the Nilsson model. The speed of the computations is an essential factor in applications to the fission theory where a large variety of nuclear shapes must be considered.

We start from the effective surface of the nucleon density as defined in Eq. (VII.1) and assume that the density drops exponentially to zero in a surface layer whose thickness is small compared to the mean nuclear density radius R_0. We assume the distribution of the nuclear field to follow approximately the density, although it may extend somewhat outside the density surface region due to the finite range of nuclear forces. Consequently, we introduce an effective surface for the

nuclear field whose shape is determined by the same shape function $\pi(u, v)$ as in Sec. VII.1, though with a slightly larger scale factor C_v than the scale factor C, Eq. (VII.3), for the density surface, i.e., we take a somewhat larger volume for the potential surface

$$C_v \approx C[1+(\Delta R_0/R_0)]$$

where ΔR_0 is the difference between the half-value radii of the potential and the density distribution. For simplicity, we assume the same effective surface $\pi(u, v)$ both for protons and for neutrons.

Knowing one equipotential surface, namely the effective surface for the potential, we finally need to assume a definite distribution of the others. The distribution we shall use is based on the observation that, in a phenomenological description of nuclear density distributions, the surface thickness parameter is nearly constant over the whole range of spherical nuclei, i.e., it is approximately independent of the surface curvature. Consequently, we use an expression for the nuclear potential which has the feature of varying in the surface region only in the direction perpendicular to the surface with a constant gradient in each point independent of the nuclear shape.

Another commonly used prescription for the potential distribution is to assume that the equipotential surfaces are scale transforms of each other. For deformed shapes, this assumption implies, however, that the skin thickness in the normal direction to the surface varies along the surface.

In the calculations presented in this paper, we use a potential with a constant skin thickness, which can be obtained by introducing a length variable

$$l(u, v) = C_v[\pi(u, v)/|\nabla_{u,v}\pi(u, v)|] \quad \text{(VII.20)}$$

and then, in conformity with our starting point, use this in a Fermi function to give the "radial" dependence

$$V(l) = V_0/[1+\exp(l/a)] \quad \text{(VII.21)}$$

where a is the surface thickness parameter for the potential, and V_0 is its value in the nuclear interior.

Without implying any further restrictions, we may obtain the correct asymptotic behavior by assuming the length variable $l(u, v)$ to be always positive outside and negative inside the potential surface at which, by definition, it is zero. The definition of the potential by Eqs. (VII.20) and (VII.21) ensures, as may easily be verified, that the field in the neighborhood of the potential surface varies only perpendicular to the surface. It has a constant gradient in this direction independent of the point on the surface equal to $\frac{1}{4}(V_0/a)$ and, as long as $|l| \lesssim a$, the length variable l may, for any shape $\pi(u, v)$, be identified with the distance from the surface $\pi(u, v) = 0$.

Summarizing, we see that as soon as the function $\pi(u, v)$ is given, the procedure described defines the potential uniquely, except for the extremum points of the function $\pi(u, v)$, where $\nabla\pi(u, v) = 0$. As we shall see, these special points may be interpreted as geometric centers of the shape determined by the equation $\pi(u, v) = 0$. The length variable l becomes singular in these points, which may have unpleasant consequences such as, for example, that the value of the potential (VII.21) in such a point may depend on the manner in which one approaches the singularity point.

The difficulty may be partly avoided by using the inherent arbitrariness left over in our definition of the shape by the function $\pi(u, v)$. This means that identical shapes are obtained if the function $\pi(u, v)$ is replaced by any other function $\Pi(u, v)$, which is expressible as a functional of $\pi(u, v)$

$$\Pi(u, v) = \Phi[\pi(u, v)], \quad \text{(VII.22)}$$

where the function $\Phi(x)$ satisfies our sign convention and is zero for $\pi(u, v) = 0$, viz.

$$\Phi(x) \gtrless 0 \quad \text{for} \quad x \gtrless 0 \quad \text{(VII.23)}$$

and

$$\Phi(0) = 0. \quad \text{(VII.24)}$$

The additional freedom may be used in different ways. We have found it convenient to choose $\Pi(u, v)$ in such a way that l, now determined by

$$l = C_v[\Pi(u, v)/|\nabla_{u,v}\Pi(u, v)|] \quad \text{(VII.25)}$$

in the spherical case always becomes identical to the usual radial variable $r - R_0$. This is also true near each sphere, if the equation $\Pi(u, v) = 0$ describes a number of identical separted spheres.

Such a transformation is useful in the sense that, with the modified length variable l given by Eq. (VII.25), one is able to define a Woods–Saxon potential which, starting from a spherical shape, continuously transforms into a number of identical spherical potentials of the same type, paralleling the corresponding transformation of the nuclear shape. The potential always preserves the feature of saturation, i.e., its depth in the nuclear center (or centers) remains constant.

When we parametrize distortions as described by Eqs. (VII.4) or (VII.5) in Sec. VII.1, a function $\Pi(u, v)$ with the above-mentioned properties may be found by setting

$$\Pi(u, v) = [\pi(u, v) - \pi_{\min}]^{1/2} - [-\pi_{\min}]^{1/2}, \quad \text{(VII.26)}$$

where $\pi_{\min}$ is the minimal value of $\pi(u, v)$. As all the extrema of the function $\pi(u, v)$ in our parametrization are situated on the line $v = 0$, i.e., the z axis, one may conveniently classify the different shapes as one- or two-center shapes according to the number of minima of $\pi(u, v)$. This number depends on the specific values of the deformation parameters appearing in the shape function $\pi(u, v)$. We find, e.g., among the symmetric shapes ($\alpha = 0$) determined by Eq. (VII.4) that we

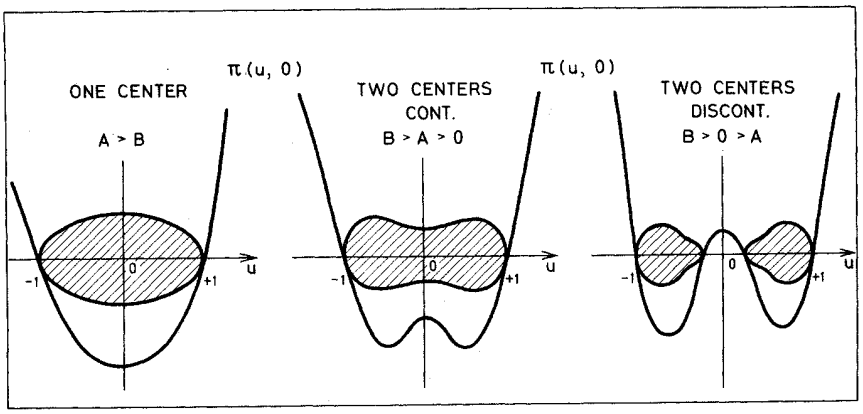

FIG. VII-7. Qualitative illustration of the connection between the shape and the function $\Pi(u, v)$ taken along the u axis. It shows that one may interpret the extrema of the function $\Pi(u, 0)$ as geometrical centers of the shape.

have one-center shapes if $A>B$, in which case

$$u_{\min}=0, \qquad \pi_{\min}=-A, \tag{VII.27}$$

and two-center shapes if $A<B$, in which case

$$u_{\min}=\pm\{\tfrac{1}{2}[1-(A/B)]\}^{1/2},$$
$$\pi_{\min}=-\tfrac{1}{4}[(A-B)^2/B]. \tag{VII.28}$$

The two-center shapes are continuous for $B>A>0$ and discontinuous for $B>0>A$, see Fig. VII-7. In the case of two-center shapes, $l(u, v)$ is still singular for $u=0$. This singularity however, gives, rise to undesirable effects if the neck radius

$$r_{\min}=C_v v(0)=C_v A^{1/2} \tag{VII.29}$$

is smaller than the diffuseness parameter a. Shapes for which this is true are hardly of any interest in this connection as the LDM description is meaningless when the neck radius becomes so small. In addition, there are reasons to believe that physical scission takes place just at the exit from the LDM valley, i.e., before the neck radius has become so small. For the exit shapes determined from Fig. VII-3, the neck radius is still considerably larger than a. In order to give an impression of our parameter choice as well as of the field resulting from the method described, Fig. VII-8 shows the distribution of equipotential surfaces for several shapes of the nuclear surface.

The occurrence of a rather strong spin–orbit coupling in the nucleonic interaction, combined with the assumption that the range of interaction is small compared to the surface thickness of the density distribution, leads to a spin–orbit coupling in the average potential of the form

$$V_{so}=k_\rho(\mathbf{l}\cdot\mathbf{s})r^{-1}[\partial\rho(\mathbf{r})/\partial r] \tag{VII.30}$$

where k_ρ is a constant, and $\rho(\mathbf{r})$ the density distribution. In actual calculations, we have used another form for the spin–orbit term, but one which is analogous to that used traditionally in the shell model, i.e.,

$$V_{so}(u, v)=-\kappa[\nabla V\times\mathbf{p}]\cdot\boldsymbol{\sigma}, \tag{VII.31}$$

where $V(u, v)$ is evaluated by Eqs. (VII.21) and (VII.25) up to the fact that the density–volume normalization condition, C, Eq. (VII.3), is used instead of C_v for defining the radial variable l, Eq. (VII.25). The choice of a spin–orbit radius somewhat smaller than the potential radius may also find support in calculations which aim at finding the one-body potential suitable for specific nuclei by fitting the ex-

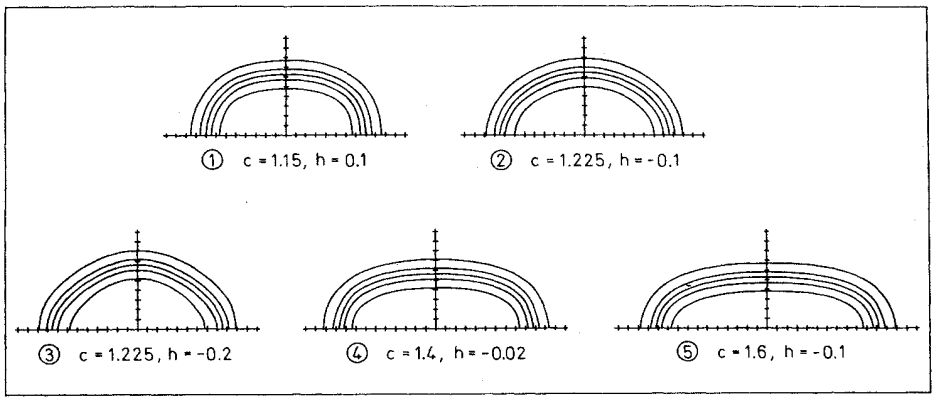

FIG. VII-8. Equipotential lines for some shapes in the $\{c, h\}$ parametrization. The equipotential lines refer to the energies 0.1 V_0, 0.3 V_0, 0.5 V_0, 0.7 V_0, and 0.9 V_0, where V_0 is the well depth in the center. Each division on the axis represents 1 F. The spherical radius is taken equal to 7 F.

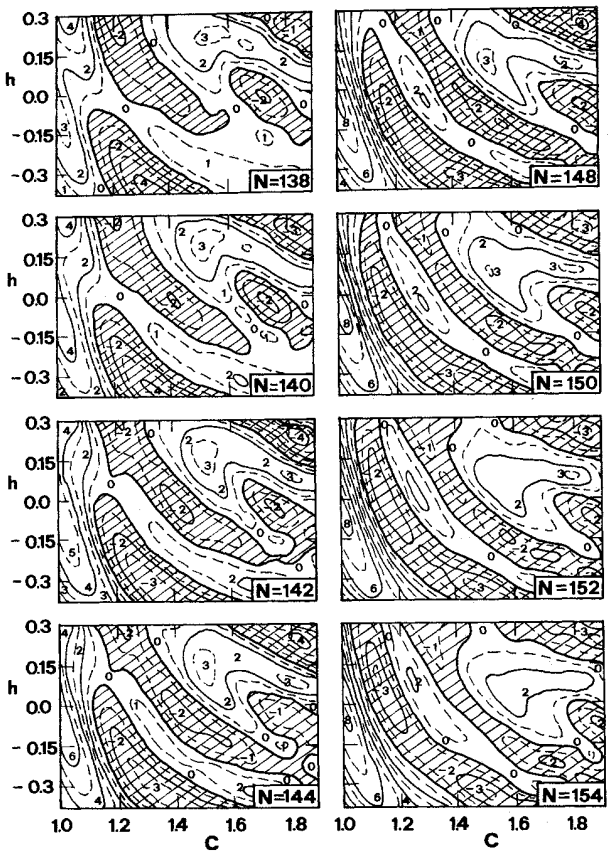

FIG. VIII-1. Contour maps of the shell-energy correction $\delta U_n+\delta P_n$ for neutrons in the actinide region. Numbers are given in MeV. The equidistance for the full lines is 2 MeV. For the parameters of the single-particle potential used, see Table VIII.1. The deformation parameters $\mathbf{c}$ and h are defined in Sec. VII. The uniform pairing gap $\bar{\Delta}$ is kept constant over the whole $\{\mathbf{c}, h\}$ region and chosen to equal $\bar{\Delta}=12\ A^{-1/2}$ MeV, as in all figures of this section. Note that there are up to four regions of negative energy corrections (shadowed).

perimental single-particle levels. Thus, the spin–orbit potential will be peaked slightly inside the half-potential radius R_v. Such a step increases the influence of the spin–orbit potential on the distribution of levels at the Fermi energy.

Another important component of the nuclear average field is the Coulomb field. As mentioned above, this was evaluated by assuming the nuclear charge to be uniformly distributed within the nuclear surface. It is given by (VII.12).

VIII. THE DEFORMATION ENERGY OF HEAVY NUCLEI

Large deformations of the nucleus have so far been studied only in the fission process. In this section we try to give a quantitative discussion of the role of the shell structure in the deformation energy of fissioning nuclei, and to examine to what extent the occurrence of shells can be related to experimental results, some of which have puzzled nuclear physicists in the past. A complete treatment of the fission process, especially the discussion of the stability of nuclei against division, must involve dynamics, to which the next section is devoted. However, the deformation energy alone is conclusive with respect to the relative energies of the stationary points, i.e., the saddle and the ground-state shapes. Without too much ambiguity these quantities can also be compared to experimental results (Lynn and Bjørnholm, private communication).

The single-particle calculations, on which the results presented below are based, have been performed by fast numerical methods, using an average potential of the Woods–Saxon type described in Sec. VII. The application of such a potential implies in principle the need of a calculation for each isotope separately. But for neighboring nuclei, the single-particle level distribution changes slowly and monotonically, and the increased radius of the average potential can easily be corrected for by a scale factor varying like Nilsson's $\hbar\omega_0$ with $A^{-1/3}$ (cf. Sec. V). Thus, we have found it sufficient in the region of heavy elements ($A\gtrsim 220$) to use only two level schemes, one for the known fission region around ^{240}Pu, and one for the hypothetical superheavy region around $^{298}114$. The parameters of the average potential used for those nuclei are compiled in Table VIII.1.

In order to ensure this assumption, we have done some check calculations with the levels of ^{230}Th; there the deformation energy should be more sensitive to the spectrum of states since it is a nucleus in the transition region from spherical to deformed shapes. But even in that case, the change in the shell-correction energy by using $A^{-1/3}$ scaling of the ^{240}Pu level scheme was at all deformations less than 0.5 MeV, which number we consider as a kind of error limit—both physically and numerically.

1. The Deformation Energy for Symmetric Shapes

We first restrict the discussion of the deformation energy to the case of symmetric shapes, i.e., to the shapes described by Eqs. (VII.4) and (VII.5) with $\alpha=0$. In the numerical computations, the increments of the deformation variables were chosen equal to $\Delta\mathbf{c}=0.06$ and $\Delta h=0.075$, which ensured that no significant extrema of δU were missed. For the reasons mentioned in Sec. VII.3, we have confined ourselves to the region of the LDM valley, i.e., to $1.0\leq\mathbf{c}\leq 1.9$, and $-0.375\leq h\leq 0.3$.

In Figs. VIII-1 and VIII-2, we present the shell correction energies for neutrons and protons, respectively, for the most important nucleon numbers in the actinide region. They include the pairing correction δP (see Sec. V.4). We did not assume here any dependence of the pairing energy on the nuclear surface, i.e., the coupling constant G was taken to be constant all over.

In the same way as in the rare earth region, the

TABLE VIII.1. The parameters of the single-particle potentials. These parameters were taken from the droplet model (Myers, 1969) except for the depth of the potential and the spin–orbit coupling constant, which were obtained by a fit to the levels of ^{208}Pb.

	^{170}Yb		^{240}Pu		^{298}114	
	Protons	Neutrons	Protons	Neutrons	Protons	Neutrons
Central potential						
R_V (F)	6.91	6.81	7.79	7.72	8.40	8.32
a_V (F)	0.66	0.66	0.66	0.66	0.66	0.66
$-V_0$ (MeV)	61.0	49.0	60.4	46.8	61.1	46.1
Spin–orbit potential						
R_ρ (F)	6.21		7.06		7.65	
a_ρ (F)	0.55		0.55		0.55	
κV_0 (MeV)	12.0		12.0		12.0	

neutron energy corrections oscillate around zero with an amplitude of ≈3 MeV, which is larger than that of the protons (≈1.5 MeV). Thus, the neutrons play a dominant role in the total deformation energy, as we shall see later.

The contour maps in Figs. VIII-1,2 show clearly a number of shell-correction minima, reflecting shell closures. In the total deformation energy, these minima lead in most cases to two locally stable configurations, namely the ground state and the second minimum.

As the shell structure is most important along the bottom of the LDM valley, i.e., for $h\approx 0$, the first minimum of the neutron energy corrections at $c\approx 1.2$ is decisive in determining the ground-state shape. This minimum is most pronounced around the magic number $N=152$, which also has been observed experimentally (Ghiorso *et al.*, 1954).

The second minimum, which is responsible for the existence of fission isomers in many heavy nuclei, occurs at $c\approx 1.4$. Its magic number, $N=146$ or 148, is in agreement with the conclusions drawn from studies of spontaneous fission isomers and other data (Bjørnholm and Strutinsky, 1969).

For some neutron numbers, there is also a third minimum of the energy shell corrections at a very large deformation ($c\approx 1.7$–1.9). However, as the LDM energy falls off very steeply there, the existence of a third minimum in the total deformation energy is rather unlikely. A minimum in δU_n may, however, influence the exit, once the nucleus has passed the saddlepoint (see Strutinsky and Pauli, 1969).

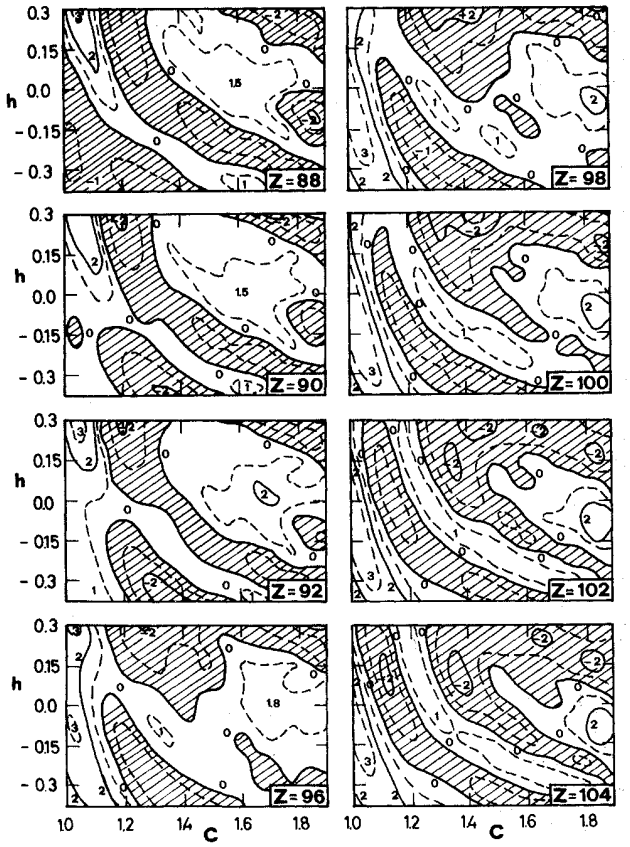

FIG. VIII-2. The same as in Fig. VIII-1 for protons in the actinide region.

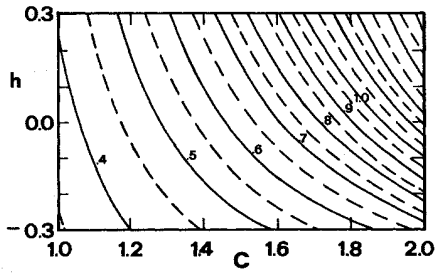

FIG. VIII-3. Plot of lines of constant mass center distance ρ_{om} in the {c, h} plane. The equidistance of the full lines is 0.1. The definition of ρ_{om} is given in Eq. VII.17a.

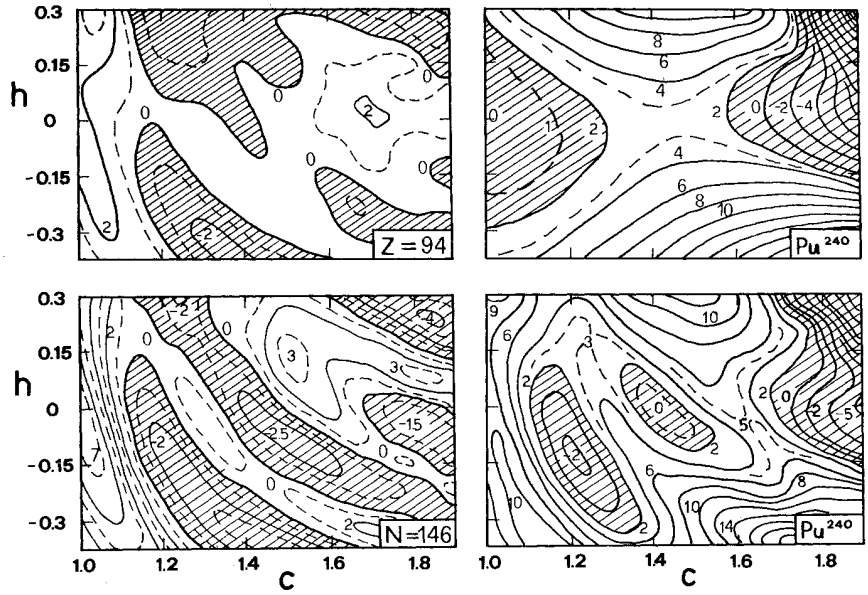

FIG. VIII-4. Left hand side: Contour maps of the energy shell corrections of $Z=94$ protons (above), and $N=146$ neutrons (below), as in Figs. VIII-1 and 2. Right hand side: Above: Contour map of the LDM energy of ^{240}Pu (normalized to 0 MeV for the spherical shape). Below: Contour map of the total deformation energy of ^{240}Pu (i.e., the sum of the quantities in the three other maps). Equidistance 2 MeV. For convenience, the regions below 2 MeV are shadowed here.

An interesting feature of the landscapes shown in Figs. VIII-1,2 shall only be touched here: A clear orientation of the "valleys" and "ridges" in the $\{\mathbf{c}, h\}$-plane can be noticed both in proton and neutron maps, irrespective of the nucleon number. It is most pronounced for the neutron numbers around $N=150$. It turns out that these orientations almost coincide with the lines of constant ρ_{em}, where ρ_{em} is the distance of the mass centers discussed in Sec. VII.4 (see Fig. VIII-3).

For the discussion of the detailed interplay between the shell corrections and the LDM energy, we show in Fig. VIII-4 the energy surfaces of ^{240}Pu as a typical example. Further contour maps of the total energies, calculated for a series of heavy nuclei, are collected in Appendix A (Fig. A-1).[10]

Figure VIII-4 shows the proton and the neutron shell corrections of ^{240}Pu separately on the left-hand side. On the right-hand side, the LDM energy (upper diagram) and the total deformation energy (lower diagram) of ^{240}Pu are shown. The shapes at both the ground state and the second minimum are determined mainly by the neutron shell correction, as we have mentioned above (for the second minimum, ^{240}Pu has a magic neutron number, see above). The ground state has the typical deformation coordinates $\mathbf{c}\approx 1.20$, $h\approx -0.15$. For the region of actinides calculated ($228\leq A\leq 252$), the elongation coordinate of the ground state moves within the limits $1.12\leq \mathbf{c}\leq 1.22$, and has its maximum value for the nuclei around ^{232}Th and ^{236}U. For the neck coordinate of the ground state, systematics similar to that of the rare earths are found (see Sec. V and especially Fig. V-3, there). It is negative for the lighter actinides ($h\approx -0.2$ for ^{228}Ra), goes towards zero with increasing mass number A, and is positive for nuclei with $A\gtrsim 252$.

The second minimum (isomer state) occurs for approximately the same shape for all the actinides: $(\mathbf{c}, h)\approx(1.4, 0.0)$. Between the two minima, there is a saddlepoint connected to the so-called first barrier. As the saddle is very shallow in the h direction (i.e.,

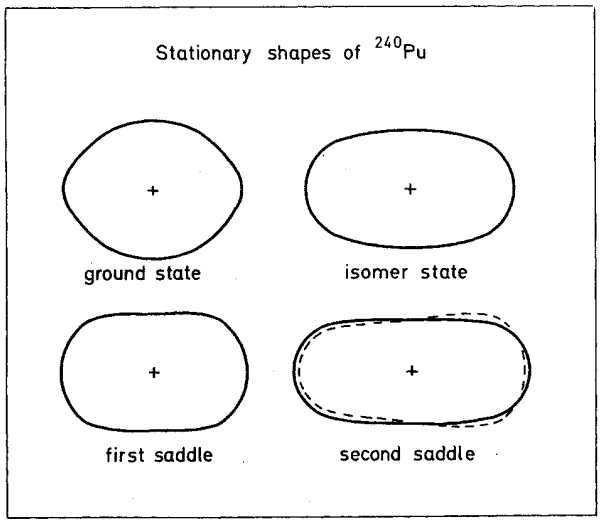

FIG. VIII-5. The four symmetrical, stationary shapes (full lines) of ^{240}Pu, found from the total energy surface in Fig. VIII-4: The ground state ($\mathbf{c}=1.21$, $h=-0.15$), the isomer state ($\mathbf{c}=1.41$, $h=0.0$), the first saddle ($\mathbf{c}=1.24$, $h=0.18$), and the second saddle ($\mathbf{c}=1.62$, $h=-0.04$). The dotted lines show the asymmetric second saddle shape as found from Fig. VIII-7 below (see also Sec. VIII.2).

[10] The superheavy nuclei (with $Z>104$) are treated in Sec. VIII.4.

along $\mathbf{c}=$ const.), its position in the $(\mathbf{c}, h)$ plane varies rather strongly with the mass number of the nucleus. The outer saddlepoint ("second barrier"), which separates the second minimum from the exit region, corresponds also to a more or less constant shape within the actinide region $(\mathbf{c}, h)\approx(1.6, -0.05)$.

In Fig. VIII.5 we show the four shapes corresponding to the stationary points in the energy surface of ^{240}Pu. It is significant that these four points in the $(\mathbf{c}, h)$ plane do not lie on a straight line. Thus, the problem of finding a reasonable trajectory—which for the pure LDM can be approximated by a one-dimensional path $(h=0)$—will in any case (including dynamics or not) be a multidimensional one.

The height of the higher barrier of ^{240}Pu, taken from Fig. VIII-4, is about 7 MeV, measured from the ground state. To it, the LDM contributes only $\approx$1 MeV. The remaining 6 MeV come from the shell correction. The same holds for the other actinides which we have considered: The main contribution to the barrier (6–9 MeV) always comes from the shell corrections. Thus, the comparison with experimental barrier heights is a rather crucial test of our calculations. The observed role of the shell structure explains, as a matter of fact, why the experimental fission barriers do not follow the LDM prediction for heavy nuclei (see Sec. I and Fig. I-2, therein).

In Table VIII.2, the heights of the barriers and the depths of the isomer minima for some actinides, as found by analyzing different experimental results (Lynn and Bjørnholm, private communication), are listed. Comparing the numbers in Table VIII.2 with the results presented in Figs. VIII-4 and A-1, it appears that the computed threshold energies are considerably higher than the experimental ones. In particular, the second barrier is, in most cases, too high as compared to the first one.

This defect can be removed only to some extent by a better choice of the LDM parameters. For example, fitting the higher barriers to the experimental thresholds, the inner barrier would be consistently too low as compared to the values deduced from experiment, and we would end with the problem of increasing the lower instead of decreasing the higher barrier. The relative size of the two barriers is deterimined mainly by the shell structure, as seen above.

Qualitatively the same results were obtained also by Nilsson *et al.* (1969) and Pashkevich (1969), although these authors used rather different single-particle models and parameterizations of the shape.

In order to remove this disagreement with experiment we have performed a number of computations involving different definitions of the nuclear surface (though still symmetric) and different radial dependences of the single-particle potential—all with negative result. Even chaining the spin–orbit coupling constant beyond physically reasonable limits, e.g., so far that the magic number for spherical shapes were shifted, did not reduce the second barrier to a sufficient extent. The introduction of a surface-dependent pairing coupling constant, as suggested by Nilsson *et al.* (1969), does not help either. It mainly gives a smooth contribution to the total energy (see Fig. V-12), which can be accounted easily for by choosing slightly different values of the surface energy coefficient or of the parameter $(Z^2/A)_{\text{crit}}$ in the LDM energy.

TABLE VIII.2. Information on double hump barriers as inferred from experimental results by Lynn and Bjørnholm (private communication). Only the results for the nuclei appearing in Table VIII.3 have been listed.

	Ground state (in MeV relative to spherical LDM)	Isomer state	Inner saddle	Outer saddle
		(given in MeV, relative to the ground state)		
^{232}Th	0.44		5.9±0.2	6.1±0.2
^{236}U	−0.15	2.5±0.2	5.9±0.2	6.0±0.2
^{240}Pu	−0.71	2.0±0.2	6.0±0.2	5.4±0.2
^{244}Cm	−1.26			

2. The Deformation Energy for Left–Right Asymmetric Shapes

The asymmetry in the distribution of the fission fragments, i.e., the fact that the fissioning nucleus breaks into pieces of unequal sizes, has early in the history of fission been related to shell structure (e.g., Meitner, 1950, 1952). The lighter fragments are indeed close to a doubly magic nucleus with $N=82$, $Z=50$. We shall, however, not investigate here the shell structure in the fragments. We shall rather ask the question, whether the asymmetry of the fission products is already being determined or partially caused by shell structure of the total deformation energy on the way to fission.

That the LDM energy for continuous shapes is stable against asymmetric shape variations (Cohen and Swiatecki, 1962) can also be seen in our calculations on Fig. VII-5: At each point of the $\{\mathbf{c}, h\}$ landscape, the energy is increased as soon as $\alpha\neq 0$. Thus, only the shell-correction part of the total deformation energy can give rise to a possible instability against asymmetry.

Recently, Møller and Nilsson (1970) have shown, using a suitable combination of P_3 and P_5 deformations, that the variation of the shell-correction energy produced by reflection-asymmetry shape variations may lower the deformation energy significantly, especially at the second barrier of the actinide nuclei.

At present, we use the $\{\mathbf{c}, h, \alpha\}$ parametrization of the surface given in (VII.4), where α is the asymmetry parameter. We have ensured that the ground-state region is stable against asymmetry, a result which was reported earlier also by Vogel (1968). We found

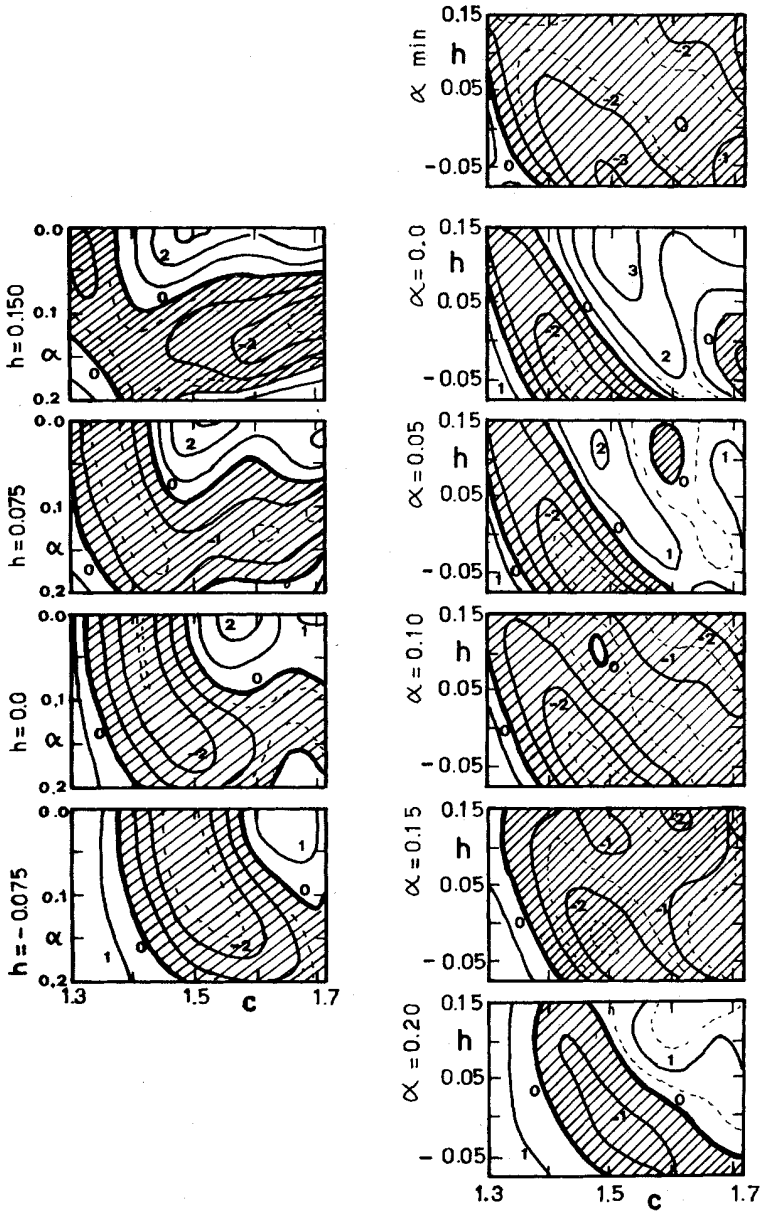

FIG. VIII-6. Neutron energy shell correction $\delta U_n+\delta P_n$ for asymmetric shapes. Only the region around the second minimum and the second barrier is shown. Equidistance of the full lines: 1 MeV. Left side: $\{c, \alpha\}$ contour maps for different values of the neck parameter h. Right side: $\{c, h\}$ contour maps for different values of the asymmetry parameter α. The topmost map (α_{min}) was obtained by minimizing $\delta U_n+\delta P_n$ with respect to α in each point $\{c, h\}$.

instabilities against the asymmetric deformations, however, for the spherical shapes of the deformed nuclei and especially at the second barrier of all actinide nuclei (Pauli *et al.*, 1971). While the former case is merely interesting for the systematics of shell effects, the latter case is of important physical significance. Therefore, we have restricted our further calculations with asymmetry to the most important region in the $\{c, h\}$ plane, which contains the two barriers and the second minimum in the actinide region.

In Fig. VIII-6, we present the results obtained for the neutron shell corrections which are a decisive part of the total deformation energy. On the left-hand side of the figure, four $\{\alpha, c\}$ contour maps of the total energy correction $\delta U_n+\delta P_n$ are shown, calculated for the neutron number $N=146$. For $c\approx 1.3$, i.e., at the left edge of the maps, symmetric shapes are favored in all cases. These are the regions of the first barrier and the second minimum. For larger c, in the region of the second barrier, the instability sets in. The occurrence of pronounced shell closures obviously can be connected also with left–right asymmetric shapes. In some cases, up to 5 MeV can be won by minimizing $\delta U_n+\delta P_n$ with respect to the α degree of freedom. Although this is

largely balanced by the increase in the LDM energy, one finds remarkable effects in the total deformation energy especially around the second barrier (with $c \approx 1.6$).

In the right-hand side of Fig. VIII-6, we see some $\{c, h\}$ maps of the same results for different values of α. While the region of lower c and h values is not affected by α, the shell structure in regions of larger deformations is clearly changed with increasing asymmetry. The topmost map on the right-hand side was obtained by minimizing the shell energy correction with respect to the asymmetry.

It is now interesting to see how these results affect the total deformation energy. This is shown in Fig. VIII-7. Above we see the total energy surface of ^{240}Pu in a $\{c, h\}$ map for $\alpha=0$ (which is a part of the corresponding map in Fig. VIII-4). Below, an analogous surface is shown, but here the total energy has been minimized locally in each point (c, h) with respect to α. One clearly recognizes that the second minimum region is unaffected, whereas the outer barrier is slightly shifted from $(c, h) \approx (1.6, -0.05)$ to $(c, h) \approx (1.54, 0.0)$, its energy being lowered by approximately 2 MeV. It is important to realize that the second barrier is not only unstable against asymmetry, but also that its position in the (c, h) plane is shifted towards a deformation

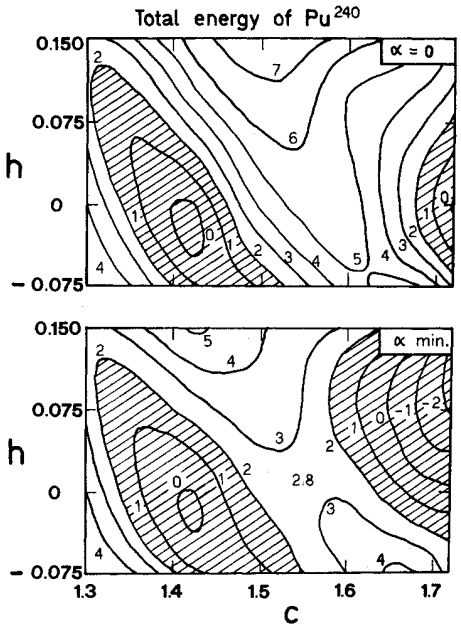

FIG. VIII-7. Total deformation energy of ^{240}Pu for symmetric (above, $\alpha=0$) and asymmetric shapes (below, α_{min}). Equidistance: 1 MeV. Only the region of the outer minimum and saddle is shown. The upper map is a part of the corresponding map in Fig. VIII-4. The lower map has been obtained by minimizing the total energy with respect to α in each point $\{c, h\}$. The minimum is symmetric, whereas the saddle is lowered by the asymmetry by approximately 2.2 MeV. Note that the position of the saddle point is shifted in the $\{c, h\}$ plane.

TABLE VIII.3. The calculated energies for local extrema of the deformation energies in the actinide region. The higher of the barriers is marked by an asterisk (*). The shell corrections were computed using an average potential of the Woods–Saxon type (see Sec. VII) with parameters given in Table VIII.1. Left–right asymmetry is included. For the liquid-drop energy a value of $(Z^2/A)_{crit}=45$, and a surface energy coefficient of 17 MeV was assumed. No special fit to experimental threshold was undertaken [see however Pauli and Ledergerber (1971)].

	Ground state in MeV relative to spherical LDM)	Isomer state	Inner saddle	Outer saddle
		(given in MeV, relative to the ground state)		
^{228}Ra	−0.4	2.2	2.4	8.2*
^{232}Th	−1.1	2.3	3.9	6.8*
^{236}U	−1.7	2.2	4.4	6.1*
^{240}Pu	−2.3	2.5	5.2*	5.1*
^{244}Cm	−2.7	2.0	6.0*	4.1
^{248}Cf	−3.5	2.1	7.4*	3.2
^{252}Fm	−3.8	1.6	7.8*	2.0
^{256}No	−4.2	0.8	7.6*	0.9
^{260}Ku	−5.2	0.4	7.0*	0.8

with a thinner neck, when the shape asymmetry is included. The nuclear elongation is reduced at the exit point and correspondingly a higher value of the Coulomb repulsion at the exit, i.e., a higher kinetic energy of the fragments is expected for the asymmetric mass division. This result agrees qualitatively with the experimental observation that the kinetic energy of the fission fragments is about 20 MeV higher for asymmetric fission.

Similar results are obtained for the other nuclei in the actinide region, whose maps are collected in Appendix A (Fig. A-2). Summing up the results, we can state the following points:

The shapes corresponding to the two minima and the first barrier are symmetric for all the actinides. The second barrier is unstable against asymmetry for all actinides. The energy of the saddlepoint is shifted towards a thinner neck (h) and a somewhat smaller elongation (c).

Our results confirm the above-mentioned report of Møller and Nilsson (1970). Also, the recent calculations of Pashkevich (1970) seem to agree, although the shapes and parameters of the Woods–Saxon potential which he used were somewhat different. [He considers a family of shapes, which are based on the lemniscate shapes and parameters of the Woods–Saxon potential, which ressemble those of Rost (1968).]

This qualitative agreement of calculations using different shapes and different single-particle models indicates once more that the result is not sensitive to details of the single-particle potential.

For more quantitative results, this problem of asymmetric fission must be treated in a more general way. Also, the dynamic features of the distorted nucleus

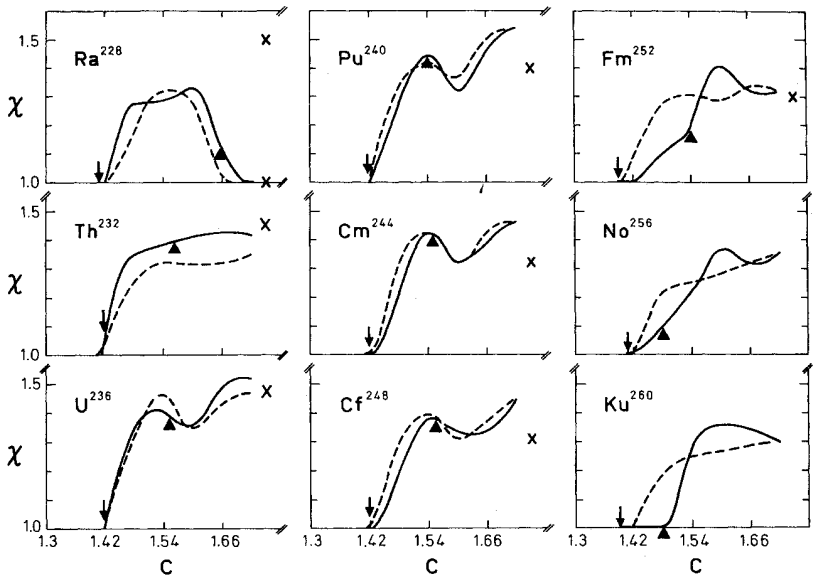

FIG. VIII-8. Theoretical mass ratios χ (for definition see the text) of some nuclei in the actinide region, plotted against c. The full and dotted lines correspond to two paths in the $\{c, h\}$ plane shown in the energy surfaces of these nuclei in Fig. A-2. Arrows ($\downarrow$) mark the isomer state shapes (symmetrical in all cases, therefore $\chi=1.0$), triangles (▲) mark the second saddle shapes. The crosses (×) mark the experimentally measured mass ratios of the fission fragments (Hyde *et al.*, 1964). Note the two crosses for ^{228}Ra, which has three peaks in the fragment mass distribution.

must be taken into account. Nevertheless, it seems plausible to conclude at this stage that the deformation energy favors asymmetric shapes at the outer barrier and in the exit region. It seems to us that these results may be considered as a basis for an explanation of the asymmetry in nuclear fission. It is, indeed, a shell-structure effect, although the shells responsible for it have hardly much to do with the magicity of spherical fragments.

It is thus tempting to estimate the mass ratios χ of the fragments which can be expected from these results. Let us define χ as the ratio of the volumes on each side of the $\chi=0$ plane. This definition is of course somewhat arbitrary but it is simple and should reveal the main features of the real mass ratio. Therefore χ is useful as a guide. In Fig. VIII-8, we have plotted χ against the elongation variable **c**. The two curves shown for each nucleus correspond to the two trajectories shown in Fig. A-2 in Appendix A. Along these paths, the mass ratio χ increases rather rapidly just behond the second minimum (marked by an arrow $\downarrow$), where we have found it above to be unity. In almost all cases it is more or less constant along the way from the second saddle (marked by a triangle ▲) towards scission. With the assumption that this mass ratio does not change during scission, it should be a rough estimate for the measured mass ratio of the fission fragments. The experimental points in Fig. VIII-8, which are the peak-to-peak ratios of the measured mass distributions, show that our estimates of χ are reasonable. It seems to us that more reliable than the absolute values of the calculated χ, as the assumptions made are hard to prove, are the systematics: the existence of a symmetric fission mode of ^{228}Ra and the slow decrease of the mass ratios with increasing mass number for $A \geq 240$ is roughly reflected in these preliminary results (see also Pauli *et al.*, 1971).

3. The Heights of the Fission Barriers of the Actinides

In Table VIII.3 we present the energies of the four stationary points of the total deformation energy as obtained from the maps presented in Figs. VIII-7 and A-2. The calculated fission thresholds—i.e., the higher of the two barriers, measured from the ground state—agree in general with the known experimental values (Table VIII.2) within our estimated error limit of about 0.5–1 MeV. This result could certainly be improved by a final fit of the LDM parameters, which was not performed here. The relative height of the two barriers is appreciably improved by the allowance of asymmetric shapes and now agrees better with the conclusions of Lynn and Bjørnholm (private communication) drawn from a compilation of various experiments. We mention especially the equal height of the barriers of ^{236}U. For lighter nuclei the outer barrier, and for heavier nuclei, the inner barrier is the higher one. These thresholds do not expose any tendency to decrease with increasing Z^2/A, as was predicted by the liquid-drop model. On the contrary, for the heavier actinides, they increase up to about 7 MeV for ^{260}Ku. This does, however, not necessarily contradict the lifetime systematics, as we shall see later in Sec. IX.

The thorium isotopes are somewhat pertinacious nuclei. We get there a too low inner barrier, viz. 3.8 MeV for ^{232}Th and even less for ^{230}Th, whereas the experiments seem to suggest at least 5.5 MeV in order to explain a rather high intermediate vibrational state (Lynn, 1966; Vorotnikov *et al.*, 1967). As mentioned above, this lack could not be removed by improvements of the single-particle model and seems to be serious.

A way to improve the results would be a new adjustment of the liquid-drop model. Actually, in all our

calculations the LDM parameters must be fitted anew after addition of the calculated shell corrections to the LDM energies. Thereby, it will be a somewhat cumbersome problem to determine which one of the two barriers in the deformation energies of the actinide nuclei corresponds to the experimental fission thresholds. Such a fit—simultaneously done for both ground-state masses and fission thresholds—may definitely improve the results. The lighter fissioning nuclei like thorium will be more sensitive to this correction, as for those the shape of the LDM saddlepoint is more critical than for the heavier nuclei.

With our choice of two symmetric and one left–right asymmetric shape parameters, we may still have restricted too much the possible shape variations of the nuclear surface. Even small amounts of more complicated shape distortions may lead to a gain of some MeV in the deformation energy. For example, a degree of freedom which breaks the axial symmetry may be important at larger deformations. Recently, Pashkevich (1969) has reported an instability of the first barrier against γ deformations, going along spheroidal deformations in a Nilsson potential well. It has to be investigated, whether this instability is still present in a more realistic (e.g., the Woods–Saxon) potential, using the (asymmetric) saddle-point shapes which we have investigated.

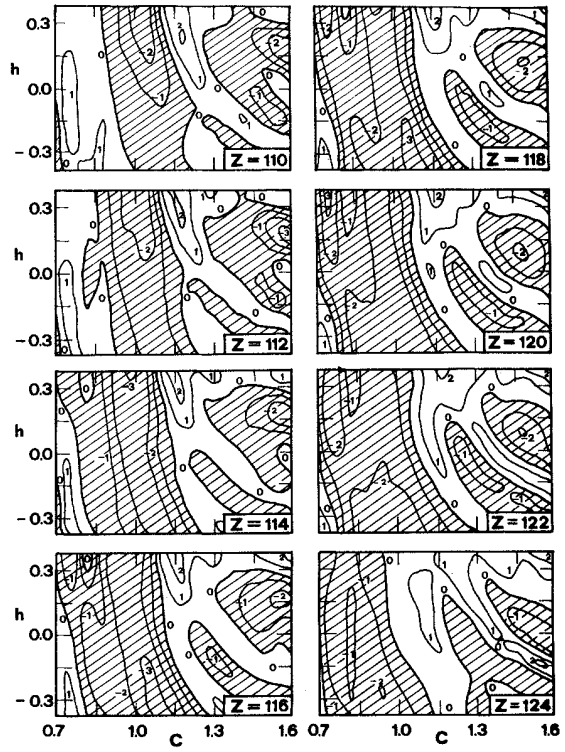

FIG. VIII-9. Shell-corrections $\delta U+\delta P$, as in Fig. VIII-1, for protons in the superheavy region (Equidistance of the contour-lines is 1 MeV here).

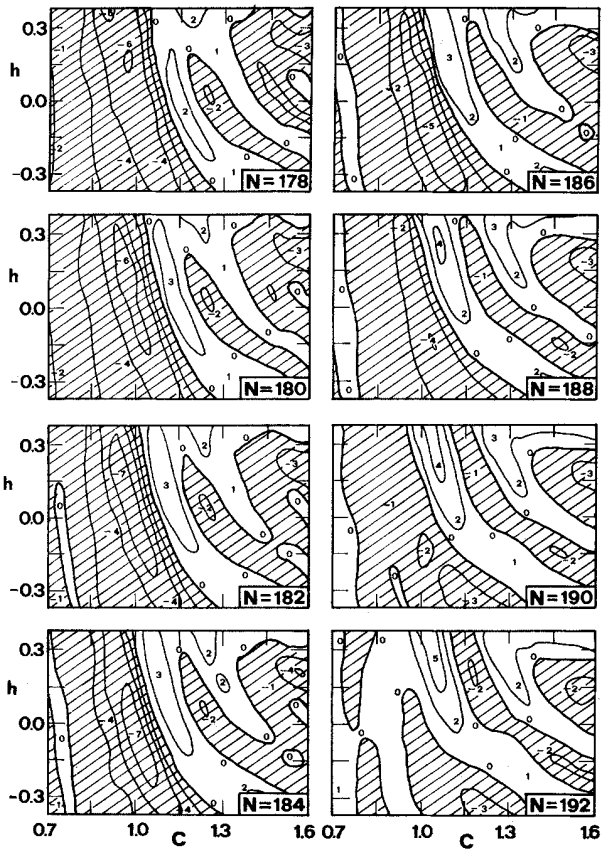

FIG. VIII-10. Shell-corrections $\delta U+\delta P$, as in Fig. VIII-1, for neutrons in the superheavy region.

In connection with the ground-state masses (Sec. VI), we have mentioned the problem of the zero-point energies of vibrations in the potential wells formed by the deformation energy surface. Should these energies differ in the two wells, the neglect of this effect may give rise to errors of up to 1 MeV, as the lowest vibrational states are known to lie at energies of this magnitude.

4. The Deformation Energy for Superheavy Nuclei

In the liquid-drop model, the upper limit for the stability of nuclei against fission is reached when the fissility parameter x [see Eq. (VII-14)] is equal to 1. It was pointed out earlier (e.g., Myers and Swiatecki, 1966a) that the increased stability due to shell structure may lead to islands of nuclei in the Periodic Table beyond this limit of $(Z^2/A)_{\text{crit}}$. As the shell structure is especially pronounced in spherical magic nuclei, possible candidates for such superheavy nuclei should favorably be compositions of the magic nucleon numbers 82, 126, 184···. For the neutrons, this outer magic number 184 is well established (see however, Meldner, 1969), but there is less agreement on the proton number. The importance of the Coulomb field for the distribution of shells increases with the increasing charge of the nucleus.

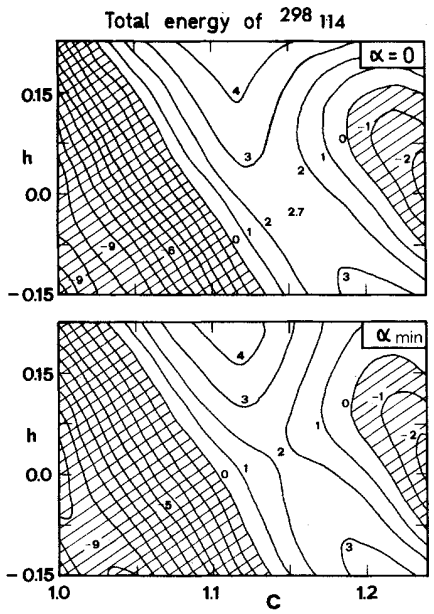

FIG. VIII-11. The same as in Fig. VIII-7 for the hypothetical superheavy nucleus $^{298}114$.

As a consequence, the original shell at $Z=126$ is widened and centered around $Z\approx114$–120. This effect can be seen in Fig. V-1, 2, where shell corrections are plotted against the nucleon numbers.

We have thus, for this discussion, carried out some calculations using the deformed Woods–Saxon potential of a hypothetical nucleus with $Z=114$ and $N=184$. The parameters of the LDM and the average potential were obtained by the straightforward extrapolation and are presented in Table VIII.1. As we, of course, are interested mainly in deformations closer to sphericity than for the actinides, we have used the range of deformations $0.7\leq c\leq1.6$, $-0.375\leq h\leq0.375$, and $0\leq\alpha\leq0.2$.

The contour maps of the energy shell corrections for $110\leq Z\leq126$ (protons) and $178\leq N\leq192$ (neutrons) are shown in Figs. VIII-9 and VIII-10, respectively. They show essentially the same pattern as the energy corrections of the actinides (comp. Figs. VIII-1, 2).

Maps of the total energy for a series of superheavy nuclei can be found in Figs. A-3 and A-4 in Appendix A. It turns out that the most favorable magic neutron number is indeed $N=184$, even when the LDM is added, whereas for the protons $Z=114$ and $Z=120$ lead to deep shell minima, both at spherical shapes. Thus, the hypothetical nuclei $^{298}114$ and $^{314}120$ are spherical magic nuclei of interest. Their fission thresholds are seen to be ≈13 MeV. Other than spherical shapes cannot be expected to be stable in this region, as the LDM energy falls off very rapidly, moving away from sphericity. Of the two candidates, the former, i.e., $^{298}114$, is supposed to be more stable against α decay (see e.g., Nilsson *et al.*, 1969; Muzycka, 1970). Therefore we show here the total energy map of this nucleus in Fig. VIII-11, both for symmetrical shapes (above), and minimized with respect to the asymmetry parameter α (below). The barrier height is not affected much by the asymmetry and the resulting value of 12.7 MeV is still high enough to make a relatively long lifetime possible. A definite answer to this question can, however, only be given within the framework of a dynamic theory (see Sec. IX below).

How reliable are the numbers presented here? One should keep in mind that we have extrapolated both the single-particle and the liquid-drop model.

As we have discussed in Sec. VI for the ground-state masses of spherical nuclei, the shell corrections are not very sensitive to the exact position of individual levels or even degenerate spherical subshells. Instead, the shell corrections are sensitive to the spacing between the mean energies of the upper- and lower-level bunches and their relative widths. We believe that these quantities are also quite reliably reproduced in the extrapolated region of the single-particle model. Thus we tend to believe that the shell corrections presented are as reliable as the shell correction to the ground-state mass of ^{208}Pb discussed in Sec. VI.

IX. ON THE DYNAMICS

In this section, some problems concerning fission dynamics are discussed. A possibility of circumventing some still poorly understood dynamic features of the nuclear shape distortion by considering a least-action trajectory in the space of deformation coordinates is described. The approximation implied by using the least-action trajectory is expected to give at least an order-of-magnitude estimate of the spontaneous fission problem. But, in order to apply this approximation, we must know the mass tensor connected with the trajectory. The evaluation of this tensor in the cranking model and the results obtained for lifetime estimates are discussed subsequently. Finally, we present some calculations of the moments of inertia for fissioning nuclei.

1. Inertial and Friction Forces and the Dynamics of Fission

In a more complete theory of the fission process, the deformation energy surface described in the preceding section constitutes only a part of the required data. Considered as a function of the deformation parameters, the deformation energy gives the generalized forces acting on the nuclear shape. For a description of the process of fission, one should also know how the nucleus reacts to these forces. This is another piece of the information required, which is contained in the so-called tensor of inertial coefficients of the system, B_{ij}. In the case of dissipation, the tensor of the friction forces γ_{ij} is also of importance. Here, the indices denote different

degrees of freedom as they appear in the definition of the nuclear shape, e.g., in terms of the shape function $\Pi(\beta, u, v)$. In each of the two tensors, one has for n deformation coordinates, $\frac{1}{2}n(n+1)$ independent quantities. They are all complicated functions of the deformation coordinates (Damgaard *et al.*, 1969b).

Of course, one must also know the equation of motion characteristic of the fission process in terms of the shape coordinates. Unfortunately, not much is known about such an equation and, at present, one can even hardly decide what kind of dynamics it should describe. The latter may also depend on the excitation energy of the compound nucleus since, at larger excitation energies, the interaction between the collective and intrinsic degrees of freedom seems to play an increasingly important role.

Some confirmation of such a dependence may be found in the fact that—as in Bohr and Wheeler's paper of 1939—one has always assumed statistical equilibrium in order to determine the fission rate in terms of the statistical phase-space density of the nucleus at the fission barrier

$$\Gamma_f \propto (N_f/2\pi)D. \qquad \text{(IX.1)}$$

Here, N_f is the number of excited states available at the barrier, and D is the level spacing of the initial compound nucleus. In a number of critical reviews on empirical data (e.g., Vandenbosch and Huizenga, 1958), it has been demonstrated that this simple equation agrees well with the data concerning both the energy dependence of Γ_f and its variation with Z and A.

In 1940, Kramers showed, however, that the Bohr–Wheeler equation (IX.1) requires a finite viscosity for the collective motion. Equation (IX.1) is valid only if the viscosity coefficient ν is of the order of the characteristic frequency of the collective mode, ω_{coll}. The magnitude of Γ_f is then nearly independent of the specific value of the viscosity. For a very small ratio ν/ω_{coll}, Γ_f is proportional to the viscosity coefficient ν, because it is only due to the interaction with the intrinsic motion that the thermal energy in the excited nucleus concentrates back in a collective mode. Contrary to this, for large viscosity, Γ_f is inversely proportional to ν as the collective motion dissipates too fast.

The available data on Γ_f are not yet accurate enough to deduce the viscosity connected with the collective motion in the fission mode. It appears only in a slowly varying pre-exponential factor in Γ_f (see Kramers, 1940). However, the very success of the Bohr–Wheeler equation suggests that, in the excited nucleus, the viscosity of the shape variations must be at least a few hundred keV or more, which is comparable to the estimated fission mode frequency of the order of 0.5 MeV.

In contrast, the model of purely mechanical, i.e., nondissipative, motion seems to work well for the lowest excitation, particularly when used to estimate the rate of spontaneous fission. Here again one hardly has any direct evidence that this assumption is relevant, except for the fact that simple estimates of the spontaneous fission lifetimes in this model are in at least qualitative agreement with the empirical values.

The problem of formulating the equation of motion for the fission process is intimately related to one of the most exciting problems of modern nuclear physics, i.e., the dynamic properties of nonequilibrium states in a large piece of nuclear matter. In many respects, it is a new problem, as the main efforts were concentrated so far on a discussion of small perturbations of the ground states.

The dissipation problem is a hard nut in the microscopic theories of nearly all classical media; there is no reason why it should be simple in a relatively small and strongly bound quantal system such as the nucleus. Therefore, one should not be discouraged by the fact that, in the fission theory, the discussion of this important problem has been limited so far to ambiguous estimates which only explore the field; see, e.g., Wilets (1959).

The situation is, however, not as hopeless as one might conclude from the foregoing. Although one can hardly be very enthusiastic about having a ready-to-use detailed theory of fission in a very near future, in many instances one will probably not need it for a description of at least some of the features of practical importance. As an example, one may refer to the data described in Sec. VII, where it has been shown how some qualitative pecularities of the LDM energy surface help to draw a reasonably qualitative picture of the process, in which the intrinsic structure of the nucleus as well as dynamic and quantal features of the deformation play probably only a secondary role—though undoubtedly important for finer details.

2. The Least-Action Trajectory

In an analogous manner, the theory of spontaneous fission is considerably simplified due to the fact that the probability of the process is determined by the exponentially small penetration factor

$$\tau^{-1} = A \exp(-2S/\hbar), \qquad \text{(IX.2)}$$

where

$$S \gg 1. \qquad \text{(IX.3)}$$

The quantity S is the classical action integral taken along the trajectory of least action of a given energy $\mathcal{E}$, connecting the positive energy regions in the ground-state well and the exit. Correspondingly, the trajectory connects the second well and the exit for the spontaneous fission isomers. In any case, it is a relatively simple classical concept which is not too sensitive to details of the equation of motion and in particular to quantal features, which would affect only the pre-exponential factor A in Eq. (IX.2), equal, by the order of magnitude, to the characteristic frequency of the collective mode.

The variation of the latter is, in fact, much less important than the action integral itself which is of the order of a few ten or a hundred units of $\hbar$.

Therefore, with logarithmic accuracy, the spontaneous fission probability may be found by means of a simple theory dealing only with the classical action integral

$$S=\int_{\sigma_1}^{\sigma_2}(2\mid\mathcal{E}-W\mid\tilde{T})^{1/2}d\sigma \qquad \text{(IX.4)}$$

$$\tilde{T}=\sum_{ij}B_{ij}(d\beta_i/d\sigma)(d\beta_j/d\sigma). \qquad \text{(IX.5)}$$

Here, the deformation parameters β_i are considered as functions of some arbitrary parameter σ. The integral is taken along some trajectory, determined in the parametrical form, between the two end points σ_1 and σ_2 corresponding to the entrance into the sub-barrier region and the exit on the other side of the potential barrier. The energy $\mathcal{E}$ of the collective motion is assumed to be conserved. Though the region of interest ($W>\mathcal{E}$) is classically forbidden, the trajectory is a classical one.

The potential energy $W(\beta_1,\cdots)$ is just the deformation energy described in the previous sections (see especially Sec. VIII). The deformation parameters $\{\beta\}=\{\beta_1,\cdots,\beta_n\}$ appear here as generalized coordinates. The inertial parameters B_{ij} are also functions of these variables. And, as discussed below, it appears that the inertial parameters are nearly as much influenced by the intrinsic shell structure as is the deformation energy itself. These variations may also be important in determining the actual trajectory. The energy consideration alone is in no case sufficient: The system may even go in a direction where the potential barrier is higher or increases faster, if the effective inertial parameter is smaller or strongly decreases in that direction.

In order to estimate the penetrability of the multidimensional potential barrier, one should find, first, such a trajectory that corresponds to the lowest value of the action integral (IX.4) among all possible trajectories which connect the two end points σ_1 and σ_2 as well as the trajectories obtained by variation of these points. For the energy-conserving system such as we assume here, this corresponds to one of the well-known formulations of the least-action principles (see, e.g., Landau and Lifschitz, 1960).

There is a formal analogy between this problem and the problem of finding a geodesic in an n-dimensional space, where the arc length element is given by the equation

$$(d\sigma)^2=\sum_{i,j=1}^{n}a_{ij}d\beta_i d\beta_j \qquad \text{(IX.6)}$$

with

$$a_{ij}=2\mid\mathcal{E}-W\mid B_{ij}(\beta). \qquad \text{(IX.7)}$$

The path of lowest action is one of the geodesics which are determined by the following system of n Euler equations:

$$\Phi_{\beta_i}(\beta_i,\dot{\beta}_i)-(d/d\sigma)\Phi_{\dot{\beta}_i}(\beta_i,\dot{\beta}_i)=0. \qquad \text{(IX.8a)}$$

Here we have

$$\Phi(\beta_i,\dot{\beta}_i)=\sum_{i,j}a_{ij}\dot{\beta}_i\dot{\beta}_j \qquad \text{(IX.8b)}$$

and

$$\dot{\beta}_i=d\beta_i/d\sigma.$$

In Eq. (IX.8a) the subscripts β_i and $\dot{\beta}_i$ mean differentiation with respect to these variables. To Eq. (IX.8) we can add the subsidiary condition

$$\Phi=1. \qquad \text{(IX.9)}$$

This subsidiary condition specifies the variable σ in such a way that it becomes equal to the arc length of the curve

$$\beta_i=\beta_i(\sigma) \qquad i=1,2,\cdots,n \qquad \text{(IX.10)}$$

in n-dimensional space (Smirnov, 1964).

By means of the Christoffel symbols, Eqs. (IX.8) are resolved with respect to the second derivatives:

$$\ddot{\beta}_i+\sum_{p,q}\begin{Bmatrix}pq\\ i\end{Bmatrix}\dot{\beta}_p\dot{\beta}_q=0 \qquad 1\le i,p,q\le n, \qquad \text{(IX.11)}$$

where

$$\begin{Bmatrix}pq\\ i\end{Bmatrix}=\sum_{j=1}^{n}a^{ij}\begin{bmatrix}pq\\ j\end{bmatrix}. \qquad \text{(IX.12)}$$

The Christoffel symbol of the first kind is denoted by

$$\begin{bmatrix}pq\\ i\end{bmatrix}=\frac{\partial a_{pi}}{\partial\beta_q}+\frac{\partial a_{qi}}{\partial\beta_p}-\frac{\partial a_{pq}}{\partial\beta_i}$$

and the quantity a^{ik} is the inverse and transpose matrix of the matrix a_{ik} defined by Eq. (IX.7).

The boundary conditions are also determined by the requirement that the action integral is stationary against variation of the endpoints σ_1 and σ_2, which rest on the equipotential surface

$$W(\beta_1,\cdots,\beta_n)=\mathcal{E}. \qquad \text{(IX.13)}$$

Thus, the variation of the action integral equals

$$(F-\sum_{i=1}^{n}\dot{\beta}_iF_{\dot{\beta}_i})\delta\sigma+\sum_{i=1}^{n}F_{\dot{\beta}_i}\delta\beta_i=0 \qquad \text{(IX.14)}$$

where F is the integrand of the action integral (IX.4),

$$F=\Phi^{1/2}. \qquad \text{(IX.15)}$$

The variations $\delta\sigma$ and $\delta\beta_i$ must also satisfy equation

(IX.13)

$$\delta W=0=\sum_{i=1}^{n}\frac{\partial W}{\partial\beta_i}\delta\beta_i, \tag{IX.16}$$

and these equations lead to n boundary conditions in the endpoints,

$$F-\sum_{i=1}^{n}\dot{\beta}_i F_{\dot{\beta}_i}=0 \tag{IX.17}$$

and $n-1$ equations relating the partial derivatives of the function F and the generalized forces

$$\mathfrak{F}_i=\partial W/\partial\beta_i. \tag{IX.18}$$

These equations are

$$F_{\dot{\beta}_i}/\mathfrak{F}_1=\cdots=F_{\dot{\beta}_n}/\mathfrak{F}_n. \tag{IX.19}$$

Now, taking into account the specific form of the integrand F, Eq. (IX.19) can also be written as

$$T_{\dot{\beta}_1}/\mathfrak{F}_1=T_{\dot{\beta}_2}/\mathfrak{F}_2=\cdots=T_{\dot{\beta}_n}/\mathfrak{F}_n \tag{IX.20}$$

where $T(\beta,\dot{\beta})$ is the kinetic energy part of F:

$$T=\tfrac{1}{2}\sum_{i,j}B_{ij}\dot{\beta}_i\dot{\beta}_j. \tag{IX.21}$$

The condition (IX.17) is identical to Eq. (IX.13). Here, we have assumed that the inertial parameters are functions of the coordinates β_i only, and T is a homogeneous function of the second order of the derivatives $\dot{\beta}_i$.

The system of the differential equations (IX.8) together with the boundary conditions (IX.13) and (IX.20) determine several trajectories which give extrema of the action integral (IX.4) evaluated along such trajectories. Among them, the one which gives the lowest value of the integral (IX.4) must be chosen.

Apparently, the problem of solving these equations is not an easy one even in such a limited formulation of the problem. One must know not only the deformation energy and the inertial parameters as functions of the deformation coordinates, but also their partial derivatives. In addition, Eq. (IX.4) has a singularity in the classical turning points, and special measures must be taken to overcome this difficulty.

Nevertheless, one can consider these equations as a kind of first approximation to a complete dynamic theory of the fission process. They are rather complicated, but one should note that for their derivation, no knowledge of the Schrödinger equation for collective shape variation is required; to develop the latter for a system whose inertial parameters depend significantly on the coordinates is in itself a problem.

The choice of the arc length σ as the independent variable is in no case necessary. Its only advantage is that with it the Euler equations for geodesics take a more symmetric form. Instead, any other function of the coordinates β_i may be used or one of them may be taken as an independent variable, the others being considered as functions of it.

Taking one of the deformation coordinates, say the elongation parameter, as an independent variable, one obtains the following system of $n-1$ differential Euler equations:

$$T(KT_{y_i}+TK_{y_i})-T[K(d/dx)T_{\dot{y}_i}+\tfrac{1}{2}T_{\dot{y}_i}(dK/dx)]+\tfrac{1}{2}KT_{\dot{y}_i}(dT/dx)=0, \tag{IX.22}$$

where we denote the independent variable by x, and $y_i(x)$ are the other coordinates which, as functions of x, determine the trajectory. As before, the subscripts y_i and $\dot{y}_i$ denote the partial derivatives with respect to y_i and to dy_i/dx which appear as arguments in the "kinetic energy" function T and in the actual kinetic energy K

$$K=|\,\mathcal{E}-W(\beta_1,\cdots,\beta_n)|. \tag{IX.23}$$

It might be instructive to consider the case of only two deformation coordinates. When we drop the index i, we find a single differential equation for this case. Denoting as a, b, and c the three independent components of the inertial tensor B_{ij} in

$$\tilde{T}=a+2b(dy/dx)+c(dy/dx)^2, \tag{IX.24}$$

we find the following equation for $y=y(x)$:

$$K[2\ddot{y}(b^2-ac)+a_x(b+c\dot{y})+a_y(a+3b\dot{y}+2c\dot{y}^2)-2b_x(a+b\dot{y})+2b_y\dot{y}^2(b+c\dot{y})-c_x\dot{y}(2a+3b\dot{y}+c\dot{y}^2)-c_y\dot{y}^2(a+b\dot{y})]+\tilde{T}[(a+b\dot{y})K_y-(b+c\dot{y})K_x]=0. \tag{IX.25}$$

The transversality condition Eq. (IX.20) at the end points just means that the term included in the squared brackets in the second term should become zero there. The Eq. (IX.25) also has another singularity at these points: the coefficient of the second derivative equal to

$$2K(b^2-ac) \tag{IX.26}$$

is zero there, alongside the actual kinetic energy K.

Therefore, the transversality condition insures that a physically reasonable solution exists, which has a finite second derivative at the endpoints. Close to them, the solution may be found in the usual way by equating the coefficients in the Taylor expansions.

With the inertial parameters a, b, c depending significantly upon the coordinates, it is not an easy task to find the solution of Eq. (IX.25); neither can one describe even qualitative features of the best trajectory.

Practical evaluation of the potential energy of the deformation and the related forces as well as of the inertial parameters and their derivatives is still labor consuming and one can only postpone a rigorous solution to the near future, when more knowledge is acquired concerning the behavior of these important

physical quantities, as well as more general dynamic features of the deformations.

A simple solution can be obtained only for the case of a constant inertial parameter in the region near the extremum of the potential, where the potential can be represented as a homogeneous polynomial of the power p

$$W=\sum_{i=0}^{p}\alpha_i x^i y^{p-i}, \tag{IX.27}$$

where α_i are the expansion coefficients of the potential energy W normalized to zero at the extremum point $x=y=0$. For this special case, straight line trajectories crossing the extremal point are a solution. Assuming

$$y=\Delta x, \tag{IX.28}$$

where Δ is a constant, we find from Eq. (IX.25) the following equation for Δ:

$$(a+b\Delta)K_y(1,\Delta)-(b+c\Delta)K_x(1,\Delta)=0 \tag{IX.29}$$

which is satisfied with one or more constant values of the slope Δ.

For $p=2$, Δ is found from the following quadratic equation:

$$\Delta^2(2b\alpha_0-c\alpha_1)+2\Delta(a\alpha_0-c\alpha_2)+(a\alpha_1-2b\alpha_2)=0 \tag{IX.30}$$

in which α_0, α_1, and α_2 are the coefficients in Eq. (IX.27). The solutions of this equation determine the slopes of the two trajectories of extremal action corresponding to the smallest and the largest values of the action integral (IX.4). They are also trajectories of the two normal modes of motion. These trajectories, in general, coincide neither with the direction of the steepest variation of the potential energy nor with that of the kinetic energy, which would be the case only for rotational invariance of the quadratic form of the potential energy W, or of the kinetic energy K in Eq. (IX.23).

Another interesting case is the approximation of steepest descent. It is obtained from Eq. (IX.25) on the assumption that the kinetic energy of the system is small compared to the potential energy. Neglecting all terms proportional to K in Eq. (IX.25) we obtain the following equation:

$$[a+b(dy/dx)]\mathcal{F}_y-[b+c(dy/dx)]\mathcal{F}_x=0. \tag{IX.31}$$

In this equation, $\mathcal{F}_x$ and $\mathcal{F}_y$ are the two partial forces defined as in Eq. (IX.18)

$$\mathcal{F}_x=\partial W/\partial x=\partial K/\partial x$$
$$\mathcal{F}_y=\partial W/\partial y=\partial K/\partial y. \tag{IX.32}$$

This equation determines locally the slope of the steepest descent trajectory

$$dy/dx=(a\mathcal{F}_y-b\mathcal{F}_x)/(c\mathcal{F}_x-b\mathcal{F}_y). \tag{IX.33}$$

For two orthogonal coordinates ($b=0$), the slope is proportional to the ratio of the forces divided by the corresponding partial masses. Thus, Eq. (IX.33) may be considered as a form of the steepest descent condition, generalized for the case of nonorthogonal coordinates and nonequal masses.

An even more general form is given by the transversality condition (IX.20) which can also be expressed in the following way:

$$\sum_{j=1}^{n}B_{1j}\dot{\beta}_j/\mathcal{F}_1=\sum_{j=1}^{n}B_{2j}\dot{\beta}_j/\mathcal{F}_2=\cdots=\sum_{j=1}^{n}B_{nj}\dot{\beta}_j/\mathcal{F}_n. \tag{IX.34}$$

Considered locally in each point of n-dimensional space, these equations determine the direction of smallest (or largest) local variation of the action integral.

It should be noted, however, that the arguments on which Eq. (IX.34) are based are in conflict with the original assumption of energy conservation in the system. In any system of this kind, the kinetic energy is, on the average, of the same order of magnitude as the potential energy. Consequently, the case of slow motion is realized only in systems with strong dissipative forces, and in this case the partial friction forces are at least as important as the effective inertial parameters.

3. The Effective Mass Parameters

The nucleons rearrange themselves in each state of the average potential in such a way that the total energy of the system has its lowest possible value. With a potential, i.e., with deformation parameters $\{\beta\}$ depending on the time, this so-called adiabatic assumption is of course only justified if the motion of the nucleons and the transitions from one level to another are so fast that the nucleon density distribution follows the average field at each moment. The nuclear composition is thus supposed not to depend on the history of the process.

This assumption justifies the expansion of the total energy in the time derivatives of the deformation parameters

$$\mathcal{E}=\mathcal{E}[\beta(t_0+\delta t)]\approx\mathcal{E}[\beta(t_0)]+T[\beta(t),\dot{\beta}(t)]. \tag{IX.35}$$

The second term T is interpreted as the kinetic energy of the collective motion and is to lowest order in $\dot{\beta}$ given by

$$T=\tfrac{1}{2}\sum_{i,j}B_{ij}(\beta)\dot{\beta}_i\dot{\beta}_j. \tag{IX.36}$$

The first term $\mathcal{E}[\beta(t_0)]$ may be identified with the deformation energy $W(\beta)$—described in Secs. V and VIII—and plays the role of a potential in the Hamiltonian of the collective motion.

The effective mass parameters $B_{ij}(\beta)$ are given by the cranking model formula (Inglis, 1954)

$$B_{ij}(\beta)=2\hbar^2\sum_m\frac{\langle 0\mid\partial/\partial\beta_i\mid m\rangle\langle m\mid\partial/\partial\beta_j\mid 0\rangle}{E_m-E_0}, \tag{IX.37}$$

where $|0\rangle$ and $|m\rangle$ denote the ground and an excited state of the system, respectively. No specific assumptions are made on these wave functions—provided one knows their dependence on the deformation parameters $\{\beta\}$.

Frequently, constraints on the motion of the individual particles are introduced at each deformation, in order to ensure that certain collective operators such as, e.g., the quadrupole moment have a particular value. This is usually achieved by means of the Lagrange multiplier method. The multipliers, introduced in this way, are then treated as dynamic variables. However, one hardly needs to do so in our case, where the collective variables are determined by the shape of the effective nuclear surface. By the very definition of the deformed shell-model potential (Sec. VII), one imposes constraints on the motion of the individual particles, by putting them into a potential well of a given shape. There is little doubt that, in this way, one has a consistent definition of the nuclear shape coordinates, by simply using the shape parameters of the potential as collective variables.

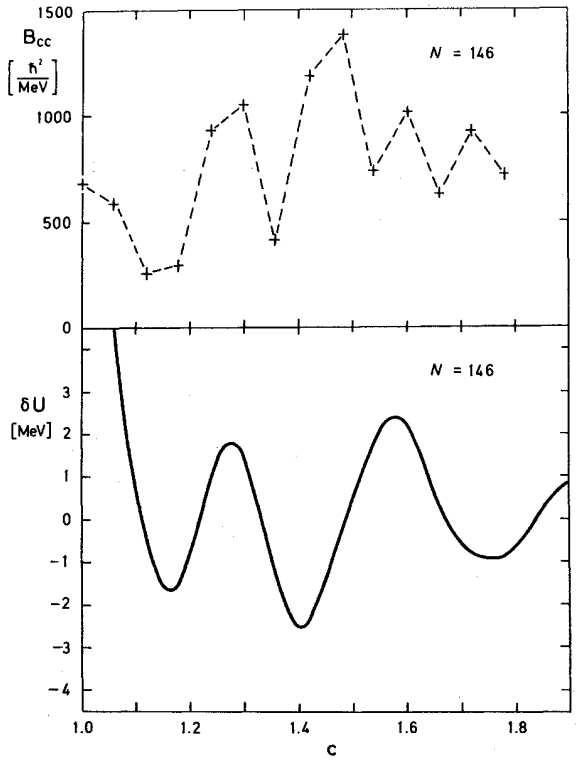

FIG. IX-1. Above: Mass parameter B_{cc} plotted versus the deformation parameter c ($h=0$, $\alpha=0$). Below: Shell energy correction $\delta U+\delta P$ plotted versus c ($h=0$, $\alpha=0$). Both curves are calculated for $N=146$ neutrons using a constant uniform pairing gap $\tilde{\Delta}=12\ A^{-1/2}$ MeV. For smaller deformations ($c\lesssim 1.4$) the fluctuations in the two quantities parallel each other, which reflects the role of the effective level density in the mass parameter [see Eq. (IX.48)].

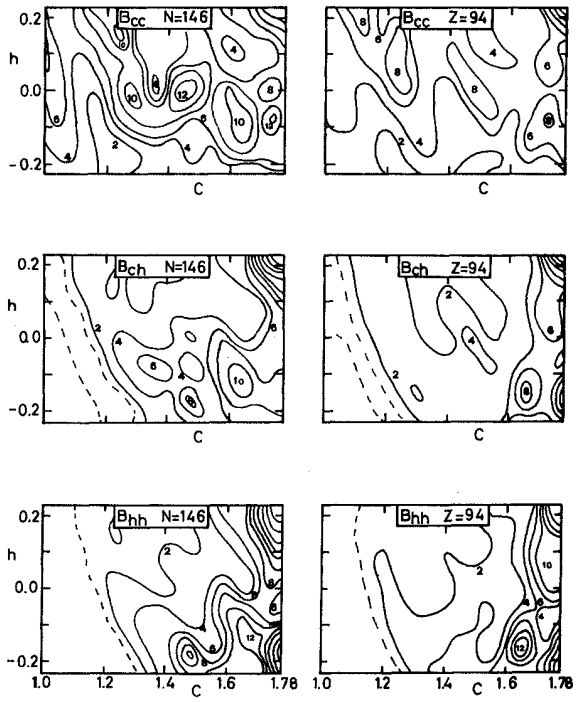

FIG. IX-2. Contour maps of the three mass parameters B_{cc}, B_{ch}, and B_{hh} for symmetric $\{c, h\}$ shapes. The neutron part (left side) and the proton part (right side) of ^{240}Pu separately. Numbers are in units of 100 $\hbar^2$/MeV; equidistance of full lines: 200 $\hbar^2$/MeV. The uniform pairing gap has been taken constant ($\tilde{\Delta}=12\ A^{-1/2}$ MeV). The plots demonstrate the shell structure for the two-dimensional case also. Observe the increase of the mass parameter at larger c values. Several local divergencies, which are connected to the short-comings of the formula (IX.37), as discussed in the text, can be observed.

Applying the cranking model formula (IX.37), one usually assumes (Bès, 1961; Kumar and Baranger, 1968), that the excited states $|m\rangle$ in Eq. (IX.37) are superpositions of two quasiparticle excitations $|\mu\nu\rangle$ with the energy $E_\mu+E_\nu$, where $E_\mu=[(\varepsilon_\mu-\lambda)^2+\Delta^2]^{1/2}$, and λ and Δ are the Fermi energy and energy gap of the system. Together with the relation (e.g. Wilets, 1964)

$$(E_m-E_0)\langle m\,|\,\partial/\partial\beta\,|\,0\rangle=\langle m\,|[\mathfrak{IC},\partial/\partial\beta]|\,0\rangle$$
$$=-\langle m\,|\,\partial\mathfrak{IC}/\partial\beta\,|\,0\rangle, \qquad \text{(IX.38)}$$

this leads to the following simple expression for the matrix elements of the operators $\partial/\partial\beta_i$

$$\langle\mu\nu\,|\,\partial/\partial\beta_i\,|\,0\rangle=-(u_\mu v_\nu+u_\nu v_\mu)/(E_\mu+E_\nu)$$
$$\times\langle\mu\,|\,\partial\mathfrak{IC}/\partial\beta_i\,|\,\nu\rangle; \qquad (\mu\neq\nu) \qquad \text{(IX.39)}$$

in terms of single-particle wave functions $|\mu\rangle$ and $|\nu\rangle$. u_ν, v_ν are the usual factors appearing in pairing theory (see Belyaev, 1959). The effects, due to variations in the occupation numbers as a function of deformation come from the "diagonal" matrix element, where the one quasi-particle is in the time-reversed state of the

other, and the matrix element is:

$$\langle \nu\bar{\nu} \mid \partial/\partial\beta_i \mid 0\rangle = (1/2E_\nu^2)[-\Delta\langle \nu \mid \partial\mathcal{H}/\partial\beta_i \mid \nu\rangle + \Delta(\partial\lambda/\partial\beta_i) + (\varepsilon_\nu - \lambda)(\partial\Delta/\partial\beta_i)]$$

where

$$\partial\lambda/\partial\beta_i = (ac_i + bd_i)/(a^2+b^2);$$
$$\partial\Delta/\partial\beta_i = (bc_i - ad_i)/(a^2+b^2); \qquad \text{(IX.40)}$$

with

$$a = \Delta \sum_\nu (1/E_\nu^3);$$
$$b = \sum_\nu (\varepsilon_\nu - \lambda)/E_\nu^3;$$
$$c_i = \Delta \sum_\nu \langle \nu \mid \partial\mathcal{H}/\partial\beta_i \mid \nu\rangle/E_\nu^3;$$
$$d_i = \sum_\nu (\varepsilon_\nu - \lambda)\langle \nu \mid \partial\mathcal{H}/\partial\beta_i \mid \nu\rangle/E_\nu^3.$$

Thus, the effective mass parameters are given by

$$B_{ij} = 2\hbar^2 \left[\sum_{\mu,\nu} \frac{\langle \mu \mid \partial\mathcal{H}/\partial\beta_i \mid \nu\rangle\langle \nu \mid \partial\mathcal{H}/\partial\beta_j \mid \mu\rangle}{(E_\mu + E_\nu)^3} \times (u_\mu v_\nu + v_\mu u_\nu)^2 \right] + P_{ij}, \qquad \text{(IX.41a)}$$

where the term

$$P_{ij} = \frac{\hbar^2}{4} \sum_\nu \frac{1}{E_\nu^5} \left[\Delta^2 \frac{\partial\lambda}{\partial\beta_i}\frac{\partial\lambda}{\partial\beta_j} + (\varepsilon_\nu - \lambda)\frac{\partial\Delta}{\partial\beta_i}\frac{\partial\Delta}{\partial\beta_j} + \Delta(\varepsilon_\nu - \lambda)\left(\frac{\partial\lambda}{\partial\beta_i}\frac{\partial\Delta}{\partial\beta_j} + \frac{\partial\lambda}{\partial\beta_j}\frac{\partial\Delta}{\partial\beta_i}\right) - \Delta^2\left(\frac{\partial\lambda}{\partial\beta_i}\langle \nu \mid \frac{\partial\mathcal{H}}{\partial\beta_j} \mid \nu\rangle + \frac{\partial\lambda}{\partial\beta_j}\langle \nu \mid \frac{\partial\mathcal{H}}{\partial\beta_i} \mid \nu\rangle\right) - \Delta(\varepsilon_\nu - \lambda)\left(\frac{\partial\Delta}{\partial\beta_i}\langle \nu \mid \frac{\partial\mathcal{H}}{\partial\beta_j} \mid \nu\rangle + \frac{\partial\Delta}{\partial\beta_j}\langle \nu \mid \frac{\partial\mathcal{H}}{\partial\beta_i} \mid \nu\rangle\right)\right] \qquad \text{(IX.41b)}$$

gives the contribution, due to the change of the occupation number, when the deformation varies.

3a. *The One-Dimensional Case*

The derivatives of the Hamiltonian with respect to the deformation variables in Eq. (IX.39) can be replaced by their leading terms, i.e., by the derivatives of the central potential,

$$\partial\mathcal{H}/\partial\beta_i \approx \partial V/\partial\beta_i, \qquad \text{(IX.42)}$$

the derivatives of the spin–orbit and the Coulomb potential being comparatively less important (Bès, 1961).

For our calculations, the derivative of the potential can for the general case be conveniently expressed in terms of the "quasiradius", l, introduced in Sec. VII, see, e.g., Eq. (VII.25):

$$\frac{\partial V}{\partial\beta_i} = \frac{\partial V}{\partial l}\cdot\frac{\partial l}{\partial\beta_i} = \frac{V_0}{a}\frac{\exp(-l/a)}{[1+\exp(-l/a)]^2}\frac{\partial l}{\partial\beta_i}. \qquad \text{(IX.43)}$$

The partial derivatives $\partial l/\partial\beta_i$ of this quantity are expressed in terms of partial derivatives of the shape function II in the following way

$$\frac{\partial l}{\partial\beta_i} = \frac{\Pi}{|\nabla\Pi|}\frac{\partial C}{\partial\beta_i} - C\frac{\Pi}{|\nabla\Pi|^2}\frac{\partial}{\partial\beta_i}|\nabla\Pi| + C|\nabla\Pi|^{-1}\frac{\partial\Pi}{\partial\beta_i}. \qquad \text{(IX.44)}$$

The derivatives (IX.44) become somewhat complicated by the definition of the shape function II [Eq. (VII.26)]. Let us first express the derivative of II with respect to β_i:

$$\frac{\partial\Pi}{\partial\beta_i} = \frac{1}{2[\pi(\beta,u,v)-\pi_{\min}]^{1/2}}\left[\frac{\partial\pi(\beta,u,v)}{\partial\beta_i} - \frac{\partial\pi_{\min}}{\partial\beta_i}\right] + \frac{\partial\pi_{\min}/\partial\beta_i}{2[-\pi_{\min}]^{1/2}}. \qquad \text{(IX.45)}$$

where π is the initial shape function, Eqs. (VII.4) and (VII.5).

The derivatives of the gradient are

$$\frac{\partial}{\partial\beta_i}|\nabla\Pi| = -\frac{|\nabla\Pi|}{2[\pi(\beta,u,v)-\pi_{\min}]}\times\left[\frac{\partial\pi(\beta,u,v)}{\partial\beta_i} - \frac{\partial\pi_{\min}}{\partial\beta_i}\right] + \frac{1}{2\{[\pi(\beta,u,v)-\pi_{\min}](\pi_u^2+\pi_v^2)\}^{1/2}}\times\left[\pi_u\frac{\partial\pi_v}{\partial\beta_i} + \pi_v\frac{\partial\pi_u}{\partial\beta_i}\right]. \qquad \text{(IX.46)}$$

Thus, the required derivatives of II are expressed in terms of π and its derivatives with respect to u and v, i.e. π_u and π_v. Care should be taken concerning the partial derivatives with respect to β_i, as the appropriate values of u and v also depend on the deformation parameter via the volume conservation constant C. Recalling the definition of u and v, i.e., $Cu=z$ and $Cv=\rho$ [see Eq. (VII.2)], and keeping in mind that, for asymmetric degrees of freedom, the deformation-dependent mass point has to be kept at rest, one obtains for these derivatives

$$\frac{\partial\pi}{\partial\beta_i} = \pi_{\beta_i} - C^{-1}(v\pi_v + u\pi_u)\frac{\partial C}{\partial\beta_i} + \pi_u\left(\frac{\partial\bar{u}}{\partial\beta_i} + \frac{\bar{u}}{C}\frac{\partial C}{\partial\beta_i}\right). \qquad \text{(IX.47)}$$

In this equation $\bar{u}$ denotes the u coordinate of the

center of mass of the shape considered. Analogous relations hold for the derivatives $\partial\pi_u/\partial\beta_i$ and $\partial\pi_v/\partial\beta_i$.

Though the above formalism is somewhat cumbersome, it does not introduce any serious complications for numerical calculations, as one needs in addition to the first derivatives—as used in the single-particle Hamiltonian (Damgaard *et al.*, 1969a)—only the second partial derivatives of the shape function π, i.e., π_{uu}, π_{vv}, π_{uv}, $\pi_{u\beta_i}$, and $\pi_{v\beta_i}$, which are found without difficulty for any reasonable definition of the nuclear shape function π.

The results, presented below, have been computed using the Woods–Saxon potential as defined in Sec. VII, with the shape variables β taken as they appear in the definition of the shape of the nuclear surface π, i.e., the coordinates $\mathbf{c}$, h, and α. As an example of the results obtained by applying the formulae derived above, we present Fig. IX-1. From this figure, it is seen that the mass parameter in the one-dimensional case shows a wiggly behavior with deformation very similar to the one found in shell-correction quantities.

3b. *The Two-Dimensional Case*

In the following, we restrict the discussion to the mass parameters connected to our two symmetric shape degrees of freedom, i.e., $\mathbf{c}$ and h. The three mass parameters B_{cc}, B_{hh}, and B_{ch} are computed by means of Eqs. (IX.41) and presented in Fig. IX-2 for the specific case of ^{240}Pu. The results expose the wiggly behavior—observed already in the one-dimensional case—which parallels the one in the energy (compare Fig. VIII-1, 2). This may be explained by means of the following considerations.

A simple approximate expression for the mass parameters can be derived if the BCS approximation is valid, i.e., for $\Delta \gg G$. In this case, the correction term P_{ij} is relatively less important and can be neglected. Restricting ourselves to the diagonal matrix elements and replacing the summation by an integration, we have

$$B_{\beta\beta} \approx \tfrac{1}{16}\hbar^2 \, |\langle \partial\mathcal{H}/\partial\beta \rangle_{\lambda\nu}|^2 (g^{sp}/\Delta^2). \qquad \text{(IX.48)}$$

The matrix element $\langle \nu \mid \partial\mathcal{H}/\partial\beta \mid \nu \rangle$ was replaced here by some average value $\langle \partial\mathcal{H}/\partial\beta \rangle_{\lambda\nu}$, which is expected to change only slowly with deformation. This equation exposes significant features of the mass parameter, especially the counter fighting effect of the effective local level density at the Fermi energy, $g^{sp}(\lambda)$, and the energy gap Δ.

This is illustrated in Figs. IX-3 and IX-1. The dependence of the mass parameter, calculated according to Eqs. (IX.40)–(IX.47), on the pairing strength, i.e., on Δ, is shown in Fig. IX-3. This dependence corresponds almost to $1/\Delta^2$ as predicted by Eq. (IX.48). The size of the gap depends on the shell structure. It may thus be surprising that the mass parameter as a function of deformation, shown in Fig. IX-1, does not

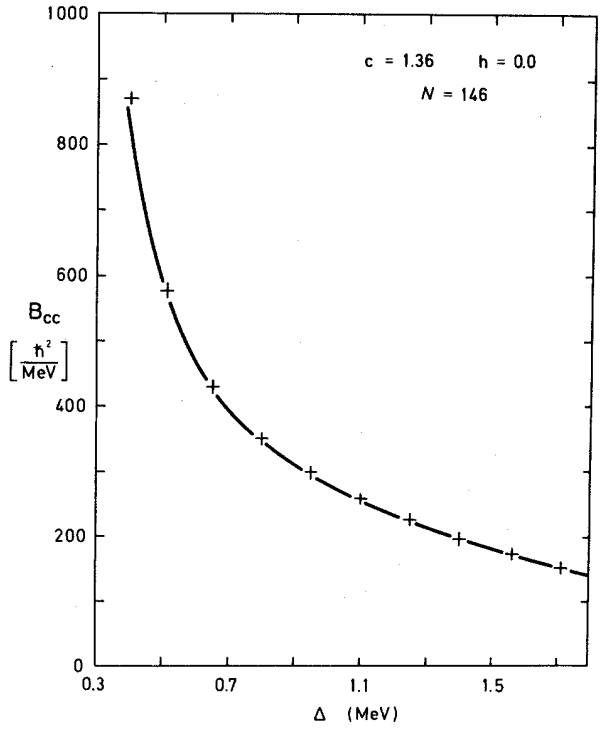

FIG. IX-3. Mass parameter B_{cc} plotted versus the pairing gap Δ. The figure is drawn on the basis of calculations done for $N=146$ neutrons at a deformation $\{\mathbf{c}, h, \alpha\}=\{1.36, 0, 0\}$. The mass parameter follows almost exactly the $1/\Delta^2$ dependence predicted by Eq. (IX.48).

vary with respect to the pairing gap as predicted by Eq. (IX.48): local minima of the energy gap coincide with minima of the mass parameter and not with its local maxima, as one would expect from Eq. (IX.48). The explanation is found in the effective local level density, $g^{sp}(\lambda)$ in Eq. (IX.48). Because of the strong energy cutoff in formula (IX.41a), in the form of E^{-3}, the effective level density varies similarly to the shell level density which, for selected cases, was shown in Fig. II-3. Thus, the result shows that the shell structure in the local level density represented by the factor g^{sp} in Eq. (IX.48) is more important than the one of the energy gap. Taken alone, the variation of $g^{sp}(\lambda)$ amounts to a factor of four between the extrema.

These results lead us to the important conclusion that the effective mass parameters are relatively large just near the shell energy maxima, compared to their smooth average. They decrease when one moves away from the maxima, and find their local minima near the local minima of the deformation energy.

The increase in the nuclear inertia near the barrier—see also Fig. IX-4—is a significant effect, which should not be neglected in estimates of the penetrability of the fission barrier and of spontaneous fission lifetimes. It is possible, though, that the data presented in Fig. IX-4

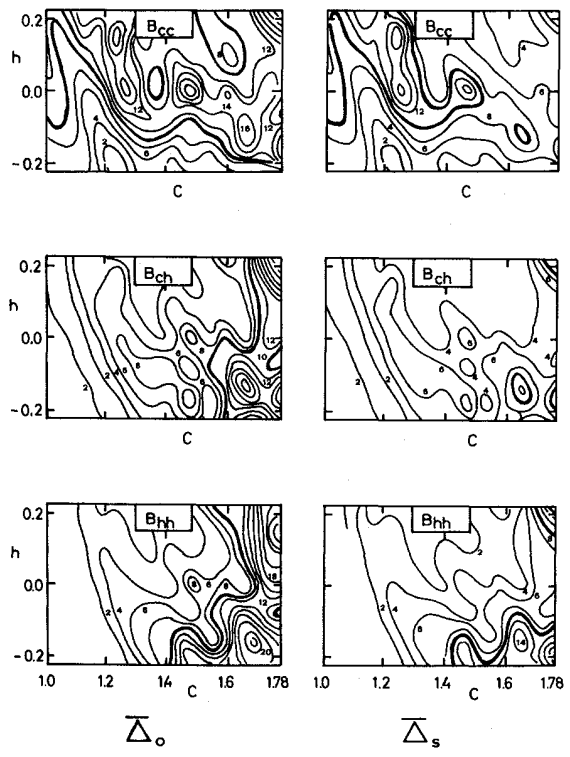

FIG. IX-4. Contour maps of the total mass parameters B_{cc}, B_{ch} and B_{hh} of ^{240}Pu. The uniform pairing gap $\bar{\Delta}$ is taken constant on the left side and surface dependent (see Sec. V) on the right. Units and equidistance as in Fig. IX-2. (Thick line for 1000 $\hbar^2$/MeV). For large deformations the mass parameters become smaller by a factor 2–3, when $\bar{\Delta}$ is surface dependent.

exaggerate the effect: the increased inertia near the barrier, which in fact is a saddlepoint in the many-dimensional space of the shape coordinates, may produce a shift of the trajectory from the saddlepoint to a sidewalk. Although the potential barrier is higher there, a smaller value for the action integral may result, due to smaller inertia.

This result demonstrates once more the importance of the level bunches close to the Fermi energy, as the main contribution to the nuclear inertia comes from a relatively narrow energy region of the order of twice the pairing gap around the Fermi energy. Special investigations of numerical calculations have shown that more than 90% of the mass parameter comes from this region, independent of deformation. However, the situation may be very different in regions of shell closures, where Δ becomes small. Indeed, one observes that at certain deformations, the mass parameters suddenly become tremendously large or even diverge. This effect has its origin in the existence of shell regions with a low pairing gap, where one or two levels come close to the Fermi energy. Then, their quasiparticle energies become very small, which may lead to a divergence of B_{ij}, due to a sudden change of the wavefunction of the occupied level at the level crossing. For these situations, residual interactions, other than pairing, become important: They remove the degeneracy near the Fermi energy, and distribute the drastic change of the wavefunction over an extended region of deformation, thus smoothing the rapid variation. Fortunately, the accidental singularities do not constitute a real difficulty in the type of calculations referred later in this section, because in a multidimensional approach as ours there is always a possible path around them.

The above should be compared to the case $\Delta = 0$, when no crossing takes place. Then, a weak variation of the single-particle wavefunctions leads to very small effective mass parameters. This is also reflected in the presence of relatively large energy denominators in Eq. (IX.37) of the order of $\hbar\omega_0 \approx 10$ MeV. As the energy denominator in the case of pairing is of the order of 2Δ, instead of $2\hbar\omega_0$, the residual interactions lead in general to increased values of the mass parameters compared to the pure independent particle value. The treatment of residual interactions other than pairing is beyond the scope of the present paper.

The effect of assuming a surface-dependent pairing for the case of ^{240}Pu is shown in Fig. IX-4.

In Fig. IX-2, one sees that the fluctuation around the mean value is less pronounced in the h direction (neck formation). This can be explained by the behavior of the average matrix element $\langle \partial V/\partial h \rangle_{Av}$ in Eq. (IX.41). Would it be possible to find another parametrization $\{\mathbf{c}, h'\}$ in such a way that the average value of the mass parameter remained constant by varying h', the plots would probably expose more similarity with the energy variation in this direction. As in the case of the deforma-

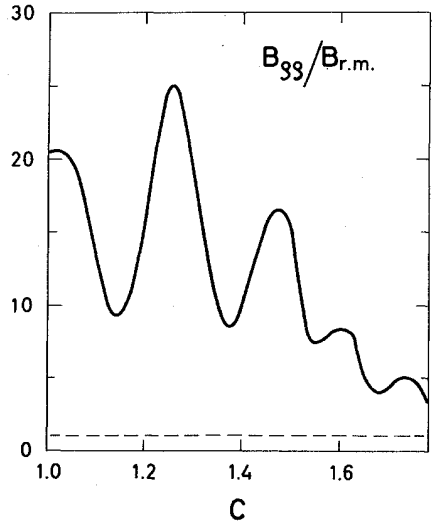

FIG. IX-5. The mass parameter $B_{\rho\rho}$ in units of the reduced mass, plotted versus the elongation $\mathbf{c}$ for (h=0) for ^{240}Pu. It is seen that we asymptotically approach $B_{\rho\rho} \sim B_{\rm rm}$ (dotted line).

tion energy, the neutrons contribute more than the protons to the mass parameters of ^{240}Pu, shown in Fig. IX-2 on the left-hand side.

A convenient unit of reference for the effective masses is the reduced mass for two equal fragments at large distances: $B_{\rm rm}=0.0240r_0^2A^{5/3}\hbar^2/\text{MeV}$. For the case of ^{240}Pu this quantity equals $\approx 330\hbar^2/\text{MeV}$. It is expected that the mass parameter approaches this value when the shape of the nucleus approaches the shape of two tangent spheres.

However, the calculated mass parameter $B_{\rm cc}$ does not seem to decrease and to approach this limiting value. It rather seems to maintain a constant value on the average. The discrepancy can be easily resolved by remembering that, for the reduced mass, the mass center distance $\rho_{\rm cm}$ as defined in Eq. (VII.17a) is important, while in the data presented we have used the longer axis as the deformation coordinate. Transforming the $B_{\rm cc}$ to the $B_{\rho\rho}$ by the equation

$$B_{\rho\rho}=B_{\rm cc}(\partial \mathbf{c}/\partial\rho)^2 \qquad \text{(IX.49a)}$$

valid for the one-dimensional case and using Eq. (VII.17a), we obtain by putting, e.g., $h=0$,

$$d\mathbf{c}/d\rho=1/(\tfrac{3}{8}+\tfrac{1}{8}\mathbf{c}^4-\tfrac{1}{10}\mathbf{c}^3) \qquad \text{(IX.49b)}$$

for continuous shapes. Thus we see that the mass parameter $B_{\rho\rho}$ does decrease to a value about equal to the reduced mass for larger values of **c**. We plot in Fig. IX-5 a graph of the ratio $B_{\rho\rho}/B_{\rm rm}$ as a function of the parameter **c** for $h=0$. Indeed, as expected, our mass parameter approaches the value of the reduced mass as the elongation increases. The fact that there is a large decrease in the ratio as **c** changes from 1.0 to 1.78 is due mostly to the factor $(\partial \mathbf{c}/\partial\rho)^2$ in Eq. (IX.49a). One can also see that our choice of the parametrization is fortunate because $B_{\rm cc}$ is not a rapidly decreasing (or increasing) function of **c**, and thus the fluctuations due to shells can be more easily identified.

The calculated mass parameters show that in general our two symmetric degrees of freedom **c** and h cannot be considered separately. This is indicated by the size of the nondiagonal inertial coefficient B_{ch} being, on the average, of the same order of magnitude as the product of the diagonal mass parameters $B_{\rm cc}$ or B_{hh} i.e.,

$$B_{ch}^2/B_{\rm cc}B_{hh}\approx 1.$$

In an ideal parametrization, this ratio should be small, but this would imply the knowledge of a fission mode which has not been found yet. In this connection, it is interesting to note that, by choosing the mass center distance $\rho_{\rm cm}$ Eq. (VII.17a) as a dynamic stretching coordinate, the interference mass parameter $B_{\rho h}$ takes substantially lower values than the two diagonal ones. Thus, also from this point of view, the mass center distance $\rho_{\rm cm}$ offers itself as a kind of natural dynamic variable (see also Sec. VIII) and would be a better choice.

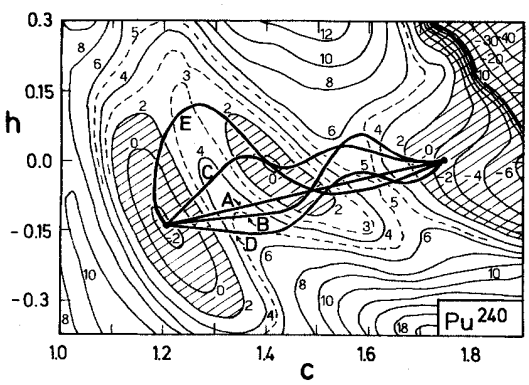

FIG. IX-6. Energy surface of ^{240}Pu. Some of the trajectories along which the action integral has been computed are shown. Each trajectory is identified by a letter. The calculated lifetime estimates were found to be: (A) 24.6, (B) 23.8, (C) 26.7, (D) 26.0, and (E) 30.2 [all in units of $\log_{10}\tau_{1/2}$ (years)]. It should be noted that the trajectory (E) touches all extremal points of the deformation energy, but has the lowest penetrability of all trajectories presented. The straight line (A) connecting the ground state and the exit region has a penetrability quite close to the trajectory of the least action (B), we have found. For all the trajectories considered the energy $\mathcal{E}$ was assumed to be -2 MeV, i.e., 0.3 MeV above the point of lowest deformation energy.

4. The Trajectory for Symmetric Distortions. Lifetime Estimates

The knowledge of the total deformation energy and of the mass parameters permits a crude estimate of spontaneous fission lifetimes. For reasons of technical simplicity, we restrict ourselves to the two symmetric degrees of freedom.

The penetrability is given by Eqs. (IX.2) and (IX.4). The pre-exponential factor is not very well defined. Although it may depend on the energy, the isotope number, etc., we identify it with the "number of assaults"

$$A=2\pi\omega_f\approx 10^{23}\,[\text{years}]^{-1}$$

obtained with $\hbar\omega_f=0.5$ MeV, where ω_f is the angular frequency of the fission mode. As we shall see later, the uncertainy of this factor is less important at the moment.

Instead of solving the equations of Sec. IX.2, we determine the trajectory approximately by searching for a path σ with the highest possible penetration, corresponding to the shortest lifetime. The mass parameters were taken along the trajectory σ so that the "kinetic energy" in Eq. (IX.5) equals

$$\tilde{T}_\sigma=\left[B_{\rm cc}\left(\frac{\partial \mathbf{c}}{\partial\sigma}\right)^2+2B_{ch}\frac{\partial \mathbf{c}}{\partial\sigma}\frac{\partial h}{\partial\sigma}+B_{hh}\left(\frac{\partial h}{\partial\sigma}\right)^2\right]. \qquad \text{(IX.50)}$$

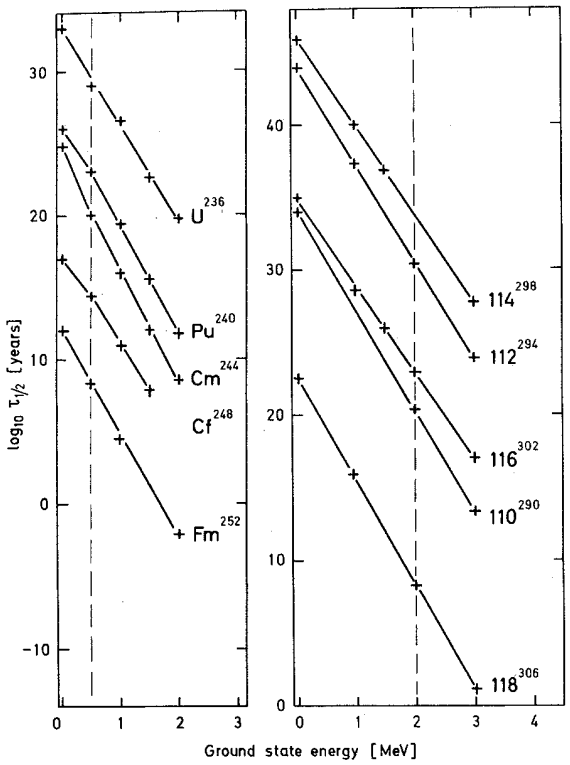

FIG. IX-7. The lifetime estimates—computed along straight line trajectories—are plotted versus the ground-state energy ε measured from the point of lowest deformation energy (see Table VIII.3) for several nuclei in the heavy and superheavy region. The estimates do not include the effects due to left-right asymmetry. An average pairing gap $\tilde{\Delta}=12.0\ A^{-1/2}$ MeV has been used independent of the surface area. It is remarkable that the slopes of the curves are about the same for all nuclei calculated.

As a starting estimate, we have computed the penetrability along a straight line, this being the shortest connection between the regions of positive energy (see Fig. IX-6). Then, σ was varied by letting it pass through several (n) fixed points between the two fixed endpoints.

These medium points were varied until no further increase in the penetrability was found, a procedure which rapidly converged. In Fig. IX-6, a few trajectories for the case of ^{240}Pu are plotted. Though this procedure is quite rough, some important conclusions can be drawn from it:

A multidimensional calculation is necessary as no unique "fission mode" is known up to now.

The trajectory, i.e., the path of lowest action, does not follow the steepest descent of the potential and does not necessarily lead through the extremal points of the deformation energy.

The straight line in the $\{c, h\}$ plane connecting the ground state and the exit has a penetrability close to that of the best trajectory found.

The best trajectory usually has a penetrability of about two to three orders of magnitude higher than the penetrability along the straight line.

If not otherwise mentioned, we assume in this paper as in others (see, e.g., Nilsson *et al.*, 1969) a zero-point energy of 0.5 MeV at the ground state.

In order to study the consequences of this assumption for the penetration estimates, we have varied this energy and present the results in Fig. IX-7. In the simplified case of a one-peaked barrier idealized by an inverted parabola, the logarithm of the penetrability is approximately proportional to the difference between threshold and ground-state energy.

It is surprising to see that our penetration estimates expose almost the same behavior, even though we include the shell structure in both the deformation and the kinetic energy. Even for different nuclei, the slopes of these curves do not vary considerably. From Fig. IX-7 we also see that changing the ground-state energy

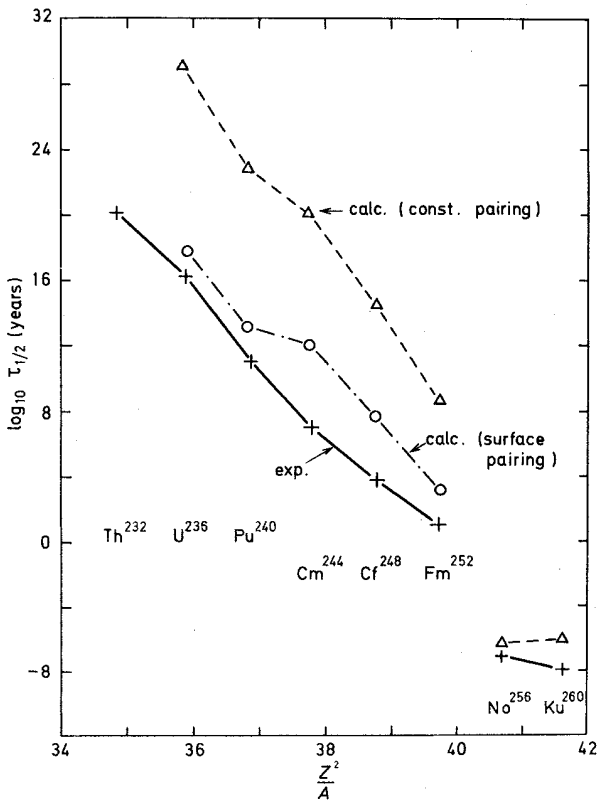

FIG. IX-8. Spontaneous fission lifetimes for several actinide nuclei. Experimental values (+) as well as our estimates with (○) and without (△) surface-dependent pairing are plotted versus Z^2/A. The total energy ε was assumed to be 0.5 MeV above the point of lowest deformation energy. Note the abrupt change in the experimental values between ^{252}Fm and ^{256}No and the closer agreement of the estimates with experiment for ^{256}No and ^{260}Ku. The presented estimates do not include any effects due to left-right asymmetry.

by $\approx$0.2 MeV, our penetration estimates vary by about two order of magnitude. Thus, the uncertainty of the ground-state energy has practically the same effect on the results as a path variation, i.e., the difference between a straight line and a "best trajectory".

The estimated lifetime for spontaneous fission are shown in Fig. IX-8 for a few actinide nuclei together with the experimental values. The systematics of the estimates follow quite well the experimental decrease in spite of the fact that the fission thresholds are almost a constant over the whole region (cf. Table VIII.3). In size, however, there is a considerable discrepancy varying between 12 and 8 orders of magnitude between uranium and fermium. This discrepancy—the huge factor of 10^{10} being related to a change of 30 percent in the actually computed action integral S, Eq. (IX.4) is certainly due to the present restriction to symmetric shape distortions, i.e., the presented estimates are computed with fission threshold too high by about 2 MeV. Considering the numerical results in detail, it turns out that more than two-thirds of the action integral comes from the region at and behind the outer barrier, where a relatively large deformation energy coincides with increased values of the mass parameters (see, e.g., Fig. IX-4). Due to the asymmetry, the second barrier is lowered, as we have seen in Fig. VIII-7, and also the mass parameters decrease, as preliminary calculations have shown. Thus, we expect a better agreement with the empirical values, once we include the asymmetric degree of freedom. Such calculations are under way.

In the case of nobelium and kurchatorium, we have performed some special calculations. As can be seen by comparing Figs. A-1 and A-2, the inclusion of the shape asymmetry for these nuclei lowers the outer barrier, obtained for symmetric shapes, so much that the system has to penetrate only the first barrier in order to fission. As we have seen this barrier is not affected by the asymmetry. Therefore, we have calculated the penetration factor not for both (symmetic) barriers but only for the inner one. The result will thus not be affected by a future inclusion of the asymmetry—and shows a surprisingly good agreement with the measured lifetimes. In this context, we may take the disrupt change of the experimental lifetimes between fermium and nobelium in the otherwise smooth curve as experimental evidence for a sudden disappearance of the outer barrier in the region around $Z=102$ and $N=152$, see Fig. IX-8.

Analogous results can also be obtained with the surface-dependent pairing. According to Eq. (IX.48), the mass parameter depends directly on the size of the pairing gap Δ, its value decreasing approximately as $1/\Delta^2$. If we increase Δ by the assumption of a surface dependence of the pairing coupling constant (see Sec. V.5), the mass parameters will at larger deformations decrease by a factor of up to two or three. This can be

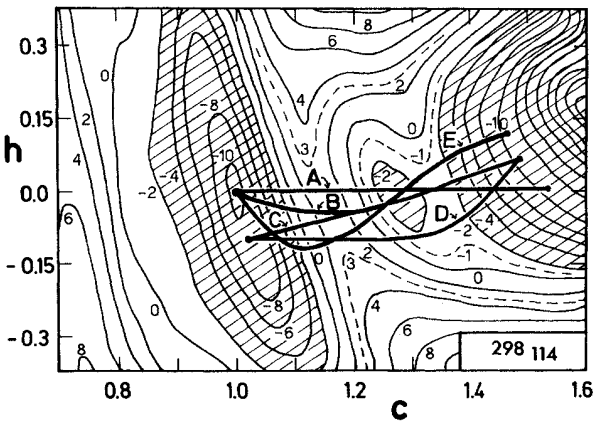

FIG. IX-9. Energy surface of the hypothetical nucleus $^{298}114$. Some of the trajectories along which the action integral was computed (as in Fig. IX–6) are plotted. The letters refer to the following lifetime estimated [$\log_{10}\tau_{112}$(years)]: 36.6 (A), 35.6 (B), 34.0 (C), and 38.8 (D). In this case, too, the straight line trajectory delivers a good estimate.

seen from Fig. IX-4 on the right-hand side. The effect on the penetrability will of course be appreciable, and the spontaneous fission lifetime decreases by more than a factor of 10^{10} in the case of ^{240}Pu. For other nuclei, the effect is similar (see, Fig. IX-8). The resulting lifetime estimates are closer to the experimental data than without surface pairing. But, as long as the effect of the asymmetry on these estimates is not cleared up, the closer agreement of the latter cases cannot be considered as an argument in favor of a surface-dependent pairing.

These difficulties seem to be related to fission of the lighter actinide nuclei, where large nuclear distortions contribute significantly to the penetration estimate. In heavier nuclei the discrepancy is smaller and thus, one may hope that a reasonable estimate may be obtained for the lifetime for spontaneous fission of the hypothetic superheavy elements, where much smaller nuclear distortions are essential.

Also for these nuclei the ground-state zero-point energy was shown in Fig. IX-7 on the right-hand side. Note that within reasonable limits the slope of the log $\tau_{1/2}$ curves for the superheavy nuclei is the same as that of the actinides. The values presented in Fig. IX-7 were obtainec by computing the action integral along straight line trajectories. How strongly this estimate is influenced by a different choice of the trajectory is shown in Fig. IX-9. Obviously, the same qualitative conclusions as for the Pu case can be drawn that a better trajectory than a straight line can indeed be found; however, it does not change the penetration estimate significantly. The estimated lifetimes fall rapidly down, away from the two nuclei $^{298}114$ and $^{304}120$, which are the most stable ones against fission. For the lighter of these nuclei we have plotted the results in Fig. IX-10. Due to the liquid-drop background, the lighter of these "off

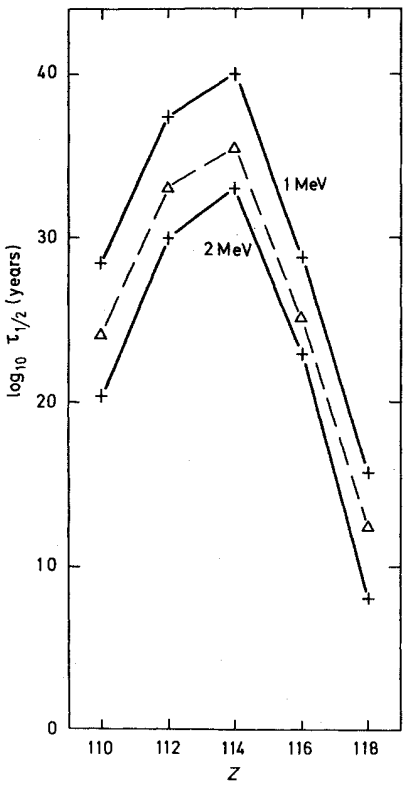

FIG. IX-10. Estimates of spontaneous fission lifetimes for a number of superheavy nuclei, plotted versus their proton number Z. The two solid curves refer to calculations using a total energy ϵ which is 1 or 2 MeV above the point of lowest deformation energy. Estimates with surface-dependent pairing are shown by the dashed curve (for $\varepsilon=1$ MeV).

center" nuclei have a longer lifetime than the heavier ones. As expected, the possible surface dependence of the pairing has less influence on the fissility of the superheavy nuclei than on the known heavy nuclei, smaller deformations and, thus, smaller surface areas being involved.

Our estimates are significantly higher than those presented by Nilsson *et al.* (1969). The difference for the superheavy nuclei is about a factor of 10^{14}, corresponding to a difference of 30% of the action integral in the exponent, Eq. (IX.14). To our larger values, the inertia at the threshold has certainly contributed. With a constant value of the mass parameter—corrected empirically for the actinide nuclei as these authors did—we approach their estimate up to a factor of 10^5, which must be attributed to our slightly increased threshold energy.

Not withstanding this difference we arrive, thus, at mainly the same conclusions as Nilsson *et al.* (1969); namely that the hypothetic superheavy elements are practically stable against spontaneous fission. Whether they disintegrate by competing processes like α or β decay (Nilsson *et al.*, 1969; Muzycka, 1970) is a question which lies beyond the scope of the present paper.

5. Moments of Inertia

So far, we have discussed only the vibrational mode of the collective motion and its application to fission. However, in a total collective Hamiltonian, the rotational energy also has to be taken into account. In this subsection, we will investigate the inertial parameters connected to the rotational degrees of freedom, i.e., the moments of inertia.

In fission theory, the so-called effective moment of inertia $\mathcal{J}_{\text{eff}}$ is of particular interest, as it determines the anisotropy of the angular distribution of the fission fragments at higher exitations (Halpern and Strutinsky, 1958). It is defined by

$$\mathcal{J}_{\text{eff}}=[(1/\mathcal{J}_{||})-(1/\mathcal{J}_{\perp})]^{-1}, \qquad \text{(IX.51)}$$

where $\mathcal{J}_{||}$ and $\mathcal{J}_{\perp}$ are the moments of inertia for rotation about the symmetry axis (or the fission axis) and the axis perpendicular to the symmetry axis, respectively. Usually, for $\mathcal{J}_{||}$ and $\mathcal{J}_{\perp}$, the rigid-body values are assumed, and then $\mathcal{J}_{\text{eff}}$ is rather strongly dependent on the shape of the nucleus at the top of the fission barrier (Strutinsky *et al.*, 1963; Cohen and Swiatecki, 1962). It becomes infinity when the saddlepoint shape becomes spherical. This should be the case of a nucleus which is very unstable against fission, and then, an isotropic angular distribution is predicted. Recently, some attempts were made to determine the limits of stability of nuclei by measuring the angular anisotropy of highly excited nuclei produced in nuclear reactions with α particles and heavy ions (Bate *et al.*, 1963; Muzycka *et al.*, 1968; Oganessian, 1968).

Experimental studies of $\mathcal{J}_{\text{eff}}$ are very important in view of the fact that they are probably the most direct way of investigating the shape of the nucleus at the barrier. However, this quantity may also be affected by the shell structure, which may be misinterpreted as due to a different shape of the nucleus. It is therefore of some interest to find out how strong the shell structure effects on the moments of inertia can be.

For the moment of inertia $\mathcal{J}_i$ for rotation about the i-axis we assume the cranking-model formula (Inglis, 1954)

$$\mathcal{J}_i=\sum_{\mu,\nu}\left\{\frac{(u_\mu u_\nu-v_\nu v_\mu)^2}{2(E_\mu+E_\nu)}\left(\tanh\frac{E_\mu}{2T}+\tanh\frac{E_\nu}{2T}\right)\right.$$
$$\left.+\frac{(u_\mu u_\nu+v_\nu v_\mu)^2}{2(E_\mu-E_\nu)}\left(\tanh\frac{E_\mu}{2T}-\tanh\frac{E_\nu}{2T}\right)\right\}|\langle\mu\,|\,M_i\,|\,\nu\rangle|^2 \qquad \text{(IX.52)}$$

where M_i is the ith component of the single-particle angular momentum operator $\mathbf{j}$ with

$$M_\perp=j_x \qquad \text{(IX.53)}$$

for $\mathcal{J}_\perp$ and

$$M_{||}=j_z \tag{IX.53}$$

for $\mathcal{J}_{||}$. The pairing interaction is treated here as temperature-dependent (Decowsky *et al.*, 1968). The quasiparticle energies E_μ and the occupation numbers u_μ and v_μ are defined as usually in the BCS theory:

$$E_\mu=[(\varepsilon_\mu-\lambda)^2+\Delta^2]^{1/2}; \qquad u_\mu=\{\tfrac{1}{2}[1+(\varepsilon_\mu-\lambda)/E_\mu]\}^{1/2} \tag{IX.54}$$

$$v_\mu^2=1-u_\mu^2,$$

where the single-particle energies ε_μ are found as described in Sec. VII for any given average nuclear potential. The parameters λ and Δ in Eq. (IX.54) are determined by the temperature-dependent gap equation

$$\frac{2}{G}=\sum_\mu \frac{\tanh\,(E_\mu/2T)}{E_\mu} \tag{IX.55}$$

and the conservation condition for the particle number N:

$$N=\sum_\mu \{1-[(\varepsilon_\mu-\lambda)/E_\mu]\tanh\,(E_\mu/2T)\}. \tag{IX.56}$$

The nuclear temperature T is considered here as a free parameter, which, however, is related in a definite way to the excitation energy.

The strength of the pairing interaction, G, is found in the way described in Sec. V, using the uniform gap $\tilde{\Delta}$ as an input parameter. The expression (IX.52) and the above-mentioned quantities refer to either protons or neutrons. The total $\mathcal{J}_i$ for a specific nucleus is then the sum of the contributions from neutrons and protons.

A convenient unit of $\mathcal{J}_i$ is the so-called "rigid-body value" $\langle \mathcal{J}_i^{\mathrm{RB}}\rangle$, i.e. the moment of inertia of a uniform mass distribution with a sharp surface, which has the same shape as the average potential used for the evaluation of the eigenenergies ε_μ and the eigenfunctions ϕ_μ.

We have done calculations with two different potentials:

1. *NM*: *The Nilsson potential with pure ellipsoidal deformation.* The deformation parameter is the ratio of the axes d of the mass distribution. With this, we have

$$\langle \mathcal{J}_{||}^{\mathrm{RB}}\rangle=\tfrac{2}{5}mNR_0^2d^{-2/3}, \tag{IX.57}$$

$$\langle \mathcal{J}_\perp^{\mathrm{RB}}\rangle=\tfrac{1}{5}mNR_0^2(1+d^2)d^{-2/3}. \tag{IX.58}$$

The nuclear radius, R_0, is assumed to be $R_0=1.2A^{1/3}$ F; m is the nucleon mass, and N the number of nucleons involved (either proton, neutron, or total mass number).

In this model, the parameter $\hbar\omega_0$ has been fixed by the requirement that the states near the Fermi level should have a value of $\langle r^2\rangle$ equal to $\frac{3}{5}R_0^2$. With $r_0=1.2$ F, this gives

$$\hbar\omega_0=55A^{-1/3}\ \mathrm{MeV}.^{11} \tag{IX.59}$$

2. *WS*: *A Woods–Saxon potential with constant skin-thickness (see Sec. VII) and the shapes* $\{\mathbf{c}, h\}$ *(see Eq. VII.4).* The rigid-body values of the moments of inertia along the LDM valley ($h=0$) are

$$\langle \mathcal{J}_{||}^{\mathrm{RB}}\rangle=\tfrac{2}{5}mNR_0^2[\mathbf{c}^{-1}-\tfrac{2}{35}\mathbf{c}^2(\mathbf{c}-1)+\tfrac{4}{525}\mathbf{c}^5(\mathbf{c}-1)^2] \tag{IX.60}$$

$$\langle \mathcal{J}_\perp^{\mathrm{RB}}\rangle=\tfrac{1}{2}\langle \mathcal{J}_{||}^{\mathrm{RB}}\rangle+\tfrac{1}{5}mNR_0^2[\mathbf{c}^2+\tfrac{4}{35}\mathbf{c}^5(\mathbf{c}-1)]. \tag{IX.61}$$

For the parallel moment of inertia $\mathcal{J}_{||}$, Eq. (IX.52) reduces to

$$\mathcal{J}_{||}=(4T)^{-1}\sum_i \frac{K_i^2}{\cosh^2\,(E_i/2T)}, \tag{IX.62}$$

where K_i is the projection of the angular momentum of the ith state on the symmetry axis. The quantity $\mathcal{J}_{||}$ can be estimated by replacing the summation by an integration. Defining the continuous functions $g^{\mathrm{SP}}(\varepsilon)$ and $g_K^{\mathrm{SP}}(\varepsilon)$, respectively, as the single-particle level density and the density of single-particle states with a definite K value, one gets approximately

$$\mathcal{J}_{||}\approx(4T)^{-1}\int_{-\infty}^{+\infty} g^{\mathrm{SP}}(\varepsilon)\frac{K^2(\varepsilon)}{\cosh^2\,(E^{\mathrm{QP}}/2T)}\,d\varepsilon, \tag{IX.63}$$

where

$$E^{\mathrm{QP}}=[(\varepsilon-\lambda)^2+\Delta^2]^{1/2}$$

and

$$\langle K^2(\varepsilon)\rangle=[g^{\mathrm{SP}}(\varepsilon)]^{-1}\int_{-\infty}^{+\infty} K^2 g_K^{\mathrm{SP}}(\varepsilon)dK. \tag{IX.64}$$

Equation (IX.63) suggests expressing $\mathcal{J}_{||}$ as a product of some level density and the average of K^2 for the levels around the Fermi energy λ. Using WKB estimates, one finds the rigid-body value of $\mathcal{J}_{||}$ given as

$$\mathcal{J}_{||}^{\mathrm{RB}}\approx g^{\mathrm{SP}}(\lambda)\,\langle K^2(\lambda)\rangle. \tag{IX.65}$$

In order to write $\mathcal{J}_{||}$ in a similar way, including temperature and pairing interaction, we define the following quantities:

$$g_T^{\mathrm{QP}}(\lambda)=(4T)^{-1}\sum_i \frac{1}{\cosh^2\,(E_i/2T)} \tag{IX.66}$$

and

$$\langle K^2(\lambda)\rangle_T=(4T)^{-1}\sum_i \frac{K_i^2}{\cosh^2\,(E_i/2T)}\Big/ g_T^{\mathrm{QP}}(\lambda). \tag{IX.67}$$

[11] The value of $\hbar\omega_0=41\ A^{-1/3}$ MeV, normally used in the Nilsson model, is obtained by averaging r^2 over *all* occupied states. In the discussion of shell structure, which is determined by a relatively narrow region around the Fermi energy, we prefer, however, the value (IX.59).

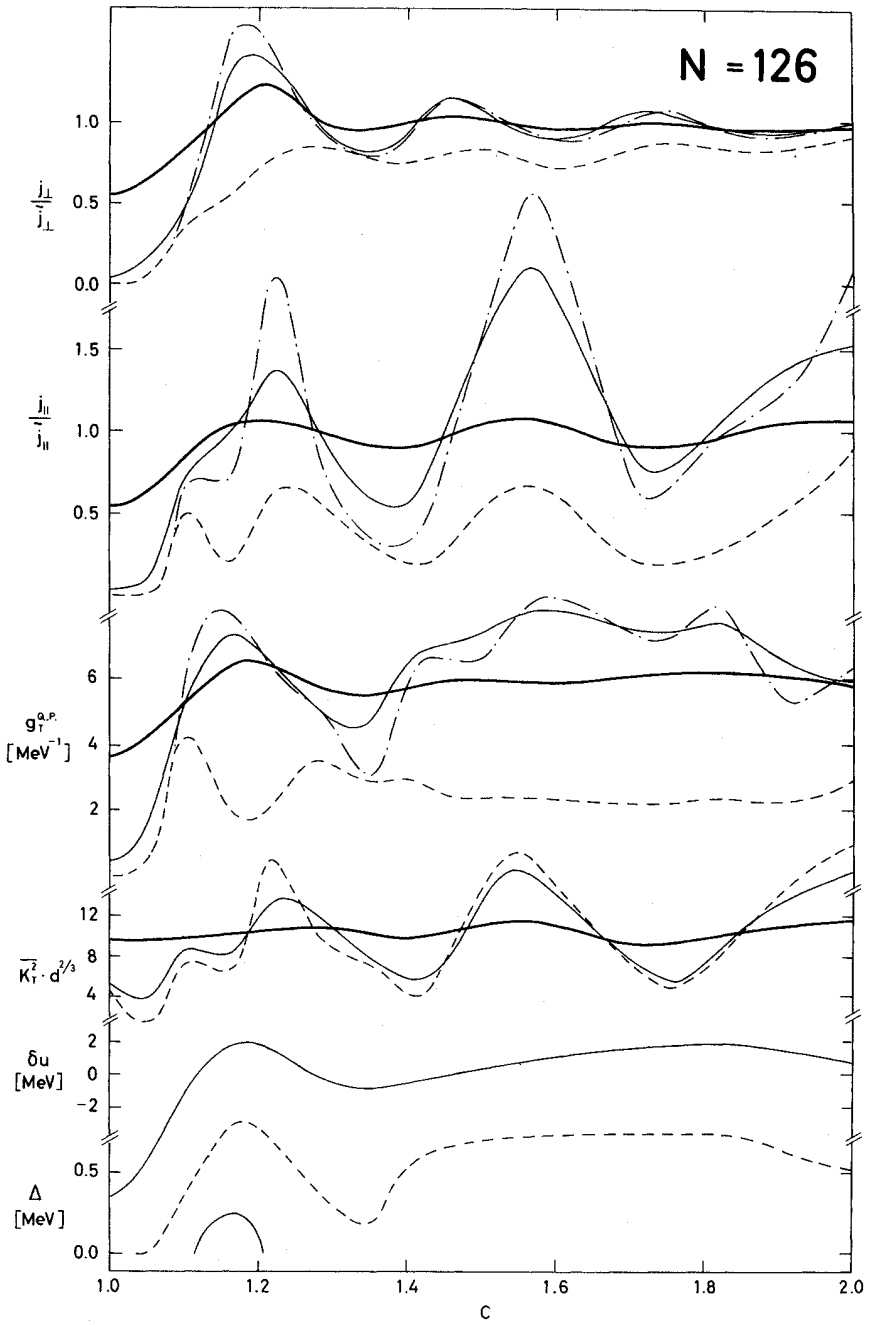

FIG. IX-11. Moments of inertia and related quantities at different temperatures, shown as functions of the elongation c (Nilsson model for $N=126$). The moments of inertia $\tilde{\mathcal{J}}_{||}$ and $\tilde{\mathcal{J}}_\perp$ are plotted in units of their rigid body values [Eqs. (IX.57, IX.58); $c=d^{2/3}$]. The quasiparticle level density g_T^{QP} and the mean value of K^2 are defined by Eqs. (IX.66) and (IX.67), respectively. The latter is multiplied by its inverse deformation dependence [see Eqs. (IX.68) and (IX.57)]. The energy shell-correction δU (see Sec. IV) is shown for comparison. The pairing gap Δ (calculated with $\tilde{\Delta}=0.6$ MeV) is shown to disappear at larger temperatures. The temperatures chosen are: 1.32 MeV (thick solid lines), 0.84 MeV (thin solid lines), and 0.28 MeV (dashed lines). The results obtained *without* pairing are indicated (dashed-dotted lines) for the lowest temperature only; for the mean value of K^2 no effect can be seen.

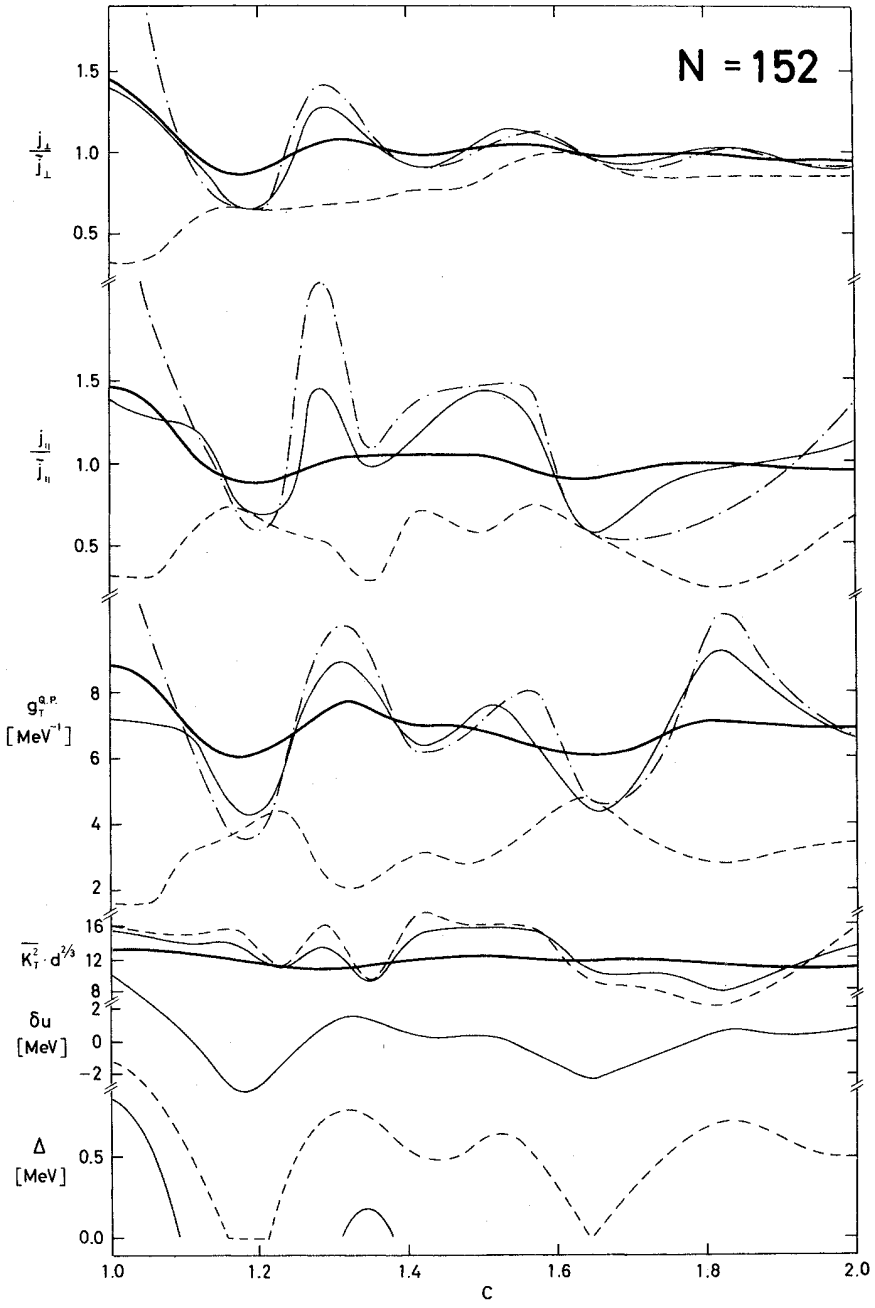

FIG. IX-12. Same as Fig. IX-11, for $N = 152$.

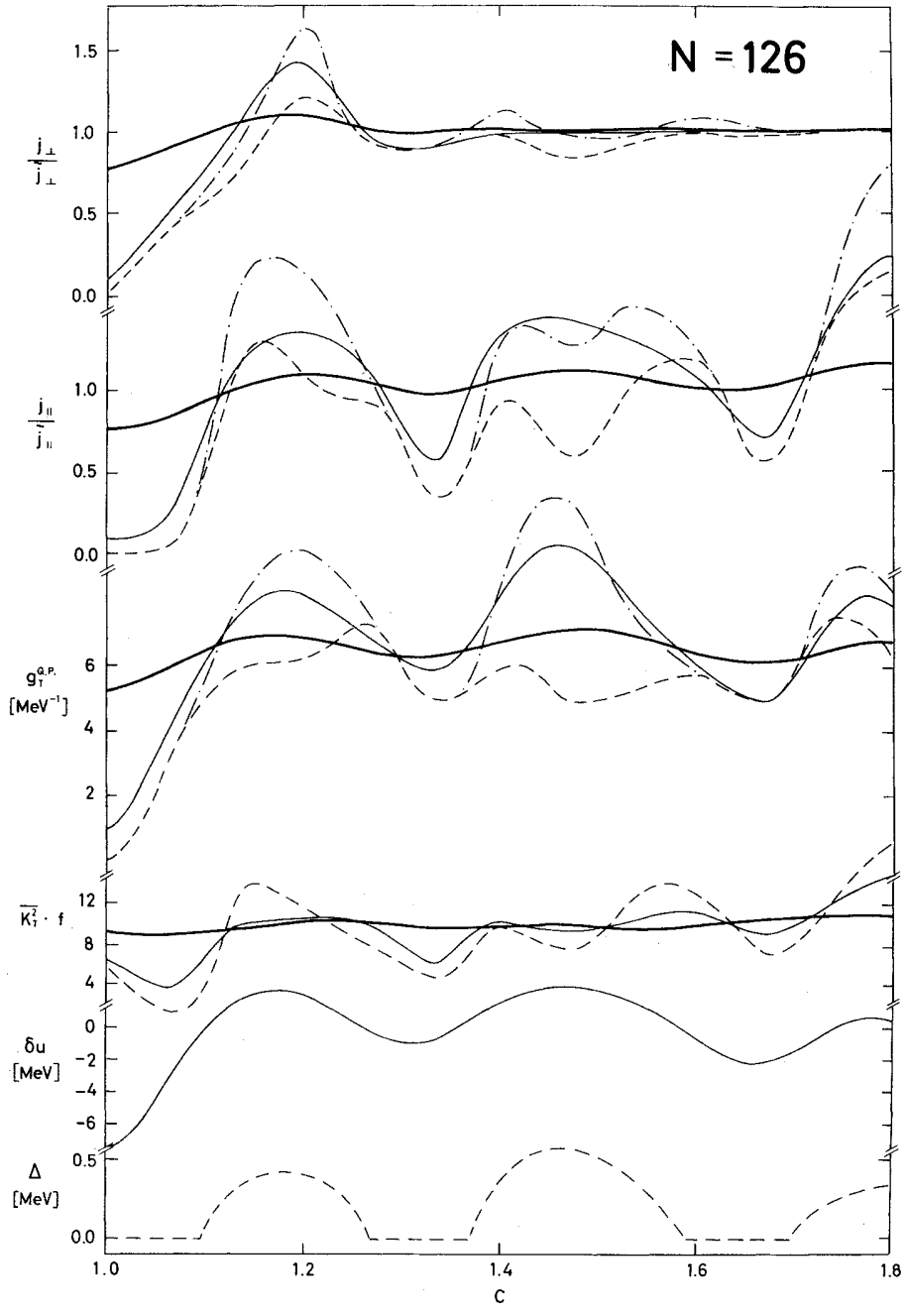

FIG. IX-13. Same as Fig. IX-11, calculated with the Woods–Saxon model for $N=126$.

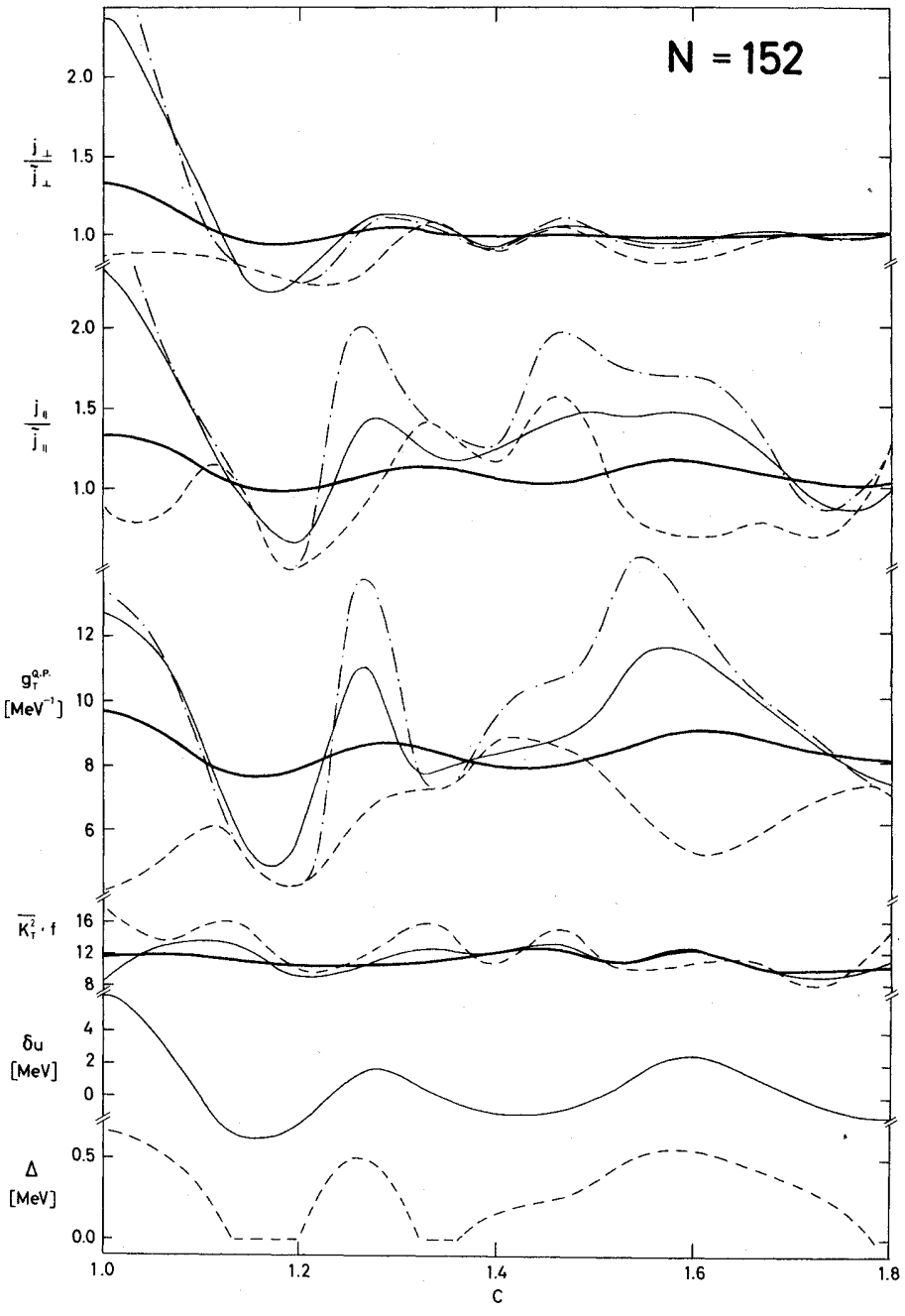

FIG. IX-14. Same as Fig. IX-12, calculated with the Woods-Saxon model for $N=152$.

Then, we find

$$\mathcal{J}_{||}=g_T^{QP}(\lambda)\langle K^2(\lambda)\rangle_T. \quad \text{(IX.68)}$$

The quantity $g_T^{QP}(\lambda)$ is thus the density of quasiparticle states.

For a fixed value of T, we can see now from Eq. (IX.68) how these functions are expected to behave. First of all, we note from the exponential cutoff that only those levels which lie within an energy interval $2T$ around λ contribute appreciably in the summations. From our knowledge of the level density behavior (see Sec. II) we can expect that all three functions (IX.66), (IX.67), and (IX.68) will fluctuate with deformation, reflecting the changing shell structure near the Fermi energy. The amplitude of these oscillations decreases as T increases, because then a larger number of levels contribute in the averaging procedure, thereby making all quantities less sensitive to the shells. In the limit of high temperature, there should not be any fluctuations at all, and we expect $\mathcal{J}_{||}$ to approach the rigid-body value $\langle\mathcal{J}_{||}^{RB}\rangle$.

When T is larger than the critical temperature of the pairing correlation T_c, at which Δ disappears, the quasiparticle level density $g_T^{QP}(\lambda)$ is the same as the single-particle level density $g^{SP}(\lambda)$. In the other limit $T\ll\Delta$, one finds (Grin, 1963) the approximate expression

$$g_T^{QP}(\lambda)=(2\pi\Delta/T)^{1/2}\exp(-\Delta/T)g^{SP}(\lambda). \quad \text{(IX.69)}$$

The gap parameter Δ is known to increase when the local density of the single-particle states near the Fermi energy increases (see Sec. V). This can lead to a reversed effect in the quasiparticle density (IX.69), which exponentially decreases with increasing Δ. Therefore, it is expected that, at higher excitations, maxima and minima of $\mathcal{J}_{||}$ should approximately correspond to those of the single-particle level density while, at low excitations, maxima of $\mathcal{J}_{||}$ correspond to minima of g^{SP} (i.e., to maxima of the quasiparticle level density), and vice versa. While this is approximately valid for high excitations, the actual correlation at low excitations is more complicated because there is also a shell effect in the averaged value of K^2. Indeed, for small temperatures, only a few states contribute to the averaging of K^2. It is known that the energies of the single-particle states with higher K values go up with deformation while those with lower K values go down. Therefore, the average value of K^2 oscillates about as frequently as does the energy shell-correction but with a different phase.

As we have described in Sec. VII, we calculate our single-particle states by a diagonalization method, using the harmonic oscillator states as a basis. For the calculation of $\mathcal{J}_\perp$, we thus need in Eq. (IX.52) the matrix elements of $M_\perp$ between the harmonic oscillator states. The nonvanishing matrix elements are

$$\langle N, n_z, \Lambda, K+1 \mid M_\perp \mid N, n_z, \Lambda, K\rangle=\tfrac{1}{2}\hbar \quad \text{(IX.70)}$$

and

$$\begin{aligned}
&\langle N, n_z+1, \Lambda\pm1, K\pm1 \mid M_\perp \mid N, n_z, \Lambda, K\rangle \\
&\qquad=\alpha_1[(n_z+1)(N-n_z\mp\Lambda)]^{1/2}, \\
&\langle N, n_z-1, \Lambda\pm1, K\pm1 \mid M_\perp \mid N, n_z, \Lambda, K\rangle \\
&\qquad=\alpha_2[n_z(N-n_z\pm\Lambda+2)]^{1/2}, \\
&\langle N+2, n_z+1, \Lambda\pm1, K\pm1 \mid M_\perp \mid N, n_z, \Lambda, K\rangle \\
&\qquad=\alpha_1[(n_z+1)(N-n_z\pm\Lambda+2)]^{1/2}, \\
&\langle N-2, n_z-1, \Lambda\pm1, K\pm1 \mid M_\perp \mid N, n_z, \Lambda, K\rangle \\
&\qquad=\alpha_2[n_z(N-n_z\mp\Lambda)]^{1/2}, \quad \text{(IX.71)}
\end{aligned}$$

where

$$\begin{aligned}
\alpha_1&=-\tfrac{1}{4}\hbar[(\omega_\perp/\omega_{||})^{1/2}+(\omega_{||}/\omega_\perp)^{1/2}], \\
\alpha_2&=-\tfrac{1}{4}\hbar[(\omega_\perp/\omega_{||})^{1/2}-(\omega_{||}/\omega_\perp)^{1/2}]. \quad \text{(IX.72)}
\end{aligned}$$

Using these matrix elements and the expansion coefficients obtained from the diagonalization, it is easy in principle to find $\langle 1 \mid M_\perp \mid 2\rangle$ and finally to compute $\mathcal{J}_\perp$ by means of Eq. (IX.52). A straightforward calculation shows that, in the spherical case, both moments of inertia are equal, i.e.

$$\mathcal{J}_\perp(T)=\mathcal{J}_{||}(T) \quad \text{(IX.73)}$$

for all nuclei and temperatures.

For zero temperature ($T=0$), the energy interval which contributes to $\mathcal{J}_\perp$ increases with increasing deformation. The matrix element of $M_\perp$ between different subshells and shells increases with larger deformations. Therefore, also, states relatively far away from the Fermi energy contribute (see, e.g., Bohr and Mottelson, to be published), and the increased number of states makes $\mathcal{J}_\perp$ less sensitive to the level properties at the Fermi energy. The amplitudes of the oscillations and the influence of pairing are therefore expected to decrease with deformation.

As a function of temperature, we expect $\mathcal{J}_\perp$ to approach its rigid-body value in the limit of large T. This has been shown for the harmonic-oscillator potential at the equilibrium deformation and also in the approximation where one considers only the diagonal matrix elements of $M_\perp$ (Migdal, 1959), which corresponds to the WKB case of an infinitely large system. It is not very clear what this limit should be in the finite

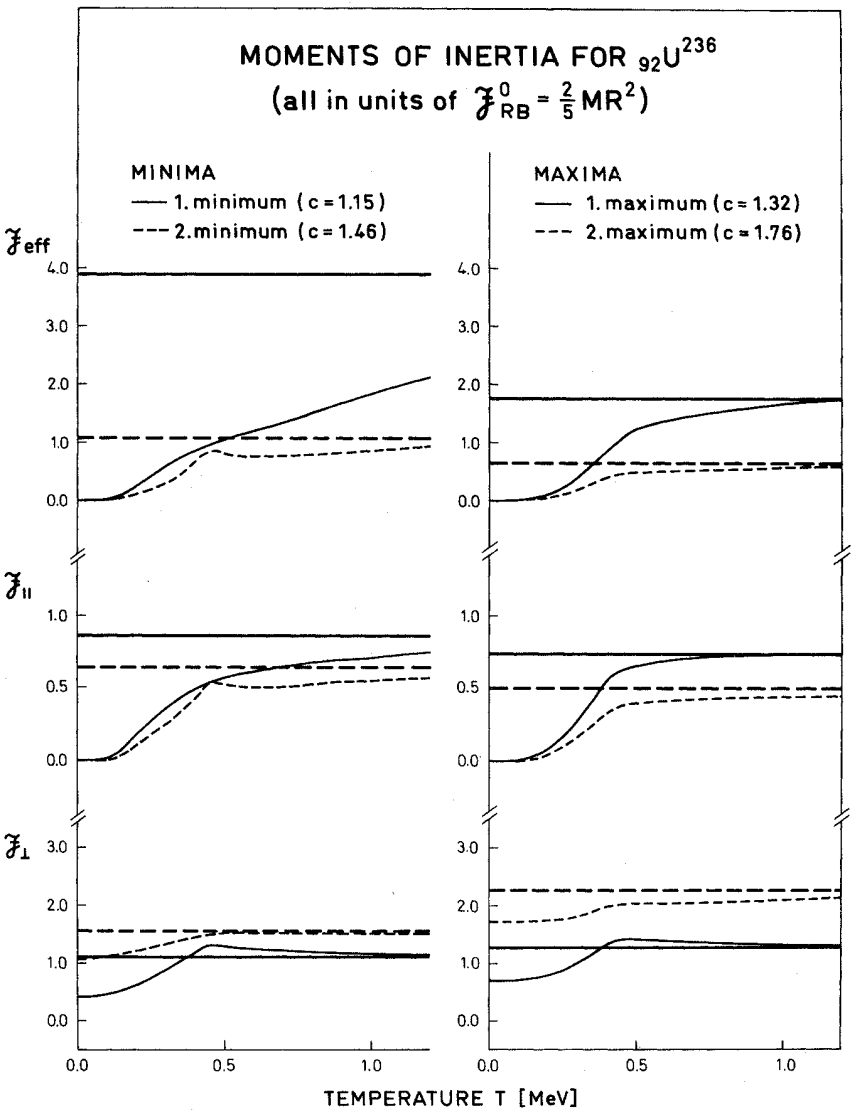

FIG. IX-15. The moments of inertia $\mathcal{J}_{\text{eff}}$, $\mathcal{J}_{||}$, and $\mathcal{J}_{\perp}$ for ^{236}U, evaluated in the Woods–Saxon model (WS), are shown as a function of the nuclear temperature for the deformations at the ground state (c = 1.15), the second minimum (c = 1.46), the first barrier (c = 1.32), and the second barrier (c = 1.76). All the moments of inertia are expressed in units of the rigid-body value for a sphere, $\mathcal{J}_{RB}{}^0$. In all cases, the thick horizontal lines represent the rigid body values. These values are reached at high temperatures.

nuclei. It can, however, be found numerically in our calculations.

In Figs. IX-11–IX-15, some numerical results are presented, which illustrate the influence of pairing, shell structure, and model dependence of the quantities introduced above. Here $\langle K^2(\lambda)\rangle_T$ remains almost unaffected by the pairing, while the other functions are more sensitive. This is, however, not true for $\mathcal{J}_{\perp}$, where the pairing effect, as in all other structure, is seen to decrease with deformation. When $\Delta \lesssim T$, all quantities behave qualitatively in the same way with and without pairing. When $T \ll \Delta$, we note the opposite behavior of the two level densities $g_T{}^{QP}$ and g^{SP} as functions of deformation. Because of the pairing independence of K^2, this anticorrelation is also present in $\mathcal{J}_{||}$, with and without pairing.

There is no clear correlation between $\mathcal{J}_{||}$ and either of the two functions $\langle K^2(\lambda)\rangle_T$ and $g_T{}^{QP}$. The drawings indicate that $g_T{}^{QP}$ in many cases is the more significant, but when $g_T{}^{QP}$ is not fluctuating very much, $\mathcal{J}_{||}$ will essentially be determined by $\langle K^2(\lambda)\rangle_T$. Therefore, one can say that $\mathcal{J}_{||}$ is definitely determined by the shell structure around λ, but not in a simple way. Sometimes it is the variation of the level density that is more important, and sometimes it is the variation of the average of $\langle K^2(\lambda)\rangle_T$. In a way $\mathcal{J}_{\perp}$ behaves similarly. For small deformations, it seems to be correlated with the level density. As the deformation increases, this correlation

is destroyed, but also shell structure and pairing effects become less pronounced.

With increasing T, the shell structure disappears and at $T \gtrsim 1$ MeV all functions approach their asymptotic values.

The discussion above was a general one and did not refer to a specific model. If we compare corresponding moments of inertia calculated in different models (NM: Figs. IX-11, 12, WS: Figs, IX-13, 14), we observe a very similar behavior even if the shapes are different.[12] However, there are differences, and if quantitative results are wanted, one must be careful in the choice of the model.

The limiting values of $\mathcal{J}_{||}$ and $\mathcal{J}_{\perp}$ at large T are, as mentioned, expected to be the rigid-body values. To what extent this is the case can be seen in Fig. IX-15. There, the quantities $\mathcal{J}_{\text{eff}}$, $\mathcal{J}_{||}$, and $\mathcal{J}_{\perp}$ are shown as functions of the temperature T, evaluated for the most interesting shapes of the nucleus ^{236}U, namely the ground-state deformation, the second minimum, and the two barriers. It can be seen that, for the first and second barriers, the rigid-body values of the moments of inertia are essentially reached at a nuclear temperature of $T_s \approx 0.8$–1.0 MeV. This value is close to that for the critical temperature at which the shell-structure effects in the level density disappear, as was found earlier (Pavlinchuk, 1967). It is also higher than the critical temperature T_c, at which the pair correlation effects disappear ($T_c \approx 0.4$–0.5 MeV).

The evaluated moments of inertia may be applied to the analysis of the angular anisotropy in the neutron-induced fission at lower excitations. The angular dis-

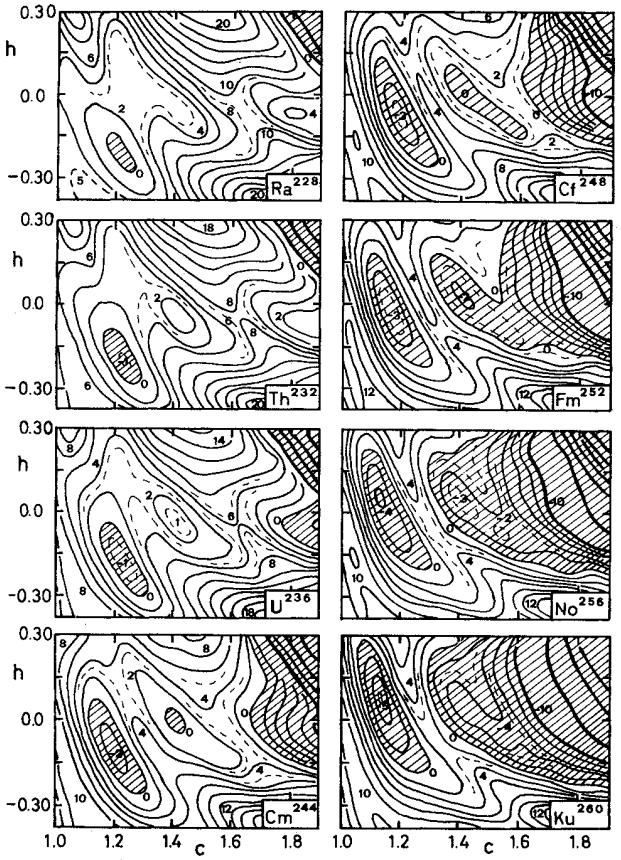

FIG. A-1. Potential energy surfaces for some nuclei in the actinide region, calculated for symmetric shape degrees of freedom. Units and equidistance of the contour lines as in Fig. VIII-1.

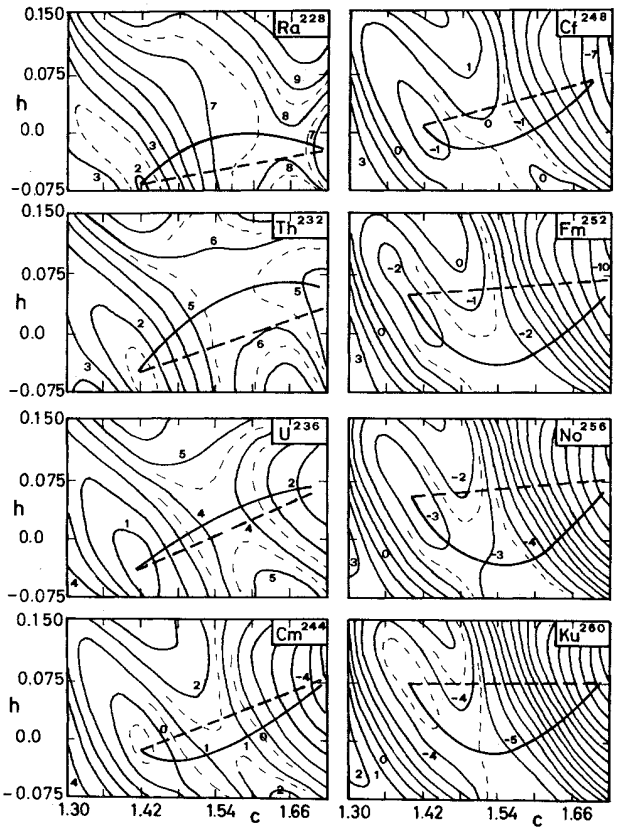

FIG. A-2. Same as Fig. A-1, but with the energy minimized in each point (c, h) with respect to the asymmetric degree of freedom α. Only the region of the isomer minimum and the second barrier is shown. The two trajectories shown are the ones used in the calculations to Fig. VIII-8. (See also text in Sec. VIII.2.)

[12] In order to make a comparison easier, we use the deformation parameter c also in the figures of the NM calculations [instead of d, Eqs. (IX.57), (IX.58); $c = d^{2/3}$].

tribution of the fragments is in this case described approximately by (Halpern and Strutinsky, 1958)

$$W(\theta)/W(90°)=1+(5E_n/8T\mathcal{J}_{\text{eff}})\cos^2\theta. \quad \text{(IX.74)}$$

For the specific case of the reaction $^{235}\text{U}(n,f)$ with $E_n=3$ MeV neutrons, the value of the temperature is found to be equal to 0.28 MeV at the first barrier and $T=0.33$ MeV at the second barrier (with the rigid-body values, these would be equal to 0.05 MeV and 0.14 MeV, respectively, which values are too low).

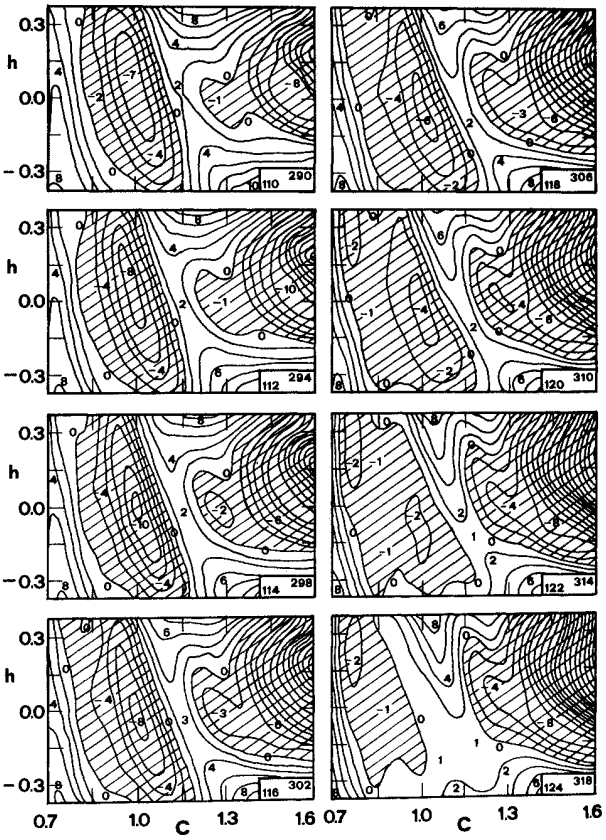

FIG. A-3. Same as Fig. A-1 for some hypothetical superheavy nuclei. (Symmetric deformations.)

The asymptotic values of the moments of inertia can be used for finding $\hbar\omega_0$ for the Nilsson model by requiring that they coincide with the corresponding rigid-body value. From the discussion above it is clear that this would give the value (IX.59). Usually, another value, which is obtained from the condition that r^2, averaged over *all* nucleons, is equal to the same quantity for uniformly distributed matter, is used. In applications, one is rather interested in a better fit near the Fermi energy. With the normal $\hbar\omega_0$, the potential would be somewhat too broad in this energy region. Another way of finding $\hbar\omega_0$ is to require that the Nilsson model on the average has the same level spacing as the Woods–Saxon model or, in other words, that the asymptotic value of g^{SP} be the same in both models. This will give a slightly smaller value than the one we have used. Still another way could be the fit of the ground-state moments of inertia. These, however, are relatively insensitive to $\hbar\omega_0$, as was noted by Nilsson and Prior (1961).

ACKNOWLEDGMENTS

The authors would like to express their thanks to Professor A. Bohr for the warm hospitality and support extended to them at the Niels Bohr Institute. We are very grateful to him and Professor B. Mottelson for numerous discussions, suggestions, and criticism. We are indebted to Dr. S. Bjørnholm, Professors H. Bethe, G. Brown, and K. Dietrich for their willingness to read parts of the manuscript and contribute with many suggestions and valuable criticism. We have greatly enjoyed the close cooperation with Dr. W. D. Myers, Dr. V. V. Pashkevich, Dr. V. M. Kolomietz, and Dr. T. Ledergerber. The assistance and advice of Mrs. S. Hellmann in preparing the manuscript and polishing the language is highly appreciated.

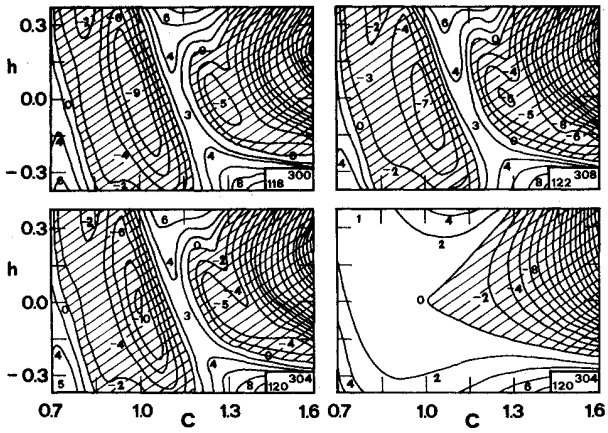

FIG. A-4. Same as Fig. A-3 for some other combinations of proton and neutron numbers. The lower map at the right-hand side shows, as an illustration, the LDM energy alone for the hypothetical $^{304}120$.

APPENDIX

In this Appendix, we present for completeness some contour maps of deformation energies which we have

not shown in Sec. VIII above, in order not to make the presentation of results too confusing there. The results have, however, been discussed in general in Sec. VIII and need therefore not to be repeated.

BIBLIOGRAPHY

1. Conferences

Proceedings of the Second United Nations International Conference on the Peaceful Uses of Atomic Energy, Geneva, 1–13 September, 1958, (United Nations Publications) Vol. 15.

Proceedings of the International Conference on Nuclear Structure, Kingston, Canada, 29 August–3 September 1960, edited by D. A. Bromley and E. W. Vogt (North Holland Publ. Co.).

Proceedings of the Second International Conference on Nuclidic Masses, Vienna, Austria, 15-19 July 1963, edited by W. H. Johnston, Jr., (Springer-Verlag).

Proceedings of the Symposium on the Physics and Chemistry of Fission, held by IAEA, Salzburg, Austria, 22-26 March 1965.

Proceedings of the International Symposium on, why and how should we investigate Nuclides far off the Stability Line, Lysekil, Sweden, 21-27 August 1966 (Almqvist and Wiksell, Stockholm).

International Nuclear Physics Conference, Gatlinburg, Tennesee, 12–17 September 1966, edited by R. L. Becker, C. D. Goodman, P. H. Stelson, and A. Zucker, (Academic, New York).

Proceedings of a Conference on Nuclear Data—Microscopic Cross-sections and Other Data Basic for Reactors, held by IAEA, Paris, 17–21 October 1966.

Proceedings of the Third International Conference on Atomic Masses, Winnipeg, Canada, 28 August–1 September 1967, edited by R. C. Barber, (University of Manitoba Press).

Proceedings of the Second IAEA Symposium on the Physics and Chemistry of Fission, Vienna, 28 July–1 August 1969.

Proceedings of the International Conference on Properties of Nuclear States, Montréal, Canada, 25–30 August 1969 (University of Montréal Press).

2. References

Abramowitz, M., and I. A. Segun, Eds., 1964, *Handbook of Mathematical Functions* (Dover, New York).

Albrecht, K., *et al.*, 1970, Phys. Letters **32B,** 229.

Andersen, B. L., *et al.*, 1970, Nucl. Phys. **A159,** 337.

Androsenko, K. D., *et al.*, 1969, Vienna, p. 419.

Balian, R., and C. Bloch, 1970, Ann. Phys. **60,** 401.

——, and C. Bloch, 1971, Ann. Phys. **64,** 271.

Baranger, M., and K. Kumar, 1968, Nucl. Phys. **A122,** 241.

Bassichis, W. A., *et al.*, 1971, Livermore Preprint UCRL-73044.

Bate, G. L., *et al.*, 1963, Phys. Rev. **131,** 722.

Batty, C. J., 1970, Phys. Letters **31B,** 496.

——, and G. W. Greenless, 1969, Nucl. Phys. **A133,** 673.

Batty, C. J., and G. W. Greenless, 1969, Nucl. Phys. **A133,** 673.

Belyaev, S. T., 1959, Kgl. Danske Videnskab. Selskab, Mat.-Fys. Medd. **31,** No. 11.

Belyakov, V. A., 1964, Sovjet Phys.—JETP **19,** 1103.

Bès, D. R., 1961, Kgl. Danske Videnskab. Selskab, Mat.-Fys. Medd. **33,** No. 2.

——, and Z. Szymánski, 1961, Nucl. Phys. **28,** 42.

Bethe, H. A., and R. F. Bacher, 1936, Rev. Mod. Phys. **8,** 82.

——, 1968, Phys. Rev. **167,** 879.

Bjørnholm, S., and V. M. Strutinsky, 1969, Nucl. Phys. **A136,** 1.

Bloch, C., and R. Balian, 1969, private communication.

Bohr, Å., 1952, Kgl. Danske Videnskab. Selskab, Mat-Fys. Medd. **26,** No. 14.

——, and B. Mottelson, 1953, Kgl. Danske Videnskab. Selskab, Mat.-Fys. Medd. **27,** No. 16.

——, and B. Mottelson, 1969, *Nuclear Structure*, (Benjamin Inc., New York), Vol. 1.

——, and B. Mottelson, to be published, *Nuclear Structure* (W. A. Benjamin Inc., New York), Vols. 2, 3.

Bohr, N., and F. Kalckar, 1937, Kgl. Danske Videnskab. Selskab, Mat.-Fys. Medd. **14,** No. 10.

——, and J. A. Wheeler, 1939, Phys. Rev. **56,** 426.

Bolsterli, M., *et al.*, 1971, Los Alamos Preprint LA-DC-12817.

Brack, M., and H.-C. Pauli, 1971, Preprint, Basel University.

Bromley, D. A., and J. Weneser, 1968, Comments Nucl. Part. Phys., **2,** 151.

Brown, G. E., 1969, Comments Nucl. Part. Phys., **3,** 136.

Bunatyan, G. G., V. M. Kolomietz, and V. M. Strutinsky, 1972, to be published.

Cohen, S., and W. J. Swiatecki, 1962, Ann. Phys. **19,** 67.

——, and W. J. Swiatecki, 1963, Ann. Phys. **22,** 406.

Damgaard, J., *et al.*, 1969a, Nucl. Phys. **A135,** 432.

——, 1969b, Vienna, p. 213.

Decowsky, P., *et al.*, 1968, Nucl. Phys. **A110,** 129.

Feenberg, E., 1955, *Shell Theory of the Nucleus* (Princeton U. P.).

Fong, P., 1969, Statistical Theory of Nuclear Fission (Gordon and Breach, New York).

Ford, G. P., *et al.*, 1970, Los Alamos Report, LA-4329.

Frenkel, J., 1939, Soviet Phys.—JETP, **9,** 641.

——, 1939, Phys. Rev. **55,** 987.

Gareev, F. A., *et al.*, 1970, Sov. J. Nucl. Phys. **11,** 667.

Geilikman, B. T., 1960, Kingston, p. 874.

——, 1965, Salzburg, **1,** 121.

——, and G. N. Khlebnikov, 1968, Yad. Fiz. **7,** 215.

Ghiorso, A., *et al.*, 1954, Phys. Rev. **95,** 293.

Goeppert-Mayer, M., and J. H. D. Jensen, 1955, *Nuclear Shell Structure* (Wiley, New York).

Grin, T., 1963, Soviet Phys.—JETP **16,** 1327.

Gustafson, C., *et al.*, 1966, Lysekil, p. 613.

Hahn, O., and F. Strassman, 1939, Naturwissenschaften **27,** 11.

Halpern, I., and V. M. Strutinsky, 1958, Geneva, p. 408.

Hasse, R. W., 1969, Vienna, p. 33.

Haxel, O., *et al.*, 1949, Phys. Rev. **75,** 1766.

Heisenberg, J., *et al.*, 1969, Phys. Rev. Letters **23,** 1402.

Hendrie, D. L., *et al.*, 1968, Phys. Letters **26B,** 127.

Hill, D. L., and J. A. Wheeler, 1953, Phys. Rev. **89,** 1102.

Hyde, E. K., *et al.*, 1964, *The Nuclear Properties of the Heavy Elements*, **3** (Prentice Hall, Englewood Cliffs, New Jersey).

Inglis, D., 1954, Phys. Rev. **96,** 1059.

Johansson, S. A. E., 1962, Nucl. Phys. **22,** 529.

Kirzhnits, D. A., 1967, *Field Theoretical Methods in Many-Body Systems* (Pergamon, New York).

Kolomietz, V. M., *et al.*, 1971, Preprint ITF-71-93-R, Kiev.

Kramers, H. A., 1940, Physica **7,** 284.

Kumar, K., and M. Baranger, 1968, Nucl. Phys. **A110,** 529.

Landau, L. D., and E. M. Lifshitz, 1959, *Quantum Mechanics* (Pergamon, New York).

——, and E. M. Lifshitz, 1960, *Mechanics* (Pergamon, New York).

Lawrence, J. N. P., 1965, Phys. Rev. **B139,** 1227.

Lynn, E., 1966, Paris, **2,** 89.

——, and S. Bjørnholm, 1970, private communication.

Malov, L. A., S. M. Polikanov, and V. G. Soloviev, 1966, Gatlinburg, p. 786.

Mayer, M. G., 1949, Phys. Rev. **75,** 1969.

Meitner, L., and O. R. Frisch, 1939, Nature **143,** 239.

——, 1950, Nature **165,** 561.

——, 1952, Arkiv Fysik **4,** 383.

Meldner, H., 1969, Phys. Rev. **178,** 1815.

Migdal, A. B., 1959, JETP **37,** 249; Soviet Phys.—JETP **10** (1960), 176.

——, 1968, *Nuclear Theory, The Quasiparticle Method* (Benjamin, New York).

Mosel, U., *et al.*, 1971, Phys. Letters **34B,** 587.

Moskowski, S. A., 1970, Phys. Rev. **C 2,** 402.

Mottelson, B., and S. G. Nilsson, 1955, Phys. Rev. **99,** 1615.

——, and S. G. Nilsson, 1959, Kgl. Danske Videnskab. Selskab, Mat. Fys. Skr. **1,** No. 8.

Muzycka, Ya. A., *et al.*, 1968, Yad. Fiz. **6,** 306.

——, 1970, Yad. Fiz. **11,** 105; Sov. J. Nucl. Phys. **11,** 57.

Myers, W. D., and W. J. Swiatecki, 1966a, Nucl. Phys. **81,** 1.

——, and W. J. Swiatecki, 1966b, Lysekil, p. 343.

——, 1968, Ph. D. Thesis, Lawrence Radiation Laboratory Report UCRL-18214.

——, 1969, Nucl. Phys. **A145,** 387.

——, and W. J. Swiatecki, 1969, Ann. Phys. **55,** 395.

Möller, P., and S. G. Nilsson, 1970, Phys. Letters **31B,** 283.

Negele, J. W., 1970, Phys. Rev. **C1,** 1260.

Nemirovsky, P. E., and V. A. Chepurnov, 1966, Sov. J. Nucl. Phys. **3,** 730.

Nilsson, S. G., 1955, Kgl. Danske Videnskab. Selskab, Mat.-Fys. Medd. **29,** No. 16.
——, and O. Prior, 1961, Kgl. Danske Videnskab Selskab, Mat.-Fys. Medd. **32,** No. 16.
——, *et al.*, 1969, Nucl. Phys. **A131,** 1.
——, S. G. Thompson, and C. F. Tsang, 1969, Phys. Letters **28B,** 458.
Nix, J. R., 1969, Nucl. Phys. **A130,** 241.
Oganessian, Yu. T., 1968, preprint JINR E7-3942, Dubna.
Pashkevich, V. V., 1969, Nucl. Phys. **A133,** 400.
——, 1969, 1970, private communications; See also Nucl. Phys. **A169,** 275 (1971).
——, and V. M. Strutinsky, 1969, Yad. Fiz. **9,** 56; Sov. J. Nucl. Phys. **9,** 35.
Pauli, H. C., *et al.*, 1971, Phys. Letters **34B,** 264.
——, and T. Ledergerber, 1971, Nucl. Phys. **A175,** 545.
Pavlinchuk, V. A., 1967, private communication.
Polikanov, S. M., *et al.*, 1962, Zhur. Eksp. i Teoret. Fiz. **42,** 1464; Soviet Phys.—JETP **15,** 1016.
Quentin, P., and R. Babinet, 1970, Nucl. Phys. **A156,** 365.
Rainwater, J., 1950, Phys. Rev. **79,** 432.
Rost, E., 1968, Phys. Letters **26B,** 184.
Seeger, P., 1967, Winnipeg, p. 85.
——, and R. C. Perisho, 1967, Los Alamos Rept LA-3751.
Siemens, P., 1970, Phys. Rev. **C1,** 98.
Smirnov, V. I., 1964, *A Course of Higher Mathematics* (Pergamon, New York) Vol. 4, Chap. 2.
Stein, N., 1969, Montréal, p. 337.
Strutinsky, V. M., and A. S. Tyapin, 1963, Zhur. Eksp. i Teoret. Fiz. **45,** 960; Soviet Phys.—JETP **18,** 664.
——, *et al.*, 1963, Nucl. Phys. **46,** 639.
——, 1966, Yad. Fiz. **3,** 614; Sov. J. Nucl. Phys. **3,** 449.
——, 1966, Lysekil, p. 629.
——, 1967, Nucl. Phys. **A95,** 420.
——, 1968, Nucl. Phys. **A122,** 1.
——, and H.-C. Pauli, 1969, Vienna, p. 155.
Swiatecki, W. J., 1963, Vienna, p. 58.
——, 1970, in *Nuclear Reactions Induced by Heavy Ions*, edited by R. Bock and W. R. Hering (North Holland Publ. Co., Amsterdam) p. 729.
——, and W. D. Myers, 1970, private communication.
Szymánski, Z., 1961, Nucl. Phys. **28,** 63.
Terrell, J., 1959, Phys. Rev. **113,** 527.
Tsang, C. F., 1969, Berkeley Report UCRL-18899.
Vandenbosch, R., 1963, Nucl. Phys. **46,** 129.
——, and J. R. Huizenga, 1958, Geneva, p. 284.
Vautherin, D., and D. M. Brink, 1970, Phys. Letters **32B,** 149.
Vogel, P., 1968, Nucl. Phys. **A112,** 583.
von Weizsäcker, C. F., 1935, Z. Physik **96,** 431.
Vorotnikov, P. E., *et al.*, 1967, Sov. J. Nucl. Phys. **5,** 210.
Wilets, L., 1959, Phys. Rev. **116,** 372.
——, 1964, *Theories of Fission* (Clarendon Press, Oxford).
Zeldes, N., *et al.*, 1967, Kgl. Danske Videnskab. Selskab, Mat. Fys. Skr. **3,** No. 5.